

**WL-TR-1997-7060**

**EFFECT OF COMPRESSIBILITY ON THE  
TURBULENCE STRUCTURE AND ITS  
MODELING**

---

**Venkata Subramanian Krishnamurty**

University of Florida  
Aerospace Engineering, Mechanics and Engineering Science  
P.O. Box 116250  
Gainesville, FL 32611-6250

**Contract No. F08635-92-C-0032**

**JULY 1997**

**INTERIM REPORT FOR PERIOD JUNE 1994- DECEMBER 1996**

**APPROVED FOR PUBLIC RELEASE; DISTRIBUTION UNLIMITED.**

**DTIC QUALITY INSPECTED 3**

**WRIGHT LABORATORY, ARMAMENT DIRECTORATE**

**Air Force Materiel Command ■ United States Air Force ■ Eglin Air Force Base**

**19970825 101**

## NOTICE


When Government drawings, specifications, or other data are used for any purpose other than in connection with a definitely Government-related procurement, the United States Government incurs no responsibility or any obligation whatsoever. The fact that the Government may have formulated or in any way supplied the said drawings, specifications, or other data, is not to be regarded by implication, or otherwise as in any manner construed, as licensing the holder, or any other person or corporation; or as conveying any rights or permission to manufacture, use, or sell any patented invention that may in any way be related thereto.

This technical report has been reviewed and is approved for publication.

FOR THE COMMANDER



Lanny G. Burdge  
Technical Director, Munitions Assessment Division



Rudy Johnson  
Program Manager

Even though this report may contain special release rights held by the controlling office, please do not request copies from the Wright Laboratory, Armament Directorate. If you qualify as a recipient, release approval will be obtained from the originating activity by DTIC. Address your request for additional copies to:

DTIC-OCP  
Defense Technical Information Center  
8725 John J Kingman Road, Suite 0944  
Fort Belvoir, VA 22060-6218

If your address has changed, if you wish to be removed from our mailing list, or if your organization no longer employs the addressee, please notify WL/MNSI, Eglin AFB FL 32542-6810, to help us maintain a current mailing list.

Do not return copies of this report unless contractual obligations or notice on a specific document requires that it be returned.

REPORT DOCUMENTATION PAGE			Form Approved OMB No. 0704-0188	
Public reporting burden for this collection of information is estimated to average 1 hour per response, including the time for reviewing instructions, searching existing data sources, gathering and maintaining the data needed, and completing and reviewing the collection of information. Send comments regarding this burden estimate or any other aspect of this collection of information, including suggestions for reducing this burden, to Washington Headquarters Services, Directorate for Information Operations and Reports, 1215 Jefferson Davis Highway, Suite 1204, Arlington, VA 22202-4302, and to the Office of Management and Budget, Paperwork Reduction Project (0704-0188), Washington, DC 20503.				
1. AGENCY USE ONLY (Leave blank)		2. REPORT DATE July 1997		3. REPORT TYPE AND DATES COVERED INTERIM June 1994 - December 1996
4. TITLE AND SUBTITLE Effect of Compressibility on the Turbulence Structure and its Modeling			5. FUNDING NUMBERS C: F08635-92-C-0032 PE: 62602F PR: 2502 TA: 03 WU: 14	
6. AUTHOR(S) Venkata Subramanian Krishnamurty				
7. PERFORMING ORGANIZATION NAME(S) AND ADDRESS(ES) University of Florida Aerospace Engineering, Mechanics and Engineering Science P.O. Box 116250 Gainesville, FL 32611-6250			8. PERFORMING ORGANIZATION REPORT NUMBER  TASK: 96-01	
9. SPONSORING/MONITORING AGENCY NAME(S) AND ADDRESS(ES) Wright Laboratory, Armament Directorate (WL/MN) 101 W. Eglin Blvd., Ste. 252 Eglin AFB, FL 32542-6810 Program Manager: Rudy Johnson, WL/MNSI/ 850-882-2141, ext. 2230			10. SPONSORING/MONITORING AGENCY REPORT NUMBER  WL-TR-1997-7060	
11. SUPPLEMENTARY NOTES  Availability of this report is specified on the reverse of the front cover.				
12a. DISTRIBUTION AVAILABILITY STATEMENT  APPROVED FOR PUBLIC RELEASE; DISTRIBUTION UNLIMITED.			12b. DISTRIBUTION CODE	
13. ABSTRACT (Maximum 200 words) In the present study, the compressibility effect is investigated in the context of the two-equation k-epsilon model. Several models have been proposed to deal with the dissipative nature of compressibility and the complexities arising due to the non-divergent nature of the velocity field. In addition modifications have been proposed to address the added time-scale effect that is due to a non-equilibrium between the rates of production and dissipation of turbulent kinetic energy in complex flows. The reduced dependence, of the k-omega based models on the spatial gradients in density, has been shown to be an artifact of the neglect of cross-diffusion terms in the transport equation for omega. Through a systematic study of the exact form of the turbulence transport equations two additional source terms that are unique to compressible turbulent flows, namely the enthalpic production term and the term representing the baroclinic effect, have been identified and models are proposed.				
14. SUBJECT TERMS k-epsilon; k-omega; compressible turbulence; enthalpic production term; baroclinic effect			15. NUMBER OF PAGES 210	
			16. PRICE CODE	
17. SECURITY CLASSIFICATION OF REPORT  UNCLASSIFIED	18. SECURITY CLASSIFICATION OF THIS PAGE  UNCLASSIFIED	19. SECURITY CLASSIFICATION OF ABSTRACT  UNCLASSIFIED	20. LIMITATION OF ABSTRACT  UL	

## TABLE OF CONTENTS

	<u>page</u>
ABSTRACT .....	vi
CHAPTERS	
INTRODUCTION .....	1
REVIEW OF LITERATURE .....	4
2.1 Compressible Free Shear Layers .....	4
2.2 Compressible Boundary Layers .....	15
2.3 Summary .....	20
EDDY-VISCOSITY MODELS .....	21
3.1 Governing Equations .....	21
3.2 Turbulence Closure .....	22
3.2.1 Averaging Techniques .....	23
3.2.1.1 Reynolds average .....	24
3.2.1.2 Favre average .....	25
3.2.1.3 Relationship between Reynolds and Favre averages .....	26
3.2.2 Equations of Motion: Averaged Form .....	27
3.3 Eddy-Viscosity Based Modelling .....	29
3.3.1 Zero- and One-Equation Models .....	30
3.4 k- $\epsilon$ Model .....	31
3.4.1 Wall-Function Treatment .....	39
3.4.1.1 Wall-function: low Mach number form .....	40
3.4.1.2 Wall-function: compressible form .....	42
3.5 Other Two-Equation Models .....	45
3.6 Summary .....	48
COMPUTATIONAL METHOD .....	50
4.1 Numerical Algorithm .....	50
4.1.1 Governing Equations .....	50



4.1.2 Numerical Algorithm .....	53
4.1.3 Artificial Dissipation Schemes .....	54
4.1.3.1 Blend of second- and fourth-order differences .....	54
4.1.3.2 Flux-limited dissipation .....	56
4.1.4 Time Stepping .....	57
4.1.5 Convergence Acceleration .....	59
4.1.6 Second-Order Upwind Scheme .....	60
4.2 Code Validation .....	63
4.2.1 Aerofoil Flow-Field Computations .....	63
4.2.1.1 Inviscid computation .....	66
4.2.1.2 Laminar computation .....	67
4.2.1.3 Turbulent flow computations .....	69
4.2.2 Nozzle Flow Computations .....	72
4.3 Summary .....	76
<b>k-<math>\epsilon</math> BASED MODELLING OF COMPRESSIBLE TURBULENT FLOWS .....</b>	<b>77</b>
5.1 Introduction .....	77
5.2 Governing Equations .....	78
5.3 Modelling of Compressibility Effects .....	82
5.3.1 Dilatation Dissipation .....	82
5.3.1.1 Zeman modification .....	85
5.3.1.2 Sarkar et al. modification .....	86
5.3.1.3 El Baz modification .....	86
5.3.1.4 Comparison of dilatation dissipation modifications .....	87
5.3.2 Pressure Dilatation .....	88
5.3.2.1 Sarkar modification .....	88
5.3.2.2 Zeman modification : .....	90
5.3.2.3 El Baz modification .....	91
5.3.3 Proposed Modifications .....	92
5.3.3.1 Estimation of turbulent mass flux .....	93
5.3.3.2 Estimation of pressure dilatation .....	95
5.3.3.3 Effect of baroclinic torque .....	96
5.3.3.4 Comment on proposed modifications .....	99
5.3.4 Additional Issues .....	100
5.4 Summary .....	103
<b>COMPUTATIONAL ANALYSIS OF COMPRESSIBILITY MODIFICATIONS ..</b>	<b>104</b>
6.1 Introduction .....	104
6.2 Base Flowfield .....	106
6.2.1 Description of the Base Flowfield .....	106
6.2.1.1 Turbulent wall boundary layer .....	107
6.2.1.2 Rapid expansion region .....	108
6.2.1.3 Mixing region .....	109

6.2.1.4 Recompression region .....	110
6.2.2 Overview of Prior Computational Efforts .....	110
6.2.3 Present Computational Study .....	112
6.2.3.1 Grid independence .....	117
6.2.3.2 Treatment of convective fluxes .....	118
6.2.3.3 Non-equilibrium modifications .....	128
6.2.3.4 Compressibility modifications .....	140
6.3 Summary .....	154
6.4 Projectile Forebody Flowfield .....	155
6.4.1 Shock-Turbulence Interaction .....	158
6.4.2 Experimental Studies of Projectile Flowfield .....	161
6.5 Projectile Flowfield Computations .....	162
6.5.1 Spike-off Case .....	163
6.5.1.1 Non-equilibrium modifications .....	164
6.5.1.2 Compressibility modifications .....	169
6.5.2 Spike-on Case .....	172
6.5.2.1 Non-equilibrium modifications .....	176
6.5.2.2 Compressibility modifications .....	182
6.6 Summary .....	186
CONCLUDING REMARKS .....	189
REFERENCES .....	193

Abstract of Dissertation Presented to the Graduate School  
of the University of Florida in Partial Fulfillment of the  
Requirements for the Degree of Doctor of Philosophy

EFFECT OF COMPRESSIBILITY ON THE TURBULENCE STRUCTURE  
AND ITS MODELLING

By

Venkata Subramanian Krishnamurty

December 1996

Chairperson : Dr. Wei Shyy  
Major Department : Aerospace Engineering, Mechanics, and Engineering Science

The effect of compressibility on the structure of turbulence is an important but difficult issue in turbulence modelling. Modelling issues in both the production and dissipation of turbulent kinetic energy need to be addressed to account for Mach number effects.

In the present study, the compressibility effect is investigated in the context of the two-equation model, particularly the  $k$ - $\epsilon$  model. Several models have been proposed in the literature, that deal with the dissipative nature of compressibility and the complexities arising due to the non-divergent nature of the velocity field. In addition modifications have been proposed to address the added time-scale effect that is due to a non-equilibrium between the rates of production and dissipation of turbulent kinetic energy in complex flows. These modifications are discussed in the context of the two-equation model. The dependence, of two-equation modelling approaches on the spatial gradients in density, has been addressed. The reduced dependence, of  $k$ - $\omega$  based models on the spatial gradients in density, has been shown to be an artifact of the neglect of cross-diffusion terms in the transport equation for

ω. Through a systematic study of the exact form of the turbulence transport equations two additional source terms that are unique to compressible turbulent flows, namely the enthalpic production term and the term representing the baroclinic effect, have been identified. Models have been proposed for these two terms.

The effectiveness of the modifications in predicting flow fields of increased complexity needs to be evaluated and a computational analysis of these modelling issues has been conducted. The numerical procedure is a finite-volume, multi-stage Runge-Kutta time stepping, second-order scheme with either a central difference or an upwind difference treatment of the convection terms. Flows characterized by strong streamline curvature and inhomogenities arising due to strong shocks and rapid expansions, in the form of supersonic flow past an axi-symmetric afterbody and hypersonic flow past a projectile, have been adopted to evaluate the various modelling aspects investigated.

## CHAPTER 1

### INTRODUCTION

The study into the effects of compressibility on turbulent fluctuations is an important but difficult one. An understanding of the effect of compressibility on the turbulent flow field is important from the point of view of predicting the turbulent flow field at high speeds. These effects become particularly important when considering the aerodynamic performance of high speed flight and also the rate of mixing in shear layers, (such as found in supersonic combustion).

Two words in the title to this dissertation need to be defined. From thermodynamics (Thompson, 1972) **compressibility** can be defined as the change in density of a fluid cell, brought about by either changes in temperature or changes in pressure. While the former is of importance in combustion systems or systems with heat sources or sinks, the latter is encountered when there are appreciable variations in the Mach number. The current study focuses on changes in the density of a fluid cell brought about by changes in pressure, and the effect of compressibility on the turbulent fluctuations.

Turbulence is a stochastic process, with random fluctuations in time and three spatial directions. These fluctuations have finite correlation time and length scales. **Turbulence structure** refers to the various correlations that can be formed between the fluctuating quantities and the spectral distribution of these fluctuations. In the case of turbulent flows, the effect of fluctuations in pressure on the fluctuations of the volume of a fluid cell are referred to as the effects of compressibility (Lele, 1994), and the effect these fluctuations have on the turbulence structure is addressed in this dissertation.

In this dissertation, questions regarding the effect of compressibility on the turbulence structure parameters and parameters that quantify this effect is addressed. In particular, the focus is on the models that have been proposed in the literature to account for the effect of compressibility and the shortcomings of these modifications. Additional aspects of the compressibility effect are addressed and modifications are proposed to account for these effects. A computational study, to understand the effectiveness and implications, of these modifications is presented. These include flowfields characterized by increased complexity due to streamline curvature and strong discontinuities, such as shocks.

Chapter 2 presents a detailed discussion of our current understanding of compressible turbulent flows, based on experimental observations and direct numerical simulations (DNS). Even with the considerable effort that has gone into improving our understanding the effects of compressibility, we do not yet have a clear picture of these effects. Because of practical limitations, DNS is restricted to simple flow fields such as mixing layers and turbulent boundary layers at low Reynolds numbers. So, some of the observations and results gleaned from such simulations are sometimes unsatisfactory in predicting more complex flow fields. In fact, in some instances, modelling suggestions based on the observations of two-stream mixing layers have proven to be not applicable in the case of wall-bounded shear layers. One of the motivations of this research effort is to address the applicability of the proposed modifications, in solving problems of direct engineering relevance.

To address these goals, one needs to resort to closure models by making approximations to the transport equations, usually second-order closure models or eddy-viscosity based approximations. The two-equation based eddy-viscosity models offer the best alternative, (from economy of computation), to solve these flow fields. But there are still issues that are unresolved, in eddy-viscosity based modelling of compressible flows. Analyses of the two-equation based modelling approach (Chen and Kim, 1987 and Bernard and Speziale, 1992) suggest a need for modifications to address non-equilibrium effects and other effects that have been hitherto ignored. In the chapters that follow, these effects are

outlined and the need for modifications to improve the modelling capabilities is addressed, including modifications that have been proposed in this research study. A thorough testing of these modifications is presented and the results compared against experimental observations.

The organization of this dissertation is as follows : Chapter 2 presents a review of the effort that has gone into enhancing our understanding of the effects of compressibility, including experimental, computational and analytical observations of such high speed flows. The turbulence closure model and the inherent problems of eddy-viscosity based modelling approaches are discussed in Chapter 3. Chapter 4, presents a detailed description of the numerical algorithm and a validation of the computational procedure used in this study. Details regarding the problems with turbulence closure models in modelling compressible, turbulent flows will be presented in Chapter 5. Chapter 5, also presents the modifications that have been proposed in the literature to address the effect of compressibility on the turbulence structure and discusses the shortcomings of these modifications. Additional modifications, that have been proposed in this dissertation, are described in Chapter 5.

In Chapter 6, the focus is on the need for the modifications that have been proposed in this study and testing of these modifications against the flow past an axi-symmetric afterbody. Extensive comparison against experimental measurements is presented here. Chapter 6 also presents an evaluation of the current modifications and other modifications that have been proposed, in the literature, for inhomogeneous flow fields. This concerns the effectiveness of the modifications in predicting flow fields characterized by the interaction of turbulence fluctuations with strong shocks. Chapter 7 presents remarks that can be made regarding the outcome of this dissertation and the issues that need to be pursued to further our understanding of turbulent flows and effectively model its characteristics.

## CHAPTER 2

### REVIEW OF LITERATURE

A review of the literature on the study of the effects of compressibility in the case of high speed, compressible turbulent flows is presented here, including experimental observations, empirical correlations, direct numerical simulation (DNS), results and analysis based on order of magnitude analysis and dimensional arguments. Particularly, studies into structure of turbulent fluctuations in free shear layers and wall bounded shear layers are summarized. In addition, in the following chapters, reviews are presented of the research efforts that have gone into improving our understanding of more complicated phenomena such as the effect of rapid expansions on a separating turbulent boundary layer and the effect of shock-turbulence interactions.

#### 2.1 Compressible Free Shear Layers

Perhaps the simplest flowfield to analyze, to understand the effect of compressibility on the turbulence structure, is the free shear layer. Free shear layers at high speeds, such as turbulent jets, wakes and two-stream mixing layers have been analyzed extensively (Birch and Eggers, 1972). There are two important effects that need to be considered in the analysis of supersonic shear layers. These are the effects of varying density and varying Mach number. Some of the first studies into compressible turbulent shear layers were experimental observation of supersonic jets ejecting into a quiescent ambient. Birch and Eggers [1972] have reviewed and compiled the experimental observations on the development of these shear layers. The experimental data indicated that the growth rates of these shear layers were substantially reduced in comparison to their incompressible counterparts. Supersonic jets are characterized by high Mach numbers and therefore reduced temperatures and thus



increased density in comparison with the surrounding fluid. The reduced growth rates were, therefore, explained as a result of the increased densities. Brown and Roshko [1974] conducted an experimental analysis of incompressible, two-stream, planar mixing layers, with different densities in the two streams, as shown in Figure 2.1.

They compared the growth rate of the mixing layer in their experiments, with the results obtained for supersonic shear layers, with similar density ratios. It was observed that while the variation in density did cause a reduction in the growth rate of the shear layers, it was not sufficient enough to explain the reduced growth rates observed in supersonic shear layers. This indicated a Mach number effect on the mixing rates in these shear layers. To correlate the observed variations in high speed, free shear layers, with the variations in Mach number, Bogdanoff [1983], suggested the use of a non-dimensional parameter,  $M^+$ . Figure 2.2 below shows a sketch of the two-stream mixing layer. Assuming that the large scale structures, that are present in the mixing layer travel at a speed  $U_c$  and that the drag on these structures was zero, he equated the dynamic pressures in the two streams and defined

$$M^+ = \frac{M_1(1 - \lambda_u)}{(1 + \lambda_q^{-1/2})\lambda_\gamma^{1/4}} \text{ where } \lambda_u = U_2 / U_1, \lambda_q = Q_2 / Q_1 \text{ and } \lambda_\gamma = \gamma_2 / \gamma_1. \text{ This value of}$$

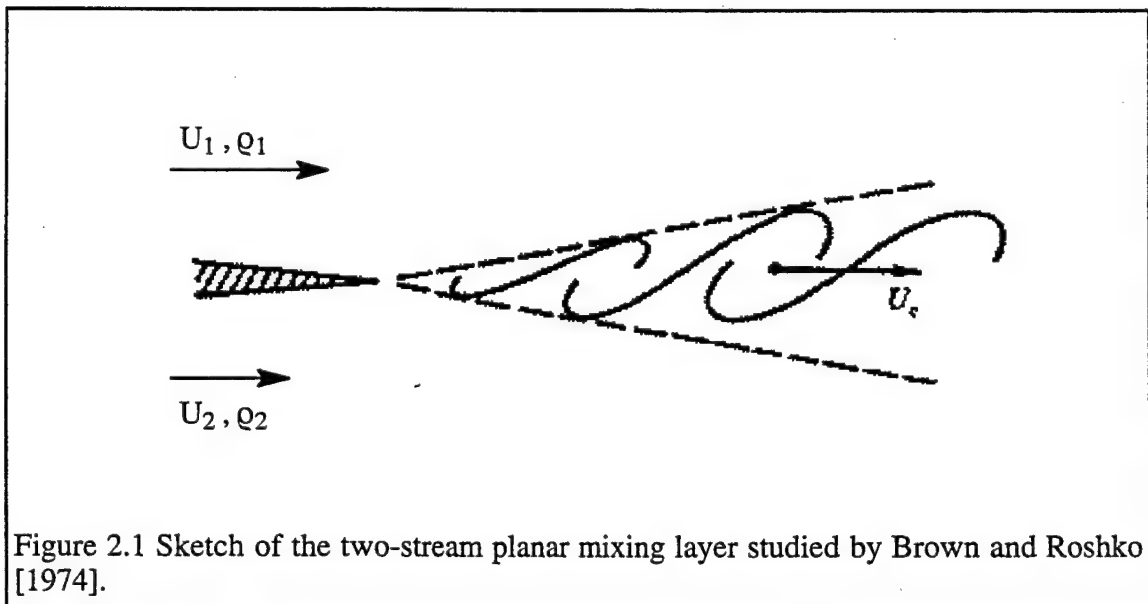


Figure 2.1 Sketch of the two-stream planar mixing layer studied by Brown and Roshko [1974].

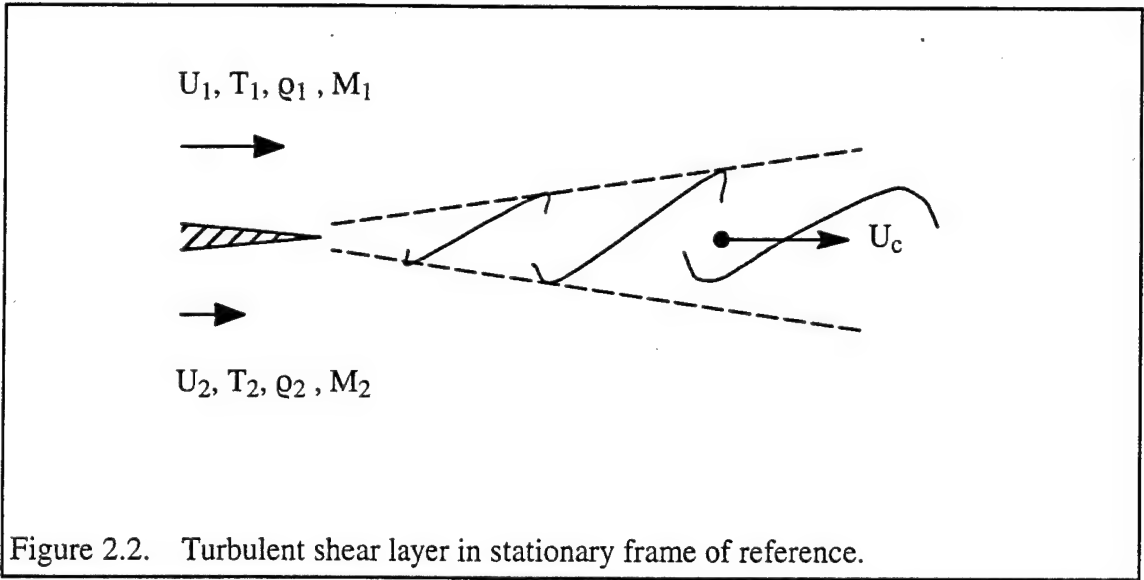


Figure 2.2. Turbulent shear layer in stationary frame of reference.

$M^+$  appears to correlate quite successfully the observed reductions in growth rates from various experimental studies.

Papamoschou and Roshko [1988] generalized this definition of the Mach number. If  $U_c$  is the velocity of the structures, then convective Mach numbers for the two streams can be defined. Accordingly,

$$\begin{cases} M_{c1} = \frac{U_1 - U_c}{a_1} \\ M_{c2} = \frac{U_c - U_2}{a_2} \end{cases} \quad (2.1)$$

where subscripts 1 and 2 represents the faster and slower streams (of a two-stream mixing layer).

If the shear layer were observed from a frame of reference moving with the structures at the velocity  $U_c$ , and if the structures vary slowly over the time it takes a fluid cell to travel through them then the flow in this reference frame can be thought of as steady. A sketch of the streamlines, from Coles [1981], in this frame of reference is shown below in Figure 2.3. The sketch shows a saddle point between the two structures, where the two fluid streams meet. If we assume that the fluid from each stream decelerates isentropically and meet at the saddle point, then the static pressure at this point is equal to the stagnation pressure of the

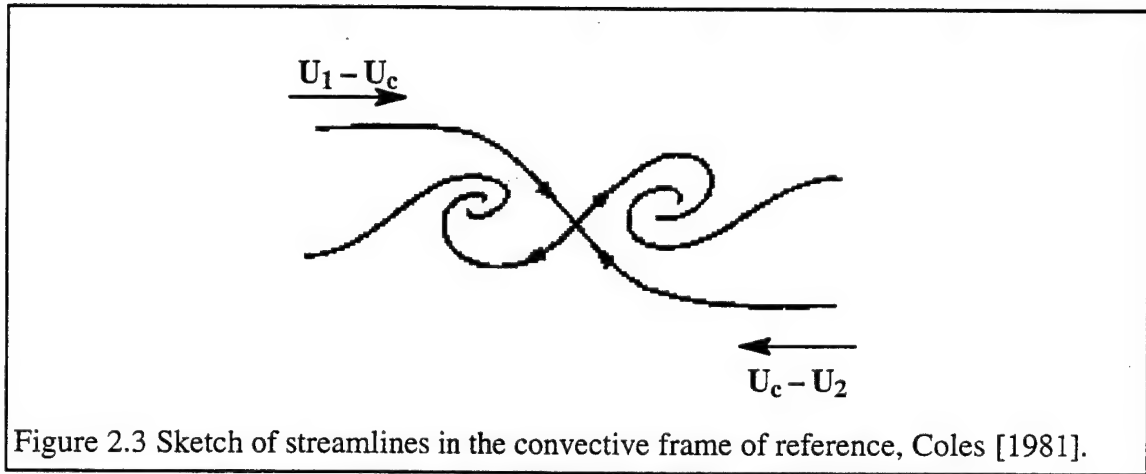


Figure 2.3 Sketch of streamlines in the convective frame of reference, Coles [1981].

two streams. Equating the stagnation pressures at this point\* (for equal static pressures) one obtains

$$\left(1 + \frac{\gamma_1 - 1}{2} M_{c1}^2\right)^{\frac{\gamma_1}{\gamma_1 - 1}} = \left(1 + \frac{\gamma_2 - 1}{2} M_{c2}^2\right)^{\frac{\gamma_2}{\gamma_2 - 1}} \quad (2.2)$$

Equation 2.2 in conjunction with equation 2.1, gives a speed-of-sound-weighted average for the convective velocity  $U_c$ ,

$$U_c = \frac{a_2 U_1 + a_1 U_2}{a_1 + a_2} \quad (2.3)$$

And for specific heat ratios not vastly different,  $M_{c1}$  and  $M_{c2}$  defined by equation 2.1 are essentially equal,  $M_{c1} = M_{c2} = M_c$  (convective Mach number). Through the rest of this dissertation we will use  $M_c$  to denote the convective Mach number.

There are several ways to define the lateral extent of the shear layer, and a variety of these definitions have been used by experimentalists to define the growth of the shear layer. These definitions have been denoted as visual thickness,  $\delta_v$ , pitot thickness,  $\delta_p$ , and  $\delta_w$ , the vorticity thickness. The vorticity thickness, sometimes referred to as the maximum slope thickness, is defined as

\* Since the static pressures of the two streams are equal, this formulation is essentially identical to the analysis of Bogdanoff [1983].

$$\delta_{\omega} = \frac{1}{|\omega_m|} \int_{-\infty}^{\infty} |\omega| dy \quad \text{where } \omega = -\frac{\partial U}{\partial y} \quad (2.4)$$

where  $|\omega_m|$  is the magnitude of the maximum value of vorticity in the shear layer.

Samimy et al. [1989], conducted experimental investigations of the mixing of compressible free shear layers and investigated the impact of a free shear layer interacting with a bow shock (the motivation here was to study the enhancement of mixing due to interaction of free shear layers with shock waves). From their results and from the results of Papamoschou and Roshko [1988], they observed that if the lateral extent of the shear layer is defined using the vorticity thickness,  $\delta_{\omega}$ , then a plot of  $\delta_{\omega} / \delta_{\omega 0}$  versus the convective Mach number (defined in equation 2.1) can reasonably correlate all the experimental data.  $\delta_{\omega 0}$  is the corresponding thickness of the shear layer at zero convective Mach number, that is incompressible flow. The non-dimensionalized value of the vorticity thickness decreases with increasing convective Mach number and reaches an asymptotic value for supersonic (convective) Mach numbers. The interaction of the bow shock with the free shear layer did not, however, produce any significant change in either the turbulence structure parameters, or the similarity profile for the mean flow velocity.

Inviscid stability analysis has been very useful in understanding some of the observed effects in the case of free shear layers. Such analyses, have been reported by Gropengesser [1970], Blumen et al. [1975], Ragab and Wu [1989], Jackson and Grosch [1989] and recently Sandham and Reynolds [1990] and Morris et al. [1990]. In such analysis the growth of the most amplified disturbance is examined as a function of the convective Mach number and also its dependence on the velocity, density and temperature ratios. These results have helped substantiate the use of  $M_c$  as a correlation parameter. These linearized analyses seem to indicate that at convective Mach numbers greater than 1.0, the convective Mach numbers  $M_{c1}$  and  $M_{c2}$  defined as in equation 2.1, are no longer equal. Strictly, the convective Mach numbers,  $M_{c1}$  and  $M_{c2}$ , need not be equal. It should be pointed out that the definition of Papamoschou and Roshko [1988] and Bogdanoff [1983] for the convective Mach number

is based on two-dimensionality of the structures and the isentropy of the structures. But recent results obtained by Papamoschou [1991] indicate that this definition of the convective Mach number is not valid in cases where the speeds of the two streams are highly disparate. This has also been shown in the inviscid stability analysis of Ragab and Wu [1990]. In a recent study, Poggie and Smits [1996] conducted an experimental analysis of the compressible turbulent shear layer at a convective Mach number of 1.1 ( $M_c = 1.1$ ). They observe that the convective velocity defined in equation 2.3 is not a constant and that it varies across the mixing layer.

Ikawa and Kubota [1975] conducted an experimental analysis of the structure of turbulence in supersonic free shear layers. They observed that, in addition to reduction in growth rates of these shear layers, they were also characterized by a reduction in the magnitude of turbulence intensity (in comparison with incompressible shear layers). Elliott and Samimy [1990] conducted an analysis of the effect of increasing convective Mach number on the turbulence structure. Their experiments, at three convective Mach numbers, showed that the magnitudes of the various turbulence correlations were markedly reduced in comparison to their incompressible counterparts. Also, the lateral extent of turbulence in the shear layer seems to decrease with increase in convective Mach number. They also present some interesting results of skewness and flatness profiles of the velocity fluctuations and these seem to confirm the previous remark on the lateral extent of turbulence activity in the shear layer.

The results from the inviscid stability analysis of Ragab and Wu [1989] and Sandham and Reynolds [1990] indicate that at convective Mach numbers greater than about 0.6 ( $M_c \geq 0.6$ ), the large structures that have been experimentally observed may no longer be two-dimensional. These studies show that at these convective Mach numbers the most amplified disturbances are the oblique ones, indicating three-dimensionality of the structures. The measurements by Samimy et al. [1992] of the correlations, also seem to suggest a three-dimensionality to the large-scale structures. Recently, Clemens and Mungal

[1995] presented a detailed visualization of the coherent structures and their development as a function of the convective Mach number. These results show that at convective Mach numbers less than 0.6 ( $M_c < 0.6$ ) the large-scale structures are well organized and indeed two-dimensional. With increase in convective Mach number, the large structures seem to be less organized and display signs of three-dimensionality.

To summarize, analysis of two-stream mixing layers indicates the following :

1. The shear layer displays large coherent structures similar to those observed by Brown and Roshko [1974]. However, the organization of these structures seem to reduce with increasing Mach numbers.
2. The growth rate of the shear layer decreases with increase in convective Mach number (defined in equation 2.1). This reduction in growth rate, though affected to a certain extent by density variations, is presumably due to varying Mach numbers.
3. The convective Mach number seems to be a valid parameter to correlate the effects of compressibility on the structure of the turbulent mixing layer.
4. The peak levels of turbulence structure parameters (correlation coefficients and spectrum shapes) also show a decrease with increase in compressibility.
5. However, for convective Mach numbers greater than unity, the convective velocity of the large structures is no longer a constant and shows variation over the lateral extent of the shear layer.
6. Inviscid stability analysis and recent experimental results indicate that the coherent structures are two dimensional at low levels of compressibility, (for  $M_c < 0.6$ ). With increasing compressibility there is a distinct three dimensionality to the structures.

All the above mentioned research efforts point to a “stabilizing effect” of compressibility on the mixing rate in high speed free shear layers. However, the reasons for the strong “stabilizing effect” remains unclear. An explanation from Sandham and Reynolds [1990] and Morris et al. [1990], drawing an analogy from the result of linear analysis indicates that the growth rate of small disturbances decreases when the convective Mach number  $M_c$  increases. Jackson and Grosch [1989] have shown that the linear analysis results, of the maximum growth rate of disturbances for a wide range of values for the free stream temperature and density, fall on essentially a single curve that is a function of  $M_c$ . The similarity between the experimentally observed variations and those predicted by linear

stability analysis has prompted the argument that linear analysis explains the effect of compressibility on mixing rate. However it is not quite clear why and how a simple linear theory can explain a fully turbulent mixing layer.

Phenomenological suggestions have been made to explain the effect of Mach number on the reduction in the rate of mixing in compressible free shear layers. Morkovin [1986] suggests that the lack of upstream and transverse propagation of information (in high speed shear layers) is responsible for the reduction in growth rates of instabilities. He suggests the existence of a zone of influence beyond which there is no propagation of information, implying a lack of communication to the extremities of the shear layer. He also suggests that the turbulent structures at high Mach numbers end up in radiating energy out, resulting in reduced energies available for entrainment and further development of the shear layer. Breidanthal [1992] recently proposed a "sonic-eddy" model to explain the reduced growth rates of free shear layers. His hypothesis suggests that turbulent eddies whose rotational Mach number exceeds unity, do not participate in the engulfment of fluid. As the relative Mach number increases, (for a simple two-dimensional mixing layer with equal densities in the two streams the relative Mach number  $M_r = 2 M_c = 2 \{U_1 - U_2\} / \{a_1 + a_2\}$ ), the proportion of such sonic eddies in the shear layer increases leading to the reduction in growth rates with increasing Mach number. A similar hypothesis has been put forth by Kim [1990] who suggests the existence of a Mach zone, beyond which information does not propagate and that with increase in the relative Mach number the lateral extent of this Mach zone reduces, resulting in the reduced communication to the edges of the shear layer leading to the reduction in shear layer growth rates. DNS studies have been attempted to provide an explanation for the reduction in mixing rate observed in free shear layers.

Papamoschou and Lele [1993] conducted an analysis of vortex shearing at various values of the relative or convective Mach number  $M_c$ . They studied the effect of shearing on a monopole placed in a stream of uniform shear. With increasing convective Mach number, they observe that the extent of the pressure variation is reduced to a narrow region

in the streamwise direction, but extending to the extremities of the shear layer. This would then negate the hypothesis of Breidenthal [1992] and Kim [1990], who propose a sonic limit beyond which communication is lost to the extremities of the shear layer. Another result of their simulations is that the streamwise extent of the Reynolds shear stress is also reduced with increase in convective Mach number. They propose that this would imply a lack of communication in the streamwise direction, and therefore a reduction in the mixing and roll-up process (amalgamation of vortices), which is known to be responsible for the growth of the shear layer. Due to this reduction in the shear stress, there is a reduction in the rate of production of turbulence energy which results in the reduced levels of turbulence observed in the experimental studies.

The transport equation describing the evolution of turbulent kinetic energy for the case of decaying compressible turbulence is equation 2.5.

$$\rho \frac{\partial q^2}{\partial t} = -2 \left( \mu \overline{\omega_j \omega_j} + \frac{4}{3} \mu (\overline{u_{jj}})^2 - \overline{p u_{k,k}} \right) \quad (2.5)$$

In the above equation,  $q^2$  represents the fluctuation kinetic energy,  $q^2 = u_j u_j$ , where  $u_j$  and  $\omega_j$  are, respectively, the fluctuation velocity and vorticity components defined using a mass-weighted Favre average. The overbars denote a Reynolds average,  $p$  represents the pressure fluctuation with respect to a Reynolds average, and  $\rho$  and  $\mu$  represent the density and molecular viscosity, respectively. Details regarding the averaging techniques can be found in Chapter 3. The first term on the right hand side of equation 2.5 represents the solenoidal dissipation rate (incompressible) due to the cascade of energy to the small scales of turbulence. The second and third terms on the right hand side represent the extra dissipation brought in due to the dilatational effects. While the second term on the right hand side represents the dilatational dissipation, the third term is referred to as the pressure dilatation term. Zeman [1990] concludes, based on the presence of eddy shocklets in compressible turbulent flow fields, that the effect of compressibility is a dissipative one, with the dilatational turbulent velocities being responsible for this extra dissipation. He derives



an expression for this extra dissipation due to dilatational effects. This extra dissipation is expressed as a function of the probability density function (pdf) of the turbulent velocity. The assumption made here is that the variance for this pdf is equal to a parameter called the turbulent Mach number,  $M_t$ . The turbulent Mach number is defined as  $M_t = \frac{\sqrt{2k}}{c}$ , where  $k$  is the kinetic energy of the turbulent fluctuations and  $c$  is the speed of sound. This Mach number is indicative of the effectiveness of turbulent fluctuations in propagation of information, in comparison with the acoustic transfer. The dilatational dissipation is therefore expressed as a function of  $M_t$  and the flatness or kurtosis of the velocity fluctuations. This expression is given below,

$$\varepsilon_d = c_d \varepsilon_s F\{M_t, K\} \quad (2.6)$$

where  $K$  is the kurtosis of the fluctuations in velocity and  $c_d$  is an adjustable constant of order one. The function  $F\{M_t, K\}$  is given as

$$F\{M_t, K\} = \left[ \frac{1}{M_t^4} \int_1^\infty \left( \frac{m_1^2 - 1}{m_1} \right)^3 p(m_1) dm_1 \right] \quad (2.7)$$

where  $p(m_1)$  is an assumed non-Gaussian pdf. Also  $m_1 = \frac{u}{a^*}$ , where  $u$  is the velocity fluctuation ahead of the shocklet, and  $a^*$  is the sonic speed. This expression is further simplified (for computational ease) to give

$$F(M_t) = 1 - \exp\left\{-[(M_t - 0.1)/0.6]^2\right\} \quad (2.8)$$

and

$$F(M_t) = 0, \text{ if } M_t < 0.1$$

Sarkar et al. [1991], using arguments based on the evolution of turbulence structures on an acoustic time scale, also proposed a model for this extra dissipation due to dilatational effects. This model is given as

$$\varepsilon_d = \alpha_1 \varepsilon_s M_t^2 \quad (2.9)$$

where  $\alpha_1$  is an order one constant. To a first order approximation, the two models are essentially identical. These modifications initially ignored the effect of pressure dilatation and combined it with the dilatational dissipation term.

More recently, El Baz and Launder [1993] proposed a model for the dilatational dissipation effect, which works out to be similar to the models proposed by Sarkar et al. [1991] and Zeman [1990], as will be demonstrated in Chapter 5. The El Baz and Launder [1993] modification offers to modify one of the constants in the modelled form of the transport equation for the rate of dissipation of turbulent kinetic energy. They obtain their modifications from an analysis of the rate of decay of compressible isotropic turbulence.

Based on a more thorough analysis of the evolution of the pressure dilatation correlation, Sarkar [1992], Zeman [1993] and El Baz and Launder [1993] have proposed models to account for this term. These modifications for the pressure dilatation term will be presented in Chapter 5 (where a comparative study, of the modifications that have been proposed to account for the effects of compressibility, is offered). Blaisdell et al. [1993] conducted a DNS study of both the decaying compressible turbulence and homogeneous shear driven turbulence. Their DNS studies confirm the existence of eddy shocklets but again the resolution used was not adequate enough to completely resolve these shocklets. The DNS studies indicate that the decay of compressible turbulence is very much dependent on the initial condition. This would then cast some doubt on the effectiveness of the algebraic modifications given above in modelling this decay of compressible turbulence. However, in the case of homogeneous shear turbulence, they observed that the ratio of dilatational dissipation to the solenoidal dissipation rate does vary as  $M_t^2$ . They also note that the Sarkar et al. [1991] model for the dilatational dissipation compares better with the results of DNS study than the Zeman [1990] model. Zemans' model [1993] for the pressure dilatation term compares better with DNS results. A more detailed discussion of these models is presented in Chapter 5.

## 2.2 Compressible Boundary Layers

Compressibility effects in high-speed mixing layers are quite different from those in high-speed wall-boundary layers. In wall-bounded turbulent shear layers, with increase in Mach number of the free stream there is a small decrease in the skin friction and the growth rate of the boundary layer thickness, which can be explained as a direct reflection of density variation from its free-stream value. This reduction in density results in a reduction in momentum transfer by Reynolds stresses.

If the root-mean-square fluctuations of the density are small then the effects of compressibility can be assumed to be minimal. This is a statement of Morkovins' hypothesis. This implies that for free-stream Mach numbers less than about 5.0 for boundary layers and jets at Mach numbers less than 1.5, the structure of turbulence is about the same as that of incompressible flows. Turbulence structure refers to the dimensionless properties like correlation coefficients and spectrum shapes. The skin friction coefficients and other ratios of turbulence quantities to mean quantities are greatly affected by density variations (mean density changes). The effect of mean density variations in  $x$  or  $y$  (spatial variation) on the turbulence structure is not covered by Morkovins' hypothesis but is often negligible at the lower Mach numbers, if the mean pressure gradients are small. Thus assumptions made about turbulence structure that give good results for incompressible or constant density flows may be applied, with suitable modifications, to compute flows with density variations for  $M_\infty \leq 5$  (for wall boundary layers) and  $M_{jet} \leq 1.5$ .  $M_{jet}$  is the Mach number defined based on the maximum velocity of the jet stream.

Fernholz and Finley [1980] offer a correlation of the various experimental measurements of compressible turbulent boundary layers and compare it with the theoretical curve fits. Overall it seems that for adiabatic walls, the van Driest transformation fits the experimental data fairly accurately. In compressible flows (Huang et al. 1994), the mixing length hypothesis yields,

$$\frac{dU}{dy} = \frac{1}{\kappa y} \left( \frac{\tau_w}{\rho} \right)^{1/2} \quad (2.10)$$

$$\frac{dT}{dy} = \frac{-q}{\rho C_p \left( \frac{\tau_w}{\rho} \right)^{1/2} \kappa_T y} \quad (2.11)$$

where  $U$  and  $T$  are the velocity and temperature, respectively.  $\tau_w$  is the wall shear stress and  $\rho$  is the local value of density.  $C_p$  is the specific heat of the fluid at constant pressure and  $\kappa$  and  $\kappa_T$  are constants.  $q$  is the heat transfer rate and is given as,  $q = q_w + U\tau_w$ , where  $q_w$  is the heat transfer rate at the wall.

Defining a friction velocity  $U_\tau = \sqrt{\frac{\tau_w}{\rho_w}}$ , equations 2.10 and 2.11 can be integrated to yield the velocity and temperature profiles, in the turbulent boundary layer. The velocity profile, in a compressible turbulent boundary layer, is therefore written as

$$\frac{U_c}{U_\tau} = \frac{1}{\kappa} \ln(y^+) + C \quad (2.12)$$

where  $\kappa$  is the von Karman constant,  $C$  is a constant of integration and  $y^+ = \left( \frac{\rho U_\tau y}{\mu} \right)$ , where  $\mu$  is the coefficient of molecular viscosity. In equation 2.12  $U_c$  is obtained using the transformation

$$U_c = \int_0^U \left( \frac{\rho}{\rho_w} \right) dU \quad (2.13)$$

and  $\frac{\rho}{\rho_w} = \left( \frac{T_w}{T} \right)$ . The velocity distribution in the compressible turbulent boundary layer can, therefore, be expressed in the functional form of equation 2.14.

$$\frac{U}{U_\tau} = f \left\{ \frac{U_\tau y}{\nu_w}, \frac{Q_w}{\rho_w C_p U_\tau T_w}, \frac{U_\tau}{a_w} = M_\tau \right\} \quad (2.14)$$

where  $U_\tau$  is the friction velocity,  $Q_w$  is the wall heat transfer rate,  $C_p$  is the specific heat at constant pressure and  $a$  is the speed of sound. The subscript “w” refers to the conditions at the wall. The velocity profile is written as

$$\frac{U_c}{U_\tau} = \frac{1}{R} \left[ \sin^{-1} \left\{ \frac{R \left( \frac{U}{U_\tau} + H \right)}{(C_1 + R^2 H^2)^{1/2}} \right\} - \sin^{-1} \left\{ \frac{RH}{(C_1 + R^2 H^2)^{1/2}} \right\} \right] \quad (2.15)$$

where,

$$\frac{U_c}{U_\tau} = \frac{1}{\kappa} \ln \left( \frac{U_\tau y}{v_w} \right) + C \quad (2.16)$$

$$R = M_\tau \left\{ (\gamma - 1) \frac{\kappa}{2K_\theta} \right\}^{1/2} \quad (2.17)$$

$$H = \frac{Q_w}{\tau_w U_\tau} = \frac{B_q}{(\gamma - 1) M_\tau^2} \quad (2.18)$$

where,  $\kappa = 0.41$  and  $K_\theta = 0.41$ .

However, this relation is usually replaced or fitted by

$$\frac{U_c}{U_\tau} = \frac{1}{\kappa} \ln \left( \frac{y U_\tau}{v} \right) + C + \frac{\Pi(x)}{\kappa} W \left( \frac{y}{\delta} \right) \quad (2.19)$$

where  $\Pi(x)$  represents the effect of pressure gradients in the outer layer of the boundary layer and  $W(y/\delta)$  represents the wake parameter (Sun and Childs, 1971). It should be noted that this van Driest transformation for the velocity profile in compressible turbulent boundary layers is applicable for flat plate boundary layers only, with no heat transfer at the wall.

In compressible turbulent flows, the velocity, temperature and density (and in high speed flows the pressure) all fluctuate. In analytical work (Kovasznay, 1953), it is more convenient to treat the equivalent fluctuations of vorticity, entropy (or total temperature) and acoustic pressure. In non-hypersonic boundary layers the acoustic mode is negligible and the entropy mode is very small for conventional rates of heat transfer (Bradshaw, 1977).

It follows from Morkovins' hypothesis that for  $\frac{p'}{p} \ll 1$  and  $\frac{T_o''}{T_o} \ll 1$ ,

$$\frac{\rho'}{\rho} = - \frac{T''}{T} = (\gamma - 1) M^2 \frac{u''}{U} \quad (2.20)$$

where the primes denote fluctuations with respect to a mean value, with a single prime denoting fluctuations with respect to a Reynolds averaged mean and a double prime denoting

fluctuations with respect to a Favre averaged mean. Further information regarding the Reynolds and Favre averaging techniques and the differences between them can be found in Chapter 3. A more rigorous derivation of the above equation can be found in Chapter 5.

Since the fractional velocity fluctuation  $u''/\tilde{U}$  is small,  $\rho'/\bar{\rho}$  is small as long as  $(\gamma - 1)M^2$  is not large compared with unity (which can be used as a convenient definition of non-hypersonic). Because velocity fluctuations in the outer layer of boundary layer are usually small,  $\frac{\sqrt{\overline{\rho'^2}}}{\bar{\rho}}$  is nowhere greater than 0.1 even at  $M_\infty = 5.0$ . At higher Mach numbers however, the wall is strongly cooled and Morkovins' hypothesis (assumption of constant stagnation temperature) breaks down. But because of wall cooling, the general level of static temperature or density fluctuations increases only slowly with Mach number. However,  $\frac{\sqrt{\overline{p'^2}}}{\bar{p}}$  increases and the interaction between vorticity and pressure modes (Bradshaw, 1977) may significantly alter the turbulence structure. The hypothesis also implies that the correlation between  $T''$  and  $u''$  is close to  $-1$ . In free mixing layers, where  $\frac{\sqrt{\overline{u'^2}}}{\tilde{U}}$  reaches 0.3, density fluctuations are larger and limit the validity of the hypothesis.

The influences of compressibility not addressed by Morkovins' hypothesis (Bradshaw, 1977) are the effects of viscosity fluctuations and the effects of spatial gradients of mean density. A turbulent eddy is likely to be affected by transverse variations in density if the fractional change in density over its width is significant. Therefore, the larger eddies that effect the entrainment of free stream fluid may be significantly affected by  $\frac{\partial \rho}{\partial y}$  even at  $M_\infty < 5$  in a boundary layer.

While it seems that the reduction in skin friction and turbulence structure parameters in the case of high-speed boundary layers can be explained on the basis of variation in density, the same arguments cannot be used to explain the reduced mixing rates in the case

of free shear layers. A better understanding of the mixing process in the case of free shear layers might help in explaining this variation in the two shear layers.

Table 2-1. Observations on the effect of compressibility in turbulent shear layers.

	Two-stream mixing layers	Boundary layers
Effect of compressibility	Reduced mixing rates : a. Reduced growth rate, and b. Reduced levels of turbulence.	Reduced thickness a. Reduced skin friction b. Increase in extent of laminar sub layer
Key parameters	$M_c, M_t, \delta_{\omega 0} / \delta_{\omega}$	$y^+, B_q, M_\tau$
Proposed Modelling options	<div style="display: flex; align-items: center;"> <div style="flex: 1;">           i. Sarkar et al., Sarkar            ii. Zeman            iii. El Baz and Launder         </div> <div style="font-size: 3em; margin: 0 10px;">}</div> <div style="flex: 1;">           Modifications for accounting for the extra dissipation due to dilatational effects.         </div> </div>	
Effectiveness of modifications	While all three modifications are effective in predicting the reduced growth rates and levels of turbulence structure parameters, they fail to offer satisfactory predictions in the case of wall boundary layers.	

The turbulence models that have been proposed to parametrize the dissipative effect of dilatational velocity fluctuations have had limited success. While they are quite capable in predicting the reduced mixing rate in the case of free shear layers (two-stream mixing layers), they have not been very successful in predicting the reductions in the case of wall boundary layers. As mentioned before, in the case of a wall shear layers, the variations in density play a more important role than in the case of free shear layers. The proposed models are ineffective in accounting for these density variations (Huang et al, 1992). A more rigorous explanation of this deficiency will be given in Chapter 5, where the models are evaluated from the point of view of eddy-viscosity based turbulence models.

### 2.3 Summary

Table 2–1 summarizes the observations on the effect of compressibility on turbulent shear layers. The above review, while not an exhaustive one, does provide a picture of the effect of compressibility on the turbulence fluctuations. Certain key parameters that can be used to characterize and to parametrize the effect of compressibility on the structure of the turbulent fluctuations have been identified. The review above has been limited to just free shear layers and wall boundary layers. In addition, there are instances where the effects of a rapid expansion or an isotropic compression on the turbulent fluctuations need to be addressed. These issues are explored in Chapter 6, where the effectiveness of the various models have been analyzed in terms of their predictive capabilities. Particularly, Chapter 6 discusses the reasons for the ineffectiveness of the various modifications that have been proposed to model the effect of compressibility in predicting a wider variety of flowfields.



## CHAPTER 3

### EDDY-VISCOSITY MODELS

In this chapter the equations of motion that govern the flowfield for compressible turbulent flows are presented. The issues of scale disparity and the closure of the mean equations are discussed. The modelling approximations that will be needed to address the closure issues for computing the mean flow are discussed, along with a discussion of the advantages and drawbacks of the various approaches. Attention is restricted to the models employing the eddy-viscosity concept.

#### 3.1 Governing Equations

The governing equations are those expressing the conservation of mass, the rate of change of momentum (in the three spatial directions) and the conservation of energy. These equations along with the equation of state are solved. The equations in their conservative form are given, in tensor notation, as

##### **Continuity**

$$\frac{\partial \rho}{\partial t} + \frac{\partial}{\partial X_i}(\rho U_i) = 0 \quad (3.1)$$

##### **Momentum**

$$\frac{\partial(\rho U_i)}{\partial t} + \frac{\partial(\rho U_i U_j)}{\partial X_j} = -\frac{\partial p}{\partial X_i} + \frac{\partial \sigma_{ij}}{\partial X_j} \quad (3.2)$$

##### **Energy**

$$\frac{\partial(\rho E)}{\partial t} + \frac{\partial(\rho U_j H)}{\partial X_j} = \frac{\partial}{\partial X_j}(U_i \sigma_{ij} - q_j) \quad (3.3)$$

### Equation of State

$$p = \rho RT \quad (3.4)$$

where repeated indices indicate summation.

In the above system of equations,  $\rho$ ,  $U_i$ ,  $p$ ,  $T$ ,  $E$  and  $H$  are the density, the velocity components, the pressure, the temperature, the total energy and the total enthalpy, respectively.  $\sigma_{ij}$  and  $q_j$  are the viscous stresses and the heat flux. The stress tensor is written as

$$\sigma_{ij} = 2\mu S_{ij} + \lambda U_{k,k} \quad (3.5)$$

where

$$S_{ij} = \frac{1}{2}(U_{i,j} + U_{j,i}) \quad ; \text{ and } \lambda = -\frac{2}{3}\mu \quad (3.6)$$

where  $U_{i,j} = \frac{\partial U_i}{\partial X_j}$ ,  $\mu$  is the molecular viscosity and  $\lambda$  is the bulk viscosity. The heat flux vector  $q_j$  is written as

$$q_j = -k \frac{\partial T}{\partial X_j} \quad \text{where } k \text{ is the thermal diffusivity.} \quad (3.7)$$

The total energy  $E$  and the total enthalpy  $H$  are written as

$$E = \frac{P}{\gamma - 1} + \frac{1}{2}\rho(u^2 + v^2) \quad (3.8)$$

$$H = E + \frac{P}{\rho} \quad (3.9)$$

where  $\gamma$  is the ratio of specific heats. In all the computations presented in this dissertation the gas is assumed to be air and the  $\gamma$  is given the value of 1.4.

### 3.2 Turbulence Closure

Turbulence is a stochastic process, characterized by eddies of varying length and time scales. The scales range from the large, energy containing eddies (slow time scale) to the small, dissipative eddies (faster time scale). While the large eddies can be of sizes comparable to the extent of the viscous layer, the small eddies are of sizes where molecular viscosity effects become important. This small scale is usually referred to as the Kolmogorov

scale. A complete description of the wide range of length and time scales in turbulent flows is given in Tennekes and Lumley [1972]. The length scales (or time scales) of the large eddies and the small Kolmogorov eddies can be related based on the Reynolds number of the flow. This relationship is given as

$$\frac{\eta}{l} = \text{Re}^{-3/4} \quad \text{where} \quad \text{Re} = \frac{ul}{\nu} \quad (3.10)$$

where  $l$  is the length scale of the large eddies and  $\eta$  represents the length scale of the Kolmogorov eddies. It is to be noted that the equation 3.10 is strictly valid only when the Reynolds number is very large. The reason is that the estimate or relationship dictated by equation 3.10 is valid only when there is a distinct inertial sub-range.

In the above system of equations, all variables are in their instantaneous form. In order to completely resolve the turbulent flowfield, the spatial resolution of the computational grid has to be of the size of the small-scale or Kolmogorov eddies. Since the spatial resolution required to adequately resolve the smallest eddies as well as the energy containing ones scales as the Reynolds number (as indicated by equation 3.10), this implies an extremely large number of grid points, especially in the case of three-dimensional computations. The current restrictions on computing power and storage do not permit us to solve, the governing equations in their exact form, for complex turbulent flows. To solve the instantaneous form of the governing equations using the direct numerical simulation (DNS) approach, inhibitions due to computing power and storage restrict the flow problems to those involving simple geometries and relatively low Reynolds and Mach numbers. In order to overcome this, use is made of some form of statistical averaging thereby permitting us to solve for the “mean flow” parameters, giving us an idea about the average variation of the flow field.

### 3.2.1 Averaging Techniques

There are several ways to define a statistical average (Monin and Yaglom, 1971). Two of the most commonly used methods to define the mean are the Reynolds average and the Favre average.

### 3.2.1.1 Reynolds average

The Reynolds average usually refers to a time average. For a variable  $\phi$ , the mean  $\bar{\Phi}$  is defined as

$$\bar{\Phi} = \frac{1}{T} \int_{t_0}^{t_0 + T} \phi dt \quad (3.11)$$

where  $T$  is a sufficiently large period of time such that it completely damps out the fluctuations in  $\phi$  about the mean. But this time period should not be too large that it subdues the variations in the mean. Time averaging can be used only in the case where the mean  $\bar{\Phi}$  is independent of  $t_0$ , that is for a stationary flow field. In cases where  $\bar{\Phi}$  is non-stationary, an ensemble average is resorted to. An ensemble average is defined as an average of an ensemble of measurements. To help understand the meaning of an ensemble average consider Figure 3.1. For the “non-stationary” flow the velocity is continually changing. A time average is not a meaningful representation of the average in this case. We have to account for the long-term and short-term variations separately. In these cases, the only

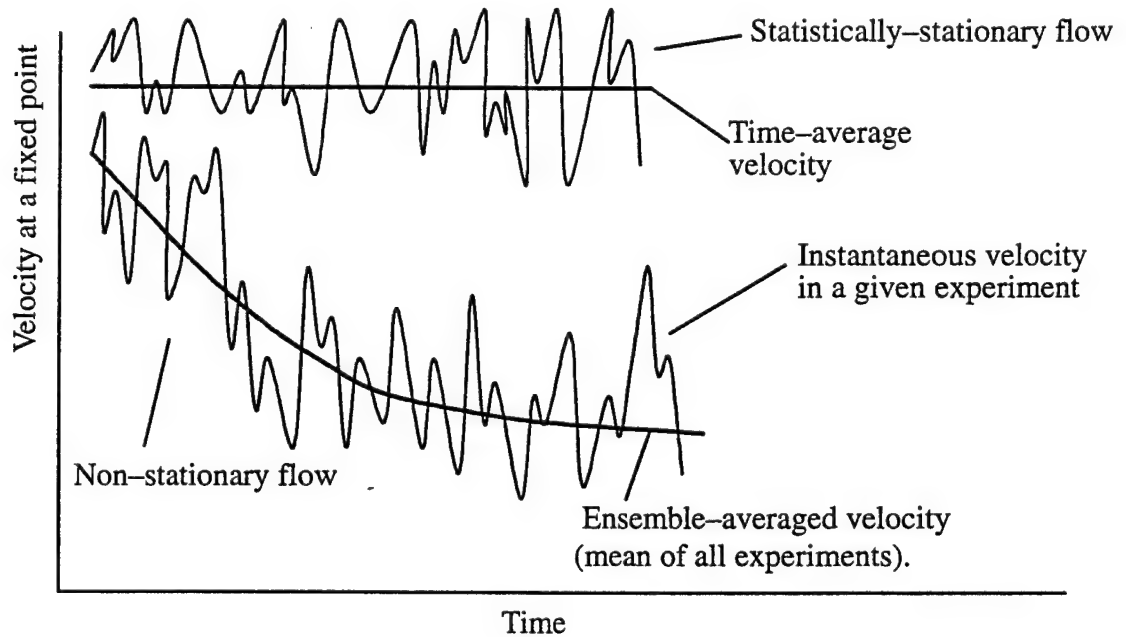


Figure 3.1. Definition of time-average and ensemble-average.

possible way to define an average would be to repeat the experiment many times, each time taking the measurement at a specific point and at a specific instant from the start of the experiment. An ensemble average would then refer to the average of all these measurements.

Throughout the remainder of this dissertation, the Reynolds average is denoted with an overbar and the fluctuations with respect to this mean by a single prime. That is,

$$\phi = \bar{\phi} + \phi' \quad (3.12)$$

where by definition,  $\bar{\phi'} = 0$ .

### 3.2.1.2 Favre average

Favre average (though first suggested by Reynolds, 1895), is a mass weighted average. The variable  $\phi$  is split into its mean and fluctuation components as

$$\phi = \tilde{\phi} + \phi'' \quad (3.13)$$

where

$$\tilde{\phi} = \frac{\overline{\rho\phi}}{\bar{\rho}} \quad (3.14)$$

and

$$\overline{\phi''} = -\frac{\overline{\rho'\phi'}}{\bar{\rho}} \quad \text{and} \quad \overline{\rho\phi''} = 0 \quad (3.15)$$

where the statement  $\overline{\rho\phi''} = 0$  implies that, when  $\phi$  represents the velocity components, there is no mass flux across the mean streamlines.

In calculating compressible turbulent flows, the Favre average is usually preferred. If the mean of the flow variables are defined using a Reynolds average, then in the case of compressible flows one ends up with terms representing the correlations involving fluctuations in density. The magnitude of these terms are not negligible and so cannot be ignored in the computations and need to be suitably modelled. Due to the lack of clear understanding of the nature of these terms, currently there are no adequate models to account for such terms. On the other hand if use is made of the Favre average, the resulting equations bear a close resemblance to the incompressible constant density equations. This enables us to model the various correlations in compressible turbulent flows using the incompressible

form of the turbulence models as a baseline. In most computational studies of compressible turbulent flows use is made of a mixed averaging technique. That is, the mean of the velocity components and temperature is defined using a Favre average and the mean density and pressure are defined using a Reynolds average.

### 3.2.1.3 Relationship between Reynolds and Favre averages

If Favre averaging is used to define the mean velocity components, then in the momentum equation (for the viscous stresses) both Favre averaged values and Reynolds averaged values appear naturally. The relationship between the definitions based on these two averaging techniques is exploited to simplify the equations. These relationships can be easily derived. For a variable  $\phi$ , we denote the Reynolds average by  $\bar{\phi}$  and the fluctuations with respect to this mean by  $\phi'$ . The Favre average is denoted by  $\tilde{\phi}$  and the fluctuations with respect to this mean by  $\phi''$ . Now based on the definitions,

$$\left. \begin{aligned} \phi &= \bar{\phi} + \phi' \\ \phi &= \tilde{\phi} + \phi'' \end{aligned} \right\} \quad (3.16)$$

Based on the rules of averaging (defined in Monin and Yaglom, 1971) we have  $\overline{\tilde{\phi}} = \tilde{\phi}$ . Therefore, from equation 3.16 we have

$$\overline{\phi''} = \bar{\phi} - \tilde{\phi} = - \frac{\overline{\rho' \phi'}}{\bar{\rho}} \quad (3.17)$$

Combining equations 3.16 and 3.17 we get

$$\phi'' = \overline{\phi''} + \phi' \quad (3.18)$$

Other relationships between mass weighted Favre averages and Reynolds averages can be found in Lele [1993]. In most numerical modelling techniques, these relationships (equation 3.17) between the Reynolds and Favre averaged values are ignored. That is,  $\overline{\phi''}$  is considered to be a negligible quantity. When  $\phi$  represents the components of velocity, this term  $\overline{\phi''}$  is referred to as the turbulent mass flux. In Chapter 5 an expression for this turbulent mass flux is derived.

### 3.2.2 Equations of Motion: Averaged Form

Through the rest of this dissertation, a mixed averaging technique is used. Using a Favre averaging technique to define the mean of the velocity components and temperature and a Reynolds averaging technique to define the mean of density and pressure, the equations governing the mean flow field can be written as given below. The split up of the variables into a mean and corresponding fluctuation is given by equation 3.19.

$$\begin{aligned}\rho &= \bar{\rho} + \rho' \\ u_i &= \tilde{U}_i + u_i'' \\ T &= \tilde{T} + T'' \\ p &= P + p'\end{aligned}\tag{3.19}$$

where, the overbar denotes a Reynolds averaged quantity and the prime denotes a fluctuation with respect to the Reynolds average. The tilde denotes a Favre averaged quantity and the double prime denotes a fluctuation with respect to the Favre average.  $P$  refers to the Reynolds averaged pressure. In terms of these mean and fluctuations, the governing equations are written as

#### Continuity

$$\frac{\partial}{\partial t}(\bar{\rho}) + \frac{\partial}{\partial X_i}(\bar{\rho}\tilde{U}_i) = 0\tag{3.20}$$

#### Momentum

$$\frac{\partial}{\partial t}(\bar{\rho}\tilde{U}_j) + \frac{\partial}{\partial X_j}(\bar{\rho}\tilde{U}_i\tilde{U}_j) = -\frac{\partial P}{\partial X_i} + \frac{\partial}{\partial X_j}\left[\underbrace{\Sigma_{ij}}_A + \underbrace{\overline{\sigma_{ij}''}}_B - \underbrace{\overline{\rho u_i'' u_j''}}_B\right]\tag{3.21}$$

#### Energy

$$\frac{\partial}{\partial t}(\bar{\rho}\tilde{E}) + \frac{\partial}{\partial X_j}(\bar{\rho}\tilde{u}_j\tilde{H}) = \frac{\partial}{\partial X_j}\left[\tilde{U}_j\left(\underbrace{\Sigma_{ij}}_C + \underbrace{\overline{\sigma_{ij}''}}_D - \underbrace{\overline{\rho u_i'' u_j''}}_D\right) + \underbrace{\overline{u_i'' \Sigma_{ij}}}_E + \underbrace{\overline{u_i'' \sigma_{ij}''}}_F - \bar{q}_j\right] \\ - \underbrace{\overline{q_j''}}_G - \underbrace{\overline{\rho u_j'' h''}}_H - \underbrace{\overline{\rho u_j'' \left(\frac{1}{2} u_i'' u_i''\right)}}_I\right]\tag{3.22}$$

where

$$\Sigma_{ij} = 2\mu S_{ij} + \lambda \tilde{U}_{k,k} \delta_{ij} ; S_{ij} = \frac{1}{2} (\tilde{U}_{i,j} + \tilde{U}_{j,i}) \quad (3.23)$$

$$\overline{\sigma_{ij}''} = 2\mu s_{ij} + \lambda \overline{u_{k,k}''} \delta_{ij} ; s_{ij} = \frac{1}{2} (\overline{u_{i,j}''} + \overline{u_{j,i}''}) \quad (3.24)$$

Through the rest of this dissertation, we will drop the *tilde* and the *overbar*. Upper case letters will be used to denote the mean quantities. Mean density will be denoted by  $\rho$ .

Before we can solve the equations of motion to obtain the mean flow field, we need to account for the various correlations (between the fluctuations). The terms that need to be modelled in the above equations are denoted as terms A through I. In most flow fields there are regions where molecular properties are more important (Rubesin, 1990). So, we can drop terms A, C, E and G. We still need to model the correlations denoted by terms B, D, F, H and I. Except for term I, which is a third order correlation, the other terms are second order correlations.

One of the ways to model these correlations is to write transport equations governing their variations. The transport equations for the second-order correlations, for example, will involve third- and higher-order moments. To account for these higher-order moments, one can derive transport equations. But these in turn will involve fourth- and higher-order moments. It is impossible to close the system of equations, (when expressing them in their mean form). This is the classical closure problem of turbulence. A detailed review of the closure problem is given in Tennekes and Lumley [1972].

There are several methods that can be employed to solve these averaged equations of motion. Large eddy simulations (LES), which occupy the rung below DNS in the ladder of turbulent flow simulations, is one such method. For high enough Reynolds numbers the small-scale eddies can be thought of as being isotropic. That is, turbulent fluctuations at these length scales are identical in the three spatial directions and invariant with respect to reflection (of the co-ordinate system). Thus, using simple models these isotropic fluctuations can be adequately modelled. In methods using LES techniques, a spatial cut-off is used to delineate the length scales that are completely resolved and those that are modelled. Eddies



whose characteristic length-scales are above this cut-off length are completely resolved while those below this spatial cut-off are modelled. These smaller eddies are usually of the order of the Kolmogorov scales. But LES has not yet developed to a level where routine calculations can be made of complex flow fields.

Another method is to model third- and higher-order moments of the correlations and solve the transport equations for the second order moments. This form of modelling is referred to as the second-order closure. A simplified form of this is the eddy-viscosity based modelling. In all the computations presented here, the eddy-viscosity based closure approximations are used. A brief description of this closure method is given here.

### 3.3 Eddy-Viscosity Based Modelling

In the above system of equations, terms such as the Reynolds stresses  $-\overline{\rho u_i'' u_j''}$ , need to be modelled to solve the system of equations for the mean flow parameters. Boussinesq (Speziale, 1992), first introduced the concept of modelling the Reynolds stresses based on the idea of a turbulent viscosity to close the system of equations (incompressible form). However, it was Prandtl (Launder and Spalding, 1972) who introduced the concept of a mixing length to compute the eddy-viscosity. The mixing length model makes a direct analogy between the transport due to turbulent fluctuations and the molecular transport. With further research it was realized that this concept was flawed, because turbulence does not have a clear demarcation of length (or time) scales. With this realization Prandtl proposed to solve a transport equation for the turbulent kinetic energy (to obtain a characteristic scale of turbulence) and use a specified length scale to compute the eddy-viscosity. Models (wherein a transport equation is solved to obtain a characteristic scale of turbulence) such as these are usually referred to as one-equation models to distinguish from the original mixing length model (referred to as the zero-equation model). A brief description of these models is given below.

### 3.3.1 Zero- and One-Equation Models

The simplest form of the eddy-viscosity based model for the Reynolds stresses is the zero-equation model. It is termed zero-equation because no extra transport equation need be solved in computing the characteristic scales of the turbulent fluctuations. The zero-equation model is originally due to Prandtl, where an analogy is drawn between the transport due to turbulent fluctuations and molecular transport. It was derived from a consideration of the flowfield in a turbulent boundary layer.

In this method, one relates the eddy-viscosity to the local mean velocity gradients by means of a mixing length,  $l_m$

$$\nu_t = l_m^2 \left| \frac{\partial U}{\partial y} \right| \quad (3.25)$$

where  $\nu_t$  is the kinematic eddy-viscosity and it has been assumed that  $y$  is a direction normal to the streamwise development of the shear layer.  $U$  is the streamwise velocity component.

One problem with mixing-length models is that they cannot model history and transport effects in a flow. Another drawback is that the length scale used is not universal and can vary from one flowfield to another and even within a given flowfield. The mixing lengths that have been estimated for predicting a particular flow most often simple boundary layers, are not strictly applicable to other flows. Furthermore, it becomes difficult to generate the mixing lengths for complex geometries.

To alleviate some of these problems one-equation models were developed. These use a transport equation for determining one of the characteristic scales of turbulence. Usually, this is the turbulent kinetic energy (TKE). By introducing such a transport equation, history and transport effects are introduced into the flow calculation. The typical modelled form of the kinetic energy is given as

$$\frac{\partial \rho k}{\partial t} + \frac{\partial}{\partial x_j} (\rho U_j k) = - \overline{\rho u_i'' u_j''} \frac{\partial U_i}{\partial x_j} - \rho \epsilon + \frac{\partial}{\partial x_i} \left[ \left( \mu_L + \frac{\mu_t}{\sigma_k} \right) \frac{\partial k}{\partial x_i} \right] \quad (3.26)$$

where  $\mu_t / \sigma_k$  is introduced to model the turbulent transport, and the pressure diffusion terms. To compute the turbulent kinetic energy dissipation rate,  $\varepsilon$ , one-equation models use a length scale model of the form

$$\varepsilon = C_D \left( \frac{k^{3/2}}{L} \right) \quad (3.27)$$

The eddy-viscosity is computed using the expression

$$\mu_t = C_{\mu} \rho \frac{\sqrt{k}}{L} \quad (3.28)$$

The length scale  $L$ , in one equation models has the same drawbacks and difficulties as the length scale  $l_m$ , in the algebraic mixing-length models. Consequently, one-equation models never became generally popular since they required considerably more computer time than the simpler zero-equation models, but did not produce significantly better results. Both zero- and one-equation models of eddy-viscosity are considered to be incomplete because they involve an arbitrary specification of one of the scales used to obtain the “turbulent-viscosity”. This led to the development of two-equation models where use is made of a transport equation for the length-scale also.

### 3.4 k- $\varepsilon$ Model

Two-equation models are considered to be the first complete model for obtaining the eddy viscosity. Rotta [1951], developed the first complete method to obtain turbulence closure. In order to compute the Reynolds stresses  $-\overline{\rho u_i'' u_j''}$ , Rotta [1951] developed the transport equations for the six components of the Reynolds stresses and their rate of dissipation. A contraction of the equations for the Reynolds stresses coupled with an eddy-viscosity hypothesis gave rise to the k- $\varepsilon$  models. A similar form of the k- $\varepsilon$  model was first obtained by Hanjalic and Launder [1976]. In these models,  $k$  represents the kinetic energy of the turbulent fluctuations  $k = \frac{1}{2} \overline{u_i'' u_i''}$  and  $\varepsilon$  represents the rate of dissipation of this kinetic energy. Using the velocity scale obtained from solving the transport equation for

$k$  and a time scale obtained from a combination of  $k$  and the solution to the transport equation for  $\epsilon$ , an expression for the turbulent-viscosity is obtained.

In the  $k$ - $\epsilon$  based models, the characteristic velocity scale is calculated as the square root of the TKE and the time scale is calculated using a combination of TKE and the rate of dissipation of TKE.

Now, defining  $k$  and  $\epsilon$  as in equation (3.29), one can derive transport equations for  $k$  and  $\epsilon$ .

$$k = \frac{1}{2} \overline{u_i'' u_i''} \quad \text{and} \quad \epsilon = \nu \overline{\frac{\partial u_i''}{\partial x_j} \frac{\partial u_i''}{\partial x_j}} \quad (3.29)$$

Thus the eddy-viscosity or turbulent-viscosity is defined as

$$\nu_t = C_\mu \frac{k^2}{\epsilon} \quad (3.30)$$

where  $C_\mu$  is a constant whose value is prescribed based on empirical observations as 0.09, and  $\nu_t$  is the eddy-viscosity.

Using this definition of eddy-viscosity the Reynolds stresses are written as

$$-\overline{\rho u_i'' u_j''} = 2\mu_t S_{ij} + \lambda_t \bar{U}_{k,k} \delta_{ij} - \frac{2}{3} \bar{\rho} k \delta_{ij} \quad (3.31)$$

where  $S_{ij} = \frac{1}{2} (\bar{U}_{i,j} + \bar{U}_{j,i})$  and  $\mu_t = \rho \nu_t$ ;  $\lambda_t = -\frac{2}{3} \mu_t$  and  $\delta_{ij}$  is the Kronecker delta.

Although this definition of eddy-viscosity and the closure of the Reynolds stress terms was obtained initially using dimensional analysis and order of magnitude arguments, rigorous methods have been developed recently to ratify\* (and modify), this formulation of the  $k$ - $\epsilon$  model. In the next few paragraphs a brief description is given of the transport equations for  $k$  and  $\epsilon$  and the modelling approximations that have been used to close these equations.

Multiplying the equation describing the rate of change of mean momentum, (equation 3.21), by  $U_i$  one can obtaining a transport equation for the rate of change of mean kinetic

\*Shih and Lumley [1993] present a continuum mechanics based procedure to ratify the form of the model used to approximate the Reynolds stresses. Speziale [1992] gives a Taylors series method to develop the model given by equation 3.31.

energy. If we replace the variables, by a mean and a fluctuating component in equation (3.2), and subtract from it the equation for the rate of change of mean momentum an equation describing the rate of change of fluctuating momentum can be obtained. Multiplying this equation by  $u_i''$  and averaging and subtracting the equation for mean kinetic energy (multiplied by  $u_i''$ ), one can obtain the equation for the rate of change of turbulent kinetic energy (TKE). This equation (in its Favre averaged form), is given below as :

### Turbulent Kinetic Energy

$$\frac{\partial}{\partial t}(\bar{\rho}k) + \frac{\partial}{\partial x_j}(\bar{\rho}\tilde{U}_j k) = P_k + \Pi - \bar{\rho}\epsilon + T_{jj} + \overline{u_i''} \frac{\partial}{\partial x_j} \Sigma_{ij} \quad (3.32)$$

where

$$P_k = - \overline{\rho u_i'' u_j''} \frac{\partial \tilde{U}_i}{\partial x_j} - \overline{u_i''} \frac{\partial P}{\partial x_i} \quad (3.33)$$

$$\Pi = \overline{p' \frac{\partial u_i''}{\partial x_i}} ; \bar{\rho}\epsilon = \overline{\frac{\partial u_i''}{\partial x_j} \sigma_{ij}''} \quad (3.34)$$

$$T_{jj} = \frac{\partial}{\partial x_j} \left[ \overline{u_i'' \sigma_{ij}''} - \overline{\rho u_j'' \left( \frac{1}{2} u_i'' u_i'' \right)} - \overline{p' u_j''} \right] \quad (3.35)$$

In the equation above the term  $P_k$  represents the production of kinetic energy due to the interaction of the turbulent field with the mean flow field. While the first term on the right hand side of equation 3.33 represents the production of TKE due to interaction with the mean velocity field, the second term represents the production of TKE due to interaction with the mean energy field\*. The term  $\Pi$  represents work done due to simultaneous fluctuations in pressure and dilatation (or volume of the fluid cell). It can be either positive or negative. The term  $T_{jj}$  represents the transport of TKE due to both molecular transport (first term in parenthesis in equation 3.35) and due to turbulent fluctuations. The last term on the right

\* As was mentioned before, the turbulent mass flux is considered to be negligible. Consequently, this production term, (enthalpic production), is usually ignored in most computational studies of compressible turbulent flows. We have derived an expression for the turbulent mass flux, (Chapter 5), and have thus been able to include the effect of this term in the evolution of the turbulent kinetic energy.

hand side of equation 3.32 represents an inertial effect. Fluid particles with lower inertia will respond much quicker to an imposed strain rather than those with larger inertia.

### Rate of Dissipation of TKE

The rate of dissipation of TKE can be defined using the enstrophy budget. The enstrophy of the turbulent fluctuations is defined as  $\frac{1}{2} \overline{\omega_p'' \omega_p''}$  with  $\varepsilon = \overline{v \omega_p'' \omega_p''}$ , where  $\omega_p''$  is the fluctuation in vorticity. The transport equation for the enstrophy budget is written as

$$\frac{\partial}{\partial t}(\rho \varepsilon) + \frac{\partial}{\partial x_k}(\rho U_k \varepsilon) = P_\varepsilon + D_\varepsilon + \Phi_\varepsilon - \nu \nabla^2 \varepsilon + B_\varepsilon \quad (3.36)$$

where

$$P_\varepsilon = -2 \overline{v \omega_p'' u_k''} \frac{\partial \Omega_p}{\partial x_k} + 2 \overline{v \omega_p'' \omega_k''} \frac{\partial U_p}{\partial x_k} + 2 \nu \Omega_k \left( \overline{\omega_p'' \frac{\partial u_p''}{\partial x_k}} \right) \quad (3.37)$$

$$D_\varepsilon = - \overline{u_k'' \frac{\partial}{\partial x_k} (v \omega_p'' \omega_p'')} + 2 \overline{v \omega_p'' \omega_k'' \frac{\partial u_p''}{\partial x_k}} \quad (3.38)$$

$$\Phi_\varepsilon = -2 \nu^2 \left( \overline{\frac{\partial \omega_p''}{\partial x_k}} \right) \left( \overline{\frac{\partial \omega_p''}{\partial x_k}} \right) \quad (3.39)$$

$$B_\varepsilon = 2 \nu \frac{\varepsilon_{pqj}}{Q^2} \left\{ \overline{\frac{\partial Q}{\partial x_q} \omega_p'' \frac{\partial p'}{\partial x_i}} + \overline{\frac{\partial P}{\partial x_i} \omega_p'' \frac{\partial Q'}{\partial x_q}} + \overline{\omega_p'' \frac{\partial Q'}{\partial x_q} \frac{\partial p'}{\partial x_i}} \right\} \quad (3.40)$$

where  $\varepsilon_{pqj}$  called the alternating tensor, is skew-symmetric (it is +1 if p, q, i are in cyclic order, -1 if p, q, i are in anti-cyclic order and 0 if any two of p, q and i are equal).

In the equations above  $P_\varepsilon$  represents the “production of dissipation”,  $D_\varepsilon$  represents the “turbulent diffusion of dissipation”,  $\Phi_\varepsilon$  represents the “destruction of dissipation”.  $B_\varepsilon$  represents the baroclinic term. In  $B_\varepsilon$ , the second term represents the “production of dissipation” and the third term represents “turbulent diffusion of dissipation”. However, in most cases (even in compressible flow simulations) this term is ignored. It will be shown in Chapter 6 that this term might be important especially in cases where the gradients of

pressure and density are not along the same direction. The fourth term in equation 3.36 represents the viscous dissipation of  $\epsilon$ .

In order to solve for  $k$  and  $\epsilon$ , the transport equations 3.32 and 3.36 have to be modelled. In solving for compressible flows, the accepted practice is to model the equations similar to their incompressible form. In the case of incompressible flows, the term  $\Pi$  is equivalently zero because of the non-divergent nature of the velocity field. But in the case of compressible flows this term is non-zero and represents the work done due to simultaneous fluctuations in pressure and dilatation of the velocity fluctuations (or the volume of the fluid cell). So this term, which does not appear in the governing equations for incompressible flows, needs to be modelled in the case of compressible flows. Certain algebraic modifications have been proposed for this term and these will be discussed in Chapter 5. The term  $T_{jj}$  in equation 3.35, represents the diffusion of turbulence and is modelled similar to the modelling used for incompressible flows. Thus,

$$T_{jj} = \frac{\partial}{\partial x_j} \left[ \left( \mu_L + \frac{\mu_t}{\sigma_k} \right) \frac{\partial k}{\partial x_j} \right] \quad (3.41)$$

The term representing the enthalpic production of turbulent kinetic energy, is usually considered to be small and is neglected. So is the term  $\overline{u_i''} \frac{\partial \Sigma_{ij}}{\partial x_j}$ , which represents the “inertial effect”.

The equation for the rate of dissipation of TKE is quite complicated even in the case of incompressible flows. The accepted practice in modelling the transport equation for  $\epsilon$  is an *ad hoc* one and is usually written as a “regular transport equation”, that is, the time rate of change of the transported quantity is equal to the rate of production of that quantity minus the rate at which it is dissipated and diffused away. Thus, this model for  $\epsilon$  leads to a transport equation which is given as

$$\frac{\partial(\rho\epsilon)}{\partial t} + \frac{\partial}{\partial x_j} (\rho U_j \epsilon) = P_\epsilon - \Phi_\epsilon + T_\epsilon \quad (3.42)$$

where the three terms on the right hand side are respectively the rate of “production of dissipation”, the rate of “dissipation of dissipation” and the rate of “diffusion of dissipation”. These terms are modelled (in comparison with the  $k$  equation) based on heuristic arguments and dimensional analysis and are given as

$$P_\varepsilon = C_{\varepsilon 1} \frac{\varepsilon}{k} P_k ; \quad \Phi_\varepsilon = C_{\varepsilon 2} \rho \frac{\varepsilon}{k} \varepsilon ; \quad T_\varepsilon = \frac{\partial}{\partial x_j} \left[ \left( \mu_L + \frac{\mu_t}{\sigma_\varepsilon} \right) \frac{\partial \varepsilon}{\partial x_j} \right] \quad (3.43)$$

The modelling constants are obtained based on empirical information from flat plate boundary layers and the rate of decay of grid turbulence. The values for the constants in incompressible flows are prescribed as  $C_{\varepsilon 1} = 1.43$  and  $C_{\varepsilon 2} = 1.92$ .

Thus the modelled form of the transport equations for  $k$  and  $\varepsilon$  is given as

### **Turbulent Kinetic Energy**

$$\frac{\partial(\rho k)}{\partial t} + \frac{\partial}{\partial x_j} (\rho U_j k) = - \overline{\rho u_i'' u_j''} \frac{\partial U_i}{\partial x_j} - \rho \varepsilon + \frac{\partial}{\partial x_j} \left[ \left( \mu_L + \frac{\mu_t}{\sigma_k} \right) \frac{\partial k}{\partial x_j} \right] \quad (3.44)$$

### **Rate of Dissipation of Turbulent Kinetic Energy**

$$\frac{\partial(\rho \varepsilon)}{\partial t} + \frac{\partial}{\partial x_j} (\rho U_j \varepsilon) = C_{\varepsilon 1} \frac{\varepsilon}{k} \left[ - \overline{\rho u_i'' u_j''} \frac{\partial U_i}{\partial x_j} \right] - C_{\varepsilon 2} \frac{\rho \varepsilon^2}{k} + \frac{\partial}{\partial x_j} \left[ \left( \mu_L + \frac{\mu_t}{\sigma_\varepsilon} \right) \frac{\partial \varepsilon}{\partial x_j} \right] \quad (3.45)$$

The modelling constants  $C_\mu$ ,  $C_{\varepsilon 1}$  and  $C_{\varepsilon 2}$  are obtained by comparing the predictions made by the model for some simple flow scenarios. For the decay of isotropic incompressible turbulence, the experimentally observed value for the rate of decay is 1.1. In this case, the equations for the transport of TKE and its dissipation rate simplify to,

$$\left. \begin{aligned} \frac{dk}{dt} &= - \varepsilon \\ \frac{d\varepsilon}{dt} &= - C_{\varepsilon 2} \frac{\varepsilon^2}{k} \end{aligned} \right\} \quad (3.46)$$

These equations can be solved analytically and the decay of TKE with time is obtained as

$$k = t^{-1/(C_{\varepsilon 2}-1)} \quad (3.47)$$

Since we know from experimental observations that the decay rate of TKE is 1.1, we fix  $C_{\varepsilon 2}$  to be 1.92 in order to obtain this decay rate.



In the case of turbulent boundary layers (incompressible) it is known that the turbulence structure parameter,  $-\overline{u'v'}/k$ , is equal to 0.3 in the log region of the boundary layer. We therefore, set  $C_\mu = 0.09$  to match this result.

In the case of incompressible flows, the velocity in the log region is expressed using the "law of the wall" and is written as

$$\frac{U}{U_\tau} = \frac{1}{\kappa} \ln \left( \frac{\rho U_\tau y}{\mu_L} \right) + 5.1 \quad (3.48)$$

where  $U_\tau$  is the friction velocity,  $U_\tau = \sqrt{\frac{\tau_{\text{wall}}}{\rho_{\text{wall}}}}$  and  $\kappa$  is the von Karman constant and is equal to 0.41. The constant  $C_{\epsilon 1}$  is obtained based on an argument that in homogeneous shear flows, the rate of production of TKE should be equal to the rate of dissipation of TKE. Based on this assumption of equilibrium between the rates of production and dissipation of turbulent kinetic energy, it can be shown that the turbulence modelling constants  $C_\mu$ ,  $C_{\epsilon 1}$  and  $C_{\epsilon 2}$  should satisfy a relation such as

$$\kappa^2 = (C_{\epsilon 2} - C_{\epsilon 1}) \sqrt{C_\mu} \sigma_\epsilon \quad (3.49)$$

In order to satisfy this relation the modelling constant  $\sigma_\epsilon$  is fit to be equal to 1.3.

With the  $k$ - $\epsilon$  model for the eddy-viscosity the various correlations that needed to be modelled in equations 3.21 and 3.22 can now be approximated as given below :

$$\left. \begin{array}{ll} \text{Term B} & -\overline{\rho u_i'' u_j''} = 2\mu_t S_{ij} + \lambda_t U_{k,k} \delta_{ij} - \frac{2}{3} \rho k \delta_{ij} \\ \text{Terms F \& I} & \overline{u_i'' \sigma_{ij}''} - \overline{\rho u_j'' \left( \frac{1}{2} u_i'' u_i'' \right)} = \frac{\mu_t}{\sigma_k} \frac{\partial k}{\partial x_j} \\ \text{Term H} & -\overline{\rho u_j'' h''} = \frac{\mu_t}{Pr_t} \frac{\partial \tilde{T}}{\partial x_j} \end{array} \right\} \quad (3.50)$$

Based on these modelling approximations, the equations of motion in their averaged form are written as

### Continuity

$$\frac{\partial \rho}{\partial t} + \frac{\partial}{\partial x_j} (\rho U_j) = 0 \quad (3.51)$$

### Momentum

$$\frac{\partial}{\partial t} (\rho U_i) + \frac{\partial}{\partial x_j} (\rho U_i U_j) = - \frac{\partial P}{\partial x_i} + \frac{\partial}{\partial x_j} \Sigma_{ij}^{\text{eff}} \quad (3.52)$$

### Energy

$$\frac{\partial}{\partial t} (\rho E) + \frac{\partial}{\partial x_j} (\rho U_j E) = \frac{\partial}{\partial x_j} \left( U_i \Sigma_{ij}^{\text{eff}} - q_j^{\text{eff}} + \Gamma_k \frac{\partial k}{\partial x_j} \right) \quad (3.53)$$

### Turbulent Kinetic Energy (TKE)

$$\frac{\partial}{\partial t} (\rho k) + \frac{\partial}{\partial x_j} (\rho U_j k) = P_k - \rho \epsilon + \frac{\partial}{\partial x_j} \left[ \Gamma_k \frac{\partial k}{\partial x_j} \right] \quad (3.54)$$

### Rate of Dissipation of TKE

$$\frac{\partial}{\partial t} (\rho \epsilon) + \frac{\partial}{\partial x_j} (\rho U_j \epsilon) = C_{\epsilon 1} \frac{\epsilon}{k} P_k - C_{\epsilon 2} \frac{\rho \epsilon^2}{k} + \frac{\partial}{\partial x_j} \left[ \Gamma_\epsilon \frac{\partial \epsilon}{\partial x_j} \right] \quad (3.55)$$

where

$$\Sigma_{ij}^{\text{eff}} = 2\mu_{\text{eff}} S_{ij} + \lambda_{\text{eff}} U_{k,k} \delta_{ij} - \frac{2}{3} \rho k \delta_{ij} \quad ; \quad S_{ij} = \frac{1}{2} (U_{i,j} + U_{j,i}) \quad (3.56)$$

where  $\mu_{\text{eff}} = \mu_L + \mu_t$  and  $\lambda_{\text{eff}} = -\frac{2}{3} \mu_{\text{eff}}$  and  $\delta_{ij}$  is the Kronecker delta.  $q_j^{\text{eff}}$  is given as

$$q_j^{\text{eff}} = (K_L + K_t) \frac{\partial T}{\partial x_j} = \frac{\gamma}{\gamma - 1} \left[ \frac{\mu_L}{Pr_L} + \frac{\mu_t}{Pr_t} \right] \frac{\partial T}{\partial x_j} \quad (3.57)$$

where the subscript L denotes the molecular or “laminar” values and subscript “t” denotes the “turbulent” values.  $\mu$  denotes the coefficient of viscosity,  $K$  denotes the thermal diffusivity and  $Pr$  the Prandtl number. In most computations  $Pr_L$  and  $Pr_t$  are assumed as constants and given the values 1.0 and 0.9 respectively.

Also in the above equations

$$P_k = - \overline{\rho u_i'' u_j''} \frac{\partial U_i}{\partial x_j} \quad (3.58)$$

$$\Gamma_k = \mu_L + \frac{\mu_t}{\sigma_k} \quad ; \quad \Gamma_\epsilon = \mu_L + \frac{\mu_t}{\sigma_\epsilon} \quad (3.59)$$

where  $\sigma_k$  and  $\sigma_\epsilon$  are assumed to be constants, whose values are prescribed to be 1.0 and 1.3, respectively. The turbulent-viscosity  $\mu_t$  is given as

$$\mu_t = C_\mu \rho \frac{k^2}{\epsilon} \quad (3.60)$$

The constants in the equation for the rate of dissipation of TKE and the definition of eddy-viscosity are given as

$$C_\mu = 0.09 \quad , \quad C_{\epsilon 1} = 1.43 \quad \text{and} \quad C_{\epsilon 2} = 1.92 \quad (3.61)$$

The k- $\epsilon$  based modelling described above is essentially the incompressible form. This is the form usually adopted to solve for compressible flows. In Chapter 5 we will return to the governing equations to investigate the problems with this modelling approach and also discuss the proposals that have been made to account for these problems.

#### 3.4.1 Wall-Function Treatment

The k- $\epsilon$  model that has been discussed above is based on the assumption that the relevant Reynolds number is very high. Thus, the form of the model given by equations 3.44 and 3.45 is strictly not valid in regions where the characteristic Reynolds number is low. One such region is that close to a wall boundary. In a turbulent boundary layer, close to the wall, there exists a thin region where the molecular effects dominate over the turbulence effects, the viscous sub-layer. Here, the turbulent fluctuations are damped out and the high Reynolds number form of the k and  $\epsilon$  equations are no longer valid. But in computational studies suitable boundary conditions need to be provided at the wall boundary. In order to estimate the magnitude of  $\epsilon$  at the wall boundary, two alternatives are available. These are the low-Reynolds number approach and the wall-function approach. In the low-Reynolds number approach, suitable damping functions are used to reduce the importance of turbulent diffusion. These damping functions are used to modify the modelling constants in the equation for eddy-viscosity and the transport equation for  $\epsilon$ . The modelling functions are derived based on empirical observations of flat plate boundary layers.

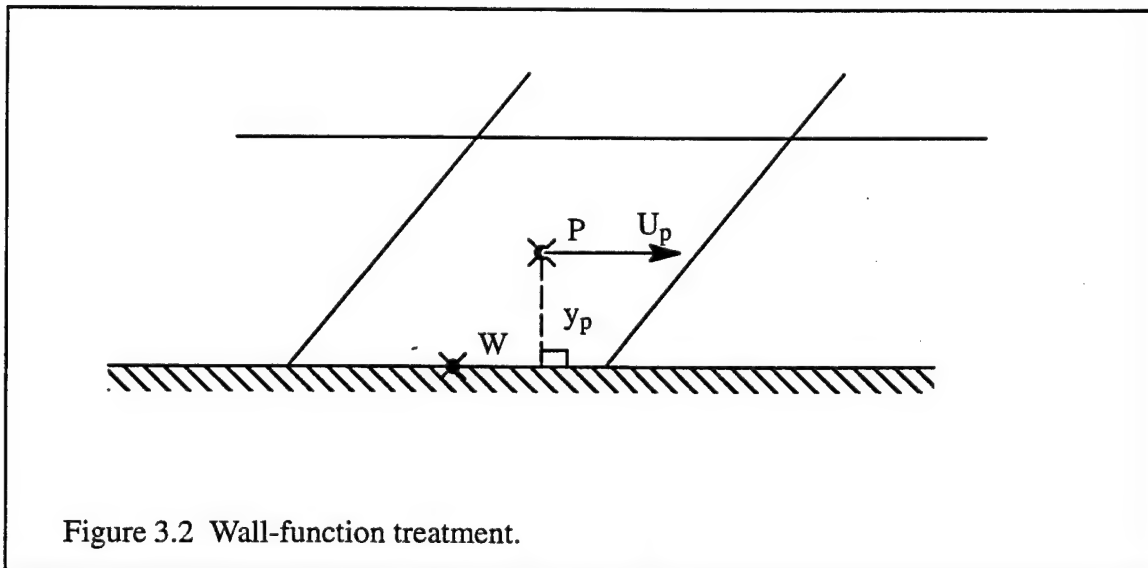
In the wall-function approach, suitable values for k,  $\epsilon$  and the wall shear stress,  $\tau_{\text{wall}}$  are prescribed. These prescriptions are also based on empirical observations of flat plate

boundary layers. The values prescribed in this approach are used at the first grid location in the computational domain and serve as boundary conditions for computing the flow field. Both the wall-function approach and the low-Reynolds number approach have their merits and demerits. There have been several proposals made to prescribe accurate damping functions for the  $k$ - $\epsilon$  model. An extensive review of some of these modifications can be found in Patel et al. [1985]. In this dissertation the simpler wall-function treatment has been used. A brief description of this technique is given below. More details regarding the wall-function treatment for compressible flows can be found in Viegas et al. [1985].

#### 3.4.1.1 Wall-function: low Mach number form

Consider the sketch shown in Figure 3.2. The sketch shows the first grid cell in the computational domain at a wall boundary. This is designated as point P and the node at the wall is designated as W.  $U_p$  is the velocity parallel to the wall and  $y_p$  is the perpendicular distance from the wall to the first grid point.

In the viscous sub-layer of a turbulent boundary layer the turbulent fluctuations are damped out and the molecular effects dominate. The velocity profile in this region is given as



$$U^+ = \frac{U_p}{U_\tau} = y^+ = \frac{\rho U_\tau y_p}{\mu_L} \quad (3.62)$$

where  $U_p$  is the velocity component parallel to the wall and  $y_p$  is the perpendicular distance to the first grid point (from the wall) as shown in Figure 3.2.  $U_\tau$  is the friction velocity and is defined as  $U_\tau = \sqrt{\frac{\tau_{wall}}{\rho}}$ .

In the log-region the turbulence effects dominate over the molecular effects and the velocity profile is given by

$$U^+ = \frac{1}{\kappa} \ln\left(\frac{\rho U_\tau y_p}{\mu_L}\right) + C \quad (3.63)$$

where  $\kappa = 0.41$  and  $C = 5.1$ .

If we assume there is a critical location in the boundary layer where the linear profile (in the viscous sub-layer) meets the logarithmic profile (in the log region), then the non-dimensionalized co-ordinate at that point can be obtained from equations 3.62 and 3.63 (Sondak and Pletcher, 1995). If we denote the critical location by “c”, then we get equating the expressions for  $U^+$  given in equations 3.62 and 3.63

$$y_c^+ = \frac{1}{\kappa} \ln(y_c^+) + C \quad (3.64)$$

The critical  $y_c^+$  can be then obtained using an iterative method like the Newton iteration method. The reason for computing this critical  $y_c^+$  is so that we can define if the first grid point in the computational domain is in the viscous sub layer or in the log layer. If the non-dimensional distance from the wall to the first grid point  $y_p^+$  is less than  $y_c^+$  ( $y_p^+ < y_c^+$ ), then this location can be assumed to be in the viscous sub layer, and the values of  $k$  and  $\varepsilon$  and the wall shear stress,  $\tau_{wall}$  are given as,

If  $y_p^+ < y_c^+$

$$\begin{aligned}
 k_{\text{wall}} &= \frac{U_\tau^2}{\sqrt{C_\mu}} \left( \frac{y_p^+}{y_c^+} \right)^2 \\
 \varepsilon_{\text{wall}} &= \frac{k_{\text{wall}}^{3/2}}{l_\varepsilon} \quad \text{where} \quad l_\varepsilon = \frac{c_i y_p}{1 + \frac{5.3}{\text{Re}_t}} \\
 \text{and } c_i &= \kappa (C_\mu)^{-3/4} \quad \text{Re}_t = \frac{\rho \sqrt{k_{\text{wall}}} y_p}{\mu_L}
 \end{aligned} \tag{3.65}$$

If  $y_p^+ \geq y_c^+$

$$\left. \begin{aligned}
 k_{\text{wall}} &= \frac{U_\tau^2}{\sqrt{C_\mu}} \\
 \varepsilon_{\text{wall}} &= \frac{U_\tau^3}{\kappa y_p}
 \end{aligned} \right\} \tag{3.66}$$

The reason for this choice comes from empirical observations of the variation of turbulent kinetic energy and its rate of dissipation. The level of TKE in the boundary layer reaches a maximum in the logarithmic layer and the non-dimensionalized value of TKE  $k^+ = \frac{k}{U_\tau^2}$  reaches a maximum value of 3.33. The wall-function is tuned to pick up this maximum value when the first grid point from the wall is in the log layer. Similarly, the level of  $\varepsilon$  is tuned to pick up its maximum value. In the viscous sub-layer, as the wall is approached, the value of TKE is an  $\mathcal{O}(y^2)$  term and  $\varepsilon$  is an  $\mathcal{O}(1)$  term. The values of  $k$  and  $\varepsilon$  are curve fit to simulate this variation, when the first grid point is in the viscous sub-layer. It should be noted that the above prescriptions for  $k$  and  $\varepsilon$  are based on incompressible flow analysis. In the case of compressible flows, the wall-function treatment has to take into account the effect of density variations. Also, the wall-function treatment has to be consistent with the van Driest transformation for the “law of the wall” given in Chapter 2.

#### 3.4.1.2 Wall-function: compressible form

In the case of compressible flows, at high Mach numbers, the variation in density across the boundary layer needs to be taken into account. There have been several “fixes”

that have been reported in the literature. Aupoix and Viala [1995], present a detailed review of these modifications to the wall function treatment. Most of these “fixes” tend to modify the definition of the non-dimensional distance,  $y^+$ , to the first grid point from the wall. Some of these definitions, briefly, are

$$\begin{aligned}
 \text{a) } y^+ &= \frac{\rho y U_\tau}{\mu_L} && \dots \text{So [1991]} \\
 \text{b) } y^+ &= \frac{\rho_{\text{wall}} y U_\tau}{\mu_{\text{wall}}} && \dots \text{van Driest} \\
 \text{c) } y^+ &= \frac{(\sqrt{\rho Q_{\text{wall}}}) y U_\tau}{\mu_L} && \dots \text{Coakley and Huang [1992]}
 \end{aligned} \tag{3.67}$$

From an analysis of the predictions made by each one of these definitions of  $y^+$  Aupoix and Viala [1995], concluded that the definition given by So et al. [1991] is the better choice for adiabatic walls, that is where  $T_{\text{wall}} = T_{\text{aw}}$ , (where  $T_{\text{wall}}$  is the wall temperature and  $T_{\text{aw}}$  is the adiabatic wall temperature, Kays and Crawford, 1980). However, for cold walls, that is where  $\frac{T_{\text{wall}}}{T_{\text{aw}}} \approx 0.2$ , they (Aupoix and Viala 1995) observe that the definition given by Coakley and Huang [1993] is a better choice.

Viegas et al. [1985] conducted a detailed analysis of the wall-function treatment for compressible flows and derived the formulation that could be used successfully to compute compressible wall-bounded flows. Given below is a brief description of this treatment for cases where the first grid point is in the log-layer. For treatments in the viscous sub-layer, refer to Viegas et al. [1985].

If the velocity is defined using the van Driest transformation, then the law of the wall can be written in a form similar to the constant property (incompressible) case. Thus

$$U_c^+ = \frac{U_c}{U_\tau} = \frac{1}{\kappa} \ln(y^+) + C \tag{3.68}$$

where  $U_\tau = \sqrt{\frac{\tau_{\text{wall}}}{\rho_w}}$  ;  $y^+ = \frac{U_\tau y}{\nu_w}$  and  $\kappa = 0.41$  is the von Karman constant.  $C$  is a constant whose value is chosen to be 5.2 (Bradshaw, 1977).  $U_c$  is the van Driest transformed velocity defined by (Bradshaw, 1977)

$$U_c = \sqrt{B} \left[ \sin^{-1} \left( \frac{A + U}{D} \right) - \sin^{-1} \left( \frac{A}{D} \right) \right] \quad (3.69)$$

where,

$$\begin{aligned} A &= \frac{q_w}{\tau_{wall}} \\ B &= \frac{2C_p T_w}{Pr_t} \\ D &= \sqrt{A^2 + B} \end{aligned} \quad (3.70)$$

It should be noted that this derivation of the velocity profile is valid for flat plate boundary layers (zero pressure gradient) only.

Close to a wall boundary the convection terms in the governing equations can be neglected in comparison to the viscous terms and the energy equation can be integrated (Huang and Coakley, 1993) to give an expression for the total heat flux as,

$$q = q_w + U\tau_{wall} \quad (3.71)$$

Equations 3.68 and 3.71 are used to bridge over to the first grid point from the solid wall. It is assumed that the first grid point is in the inner layer of the turbulent boundary layer. Based on empirical observations the values of TKE and its dissipation rate,  $k_{wall}$  and  $\epsilon_{wall}$  respectively, are “curve fit” as

$$\begin{aligned} k_{wall} &= \left( \frac{\tau_{wall}}{\rho} \right) / \sqrt{C_\mu} \\ \epsilon_{wall} &= \frac{\left( \frac{\tau_{wall}}{\rho} \right)^{3/2}}{\kappa y} \end{aligned} \quad (3.72)$$

It should be pointed out that  $\rho$  in the above equations is the local value of density.

In order to implement the “law of the wall” for compressible flows Viegas et al. [1985] suggest that the  $y^+$  of the first grid point (in the computational domain) should be between 20 and 40, with the second grid point at a distance  $\Delta y^+ = 20-40$ . The following steps have been suggested by Huang and Coakley [1993] in implementing the “law of the wall” for compressible flows (referring to Figure 3.2) :



1. Assuming  $y_p^+$  initially (or computed from the previous time step), calculate  $U_{c,p}^+$  from equation 3.68.
2. Assuming  $\frac{q_w}{\tau_{wall}}$  and  $T_w$  initially (or computed from the previous time step), calculate  $U_{c,p}$  from equation 3.69.
3. Equation 3.68 can be written in terms of a formula for the wall shear stress,  $\tau_{wall}$  :

$$\begin{aligned}\tau_{wall} &= Q_w U \tau \frac{U_{c,p}}{U_{c,p}^+} \\ \tau_{wall} &= y_p^+ \mu_w \frac{U_{c,p}}{U_p} \frac{1}{U_{c,p}^+} \frac{U_p}{y_p}\end{aligned}\tag{3.73}$$

This can be used to define an effective turbulent-viscosity connecting the wall and the first grid point. That is,

$$\mu_t \Big|_{wall} = \frac{y_p^+ \mu_w U_{c,p}}{U_p U_{c,p}^+}\tag{3.74}$$

4. Substituting equation 3.73 into equation 3.71 and assuming constant Prandtl number,  $Pr_t$ , the heat flux at the wall can be obtained :

$$q_w = - \frac{\mu_t C_p}{Pr_t} \left( \frac{T_p - T_{wall}}{y_p} \right) - \frac{\mu_t}{2} \left( \frac{U_p^2}{y_p} \right)\tag{3.75}$$

which helps in defining an effective thermal conductivity,  $\mu_t C_p / Pr_t$ , to be used to bridge over to the first grid point.

5. The Navier-Stokes equations are then solved to obtain  $U_p$  and  $T_p$ .
6. With these solutions,  $\tau_{wall}$  and  $q_w$  (or  $T_{wall}$ ) are updated using equations 3.73 and 3.75 and  $y_p^+$  is updated.

Both the level of TKE,  $k_p$ , and its rate of dissipation,  $\varepsilon_p$  at the first grid point from the wall are fixed using the values defined in equation 3.72.

### 3.5 Other Two-Equation Models

The k- $\varepsilon$  model that has been described above is the most popular turbulence model in use today. Coupled with the wall treatment, the k- $\varepsilon$  model is well behaved and provides solutions of reasonable accuracy for most engineering problems. Many important industrial applications require the integration of turbulence models directly to a solid boundary,

particularly in situations where wall transport properties are needed or where there is flow separation. The lack of exact treatment for  $\varepsilon$  at the wall and the lack of asymptotic consistency in the  $k$ - $\varepsilon$  model has led to formulations for the near wall modelling of the  $k$  and  $\varepsilon$  equations (Patel et al., 1985). These alternative formulations (low-Reynolds number versions), can be numerically stiff and involve a certain degree of empiricism (Speziale et al. 1992) and has led to the formulation of alternative forms of two-equation models. Most of the two-equation models that have been proposed involve the solutions of transport equations for  $k$  and some function of  $k$  and  $\varepsilon$ . The most notable is the  $k$ - $\omega$  model of Wilcox and Traci [1976] and Wilcox [1988].

In the  $k$ - $\omega$  model, a modelled form of the transport equations for  $k$  and a reciprocal time scale  $\omega$  ( $\omega = \frac{\varepsilon}{C_\mu k}$ ) are solved to define the turbulent-viscosity. There is evidence that the  $k$ - $\omega$  model is computationally robust for integration to a solid boundary (Menter, 1994). The form of the transport equation for  $k$  is identical to the one given by equation 3.54. The modelled form of the  $\omega$  equation is given as (Wilcox, 1988)

$$\frac{\partial(\rho\omega)}{\partial t} + \frac{\partial}{\partial x_j}(\rho U_j \omega) = C_{\omega 1} \frac{\omega}{k} P_k - C_{\omega 2} \rho \omega^2 + \frac{\partial}{\partial x_j} \left[ \Gamma_\omega \frac{\partial \omega}{\partial x_j} \right] \quad (3.76)$$

where  $P_k$  is defined as in equation 3.58 and

$$\Gamma_\omega = \mu_L + \frac{\mu_t}{\sigma_\omega} \quad (3.77)$$

The eddy-viscosity is now defined as

$$\mu_t = \frac{\rho k}{\omega} \quad (3.78)$$

The constants in the above equations are given the values

$$C_\mu = 0.09 \quad ; \quad C_{\omega 1} = \frac{5}{9} \quad ; \quad C_{\omega 2} = \frac{5}{6} \quad \text{and} \quad \sigma_\omega = 2 \quad (3.79)$$

The above form of the  $k$ - $\omega$  model has been shown to be computationally robust (in integrating directly to a solid boundary) for a variety of test cases (Menter, 1992 ; Wilcox, 1992). However, the  $k$ - $\omega$  model has been shown to predict asymptotically inconsistent

values for  $k$  near a solid boundary (Wilcox, 1988). It has been shown (Patel et al. 1985) that  $k$  varies as  $O(y^2)$  close to a solid boundary. The  $k$ - $\omega$  model with the form for the  $\omega$  equation given by equation 3.76 predicts the variation of  $k$  to be  $k = y^{3.23}$  (Wilcox, 1988). The reason for this variation is the neglecting of a cross-diffusion term in the equation for  $\omega$  (equation 3.76). The exact form of the equation for  $\omega$  which is defined as  $\omega = \frac{\varepsilon}{C_\mu k}$  can be derived, and is given in Speziale et al. [1992]. The difference between the exact form of the equation for  $\omega = \frac{\varepsilon}{C_\mu k}$  and equation 3.76 is that there is an additional cross-diffusion term missing in equation 3.76. The cross diffusion has been shown to be responsible for the inconsistent value of  $k$  predicted by the modelled form of the  $\omega$  equation given by equation 3.76 (Speziale et al. 1992). Briefly, this can be explained as follows (from Speziale et al. 1992) :

Close to a solid boundary, that is  $y \rightarrow 0$ , the balance of terms in the  $\omega$  equation reduces to (from the exact form of the equation for  $\omega = \frac{\varepsilon}{C_\mu k}$ ).

$$\frac{2\nu_L}{k} \left( \frac{\partial \omega}{\partial y} \frac{\partial k}{\partial y} \right) + \nu_L \frac{\partial^2 \omega}{\partial y^2} + \omega^2 = 0 \quad (3.80)$$

The balance of terms gives an asymptotically consistent variation for  $k$  close to the solid boundary. Whereas, according to the suggested modelled form of  $\omega$ , equation 3.76, leads to a balance of terms such as :

$$\nu_L \frac{\partial^2 \omega}{\partial y^2} - C_{\omega 2} \omega^2 = 0 \quad (3.81)$$

which leads to the asymptotically inconsistent value for  $k$ , close to a solid wall (Speziale et al. 1992). The asymptotic inconsistency has been dismissed by Menter [1992] as irrelevant as long as the model predicts the mean flow variations with reasonable accuracy. However, the cross-diffusion term is included in a "blended" form of the  $k$ - $\varepsilon$  and  $k$ - $\omega$  models (Menter, 1992).

In addition to the asymptotic inconsistency of the modelled form of the  $k$ - $\omega$  model, there exists another problem regarding the freestream dependency of the model. The

modelled form of the  $k$ - $\omega$  model given by Wilcox [1992], is highly sensitive to the values of  $k$  and  $\omega$  prescribed at the free stream boundary (Menter, 1992). Menter [1992], suggests the use of a blending function such that the virtues of the  $k$ - $\epsilon$  and the  $k$ - $\omega$  model could be exploited. That is, the  $k$ - $\epsilon$  model is known to be insensitive to the values for  $k$  and  $\epsilon$  prescribed at the free stream boundary. The  $k$ - $\omega$  model, on the other hand, is computationally robust in integrating the model equations directly to a solid boundary. The use of the blending function helps to switch to the  $k$ - $\omega$  model in regions close to a solid boundary and switch to the  $k$ - $\epsilon$  model in the outer regions of the viscous layer. The blending function treatment has had quite a bit of success.

Other two-equation models or versions of the  $k$ - $\epsilon$  and  $k$ - $\omega$  models are being continuously proposed\*. For example, Speziale et al. [1992] have proposed a  $k$ - $\tau$  model where  $\tau$  is defined as  $\tau = \frac{k}{\epsilon}$ . They argue that this  $k$ - $\tau$  model is capable of predicting asymptotically consistent values and is computationally robust when integrating to a solid boundary. But testing of this model has been limited to some simple flowfield simulations and needs to be adequately tested for a variety of engineering problems before it becomes the model of choice.

We have briefly touched upon the modelling concepts of eddy-viscosity based models. In Chapter 5, we present a more detailed analysis of the  $k$ - $\epsilon$  model as it applies to compressible flows and analyze the reported superiority (Huang et al., 1992) of the  $k$ - $\omega$  model over the  $k$ - $\epsilon$  model (in light of the cross-diffusion term).

### 3.6 Summary

In this chapter, we have presented the equations of motion in their instantaneous form and highlighted the need for turbulence closure models. The Reynolds averaging and Favre averaging techniques have been discussed. A brief summary of the zero- and one-equation

\*For example Menter [1992] proposed a shear stress transport model which is claimed to be superior in making predictions of separated flows in comparison with the  $k$ - $\epsilon$  and  $k$ - $\omega$  models.

models of turbulence has been presented with a view to making a case for two-equation models of turbulence closure.

The two-equation  $k$ - $\epsilon$  model of turbulence has been discussed in detail and the empiricism involved in the determination of the constants, that are needed to model the eddy-viscosity and the scale-determining equation. The problems associated with the  $k$ - $\epsilon$  model for turbulence in terms of integration to a solid boundary have been discussed and a detailed description of the wall-function treatment as it applies to low Mach number flows and high speed compressible flows has been provided. Additional forms of the two-equation models of turbulence have been presented with a terse description of their virtues and drawbacks.

## CHAPTER 4

### COMPUTATIONAL METHOD

In this chapter details regarding the numerical algorithm are presented. Details regarding this scheme as well as the artificial dissipation schemes that are used in conjunction with this finite volume scheme are presented. Additionally, an upwind scheme that has been used in the calculations is also described. Validation studies of the computational code, developed based on this numerical algorithm, against benchmark test cases are presented. Drawbacks or weak points of this numerical algorithm are highlighted.

#### 4.1 Numerical Algorithm

##### 4.1.1 Governing Equations

The governing equations are given in Chapter 3, equations 3.51 through 3.61. These equations are non-dimensionalized using characteristic variables defined as follows:

$$\left. \begin{aligned} x^* = L \quad ; \quad y^* = L \quad ; \quad t^* = \frac{L}{\sqrt{\frac{p_\infty}{\rho_\infty}}} \quad ; \quad U^* = \sqrt{\frac{p_\infty}{\rho_\infty}} \quad ; \quad p^* = p_\infty \\ \rho^* = \rho_\infty \quad ; \quad T^* = T_\infty \quad ; \quad \mu^* = \mu_\infty \end{aligned} \right\} \quad (4.1)$$

where  $L$  is some characteristic length scale of the flow field.  $x$ ,  $y$  and  $t$  represent the two spatial co-ordinates and time.  $U$ ,  $p$ ,  $\rho$ ,  $T$  and  $\mu$  represent, respectively, the  $x$  component of the velocity, the pressure, the density, temperature and the coefficient of molecular viscosity. The subscript  $\infty$  refers to the free-stream or main-stream conditions. The component of velocity in the  $y$  direction is non-dimensionalized using the same characteristic velocity  $U^*$ . Using these characteristic variables the governing equations are obtained in their non-dimensionalized form. These governing equations in their non-dimensionalized form can be cast into a form given below in equation 4.2.

$$\frac{\partial W_{ij}}{\partial t} + \frac{\partial F_{ij}}{\partial x} + \frac{\partial G_{ij}}{\partial y} + S_{ij} = 0 \quad (4.2)$$

where  $i$  and  $j$  represent the indices of the control volume in the computational grid. A typical control volume used is shown in the sketch below in Figure 4.1.

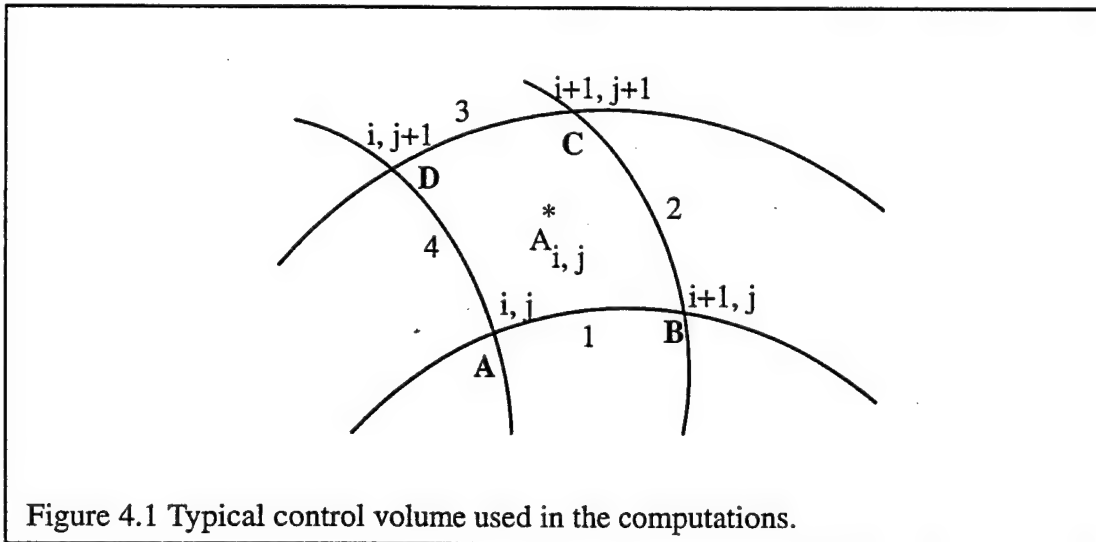
For the two-dimensional case the terms  $W_{ij}$ ,  $F_{ij}$  and  $G_{ij}$  are defined as

$$W_{ij} = \begin{bmatrix} \rho \\ \rho U \\ \rho V \\ \rho E \\ \rho k \\ \rho \epsilon \end{bmatrix} ; \quad F_{ij} = F_c + F_d ; \quad G_{ij} = G_c + G_d \quad (4.3)$$

where  $F_c$  and  $G_c$  represent the inviscid fluxes and  $F_d$  and  $G_d$  represent the viscous or diffusive fluxes. The inviscid fluxes are given as

$$F_c = \begin{bmatrix} \rho U \\ \rho U^2 + p \\ \rho UV \\ \rho UE \\ \rho Uk \\ \rho U\epsilon \end{bmatrix} \quad G_c = \begin{bmatrix} \rho V \\ \rho UV \\ \rho V^2 + p \\ \rho VE \\ \rho Vk \\ \rho V\epsilon \end{bmatrix} \quad (4.4)$$

and the viscous fluxes are given as,



$$F_d = \begin{bmatrix} 0 \\ -\sigma_{xx} \\ -\sigma_{xy} \\ -u\sigma_{xx} - v\sigma_{xy} + q_x \\ \left(\mu_L + \frac{\mu_T}{\sigma_K}\right) \frac{\partial k}{\partial X} \\ \left(\mu_L + \frac{\mu_T}{\sigma_\varepsilon}\right) \frac{\partial \varepsilon}{\partial X} \end{bmatrix} \quad G_d = \begin{bmatrix} 0 \\ -\sigma_{xy} \\ -\sigma_{yy} \\ -u\sigma_{xy} - v\sigma_{yy} + q_y \\ \left(\mu_L + \frac{\mu_T}{\sigma_K}\right) \frac{\partial k}{\partial Y} \\ \left(\mu_L + \frac{\mu_T}{\sigma_\varepsilon}\right) \frac{\partial \varepsilon}{\partial Y} \end{bmatrix} \quad (4.5)$$

where  $k$  and  $\varepsilon$  denote the turbulent kinetic energy (TKE) and its dissipation rate, respectively.

The viscous stresses and the heat fluxes are given as

$$\left. \begin{aligned} \sigma_{xx} &= 2\mu_{\text{eff}} \frac{\partial U}{\partial x} + \lambda_{\text{eff}} \left[ \frac{\partial U}{\partial x} + \frac{\partial V}{\partial y} \right] - \frac{2}{3} \rho k \\ \sigma_{yy} &= 2\mu_{\text{eff}} \frac{\partial V}{\partial y} + \lambda_{\text{eff}} \left[ \frac{\partial U}{\partial x} + \frac{\partial V}{\partial y} \right] - \frac{2}{3} \rho k \\ \sigma_{xy} &= \mu_{\text{eff}} \left( \frac{\partial U}{\partial y} + \frac{\partial V}{\partial x} \right) \\ q_x &= -K_{\text{eff}} \frac{\partial T}{\partial x} \quad ; \quad q_y = -K_{\text{eff}} \frac{\partial T}{\partial y} \end{aligned} \right\} \quad (4.6)$$

where

$$\mu_{\text{eff}} = \mu + \mu_t \quad ; \quad \lambda_{\text{eff}} = -\frac{2}{3} \mu_{\text{eff}} \quad \text{and} \quad K_{\text{eff}} = \frac{\gamma}{\gamma - 1} \left[ \frac{\mu}{\text{Pr}} + \frac{\mu_t}{\text{Pr}_t} \right] \quad (4.7)$$

where,  $\mu$  is the molecular viscosity,  $\text{Pr}$  is the Prandtl number, with subscripts “t” denoting turbulent quantities. The turbulent Prandtl number is assumed to be a constant.  $\text{Pr}$  and  $\text{Pr}_t$  are specified as 1.0 and 0.9, respectively. The turbulent-viscosity  $\mu_t$  is given as

$$\mu_t = C_\mu \frac{\rho k^2}{\varepsilon} \quad C_\mu = 0.09 \quad (4.8)$$

The molecular viscosity is computed using a power law, that is

$$\frac{\mu}{\mu_\infty} = \left( \frac{T}{T_\infty} \right)^n \quad (4.9)$$

where the exponent  $n = 0.75$ .

The source term  $S_{ij}$  in equation 4.2 is given as



$$S_{ij} = \begin{bmatrix} 0 \\ 0 \\ 0 \\ P_k - \rho \epsilon \\ C_{\epsilon 1} \frac{\epsilon}{k} P_k - C_{\epsilon 2} \frac{\rho \epsilon^2}{k} \end{bmatrix} \quad (4.10)$$

where  $P_k$  is the rate of production of TKE and is given as

$$P_k = - \overline{\rho u_i'' u_j''} \frac{\partial U_i}{\partial x_j} \quad (4.11)$$

where the indices  $i$  and  $j$  are indicative of tensor notation, (not computational grid locations).

The constants in equation 4.10 are specified as,  $C_{\epsilon 1} = 1.43$  and  $C_{\epsilon 2} = 1.92$ .

#### 4.1.2 Numerical Algorithm

The numerical algorithm is based on the finite volume formulation with a multi-stage Runge-Kutta time stepping scheme developed by Jameson et al [1981]. Details of this scheme are briefly outlined here.

Integrating the system of equations given by equation 4.5 over the control volume whose area (or in three-dimensions the volume  $V_{ij}$ ) is given by  $A_{ij}$  and making use of the divergence theorem, we can write the system of equations as

$$\frac{dW_{ij}}{dt} + \frac{1}{A_{ij}} \sum_{k=1}^4 (F_k \Delta y_k - G_k \Delta x_k) + S_{ij} = 0 \quad (4.12)$$

where  $k$  refers to the faces of the control volume. This formulation is essentially a contour integration around the boundary of the control volume. The values of the fluxes at the faces are calculated as an average of the values at the adjacent cell centers. Considering the control volume sketched in Figure 4.1, the second term in equation (4.12) can be written as

$$[F_k \Delta y_k - G_k \Delta x_k] = \left\{ (F_{AB} \Delta y_{AB} - G_{AB} \Delta x_{AB}) + (F_{BC} \Delta y_{BC} - G_{BC} \Delta x_{BC}) + \right. \\ \left. (F_{CD} \Delta y_{CD} - G_{CD} \Delta x_{CD}) + (F_{DA} \Delta y_{DA} - G_{DA} \Delta x_{DA}) \right\} \quad (4.13)$$

Referring to Figure 4.1 again, the first term on the right hand side of equation 4.13 can be written as

$$F_{AB}\Delta y_{AB} - G_{AB}\Delta x_{AB} = 0.5 * (F_{ij} + F_{i,j-1})(y_B - y_A) - 0.5 * (G_{ij} + G_{i,j-1})(x_B - x_A) \quad (4.14)$$

The fluxes on the other three sides can be written in a similar fashion. The viscous terms are evaluated in a similar fashion. For example, terms like  $\frac{\partial U}{\partial x}$  and  $\frac{\partial U}{\partial y}$  are evaluated as follows : For the control volume sketched in Figure 4.1 these terms are written as

$$\frac{\partial U}{\partial x} = \frac{1}{A_{ij}} \sum_{k=1}^4 U_k \Delta y_k \quad \text{and} \quad \frac{\partial U}{\partial y} = - \frac{1}{A_{ij}} \sum_{k=1}^4 U_k \Delta x_k \quad (4.15)$$

and an equation similar to 4.14 can be written. For example, for face 2 these work out to be

$$\left. \begin{aligned} U_{BC}\Delta y_{BC} &= 0.5 * (U_{ij} + U_{i+1,j}) * (y_C - y_B) \\ U_{BC}\Delta x_{BC} &= 0.5 * (U_{ij} + U_{i+1,j}) * (x_C - x_B) \end{aligned} \right\} \quad (4.16)$$

The control volume formulation given above, is essentially a second-order central difference scheme and hence suffers from odd-even decoupling. That is, the control volume formulation introduces dispersive errors to the solution especially in the case of flow fields with strong gradients such as shocks. In order to suppress the oscillations, induced by dispersive errors, one can add extra dissipation to the numerical procedure (Hirsch, 1990). Alternatively, an upwind type scheme implicitly contains numerical dissipation to suppress such undesirable oscillations.

#### 4.1.3 Artificial Dissipation Schemes

In order to dampen the amplitude of the oscillations introduced by the “second-order central difference scheme” explained above, a dissipation term  $D_{ij}$  is added to the fluxes in equation 4.12.  $D_{ij}$  can be defined in one of two ways. One is a blend of second- and fourth-order differences and the other is a scheme based on TVD schemes.

##### 4.1.3.1 Blend of second- and fourth-order differences

In this scheme a blend of second- and fourth-order differences of the vector  $W_{ij}$  defined by equation 4.3 is used. The basic dissipation scheme, first proposed by Jameson et

al. [1981] has been modified by Swanson and Turkel [1987] and is outlined here. According to this scheme the dissipation term,  $D_{ij}$ , is written as

$$-D_{ij} = d_{i+1/2,j} - d_{i-1/2,j} + d_{i,j+1/2} - d_{i,j-1/2} \quad (4.17)$$

Here, the 1/2 locations correspond to the faces of the control volume. The terms  $d_{i+1/2,j}$  and  $d_{i-1/2,j}$  together represent the sum of a second-order difference and a fourth-order difference. The term  $d_{i+1/2,j}$  is written as

$$d_{i+1/2,j} = \lambda_{i+1/2,j} \left\{ \begin{aligned} &\varepsilon_{i+1/2,j}^{(2)} (W_{i+1,j} - W_{i,j}) - \\ &\varepsilon_{i+1/2,j}^{(4)} (W_{i+2,j} - 3W_{i+1,j} + 3W_{i,j} - W_{i-1,j}) \end{aligned} \right\} \quad (4.18)$$

where

$$\lambda_{i+1/2,j} = \frac{1}{2} (\lambda_{\xi_{ij}} + \lambda_{\xi_{i+1,j}}) \quad (4.19)$$

$$\lambda_{\xi} = |Uy_{\xi} - Vx_{\xi}| + c \sqrt{x_{\xi}^2 + y_{\xi}^2} \quad (4.20)$$

where  $U$  and  $V$  are the cartesian components of the velocity vector and  $x_{\xi}$  and  $y_{\xi}$  are the metrics of the grid system and  $c$  is the speed of sound.

$$\varepsilon_{i+1/2,j}^{(2)} = K^{(2)} \max[v_{ij}, v_{i+1,j}] \quad (4.21)$$

$$\varepsilon_{i+1/2,j}^{(4)} = \max \left[ 0, \left( K^{(4)} - \varepsilon_{i+1/2,j}^{(2)} \right) \right] \quad (4.22)$$

$$v_{ij} = \left| \frac{p_{i+1,j} - 2p_{i,j} + p_{i-1,j}}{p_{i+1,j} + 2p_{i,j} + p_{i-1,j}} \right| \quad (4.23)$$

where  $p_{ij}$  is the pressure at the control volume defined by the index  $\{i,j\}$ . In the above equations,  $\lambda_{\xi}$  represents the maximum eigen value in the  $\xi$  direction.  $\varepsilon_{i+1/2,j}^{(2)}$  and  $\varepsilon_{i+1/2,j}^{(4)}$  are tuned based on the gradients in pressure. When there is strong jump in the pressure, such as across a shock, the second-order difference dominates and extra dissipation is added to suppress the spurious oscillations that might arise at the shock location. The fourth-order

difference is useful in smoothing out minor wiggles that arise in regions where the variations are relatively smoother.

Similar relations hold for the three other terms in equation 4.17. The terms  $K^{(2)}$  and  $K^{(4)}$  are arbitrary constants. The values for these constants range from  $0.25 \leq K^{(2)} \leq 1.5$  and  $1/512 \leq K^{(4)} \leq 1/32$ . Typically used values for  $K^{(2)}$  and  $K^{(4)}$  are  $1/4$  and  $1/256$ , respectively.

In equation 4.17, the first term on the right hand side along with a similar term for  $d_{i-1/2,j}$  represents the second-order difference and the second term on the right hand side along with a similar term from  $d_{i+1/2,j}$  represents the fourth-order difference along the  $\xi$  direction. In the absence of strong discontinuities such as shocks, the second-order term is almost negligible and the fourth-order term smooths any oscillations that might occur in the solution procedure. The second-order difference based term helps in capturing the shock and suppress the oscillations that occur at the shock location.

#### 4.1.3.2 Flux-limited dissipation

The flux-limited dissipation scheme is based on the scheme developed by Yee [1985]. The approach is to construct a scheme with TVD properties. The finite volume TVD scheme used here is obtained by constructing flux-limited dissipation terms added to the physical flux terms in such a way that the resulting semi-discrete equations have TVD properties, provided proper time stepping is used. Details of the scheme are given in Li and Kroll [1988]. The formulation used for the dissipation term is briefly outlined here.

$$D_{ij} = -\frac{1}{2} \left( T_{i+\frac{1}{2},j} \Phi_{i+\frac{1}{2},j} - T_{i-\frac{1}{2},j} \Phi_{i-\frac{1}{2},j} + T_{i,j+\frac{1}{2}} \Phi_{i,j+\frac{1}{2}} - T_{i,j-\frac{1}{2}} \Phi_{i,j-\frac{1}{2}} \right) \quad (4.24)$$

where  $T$  is the eigenvector matrix of the transformation Jacobian. The dissipation vectors  $\Phi$  are constructed in the  $i$  and  $j$  directions according to their one-dimensional forms. The schemes (Yee, 1985), can be classified into upwind and symmetric schemes. The symmetric scheme is used and is defined here. For the symmetric scheme, the  $k^{\text{th}}$  element of the vector  $\Phi$  denoted by  $\Phi^k$  is written as

$$\phi_{i+\frac{1}{2},j}^k = -\Psi\left(\lambda_{i+\frac{1}{2},j}^k\right)\left(\alpha_{i+\frac{1}{2},j}^k - \Omega_{i+\frac{1}{2},j}^k\right) \quad (4.25)$$

The function  $\Psi$  is a correction term which is written as

$$\Psi(\lambda) = \begin{cases} |\lambda| & |\lambda| \geq \delta \\ \frac{(\lambda^2 + \delta^2)}{2\delta} & |\lambda| < \delta \end{cases} \quad (4.26)$$

where  $\delta$  is a small positive number and  $\lambda^k$  is the  $k^{\text{th}}$  eigen value of the Jacobian matrix.  $\Omega$  is a limiter function. The limiter function used here is given as

$$\Omega_{i+\frac{1}{2},j} = \text{minmod}\left(\alpha_{i-\frac{1}{2},j}, \alpha_{i+\frac{1}{2},j}\right) + \text{minmod}\left(\alpha_{i+\frac{1}{2},j}, \alpha_{i+\frac{3}{2},j}\right) - \alpha_{i+\frac{1}{2},j} \quad (4.27)$$

where the minmod function is defined as

$$\text{minmod}(x, y) = \text{sgn}(x) \max\{0, \min[|x|, y \text{sgn}(x)]\} \quad (4.28)$$

and  $\alpha^k$  is the  $k^{\text{th}}$  element of the vector  $\alpha = (\alpha_1, \alpha_2, \alpha_3, \alpha_4)^T$  and

$$\alpha_{i+\frac{1}{2},j} = T_{i+\frac{1}{2},j}^{-1} (W_{i+1,j} - W_{i,j}) \quad (4.29)$$

$T^{-1}$  is the inverse of the eigen vector matrix  $T$ . The values at  $(i + 1/2, j)$  or the cell interfaces are obtained using the Roe averaging technique (Roe, 1981).

Adding the dissipation terms to equation 4.12 we can rewrite it as

$$\frac{dW_{i,j}}{dt} + Q_{i,j} - D_{i,j} = 0 \quad (4.30)$$

where

$$Q_{i,j} = \frac{1}{A_{i,j}} \sum_{k=1}^4 (F_k \Delta y_k - G_k \Delta x_k) + S_{i,j} \quad (4.31)$$

#### 4.1.4 Time Stepping

An explicit five-step, modified Runge-Kutta time stepping scheme is used in the present set of calculations. Details of this time stepping can be found in Hirsch [1990]. A brief outline is presented here. The regular Runge-Kutta scheme is fourth-order accurate. By sacrificing some of the accuracy an increase in stability of the scheme is obtained (see

Jameson et al., 1981). The result is a second-order accurate scheme, which allows the use of larger time steps. Rewriting equation with the dissipation term added, we get

$$\frac{dW_{ij}}{dt} + P_{ij} = 0 \quad \text{where } P_{ij} = Q_{ij} - D_{ij} \quad (4.32)$$

The five stages of the time-stepping scheme are given in the equation below, where superscripts have been used to denote the stages of the time-stepping scheme. Superscript (n) refers to the values of the  $W_{ij}$  vector from the previous time step, and (n+1) refers to the time step for which calculations are being made. Also  $\Delta t$  denotes the size of the time step used for the temporal marching.

$$\left. \begin{aligned} W_{ij}^{(0)} &= W_{ij}^{(n)} \\ W_{ij}^{(1)} &= W_{ij}^{(0)} - \alpha_1 \Delta t P_{ij}^{(0)} \\ W_{ij}^{(2)} &= W_{ij}^{(0)} - \alpha_2 \Delta t P_{ij}^{(1)} \\ W_{ij}^{(3)} &= W_{ij}^{(0)} - \alpha_3 \Delta t P_{ij}^{(2)} \\ W_{ij}^{(4)} &= W_{ij}^{(0)} - \alpha_4 \Delta t P_{ij}^{(3)} \\ W_{ij}^{(5)} &= W_{ij}^{(0)} - \alpha_5 \Delta t P_{ij}^{(4)} \\ W_{ij}^{(n+1)} &= W_{ij}^{(5)} \end{aligned} \right\} \quad (4.33)$$

where  $\alpha_1 = 1/4$ ,  $\alpha_2 = 1/6$ ,  $\alpha_3 = 3/8$ ,  $\alpha_4 = 1/2$  and  $\alpha_5 = 1.0$ . The time step size  $\Delta t$  is dictated by the stability condition and is determined as follows :

The permitted time step  $\Delta t$  is defined as the harmonic mean of the time steps allowed in the  $\xi$  and  $\eta$  directions. These time steps are dictated by the CFL condition. Thus,

$$\frac{1}{\Delta t} = \frac{1}{\Delta t_\xi} + \frac{1}{\Delta t_\eta} \quad (4.34)$$

$$\Delta t_\xi = \text{CFL} \frac{A_{ij}}{\lambda_\xi} \quad \text{and} \quad \Delta t_\eta = \text{CFL} \frac{A_{ij}}{\lambda_\eta} \quad (4.35)$$

where,  $\lambda_\xi$  and  $\lambda_\eta$  are the maximum eigen values in the  $\xi$  and  $\eta$  directions respectively and are given as

$$\begin{aligned}\lambda_{\xi} &= |Uy_{\xi} - Vx_{\xi}| + c \sqrt{x_{\xi}^2 + y_{\xi}^2} \\ \lambda_{\eta} &= |-Ux_{\eta} + Vy_{\eta}| + c \sqrt{x_{\eta}^2 + y_{\eta}^2}\end{aligned}\tag{4.36}$$

In evaluating the term  $P_{i,j}$  in equation 4.33 it is not necessary to evaluate the dissipation term  $D_{i,j}$  at every stage of the time-stepping, in fact, it is sufficient if they are evaluated at the first two stages of the time-stepping. The value of the dissipation that is obtained at the end of this second stage is used throughout the rest of the stages. Similarly, the viscous fluxes need to be evaluated only at the first stage of the time-stepping. These helping in reducing the computational cost. There are other ways of reducing the computational cost. Two such ways have been employed in the computational procedure used in this dissertation.

#### 4.1.5 Convergence Acceleration

Two convergence acceleration techniques have been employed in the computational procedure used here. These are the local time-stepping procedure and the residual averaging method.

In most computational procedures, the time step size is dictated by the stability of the scheme employed. In calculations of transient flow fields, the time step size is determined as the minimum of the time steps permitted in all the control volumes of the computational domain. In computing steady-state solutions it is not necessary to use the same time step size over all the control volumes in the computational domain. In fact, in most computational cases, there are regions in the flow field where the temporal variation of the flow field is almost negligible and would therefore permit the use of a larger time step. In the local time-stepping technique, each control volume is stepped in time based on the requirements of stability at that control volume (local stability requirements). Therefore, each control volume is marched to a different time level at each iteration. Since all control volumes are marching towards a steady state the local time-stepping scheme, helps in accelerating the rate of convergence of the solution.

Another way of accelerating the convergence rate is by using the residual averaging technique. This is essentially a residue smoothing procedure and more details can be found in Turkel [1984]. A diffusion equation is solved in a manner similar to the ADI (Alternating Direction Implicit) method. If  $\overline{P_{ij}}$  is the residue from a stage of the time-stepping scheme, then the smoothed out value of the residue at this stage is obtained by solving

$$(1 - \beta_x^2 \delta_{xx})(1 - \beta_y^2 \delta_{yy})P_{ij}^* = \overline{P_{ij}} \quad (4.37)$$

where,  $\delta_{xx}$  and  $\delta_{yy}$  are central difference operators and  $\beta_x$  and  $\beta_y$  are terms defined based on the largest eigen values in the  $\xi$  and  $\eta$  directions respectively. The value of  $P_{ij}^*$  is obtained by sweeping over the control volumes in the  $\xi$  direction first and then in the  $\eta$  direction. That is, equation 4.37 is solved to obtain an intermediate value of  $P_{ij}^*$  by sweeping in the  $\xi$  direction and then the same is done in the  $\eta$  direction. The sweeping can be done either explicitly or implicitly. If explicit methods are used, the equations reduce to a solution of

$$-\epsilon P_{i-1,j}^{**} + (1.0 + 2\epsilon)P_{ij}^{**} - \epsilon P_{i+1,j}^{**} = \overline{P_{ij}} \quad (4.38)$$

and,

$$-\epsilon P_{i,j-1}^* + (1.0 + 2\epsilon)P_{ij}^* - \epsilon P_{i,j+1}^* = P_{ij}^{**} \quad (4.39)$$

where,  $\epsilon$  is constant and a typically used value is 0.2 for schemes using the blend of second- and fourth-order differences based dissipation terms and is 2.0 for schemes using the TVD type dissipation scheme.

#### 4.1.6 Second-Order Upwind Scheme

As was mentioned earlier, the dissipation terms used in this finite volume scheme work to reduce the amplitude of the oscillations about a discontinuity and do not completely dissipate them. As a result, in cases with a strong shock\* these extra dissipation terms are not sufficient. Also, from an analysis of the results obtained for the axi-symmetric afterbody flowfield it was observed that the second-order scheme as described above allows the

\*In one of the test cases to be presented later, the projectile forebody problem at Mach 6.06, the bow shock formed ahead of the forebody is extremely strong that the dissipation added to inviscid fluxes is not sufficient to adequately suppress the oscillations. Therefore, results could not be obtained using the "second-order-central-difference" based treatment of the convection terms.



upstream propagation of information for supersonic flow fields. Therefore, in these cases a second order upwind scheme is used, which is based on the flux-vector-splitting technique of Steger and Warming (Shuen, 1992). The fluxes at the interfaces of the control volumes were calculated using a MUSCL extrapolation with a min-mod limiter. Brief details of this convection treatment are given below :

Equation 4.12 can be rewritten to separate the inviscid and viscous contribution to the fluxes at the cell faces and is now written as

$$\frac{dW_{ij}}{dt} + \frac{1}{A_{ij}} \sum_{k=1}^4 \left\{ (F_k \Delta y_k - G_k \Delta x_k)_{\text{inviscid}} + (F_k \Delta y_k - G_k \Delta x_k)_{\text{viscous}} \right\} + S_{ij} = 0 \quad (4.40)$$

Defining two new fluxes,  $Q_{ij}^c$  and  $Q_{ij}^d$  representing the inviscid and viscous contributions respectively, the inviscid fluxes  $Q_{ij}^c$  are evaluated as

$$Q_{ij}^c = F_c l_{i+1/2,j} - F_c l_{i-1/2,j} + G_c l_{i,j+1/2} - G_c l_{i,j-1/2} \quad (4.41)$$

where  $F_c$  and  $G_c$  are defined in equation 4.4. There is no change in the evaluation procedure for the viscous fluxes. The viscous fluxes are evaluated in the same manner that was outlined previously.

The terms in equation 4.41, represent the inviscid fluxes at the control volume interfaces. These are defined as

$$F_c l_{i+1/2,j} = F^+(Q_{i+1/2,j}^L) + F^-(Q_{i+1/2,j}^R) \quad (4.42)$$

$Q_{i+1/2,j}^L$  and  $Q_{i+1/2,j}^R$  are defined as

$$Q_{i+1/2,j}^L = Q_{ij} + \phi_{i+1/2,j}^- \quad (4.43)$$

$$\phi_{i+1/2,j}^- = \frac{l_{ij}}{2} \text{minmod}[\Delta Q_{ij}^-, \Delta Q_{ij}^+] \quad (4.44)$$

where  $l_{ij}$  represents the length of the cell and the min-mod limiter has been defined earlier in equation 4.28. The terms inside the parenthesis are written as

$$\left. \begin{aligned} \Delta Q_{ij}^- &= \frac{2(Q_{ij} - Q_{i-1,j})}{l_{ij} + l_{i-1,j}} \\ \Delta Q_{ij}^+ &= \frac{2(Q_{i+1,j} - Q_{ij})}{l_{ij} + l_{i+1,j}} \end{aligned} \right\} \quad (4.45)$$

The term  $Q_{i+1/2,j}^R$  is defined in a similar way and is given as

$$Q_{i+1/2,j}^R = Q_{i+1,j} - \phi_{i+1/2,j}^+ \quad (4.46)$$

$$\phi_{i+1/2,j}^+ = \frac{l_{i+1,j}}{2} \min \text{mod} [\Delta Q_{i+1,j}^+, \Delta Q_{i+1,j}^-] \quad (4.47)$$

With the  $Q$  vectors along the left and right running characteristics, defined as above, the  $F^+$  and  $F^-$  vectors are defined as

$$\left. \begin{aligned} F^+ &= \lambda_1^+ K_1 + \lambda_2^+ K_2 + \lambda_3^+ K_3 \\ F^- &= \lambda_1^- K_1 + \lambda_2^- K_2 + \lambda_3^- K_3 \end{aligned} \right\} \quad (4.48)$$

where vectors  $K_1$ ,  $K_2$  and  $K_3$  are written as

$$K_1 = \frac{\gamma - 1}{\gamma} \begin{bmatrix} \rho \\ \rho U \\ \rho V \\ \rho \left( h_t - \frac{c^2}{\gamma - 1} \right) \\ \rho k \\ \rho \varepsilon \end{bmatrix} \quad K_2 = \frac{1}{2\gamma} \begin{bmatrix} \rho \\ \rho(U + \tilde{k}_x c) \\ \rho(V + \tilde{k}_y c) \\ \rho(h_t + \theta_k c) \\ \rho k \\ \rho \varepsilon \end{bmatrix} \quad K_3 = \frac{1}{2\gamma} \begin{bmatrix} \rho \\ \rho(U - \tilde{k}_x c) \\ \rho(V - \tilde{k}_y c) \\ \rho(h_t - \theta_k c) \\ \rho k \\ \rho \varepsilon \end{bmatrix} \quad (4.49)$$

where

$$\tilde{k}_x = \frac{k_x}{|\nabla k|} \text{ and } \tilde{k}_y = \frac{k_y}{|\nabla k|} \text{ where } |\nabla k| = \sqrt{k_x^2 + k_y^2} \quad (4.50)$$

Depending on the fluxes being evaluated, that is if  $F^+$  and  $F^-$  are being evaluated then  $k$  represents the  $\xi$  coordinate and if  $G^+$  and  $G^-$  are being evaluated then  $k$  represents the  $\eta$  direction. Also, the  $\lambda$ 's are evaluated as

$$\lambda_n^\pm = \frac{1}{2} [\lambda_n \pm |\lambda_n|] \text{ where } n = 1, 2 \text{ or } 3 \quad (4.51)$$

and

$$\left. \begin{aligned} \lambda_1 &= \beta_k \\ \lambda_2 &= \beta_k + c|\nabla k| \\ \lambda_3 &= \beta_k - c|\nabla k| \end{aligned} \right\} \quad (4.52)$$

$$\beta_k = Uk_x + Vk_y \quad \text{and} \quad \theta_k = U\tilde{k}_x + V\tilde{k}_y \quad (4.53)$$

Again depending on the flux being evaluated the values of the metrics  $k_x$  and  $k_y$  are evaluated. A similar procedure is used to define the fluxes  $G^+$  and  $G^-$ .

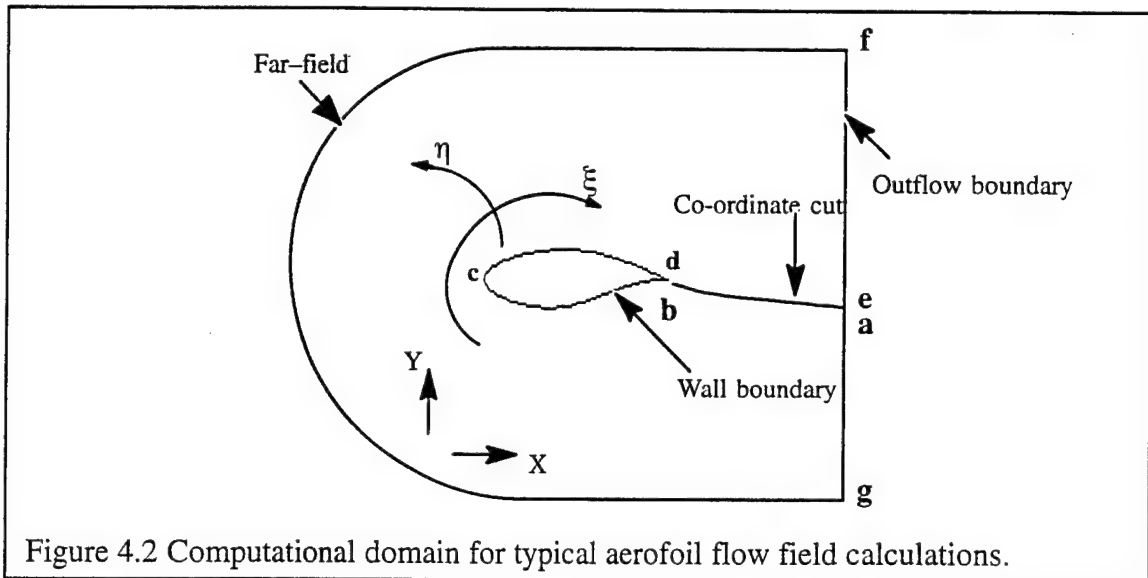
## 4.2 Code Validation

With the numerical algorithm described above a computational code was developed to conduct studies of compressible flow fields. But before any studies can be done, the computational code has to be tested and validated for computational accuracy. Such tests were conducted of both internal as well as external flowfields. For the external flow field case, tests were conducted of flow past two different aerofoil configurations. One was the symmetric NACA-0012 aerofoil and the other was the high lift RAE-2822 aerofoil. The computational results obtained from these test cases were compared against experimental data. The internal flow field that was tested is the flow through a converging-diverging nozzle configuration. Three different area ratios were tested and compared against experimental data. These test cases are described below and comparisons presented against experimental data.

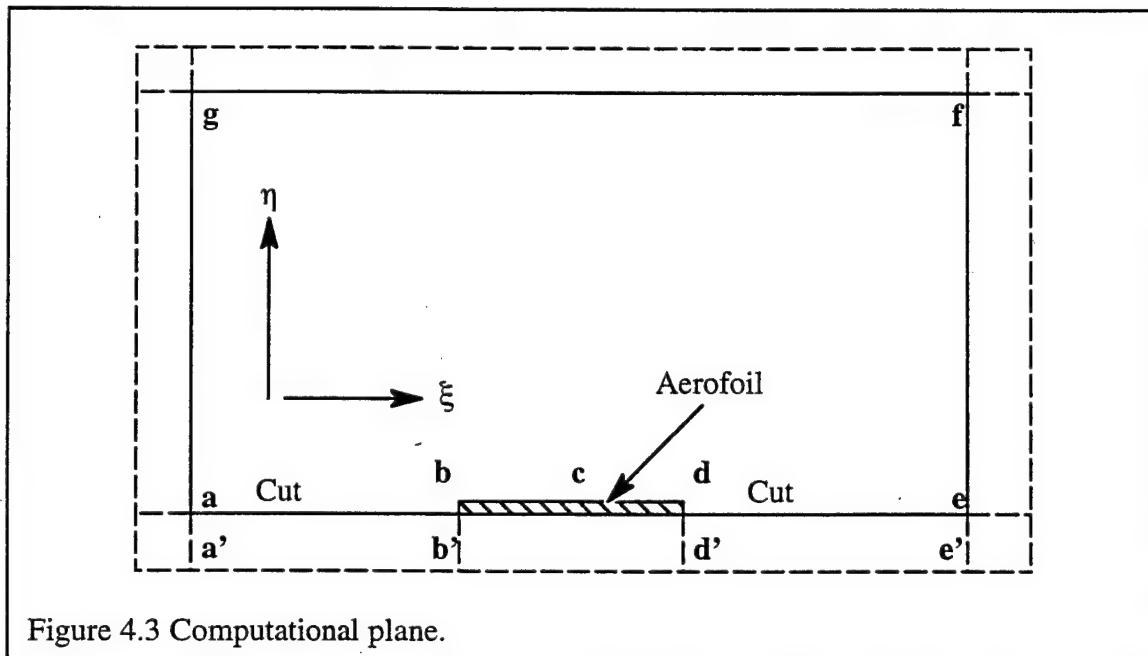
### 4.2.1 Aerofoil Flow-Field Computations

Before presenting the results obtained from the computations, the details regarding the computations, such as, boundary conditions are presented below.

For this set of computations, a conventional C-grid system was used. The grids were generated using a grid generation program described in Rizzi [1981]. The physical domain used in the computations is shown in Figure 4.2 along with the boundaries of the domain. Thus, there are outflow or far-field boundaries, wall boundary and symmetry boundaries. The co-ordinate cut represents a symmetry boundary. Conditions have to be specified at these boundaries.



Boundary conditions are prescribed, in this finite-volume formulation, using a set of dummy cells along each boundary. To understand the application of the boundary conditions in the computational method, consider the sketch shown in Figure 4.3 which shows the computational domain. The locations marked correspond to similar locations in the physical plane shown in Figure 4.2. The outer set of dashed lines depict the dummy cells used to store the information regarding the boundary condition. To be more precise, let us consider the



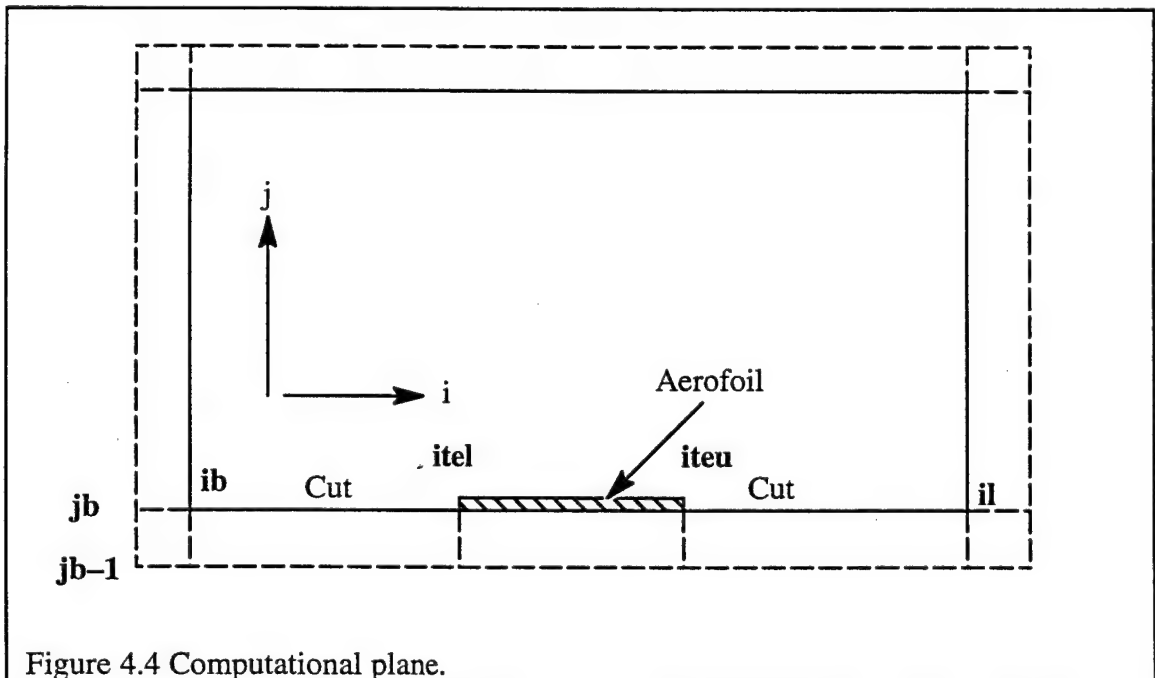
boundary “ab” and the boundary “ed”. These boundaries denote the co-ordinate cut. The cells bounded by abb’a’ get their information from the first set of cells just above “ed” and the cells bounded by edd’e’ get their information from the first set of cells just above “ab”. Thus in Figure 4.4, the information for the boundary conditions for the cells at the location  $j=j_b$  are stored in  $j=j_b-1$ . For the boundary defined by  $i=i_b-1$  to  $i=itel$  and by  $i=iteu$  to  $i=il$ , the following methodology is used. If  $W_{i,j}$  is the variable whose boundary condition is being prescribed, then

$$\begin{aligned} &\text{for } i = i_b \text{ to } itel \\ &W_{i,j_b-1} = W_{ir,j_b} \end{aligned} \quad (4.54)$$

where  $ir = il - i + 1$

and a similar boundary condition can be prescribed for  $i = iteu$  to  $il$ .

The wall boundary is modelled as a no-slip boundary in viscous computations with the wall shear stresses and the turbulent kinetic energy and its dissipation rate being prescribed using the wall function technique described in Chapter 3. In the case of inviscid computations, the computational method uses a method prescribed by Rizzi [1978]. Since the wall boundary is no longer a no-slip boundary, it is characterized by zero mass flux into



the wall. Using this and the momentum equation, a pressure boundary condition can be easily derived. At the far-field the effect of the solid boundary has to be taken into account. That is, in reality the far-field extends out to infinity. But in numerical calculations, because of practical limitations, the extent of the far-field boundary is truncated and so the conditions at this boundary, in the numerical domain, are not really free-stream conditions. Physically, the control volumes at this boundary location may be expected to feel the impact of the aerofoil. Usually far-field corrections are employed to taken into account the impact of the aerofoil on the free-stream. More details regarding the far-field correction can be found in Thomas and Salas [1986].

#### 4.2.1.1 Inviscid computation

With the specification of the boundary conditions given above, computations were made to evaluate the shock-capturing capabilities of the computational code. In order to test this, we made computations of the flow over a NACA-0012 aerofoil. Figure 4.5 shows an illustrative picture of the grid that was used in these computations. Only a portion of the grid used is shown in this picture. The computational domain extended about 5 chord lengths fore and aft of the aerofoil and 7 chord lengths in the lateral direction. The grid has 100 grid points on the aerofoil surface with 20 points in the wake region. The lateral direction was covered using 21 grid points.

The freestream Mach number is  $M_\infty = 0.85$  and the angle of attack is  $\alpha = 1.0$  (deg). The surface pressure distribution that was obtained from the computations is compared with the benchmark data for this flow field (Yoshihara and Sacher, 1985). This comparison and the pressure distribution contours (close to the aerofoil) is shown in Figure 4.6. In this figure, the pressure coefficient  $C_p$ , is defined as  $C_p = \frac{p - p_\infty}{\frac{1}{2} \rho_\infty U_\infty^2}$ , where  $p$  is the surface pressure and the subscripts  $\infty$  refer to the free-stream conditions. It should be mentioned that the benchmark data was obtained with 300 grid points on the aerofoil surface and a grid of size

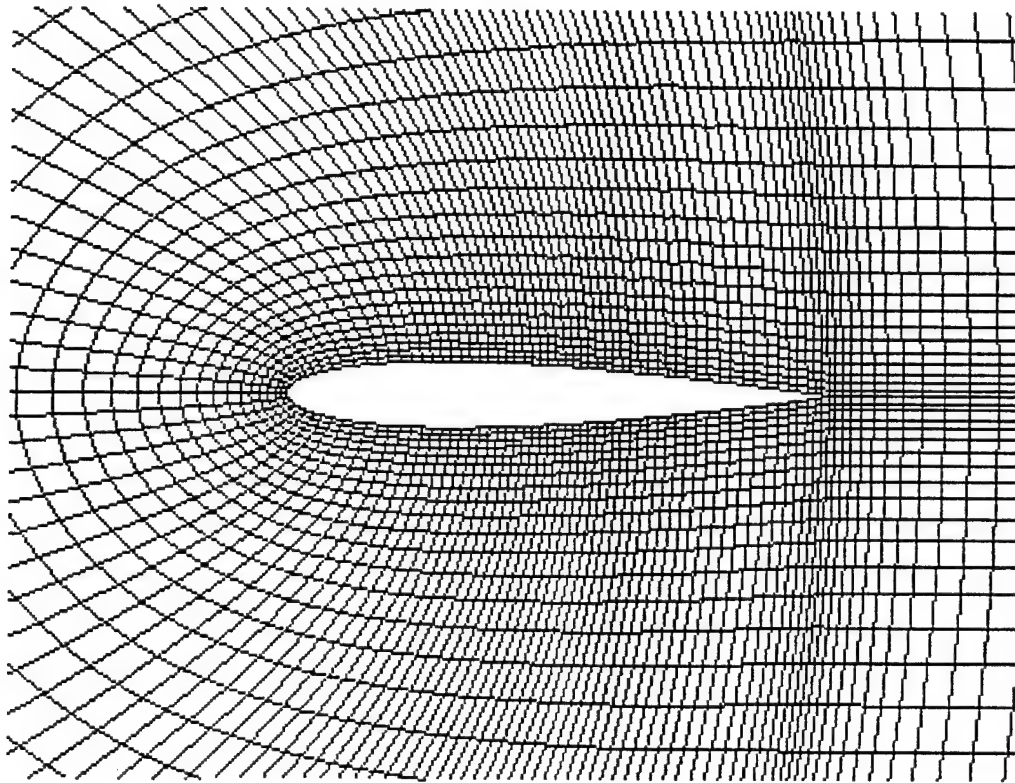


Figure 4.5 Computational grid used for the inviscid computations of flow over a NACA-0012 aerofoil.

512 x 256. Considering this the computational capabilities of the code (developed in this research effort) are quite good.

#### 4.2.1.2 Laminar computation

To test the computational capability of the code in predicting simple viscous flows, computations were made of the laminar flow over the NACA-0012 aerofoil. This computation was intended as a test of the numerical discretization of the viscous terms as well as to test the validity of the code in predicting symmetric flowfields. The boundary conditions used in this computational study were, a no-slip boundary for the velocity components and an adiabatic wall boundary for the temperature field. At the far-field, corrections prescribed by Thomas and Salas [1986] (for the finiteness of the computational domain) were employed.

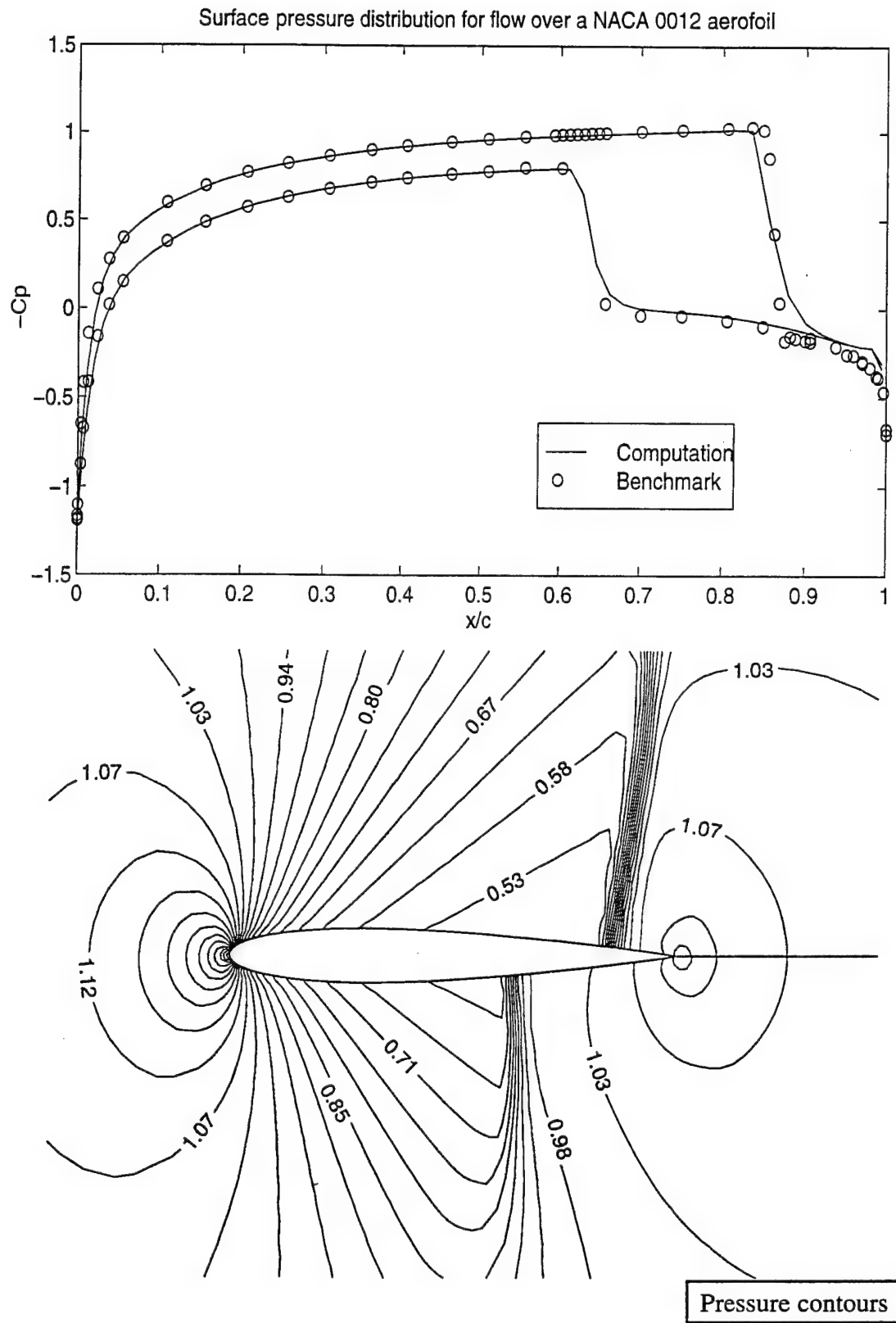


Figure 4.6 Surface pressure distribution and pressure distribution for inviscid flow over a NACA-0012 aerofoil.  $M_\infty = 0.85$ ,  $\alpha = 1.0$ .



The computational domain extended 5 chord lengths fore and aft of the aerofoil (from the leading and trailing edges, respectively) and 7 chord lengths in the lateral direction. The grid points were clustered close to the aerofoil surface in order to capture the viscous effects. The first grid point from the wall (aerofoil surface) was at a  $\Delta y = 0.005c$  (where  $c$  is the chord length of the aerofoil = 1.0). The computational grid had 120 grid points on the aerofoil surface and 40 points in the wake region. The grid size used in these computations was  $201 \times 61$ . The free-stream conditions for this laminar flow were a Mach number of 0.5 and a Reynolds number of 5000 at an angle of attack of  $0^\circ$ . The results obtained help to validate two aspects of the computational code. One is the symmetry of the solution and the other is the accuracy of the coding (in terms of the viscous fluxes). The contour plots of the pressure distribution and the surface pressure distribution are shown in Figure 4.7. The  $C_p$  profile shown in Figure 4.7 has been compared against similar computations made by Swanson and Turkel [1987]. The pressure coefficient is defined as indicated above (in the section on inviscid computations). The agreement with the results of Swanson and Turkel [1987] is very good.

#### 4.2.1.3 Turbulent flow computations

The code was next validated to determine the accuracy of coding in terms of discretization of the turbulent fluxes and the accuracy in implementation of the wall-function treatment. The same grid from the laminar computations was used for this set of calculations as well. The non-dimensional distance of the first grid point, away from the aerofoil surface, was at a  $y^+ \approx 40$ . The free-stream conditions for this case were a Mach number = 0.5 and a Reynolds number =  $2.89 \times 10^6$  at an angle of attack of  $0^\circ$ . The low Mach number form of the wall-function treatment, described in Chapter 3, was used here. Results from this computation were compared against experimental measurements (Thibert et al., 1979). The comparison of surface pressure distribution and a contour plot of the pressure distribution in the flow field is presented in Figure 4.8. The agreement with the experimental measurements is excellent.

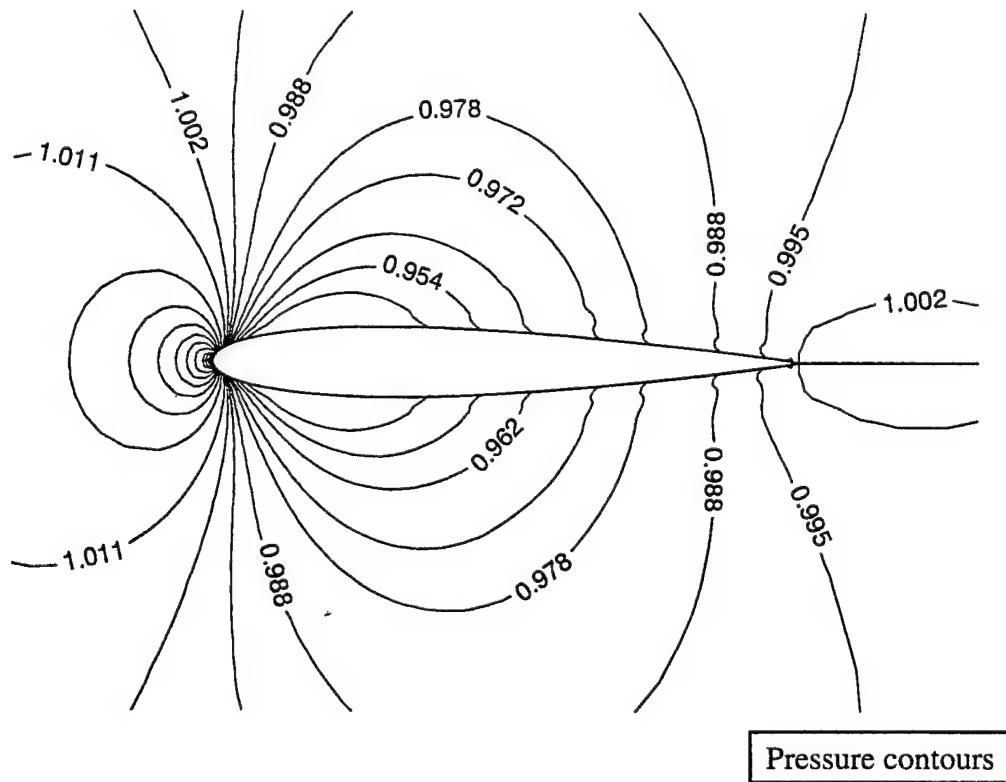
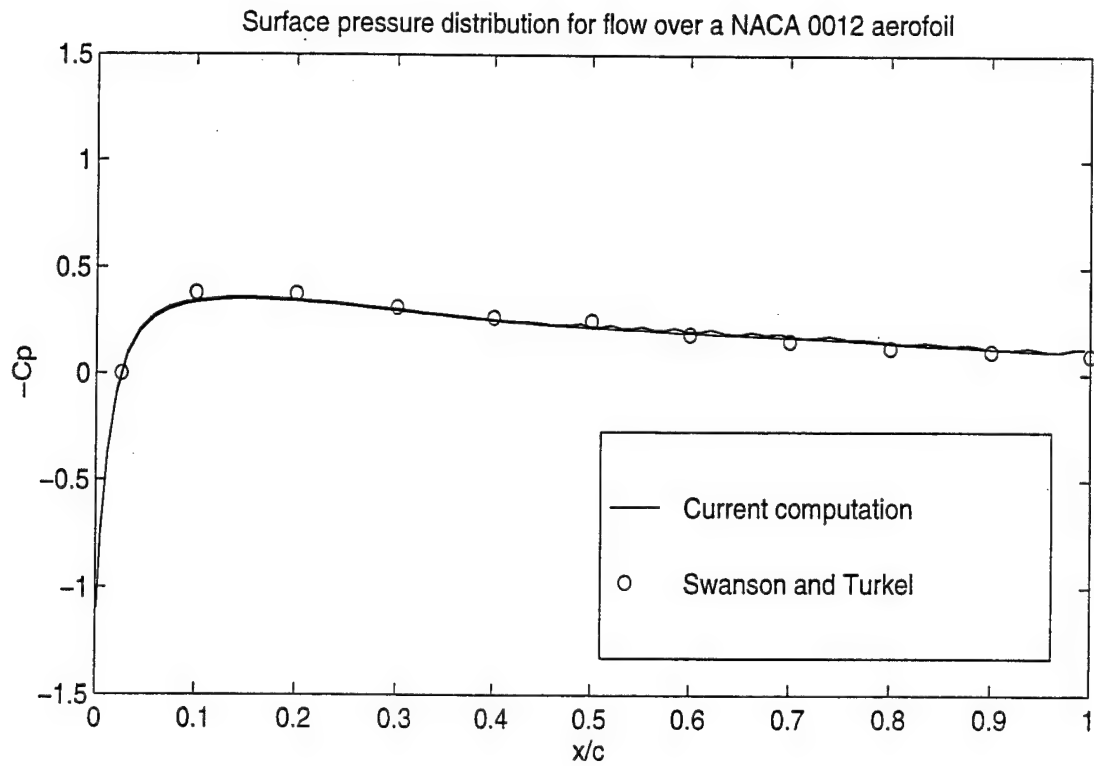


Figure 4.7 Validation of computational code for laminar flow past a NACA0012 aerofoil.  $M_\infty = 0.5$ ,  $Re = 5000$ ,  $\alpha = 0.0$  degrees.

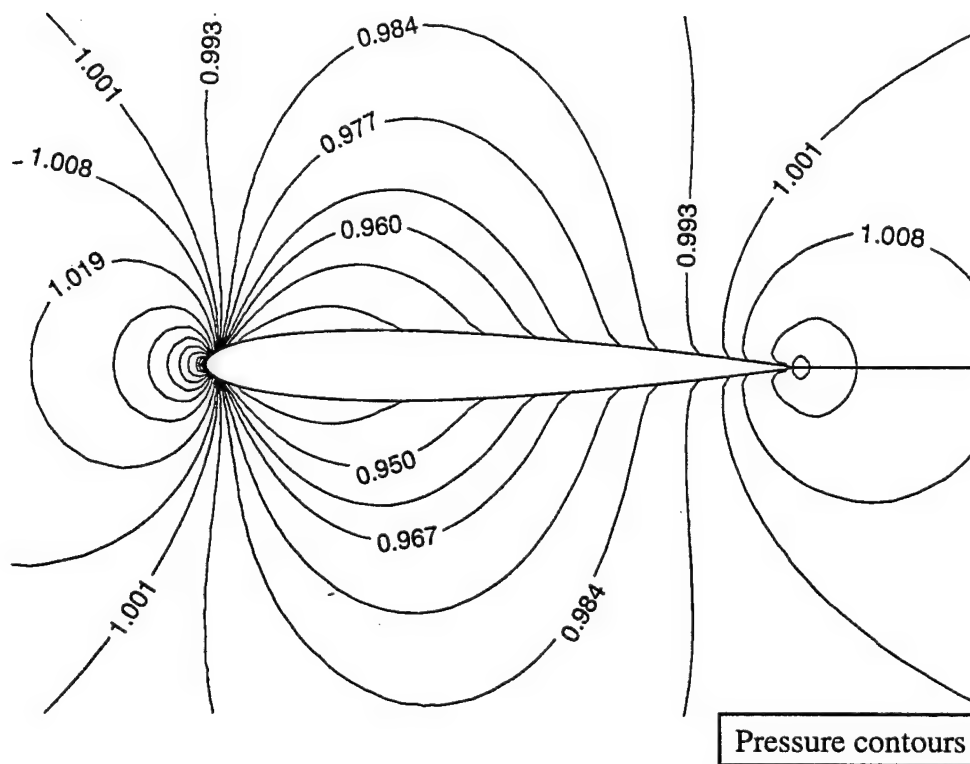
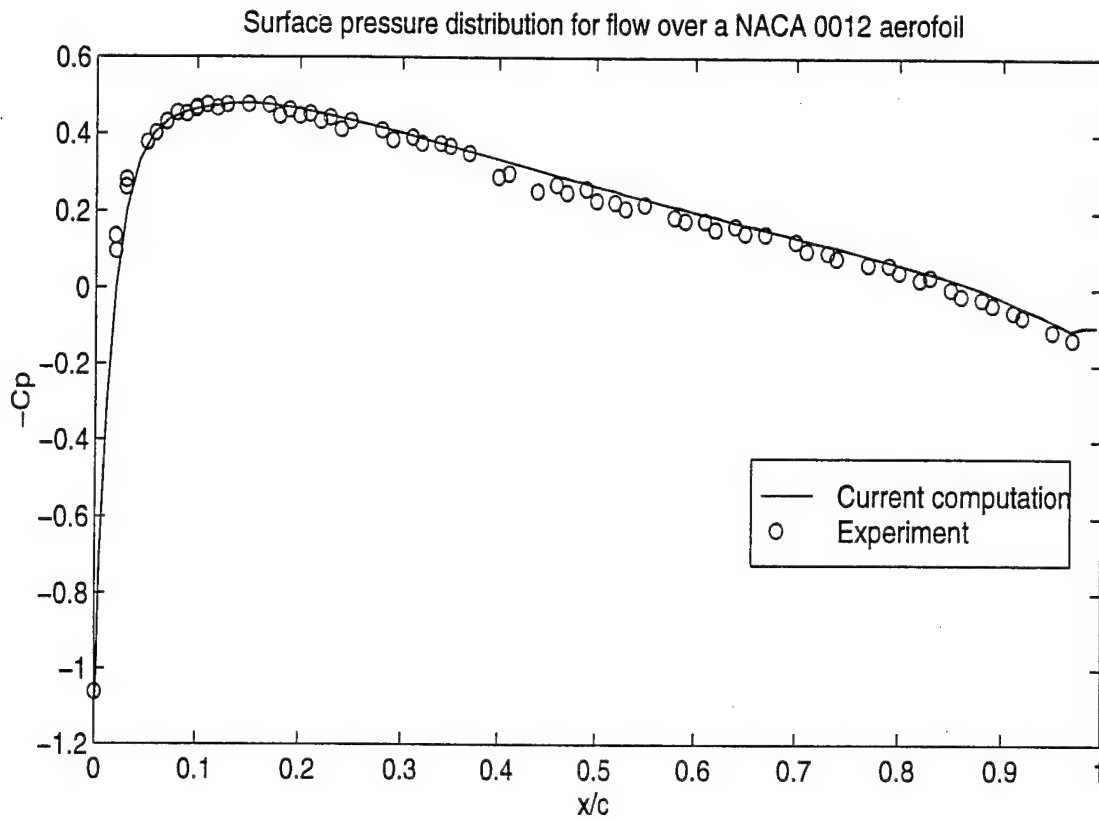


Figure 4.8 Validation of computational code for turbulent flow past a NACA0012 aerofoil.  $M_\infty = 0.5$ ,  $Re = 2.89 \times 10^6$ ,  $\alpha = 0.0$  degrees.

To further validate the code for turbulent flow computations a test, of the computational capability in predicting a sub-critical flow past the high lift RAE-2822 aerofoil, was conducted. The grid used for these computations had 221 grid points in the  $i$ -direction and 61 points in the  $j$  direction. The non-dimensional distance of the first grid point, away from the aerofoil surface, was about  $y^+ \approx 40$ . The free-stream conditions were a Mach number  $M_\infty = 0.676$  and a Reynolds number  $Re_\infty = 5.7 \times 10^6$  at an angle of attack of  $\alpha = 2.40$ . The results from this computation were compared with experimental data. The comparison indicates that the accuracy of the computations are indeed quite good. The surface pressure distribution and the pressure distribution for this case are shown in Figure 4.9.

#### 4.2.2 Nozzle Flow Computations

With the code validated for external flow field computations, we proceeded to validate the code for a set of internal flow computations. For this case, we chose the flow through a converging-diverging nozzle. This flowfield is characterized by multiple shock reflections and interactions between the compression waves and the viscous shear layer. The computations were compared against experimental measurements. Three different area ratios were tested to ascertain the computational validity of the code. A brief description of the boundary conditions used for this set of calculations and the computational grid used is given below.

The nozzle geometry is sketched in figure 4.10 below. There are essentially an inflow boundary, an outflow boundary and a solid boundary at the top and bottom of the nozzle wall. At the inflow boundary the inlet Mach number, the total pressure and the total temperature were held constant. The angle of attack at the inflow is specified to be  $0^\circ$ . At the outflow boundary, since the flow is supersonic, the variables are extrapolated. At the solid boundary, the no-slip condition is specified and also there is no heat transfer at the walls.

The nozzle area-ratio is defined as the ratio of the nozzle exit plane area to the area at the throat.. For a two-dimensional nozzle this works out to be, for unit depth into the paper,

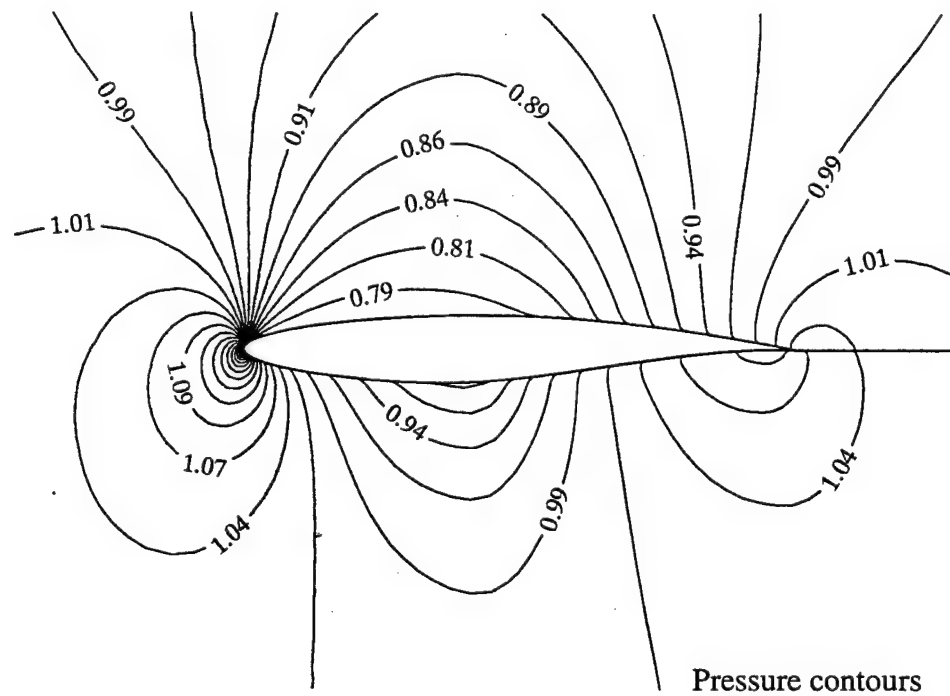
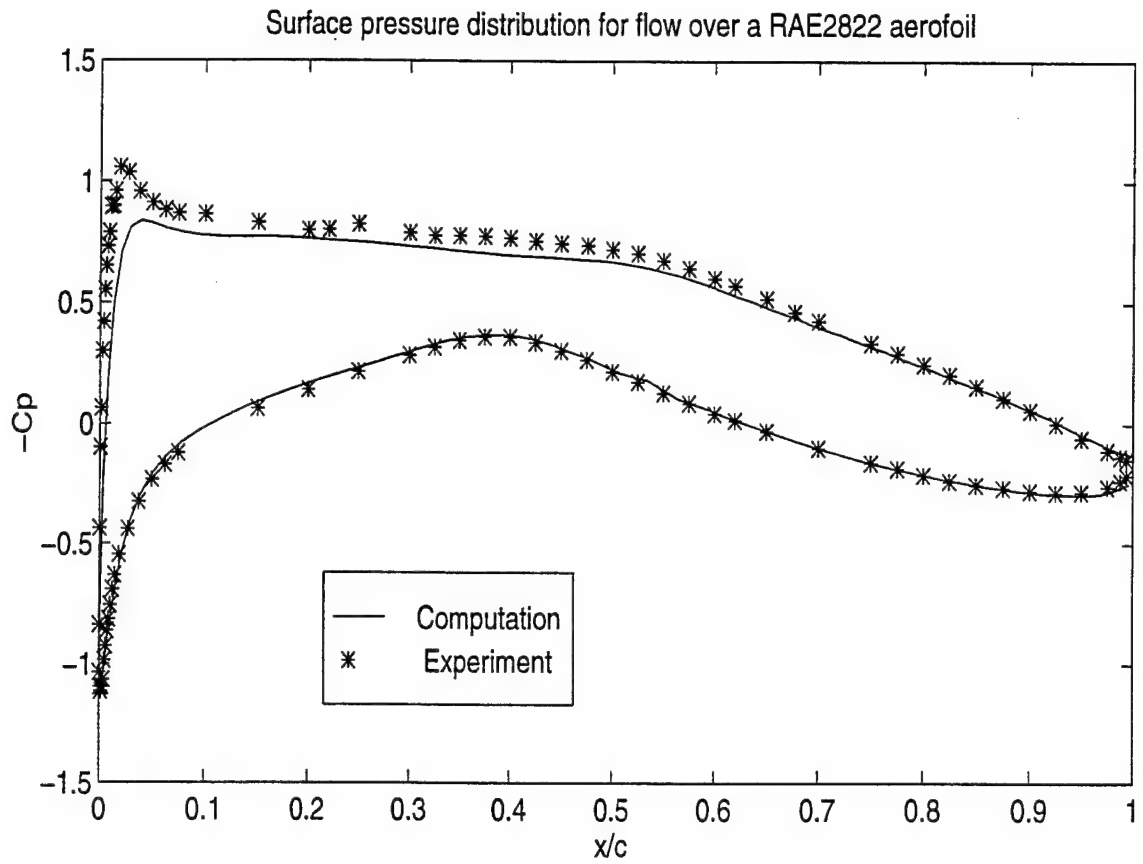
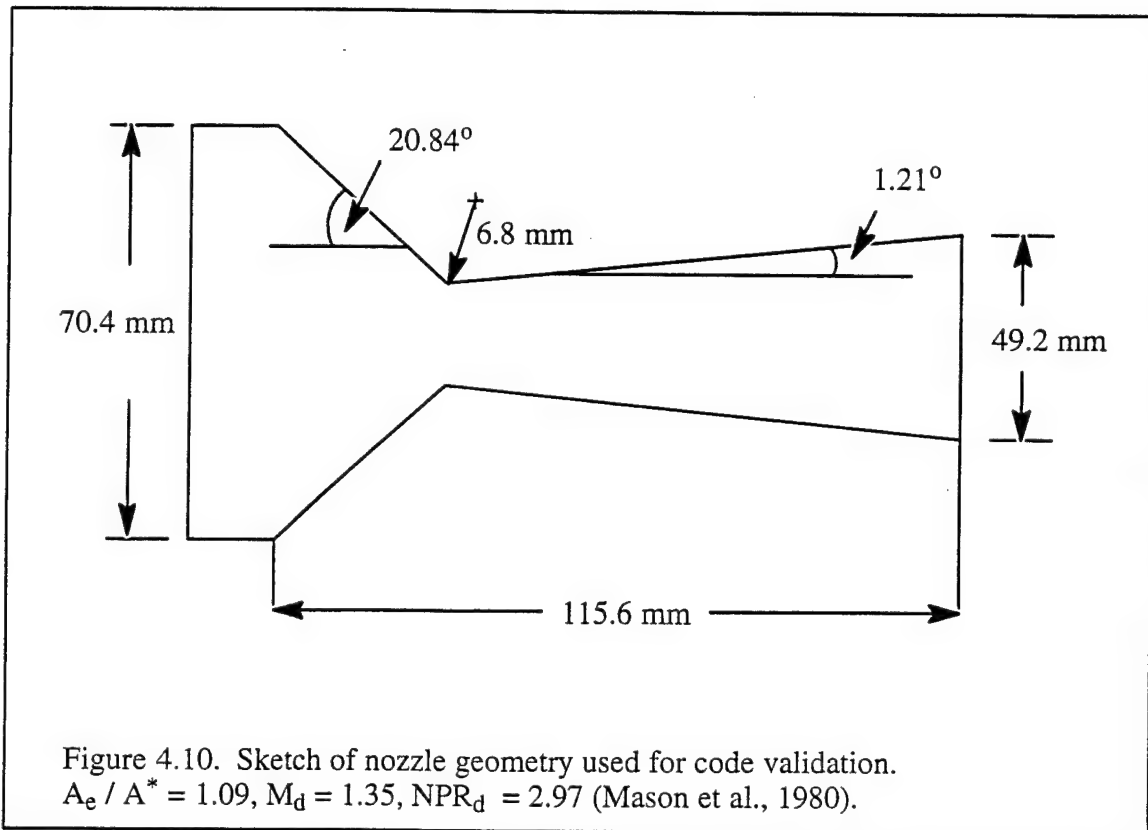


Figure 4.9 Computation of turbulent flow past a RAE 2822 aerofoil :  
 $M_\infty = 0.676$  ,  $Re = 5.7 \times 10^6$  ,  $\alpha = 2.4$



the ratio of the height at the exit plane to the height at the throat, that is (with reference to Figure 4.10), the area ratio =  $A_{\text{exit}} / A^*$ . For this validation study, three different area ratios were tested. One was for an area ratio of 1.3 and the other for an area ratio of 3.5. The inflow Mach number is 0.3 and the inflow Reynolds number is  $5.807 \times 10^6$ .

To validate the computational predictions against experimental data, another set of computations were done of the flow through the converging-diverging nozzle geometry sketched in Figure 4.10. Figure 4.10 shows a sketch of the nozzle geometry used in the code validation study. The experimental data for this study is available in Mason et al. [1980]. The pressure distribution on the upper wall of the nozzle is shown in Figure 4.11. The comparison between experimental measurements and computational predictions is quite good. Contours of static pressure distribution in the nozzle flow field are also shown in Figure 4.11.

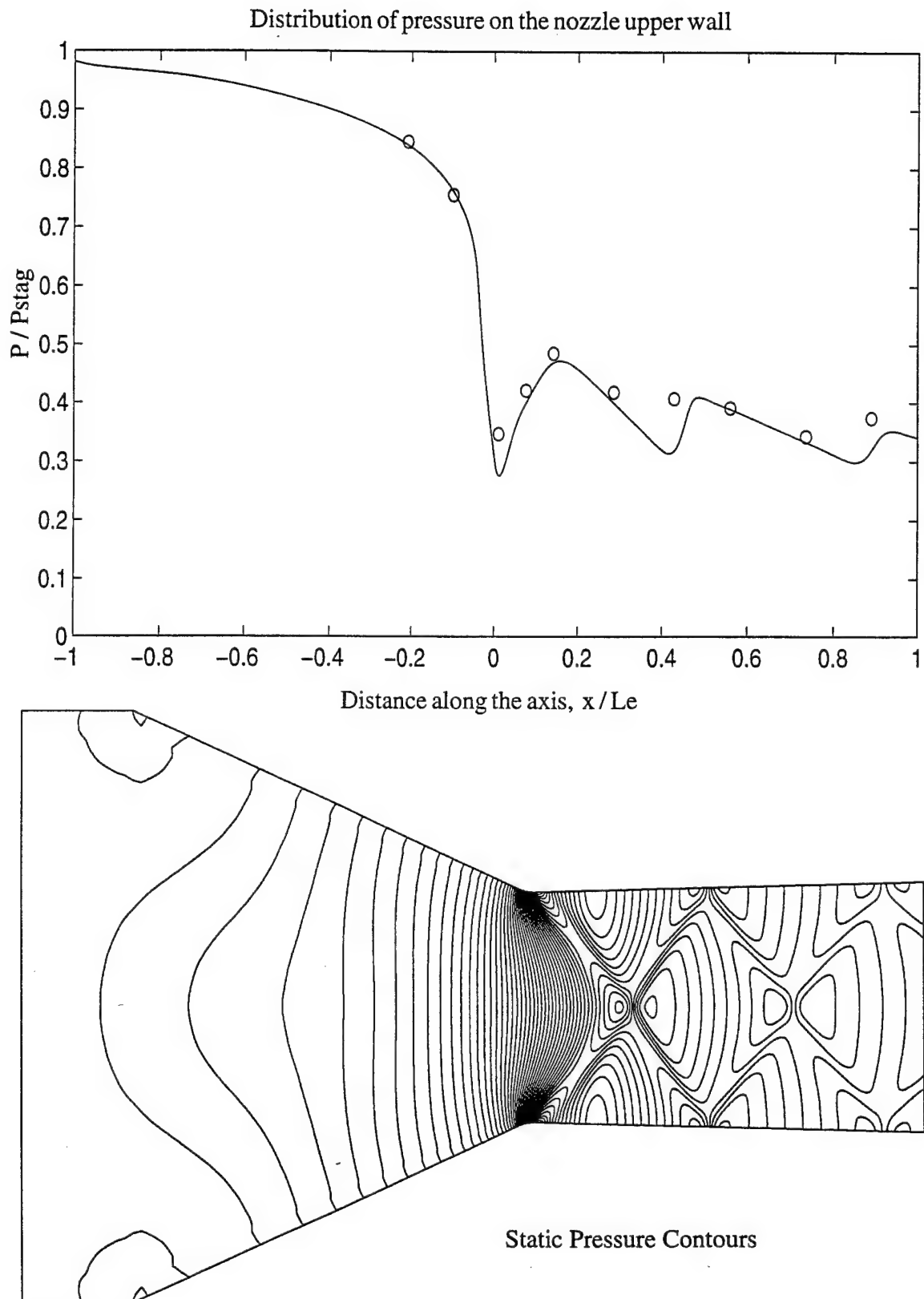


Figure 4.11. Computation of flow through a converging-diverging nozzle,  $M_d = 1.36$ ,  $NPR_d = 2.97$ .

### 4.3 Summary

In this chapter, we have presented the numerical algorithm that was used in the computational study. A brief description of the finite-volume scheme, the time-stepping and the artificial-dissipation schemes used in the computations is presented. The drawbacks of the artificial-dissipation schemes have been highlighted. The results from a code validation study, of this numerical algorithm, for a variety of test cases has been given. The results indicate the accuracy of the code and validate the use of this computational procedure in calculating other flow fields to be presented in the following chapters.

Additionally, grid independency tests (to be presented in Chapter 5) have been performed for the axi-symmetric afterbody flowfield have been performed. In that case the predictions made by the second-order, "artificial-dissipation" schemes were compared against those made using the second-order upwind scheme. The study indicated that for the afterbody flowfield, the second-order upwind scheme offers an improvement (in terms of solution accuracy) over the artificial-dissipation schemes. With this in mind, all the computational results to be presented in the following chapters have been obtained using the upwind scheme.



## CHAPTER 5

### k- $\epsilon$ BASED MODELLING OF COMPRESSIBLE TURBULENT FLOWS

The effect of compressibility on the turbulence structure is an important but difficult issue in turbulence modelling. Modelling issues in both the production and dissipation of turbulent kinetic energy need to be addressed to account for Mach number effects. Several proposed treatments dealing with the dilatation dissipation and the pressure dilatation correlation are discussed in the context of the two-equation model. Two new modifications are investigated, to account for the extra source terms that appear in the turbulence transport equations for compressible flows. Additionally, the effectiveness of proposed modifications to allow the dissipation rate to respond to the mean strain rate more effectively, are analyzed.

#### 5.1 Introduction

Compressibility refers to the fluctuations in the volume of the fluid cell corresponding to the fluctuations in pressure. The effect compressibility has on the turbulence structure (i.e., the various correlation coefficients and energy spectrum etc.) is of importance in the accurate modelling of compressible flows. Compressible turbulent shear layers are characterized by a marked reduction in growth rates (in comparison to incompressible shear layers) but retain the structure of their incompressible counterparts (see Chapter 2 for a review of compressibility effects on turbulent shear layers).

Direct Numerical Simulation (DNS) results obtained have helped in understanding some of the effects that compressibility has on the turbulence structure (Lele, 1994). But DNS is still not a feasible method in computing flow fields of engineering interest. DNS results have, however, helped in identifying a parameter that could be used to characterize the importance of compressibility on the turbulent fluctuations. This is the turbulent Mach

number, defined as the ratio of a characteristic speed of turbulence to the wave speed. Thus,  $M_t = \frac{\sqrt{2k}}{a}$ , where  $k$  is the Turbulent Kinetic Energy and  $a$  is the speed of sound.  $M_t$  is a non-dimensional parameter, a field variable representing the propagation of information by turbulent fluctuations in comparison to the acoustic propagation. DNS results have also helped in the formulation of modifications to account for the observed effects of compressibility as a function of the turbulent Mach number. These will be presented in the subsequent sections of this chapter. In computing flowfields involving a certain degree of complexity the two-equation models offer a viable alternative in terms of computational ease (Speziale, 1992). A review of the predictive capabilities of two-equation based closures is given in Chapter 3. Here the  $k$ - $\epsilon$  model is used to achieve turbulence closure.

## 5.2 Governing Equations

In the solution of turbulent flow fields the variables are usually split into a mean and a fluctuating part. The mean can be defined in one of two ways: 1) Reynolds average, or 2) Favre average. In solving for compressible flows, the use of Reynolds average introduces correlations involving density fluctuations and the modelling of these correlations is difficult. In order to overcome this a combination of Reynolds and mass weighted Favre average is used. The advantage in doing this is that the governing equations bear a close resemblance to their incompressible counterparts. Therefore incompressible methodologies can, with little modifications, be used in solving for compressible turbulent flows. Modelling of the correlations can be accomplished in a variety of ways. The exact form of the governing equations in their averaged form was presented in Chapter 3. These equations are repeated here for convenience. Additionally, terms that are important for compressible turbulent flows (as different from incompressible flows) are identified and the modelling of these terms is discussed.

The governing equations are the equations representing conservation of mass, momentum and energy. The averaged form of the equations are given below, where density and pressure are Reynolds averaged while Favre averaging is used to define the mean of the

velocity components and temperature. A tilde denotes a Favre averaged quantity and a (') denotes fluctuations with respect to the Favre mean. An overbar denotes a Reynolds average and a (') denotes fluctuations with respect to it. The variables are split up into their mean and fluctuating part as given below in equation 5.1:

$$\begin{aligned}\rho &= \bar{\rho} + \rho' \\ u_i &= \tilde{U}_i + u_i'' \\ T &= \tilde{T} + T'' \\ p &= P + p'\end{aligned}\quad (5.1)$$

where  $\rho$ ,  $u_i$ ,  $T$ , and  $p$  refer to the instantaneous density, velocity, temperature and pressure respectively.  $P$  refers to the Reynolds averaged pressure. The exact form of the governing equations, using the mixed averaging technique, is given as follows :

#### Continuity

$$\frac{\partial}{\partial t}(\bar{\rho}) + \frac{\partial}{\partial x_j}(\bar{\rho}\tilde{U}_j) = 0 \quad (5.2)$$

#### Momentum

$$\frac{\partial}{\partial t}(\bar{\rho}\tilde{U}_j) + \frac{\partial}{\partial x_j}(\bar{\rho}\tilde{U}_i\tilde{U}_j) = -\frac{\partial P}{\partial x_i} + \frac{\partial}{\partial x_j}[\Sigma_{ij} + \overline{\sigma_{ij}''} - \overline{\rho u_i'' u_j''}] \quad (5.3)$$

#### Energy

$$\begin{aligned}\frac{\partial}{\partial t}(\bar{\rho}\tilde{E}) + \frac{\partial}{\partial x_j}(\bar{\rho}\tilde{U}_j\tilde{H}) &= \frac{\partial}{\partial x_j} \left[ \tilde{U}_j \left( \Sigma_{ij} + \overline{\sigma_{ij}''} - \overline{\rho u_i'' u_j''} \right) + \overline{u_i'' \Sigma_{ij}} + \overline{u_i'' \sigma_{ij}''} - \bar{q}_j \right] \\ &\quad - \overline{q_j''} - \overline{\rho u_j'' h''} - \overline{\rho u_j'' \left( \frac{1}{2} u_i'' u_i'' \right)} \end{aligned} \quad (5.4)$$

#### Turbulent Kinetic Energy (TKE)

$$\begin{aligned}\frac{\partial}{\partial t}(\bar{\rho}k) + \frac{\partial}{\partial x_j}(\bar{\rho}\tilde{u}_j k) &= -\overline{\rho u_i'' u_j''} \frac{\partial \tilde{U}_i}{\partial x_j} - \overline{u_i''} \frac{\partial P}{\partial x_i} + \overline{u_i''} \frac{\partial \Sigma_{ij}}{\partial x_j} + \\ &\quad \frac{\partial}{\partial x_j} \left[ \overline{u_i'' \sigma_{ij}''} - \overline{\rho u_j'' \left( \frac{1}{2} u_i'' u_i'' \right)} - \overline{p' u_j''} \right] + \overline{p' \frac{\partial u_i''}{\partial x_i}} - \overline{\frac{\partial u_i''}{\partial x_j} \sigma_{ij}''} \end{aligned} \quad (5.5)$$

where

$$\Sigma_{ij} = 2\mu S_{ij} + \lambda \tilde{U}_{k,k} \delta_{ij} ; S_{ij} = \frac{1}{2} (\tilde{U}_{i,j} + \tilde{U}_{j,i}) \quad (5.6)$$

$$\overline{\sigma_{ij}''} = 2\mu s_{ij} + \lambda \overline{u_{k,k}''} \delta_{ij} ; s_{ij} = \frac{1}{2} (\overline{u_{i,j}''} + \overline{u_{j,i}''}) \quad (5.7)$$

Following the assumption that there are regions in the flow field where molecular properties are more important, terms such as  $\overline{\sigma_{ij}''}$ ,  $\overline{q_j''}$ ,  $\overline{u_i''} \Sigma_{ij}$  and  $\overline{u_i''} \frac{\partial \Sigma_{ij}}{\partial x_j}$ , in the above equations are neglected. Rewriting the modified governing equations, we have

### Continuity

$$\frac{\partial}{\partial t}(\bar{\rho}) + \frac{\partial}{\partial x_j}(\bar{\rho} \tilde{U}_j) = 0 \quad (5.8)$$

### Momentum

$$\frac{\partial}{\partial t}(\bar{\rho} \tilde{U}_j) + \frac{\partial}{\partial x_j}(\bar{\rho} \tilde{U}_i \tilde{U}_j) = - \frac{\partial P}{\partial x_i} + \frac{\partial}{\partial x_j} \left[ \Sigma_{ij} - \frac{\overline{\rho u_i'' u_j''}}{A} \right] \quad (5.9)$$

### Energy

$$\frac{\partial}{\partial t}(\bar{\rho} \tilde{E}) + \frac{\partial}{\partial x_j}(\bar{\rho} \tilde{U}_j \tilde{E}) = \frac{\partial}{\partial x_j} \left[ \tilde{U}_j \left( \Sigma_{ij} + \frac{\overline{\sigma_{ij}''}}{B} - \frac{\overline{\rho u_i'' u_j''}}{C} \right) + \frac{\overline{u_i'' \sigma_{ij}''}}{D} - \tilde{q}_j \right] \\ - \frac{\overline{\rho u_j'' h''}}{E} - \frac{\overline{\rho u_j'' \left( \frac{1}{2} u_i'' u_i'' \right)}}{F} \quad (5.10)$$

### Turbulent Kinetic Energy

$$\frac{\partial}{\partial t}(\bar{\rho} k) + \frac{\partial}{\partial x_j}(\bar{\rho} \tilde{U}_j k) = - \frac{\overline{\rho u_i'' u_j''}}{G} \frac{\partial \tilde{U}_i}{\partial x_j} - \frac{\overline{u_i''}}{H} \frac{\partial P}{\partial x_i} - \frac{\overline{\partial u_i''}}{\partial x_j} \sigma_{ij}'' + \\ \frac{\partial}{\partial x_j} \left[ \frac{\overline{u_i'' \sigma_{ij}''}}{J} - \frac{\overline{\rho u_j'' \left( \frac{1}{2} u_i'' u_i'' \right)}}{K} - \overline{p' u_j''} \right] + \overline{p' \frac{\partial u_i''}{\partial x_i}} \quad (5.11)$$

where  $k$  represents the turbulent kinetic energy and is equal to  $k = \frac{\overline{\rho u_i'' u_i''}}{\bar{\rho}}$ .

In the above equations, the terms that need to be modelled are indicated by an underscore and are denoted as terms A through K. The current modelling procedure (of these terms) based on the k- $\epsilon$  model is given below.

Terms A, C and G : These are the Reynolds stress terms. They are modelled as

$$-\overline{\rho u_i'' u_j''} \approx 2\mu_t S_{ij} + \lambda_t \frac{\partial \bar{U}_k}{\partial x_k} \delta_{ij} - \frac{2}{3} \rho k \delta_{ij} \quad (5.12)$$

where  $S_{ij}$  is defined in equation 5.6.  $\mu_t$  is the eddy viscosity and  $\lambda_t = -\frac{2}{3}\mu_t$ . Throughout the rest of this dissertation we will use capitalized notation to indicate averaged quantities (except for density, where  $\rho$  will denote the average value). Implicit in the notation used is that the pressure and density are Reynolds averaged while the velocity components and temperature are Favre averaged.

Terms D, F and J : These terms represents the diffusion of energy due to turbulent fluctuations and are modelled as

$$\overline{u_i'' \sigma_{ij}''} - \overline{\rho u_j'' \left( \frac{1}{2} u_i'' u_i'' \right)} \approx \frac{\mu_t}{\sigma_k} \frac{\partial k}{\partial x_j} \quad (5.13)$$

The effect of the term  $\overline{p' u_j''}$  on the rate of change of TKE is not explicitly accounted for and is included in the model for the diffusion terms given in equation 5.13.

Term E : This represents the turbulent heat flux and using the Reynolds' analogy (Schlichting, 1968) this term is modelled as

$$-\overline{\rho u_j'' h''} = \frac{\mu_t}{Pr_t} \frac{\partial T}{\partial x_j} \quad (5.14)$$

where  $Pr_t$  is the turbulent Prandtl number and is usually specified to be equal to 0.9.

Term I : This term represents the rate of dissipation of turbulent kinetic energy due to molecular effects and is solved for via a transport equation. That is,

$$\frac{\partial \overline{u_i'' u_i''}}{\partial x_j} \sigma_{ij}'' = \rho \epsilon \quad (5.15)$$

We will return to this definition of  $\epsilon$  when we discuss the dissipative effects of compressibility.

In the k- $\epsilon$  based modelling, transport equations for k and  $\epsilon$  are solved. With these a characteristic velocity scale and a length scale can be identified resulting in the following definition for eddy-viscosity.

$$\mu_t = C_\mu \frac{\rho k^2}{\epsilon} \quad \text{where } C_\mu = 0.09 \quad (5.16)$$

### 5.3 Modelling of Compressibility Effects

In the equations governing the compressible turbulent flow field, terms can be identified which are of relevance and different from those of incompressible flows (see Table 5-1). From the governing equations given above, the terms that are unique to compressible turbulent flows (and not accounted for in “incompressible” models) are:  $\overline{\sigma_{ij}''}$ ,  $\overline{p' \frac{\partial u_i''}{\partial x_i}}$  and  $\overline{u_i'' \frac{\partial P}{\partial x_i}}$ , in addition to the dilatational effects on the rate of dissipation of TKE.  $\overline{\sigma_{ij}''}$  is purely a result of Favre averaging and at low Mach numbers it does not represent compressibility effects (Lele, 1994). Therefore, in order to close the system of equations we need to suitably account for  $\overline{p' \frac{\partial u_i''}{\partial x_i}}$  and  $\overline{u_i'' \frac{\partial P}{\partial x_i}}$ . We will refer, henceforth, to the first term as the pressure dilatation term and the second term as the enthalpic production term. Before we discuss the modifications that have been proposed for the pressure dilatation term, let us consider the effects of compressibility on the rate of dissipation of TKE,  $\epsilon$ .

#### 5.3.1 Dilatation Dissipation

From a DNS analysis of compressible flows Sarkar et al. [1991] and Zeman [1990], concluded that the effect of compressibility on the turbulence structure was a dissipative one. Compressibility introduces an extra amount of dissipation (of the turbulent fluctuations) due to the non-divergent nature of the velocity fluctuations, as can be seen by examining the definition of the rate of dissipation of TKE. Following the definition of  $\epsilon$  given above in equation 5.15, we get (Zeman, 1990 and Sarkar et al., 1991) :

Table 5–1. Terms representing the effect of compressibility on the structure of turbulence.

Terms	Proposed Modifications	Advantages / Drawbacks
1. Dilatation Dissipation ( $\epsilon_d$ )	(a) Sarkar et al. [1991] – (Eqn. 5.30) (b) Zeman [1990] – (Eqn. 5.27) (c) El Baz and Launder [1993] – (Eqn. 5.31)	Zemans' modification requires information regarding the kurtosis of the fluctuations, which is not available in general. Both models do a good job in predicting the growth rates of mixing layers, but fail to predict the correct variations in skin friction coefficient in the case of wall boundary layers, (Wilcox, 1992).
2. Pressure Dilatation ( $\overline{p'd''}$ )	(a) Sarkar [1992] – (Eqn. 5.38) (b) Zeman [1992] – (Eqn. 5.44) (c) El Baz and Launder [1993] – (Eqn. 5.46) (d) Current [1992] – (Eqn. 5.63) (e) Rubesin [1991]	Models (a) and (c) were intended for the mixing layer. When applied to boundary layers, they yield reduced levels of TKE which is an undesirable outcome, (Huang et al. 1994). Model (b) improves the prediction of log-law profiles. Model (e) makes the system of equations very stiff and difficult to solve, (Huang et al. 1994).
3. Turbulent Mass Flux ( $\overline{u_i''}$ )	(a) Rubesin [1991] (b) Ristorcelli [1993] (c) Current (Eqn. 5.56)	Model (a) introduces an ad hoc assumption regarding the fluctuating enthalpy and requires prescription of a polytropic constant. Model (b) has not been tested.
4. Enthalpic Production ( $\overline{u_i'' dP/dx_i}$ )	Current Work	Model for $\overline{u_i''}$ enables us to compute this production term, but the model still needs to be validated, in particular for a flowfield where compressibility is an important issue.

$$\rho \epsilon = \overline{\frac{\partial u_i''}{\partial x_j} \sigma_{ij}''} \quad (5.17)$$

The fluctuating component of the viscous stresses  $\overline{\sigma_{ij}''}$ , is defined as in equation 5.7.

Assuming the fluctuations in molecular viscosity are negligible we can write

$$\rho \epsilon = 2\mu \overline{s_{ij}s_{ij}} - \frac{2}{3}\mu \overline{u_{k,k}'' u_{k,k}''} \quad (5.18)$$

where the comma is used to denote a derivative. Denoting the dilatation of the velocity fluctuations as  $d'' = \frac{\partial u_k''}{\partial x_k}$  we can write

$$\rho \varepsilon = \mu \left( 2 \overline{s_{ij} s_{ij}} - \frac{2}{3} \overline{d''^2} \right) \quad (5.19)$$

where  $\mu$  represents the coefficient of molecular viscosity. If we define the fluctuating vorticity vector as,  $\omega_p'' = (u_{ij}'' - u_{ji}'')$  we can obtain the relationship,

$$\overline{s_{ij} s_{ij}} = \frac{1}{2} \overline{\omega_p'' \omega_p''} + \overline{u_{ij}'' u_{ji}''} \quad (5.20)$$

Substituting this relationship into equation 5.19, we obtain

$$\rho \varepsilon = \mu \left( \overline{\omega_p'' \omega_p''} + 2 \overline{u_{ij}'' u_{ji}''} - \frac{2}{3} \overline{d''^2} \right) \quad (5.21)$$

The second term on the right hand side in equation 5.21 satisfies the following relation (Sarkar et al., 1991)

$$\overline{u_{ij}'' u_{ji}''} = \left( \overline{u_i'' u_j''} \right)_{,ij} - 2 \left( \overline{u_{i,i}'' u_{j,j}''} \right) + \overline{u_{i,i}'' u_{j,j}''} \quad (5.22)$$

For homogeneous turbulent flows, this relationship reduces to

$$\overline{u_{ij}'' u_{ji}''} = \overline{u_{i,i}'' u_{j,j}''} = \overline{d''^2} \quad (5.23)$$

Combining this with equation 5.21, we obtain

$$\rho \varepsilon = \mu \left( \overline{\omega_p'' \omega_p''} - \frac{4}{3} \overline{d''^2} \right) \quad (5.24)$$

The dissipation rate (of TKE) in compressible turbulent flows can be, therefore, written as a sum of a “solenoidal” dissipation rate (the first term on the right hand side of equation 5.24) and a “dilatational dissipation” rate. Thus,

$$\rho \varepsilon = \rho (\varepsilon_s + \varepsilon_d) \quad (5.25)$$

where

$$\rho \varepsilon_s = \mu \overline{\omega_p'' \omega_p''} \quad ; \quad \rho \varepsilon_d = \frac{4}{3} \mu \overline{d''^2} \quad (5.26)$$

The solenoidal dissipation rate can be thought of as the dissipation due to the regular process of cascading of energy to the smaller scales and in the absence of dilatational effects



it can be considered to be equivalent to the “incompressible” dissipation rate. The dilatational dissipation (also referred to as compressible dissipation) is due to the non-divergent nature of the velocity fluctuations.

#### 5.3.1.1 Zeman modification

Zeman [1990], assumed the presence of eddy shocklets in the compressible turbulent flow field (Passot and Pouquet, 1987) and that these eddy shocklets directly affected the dilatational dissipation rate,  $\epsilon_d$ , but not the solenoidal dissipation rate. Proceeding to model this dissipation rate as a function of a probability density function of the fluctuations in velocity he assumed that the variance of these fluctuations was equal to a non-dimensional parameter called the turbulent Mach number,  $M_t$ , which is defined as  $M_t = \frac{\sqrt{2k}}{c}$ . The turbulent Mach number is a field quantity and represents a ratio of the propagation of information by turbulence to acoustic propagation, with the turbulent kinetic energy providing a characteristic velocity scale at which turbulent fluctuations transfer information. The model proposed by Zeman [1990], for the dilatational dissipation rate is given below:

$$\epsilon_d = c_d \epsilon_s F\{M_t, K\} \quad (5.27)$$

where  $c_d$  is an adjustable constant of order one and  $K$  is the kurtosis of the fluctuations. The function  $F\{M_t, K\}$  is given as,

$$F\{M_t, K\} = \left[ \frac{1}{M_t^4} \int_1^\infty \left( \frac{m_1^2 - 1}{m_1} \right)^3 p(m_1) dm_1 \right] \quad (5.28)$$

where  $p(m_1)$  is an assumed non-Gaussian pdf. Also,  $m_1 = \frac{u}{a^*}$ , where  $u$  is the velocity fluctuation ahead of the shocklet, and  $a^*$  is the sonic speed. This expression was further approximated, (for computational ease), as

$$\begin{aligned} F(M_t) &= 1 - \exp\left\{-[(M_t - 0.1)/0.6]^2\right\} \\ \text{and} \\ F(M_t) &= 0, \text{ if } M_t < 0.1 \end{aligned} \quad (5.29)$$

### 5.3.1.2 Sarkar et al. modification

Sarkar et al. [1991] considered the evolution of the turbulence fluctuations on an acoustic time scale. They considered the effect of varying compressibility, based on the turbulent Mach number,  $M_t$ , on the rate of dissipation of TKE  $\epsilon$ . Analysis of decaying compressible turbulence indicated that the impact of varying compressibility on the solenoidal component of the dissipation rate, ( $\epsilon_s$ ) was negligible in comparison with the effect on the dilatational component, ( $\epsilon_d$ ). They also observed, that the ratio of dilatational dissipation rate to the solenoidal dissipation rate, that is,  $\left(\chi = \frac{\epsilon_d}{\epsilon_s}\right)$  varied directly as the square of the turbulent Mach number,  $M_t = \frac{\sqrt{2k}}{c}$ . Based on an analysis of the evolution of the fluctuations on an acoustic time scale, they proposed a model for the dilatational dissipation rate, which is given as,

$$\epsilon_d = \alpha_1 \epsilon_s M_t^2 \quad (5.30)$$

where  $\alpha_1$  is an arbitrary constant of  $\mathcal{O}(1)$ . The constant  $\alpha_1$  is determined from an analysis of the predictions made of decaying compressible turbulence.

### 5.3.1.3 El Baz modification

We will refer to the modification proposed by El Baz and Launder[1993] as the El Baz modification, through the rest of this dissertation. El Baz and Launder[1993] proposed a modification to account for this extra rate of dissipation due to compressibility effects. They chose to model one of the constants in the modelled form of the transport equation for  $\epsilon_s$ . The transport equation in its modelled form is given in Chapter 3, equation 3.45. In Chapter 3, we have discussed the estimation of the constant  $C_{\epsilon 2}$ . El Baz and Launder [1993] chose to modify the constant  $C_{\epsilon 2}$  to match the observed decay rate of compressible isotropic turbulence. Based on this observation, they modified this constant as

$$C_{\epsilon 2}' = \frac{C_{\epsilon 2}}{1 + 3.2M_t^2} \text{ where } M_t = \frac{\sqrt{k}}{a} \quad (5.31)$$

and used  $C_{\epsilon 2}'$  instead of  $C_{\epsilon 2}$  in the modelled form of the transport equation for  $\epsilon$ , given in equation 3.45.

#### 5.3.1.4 Comparison of dilatation dissipation modifications

All the modifications presented above are not very much different from one another. Recently Blaisdell et al. [1993], compared the predictive capabilities of the Sarkar et al. [1991] model and the model proposed by Zeman [1990]. From their study they concluded that the Sarkar et al. [1991] modification was marginally superior to that proposed by Zeman [1990]. Furthermore, they also raised the question regarding the applicability of both modifications in computing decaying compressible turbulence, because the decay rate they observed was very much dependent on the initial conditions.

To compare the modifications due to Sarkar et al. [1991] and El Baz and Launder [1993], we conducted numerical simulations of decaying compressible turbulence at three values of initial turbulent Mach number,  $M_{t0}$ . In the case of decaying isotropic compressible turbulence, the equations reduce to

Sarkar modification, (Sarkar et al., 1991) :

$$\frac{dk}{dt} = -\epsilon_s(1.0 + \alpha_1 M_t^2) \quad (5.32)$$

$$\frac{d\epsilon_s}{dt} = -C_{\epsilon 2} \frac{\epsilon_s^2}{k} \quad (5.33)$$

$$\frac{d(M_t^2)}{dt} = -\frac{\epsilon_s^2}{k} M_t^2 (1 + \alpha_1 M_t^2) [1 + 0.5\gamma(\gamma - 1)M_t^2] \quad (5.34)$$

El Baz modification, (El Baz and Launder, 1993) :

$$\frac{dk}{dt} = -\epsilon_s \quad (5.35)$$

$$\frac{d\epsilon_s}{dt} = -\left(\frac{C_{\epsilon 2}}{1 + 3.2M_t^2}\right) \frac{\epsilon_s^2}{k} \quad (5.36)$$

$$\frac{d(M_t^2)}{dt} = -\frac{\epsilon_s^2}{k} M_t^4 [1 + 0.5\gamma(\gamma - 1)M_t^2] \quad (5.37)$$

The above equations describe the evolution of the turbulence field. These equations were solved using a second-order Runge-Kutta scheme for various values of the initial Mach number,  $M_{t,0}$ . The model coefficient  $C_{\epsilon 2}$ , was chosen to be 1.83, in order to reproduce the observed decay rate in the case of high Reynolds number incompressible turbulence.

The decay of TKE is shown in Figure 5.1. In the figure,  $k_0$  and  $(\epsilon_s)_0$  refer to the initial values of TKE and the solenoidal dissipation rate, respectively. As Sarkar et al. [1991] point out, these computed values should not be compared with DNS simulations but just used to evaluate the decay rate of the TKE predicted by the two different modifications. For the lower Mach number cases, the two modifications predict the same initial decay rate. But at a later time, the El Baz and Launder [1993] modification does seem to predict a slightly greater reduction in the TKE. There are, however, distinct differences between the modifications for the initial turbulent Mach number of 0.5, which in free shear layers corresponds to a free stream Mach number of 10.

### 5.3.2 Pressure Dilatation

The pressure dilatation  $\overline{p'd''}$  where,  $d'' = \frac{\partial u_k''}{\partial x_k}$ , is one of the terms that appears explicitly in the governing equations, in the case of compressible turbulent flows, due to the non-divergent fluctuating velocity field. The pressure dilatation refers to the work done due to simultaneous fluctuations in the volume of the fluid cell corresponding to the fluctuations in pressure. It can be either positive or negative and when negative represents an extra dissipation.

Modifications have been proposed by Sarkar [1993], Zeman [1992] and El Baz and Launder [1993] to model the effect of this dilatational term.

#### 5.3.2.1 Sarkar modification

Sarkar [1992] conducted an analysis of the evolution of the pressure dilatation correlation in both decaying compressible turbulence and homogeneous shear turbulence. Writing a Poisson equation for the pressure fluctuations, the evolution of the incompressible

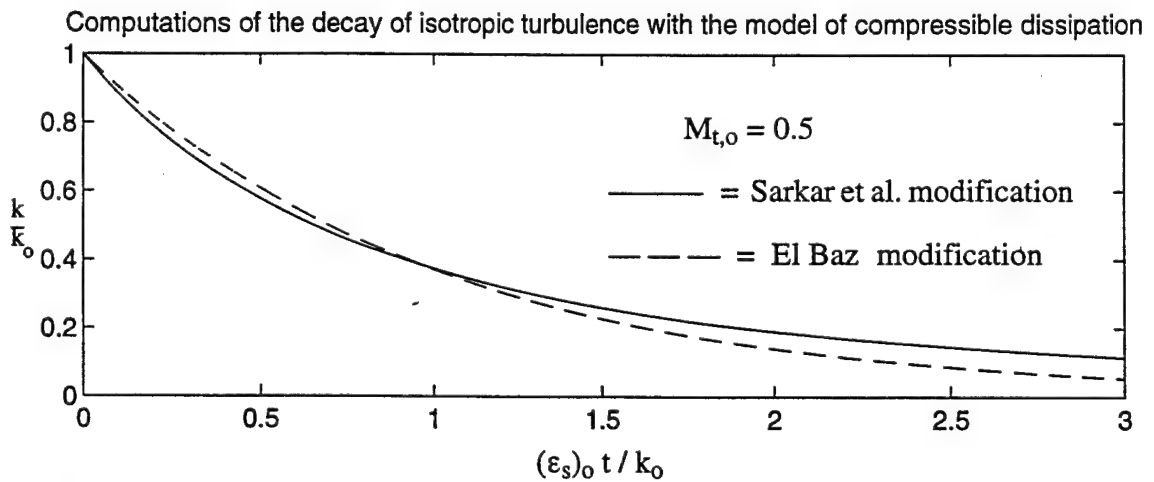
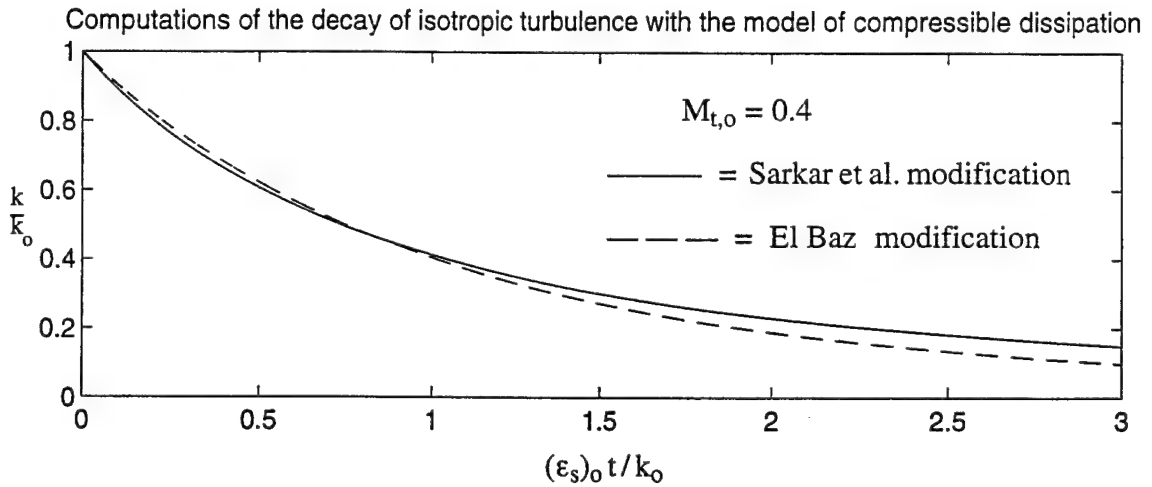
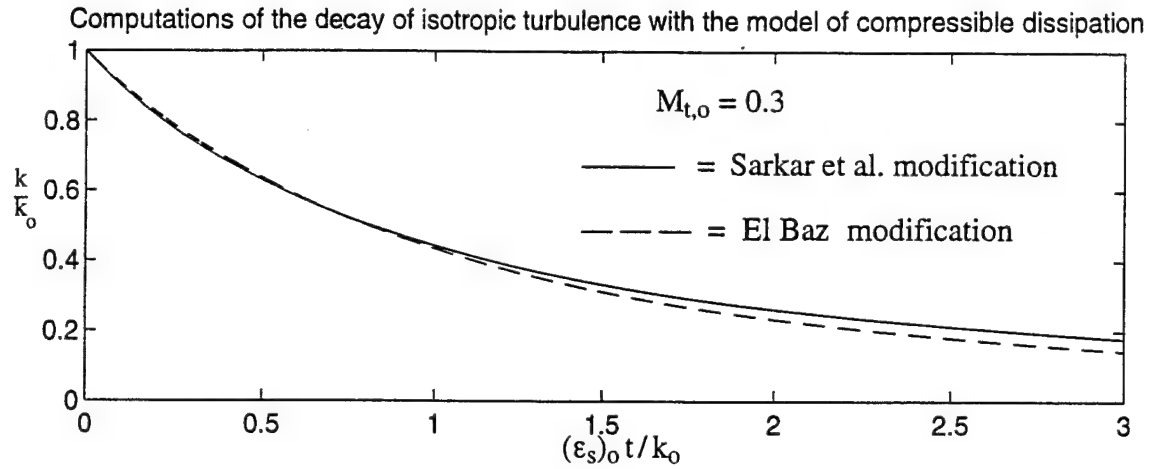


Figure 5.1 Computed decay of isotropic compressible turbulence using two different modifications for dilatational dissipation.

part and the compressible part of the pressure fluctuations was considered\*. Denoting the incompressible part of the pressure fluctuations as  $p_I'$  and the compressible part of the pressure fluctuations as  $p_c'$ , they considered the evolution of  $\overline{p_I' d''}$  and  $\overline{p_c' d''}$ . These studies seem to indicate that the  $\overline{p_I' d''}$  component of the pressure dilatation term was affected to a greater extent by compressibility than  $\overline{p_c' d''}$  (for both decaying and homogeneous shear turbulence). From an analysis of  $\overline{p_I' d''}$  (based on a decomposition of the pressure fluctuations into a rapid part and a slowly evolving part) they present modifications for the pressure dilatation term. The analysis did not take into account the contribution from  $\overline{p_c' d''}$  and was restricted by the assumption of homogeneity in the fluctuations, that is, spatial gradient of fluctuation correlations is equivalently zero. Borrowing ideas from the modelling of the pressure-strain correlations in incompressible turbulent flows the model for the pressure dilatation term is derived.

$$\overline{p' d''} = -\alpha_3 P_k M_t^2 + \alpha_4 Q \epsilon_s M_t^2 \quad (5.38)$$

where  $\alpha_3 = 0.4$ ,  $\alpha_4 = 0.2$  and  $M_t = \frac{\sqrt{2k}}{a}$ . In addition  $\alpha_1$  in equation 5.30 is set equal to 0.5. The constants are obtained from a curve fit of the model with DNS simulations.

#### 5.3.2.2 Zeman modification :

The model due to Zeman [1992] is based on the balance of the transport equation for the pressure fluctuation variance. That is,

$$\frac{1}{2} \frac{D \overline{p'^2}}{Dt} = -Q a^2 \overline{p' \frac{\partial u_i''}{\partial x_i}} - \gamma \overline{p'^2} \frac{\partial U_i}{\partial x_i} - a^2 \overline{p' u_j''} \frac{\partial Q}{\partial x_j} + \text{higher order terms} \quad (5.39)$$

Making an assumption that the variance in pressure fluctuations was small, Zeman [1992] neglected the second term on the right hand side. And assuming that the temporal variation of the pressure variance was negligible, he obtains a functional form for the pressure dilatation term.

\*Writing the Poisson equation for the pressure fluctuations, two groups of terms can be identified. The split up is based on the assumption that the mean density variations contribute to the evolution of the incompressible part of pressure fluctuations and the fluctuations in density and its gradients contribute to the evolution of the compressible part.

$$\overline{p' \frac{\partial u_i''}{\partial x_i}} = F \left\{ -\frac{1}{Q} \overline{p' u_j''} \frac{\partial Q}{\partial x_j} \right\} \quad (5.40)$$

Using the equation of state the pressure velocity correlation can be expressed as (Lele, 1994):

$$\overline{p' u_j''} = \frac{P}{Q} \overline{Q' u_j''} + \frac{P}{T} \overline{T'' u_j''} \quad (5.41)$$

With the model for the turbulent mass flux (first term on the right hand side of equation 5.41) and the model for the turbulent heat flux (second term on the right hand side of equation 5.41) he derives a model for the pressure dilatation term. The steps in this derivation are:

From Sarkar and Lakshmanan [1991]

$$\overline{Q' u_j''} = -\frac{\mu_t}{Q \sigma_Q} \frac{\partial Q}{\partial x_j} \quad (5.42)$$

where  $\sigma_Q = 0.7$

From the model for correlation between fluctuations in temperature and velocity

$$\overline{T'' u_j''} = -\frac{\mu_t}{Pr_t Q} \frac{\partial T}{\partial x_j} \quad \text{where } Pr_t = 0.9 \quad (5.43)$$

Substituting these two models into equation 5.41 and curve-fitting the model to DNS results (and invoking boundary layer assumptions) they obtain the final form of the pressure dilatation term as

$$\overline{p' d''} = g(M_t) \left( \frac{\partial Q}{\partial y} \right)^2 \frac{k a^2}{\epsilon Q} \overline{v'^2} \quad (5.44)$$

$$\text{where } g = 0.2 \left[ 1 - \exp \left( \frac{-M_t^2}{0.02} \right) \right] \quad (5.45)$$

where,  $M_t = \frac{\sqrt{2k}}{a}$ .

### 5.3.2.3 El Baz modification

The modification proposed by El Baz and Launder [1993] is referred to as the El Baz modification. The modification is largely based on the modelling of the pressure-strain correlation term in incompressible flows. Identifying (in a manner similar to the analysis of Sarkar, 1992) a rapid and a slowly evolving part of the pressure fluctuations, El Baz and

Launder [1993], proposed to model only the rapid evolution part (that is contribution to the evolution of the pressure fluctuations comes only from the mean strain). El Baz and Launder [1993] use a method similar to that prescribed by Launder, Reece and Rodi [1975] for modelling this term (for incompressible flows). The variation for compressibility comes via the introduction of a constant which is considered to be an intrinsic function of compressibility which vanishes in the incompressible limit. From a contraction of the model for the rapid part of the pressure-strain correlation they obtain a model for the pressure dilatation term as

$$\overline{p' \frac{\partial u_i''}{\partial x_i}} = F \left[ \frac{8}{3} \rho k \frac{\partial U_k}{\partial x_k} - P_k \right] \quad (5.46)$$

where  $F$  is the constant which is considered to be an intrinsic function of compressibility. This function  $F$  is assumed to be a function of the turbulent Mach number, that is,

$$F = \beta M_t^2 \quad ; \quad \text{where } M_t = \frac{\sqrt{k}}{a} \quad (5.47)$$

where  $\beta$  is an arbitrary constant whose value is prescribed to be 1.5

### 5.3.3 Proposed Modifications

The methodology predominantly used in computing compressible flow fields is to use Favre averages for velocity components and temperature and Reynolds average for pressure and density. The stress tensor and the heat flux vector are computed using Reynolds averages. The implicit assumption here is that the turbulence is homogeneous and therefore the turbulent mass flux and the fluctuating stress tensor are negligible. But as shown by Ristorcelli [1993]\*, this could be erroneous in the case of high supersonic and hypersonic flow fields. In order to accurately model the exact form of the governing equations (except for the dissipation rate transport equation) account must be made of the turbulent mass flux term. In what follows an expression is derived for the turbulent mass flux term. Two new

\*Ristorcelli [1993], refers to a DNS study of hypersonic boundary layer to show that the turbulent mass flux terms are quite substantial in comparison with the mean flow velocity components.



modifications are proposed to account for the enthalpic production term and a term to account for the effect of the baroclinic torque on the turbulent fluctuations.

### 5.3.3.1 Estimation of turbulent mass flux

The total enthalpy,  $H$ , in its instantaneous form can be written as :

$$H = h + \frac{1}{2}u_i u_i \quad (5.48)$$

where  $h$  is the static enthalpy and  $u_i$  are the components of the velocity vector. Both  $h$  and  $u_i$  are in their instantaneous form. Using Favre averages, equation 5.48 can be written in terms of mean and fluctuating quantities. The equation is then written as

$$\tilde{H} + H'' = \tilde{h} + h'' + \frac{1}{2}(U_i + u_i'')(U_i + u_i'') \quad (5.49)$$

Expanding the third term on the right hand side and rewriting the above equation, we get

$$\tilde{H} + H'' = \left[ \tilde{h} + \frac{1}{2}U_i U_i + \frac{1}{2}u_i'' u_i'' \right] + [h'' + u_i'' U_i] \quad (5.50)$$

In most modelling procedures, the average value of stagnation enthalpy,  $\tilde{H}$ , is associated with the first group of terms on the right hand side of equation 5.50. Fluctuations in stagnation enthalpy are associated with the second group of terms on the right hand side of equation 5.50. Making an assumption of constant stagnation enthalpy, an expression can be derived to relate the fluctuations in enthalpy to the turbulence intensity. From their experimental measurements of the flow past an axi-symmetric afterbody (at an inflow Mach number of 2.3) Gaviglio et al. [1977] observed that the assumption of constant total enthalpy was indeed valid. Therefore, assuming constant enthalpy the second term on the right hand side of equation 5.50 can be equated to zero. Thus,

$$h'' = -u_i'' U_i \quad (5.51)$$

Assuming that the fluctuations are isobaric, the relationship between the fluctuations in density and temperature can be expressed as

$$\frac{\rho'}{\rho} \cong -\frac{T''}{T} \quad (5.52)$$

The assumption of isobaricity has been confirmed by the experimental observations of Gaviglio et al. [1977]. If we assume constant specific heats, then equation 5.52 can be used to relate the fluctuations in density and enthalpy. Thus,

$$\frac{\rho'}{\bar{\rho}} \cong -\frac{T''}{\bar{T}} = \frac{h''}{\bar{h}} \quad (5.53)$$

The above equation coupled with equation 5.51 gives a relationship between the fluctuations in density, temperature and velocity as given by equation 5.54.

$$\frac{\rho'}{\bar{\rho}} = -\frac{T''}{\bar{T}} = \frac{(\gamma - 1)}{a^2} U_i u_i'' \quad (5.54)$$

From definition,

$$\overline{u_i''} = -\frac{\overline{\rho' u_i'}}{\bar{\rho}} \quad (5.55)$$

Multiplying equation 5.54 throughout by  $u_j'$  and averaging we can set up a functional relationship expressing the dependence of the turbulent mass flux on the gradients in temperature and the Reynolds stresses. The functional relationship is expressed in the form given by equation 5.56.

$$\overline{u_j''} = C_1 \left\{ \left( \frac{\mu_t C_p}{Pr_t} \right) \left( \frac{\gamma - 1}{\bar{\rho} a^2} \right) \frac{\partial \bar{T}}{\partial x_j} + \left[ \frac{(\gamma - 1)}{\bar{\rho} a^2} \bar{U}_i \overline{\rho u_i'' u_j''} \right] \right\} \quad (5.56)$$

where  $C_1$  is an arbitrary constant and  $C_p$  is the specific heat at constant pressure. Comparing this expression with that of Ristorcelli [1993] we get

$$C_1 = \frac{2M_t}{1 - M_t} \text{ where } M_t = \frac{\sqrt{2k}}{a} \quad (5.57)$$

It is to be noted that equation 5.56 expresses the functional dependence of the turbulent mass flux on the thermal gradients and the intensity of the velocity fluctuations. The assumption was used as a starting point for modelling the turbulent mass flux. It does not imply that the fluctuations are isobaric and if we make the assumption of isobaricity of the fluctuations, then the terms inside the parenthesis in equation 5.56 cancel each other out.

### 5.3.3.2 Estimation of pressure dilatation

The estimate for the pressure dilatation term\* follows closely the derivation for the corresponding term by Rubesin [1990].

From the continuity equation we get the transport equation for the fluctuating density

$$\frac{\partial \rho'}{\partial t} + \frac{\partial}{\partial x_k} [\rho' \tilde{U}_k + \rho u_k''] = 0 \quad (5.58)$$

Multiplying by  $(\rho')$  and rearranging the equations and neglecting the triple correlation term, we get

$$\frac{\partial}{\partial t} (\rho'^2) + \tilde{U}_k \frac{\partial}{\partial x_k} (\rho'^2) + 2\rho'^2 \frac{\partial \tilde{U}_k}{\partial x_k} + 2\rho' u_k'' \frac{\partial \bar{\rho}}{\partial x_k} + 2\rho' \bar{\rho} \frac{\partial u_k''}{\partial x_k} = 0 \quad (5.59)$$

Averaging and rearranging, we get

$$\overline{\rho' \frac{\partial u_k''}{\partial x_k}} = -\frac{1}{2\bar{\rho}} \left[ \frac{\partial}{\partial t} (\overline{\rho'^2}) + \tilde{U}_k \frac{\partial}{\partial x_k} (\overline{\rho'^2}) \right] - \left( \frac{\overline{\rho'^2}}{\bar{\rho}^2} \right) \frac{\partial \tilde{U}_k}{\partial x_k} - \overline{u_k''} \frac{\partial \bar{\rho}}{\partial x_k} \quad (5.60)$$

Defining a new variable  $\beta$  where

$$\beta = \frac{(\overline{\rho'^2})^{\frac{1}{2}}}{\bar{\rho}}; \text{ or } \frac{\overline{\rho'^2}}{\bar{\rho}^2} = \beta^2 \quad (5.61)$$

Making the assumption that the intensity of pressure fluctuations are directly proportional to the intensity of density fluctuations and writing

$$\frac{p'}{P} \approx \frac{\rho'}{\bar{\rho}} \quad (5.62)$$

We can therefore, making a change of variables to  $\beta^2$ , derive a relationship for the pressure dilatation correlation as

$$\overline{p' \frac{\partial u_k''}{\partial x_k}} = P \left\{ \frac{1}{\bar{\rho}} \frac{\partial \bar{\rho}}{\partial x_k} \overline{u_k''} - \frac{1}{2} \left[ \frac{\partial}{\partial t} (\beta^2) + \tilde{U}_k \frac{\partial}{\partial x_k} (\beta^2) \right] \right\} \quad (5.63)$$

To estimate  $\beta^2$  we use the empirical observations of Gaviglio et al. [1977] and obtain,

The derivation for the pressure dilatation term is presented here to indicate that the term can be calculated using the modification derived above for the turbulent mass flux. In the computational study given in Chapter 6 the modifications for pressure dilatation derived in this section were not used.

$$\beta^2 = \frac{\overline{\rho'^2}}{\overline{\rho}^2} = [(\gamma - 1)M^2]^2 \left( \frac{\overline{u_i'' u_i''}}{\bar{U}_i \bar{U}_i} \right) \quad (5.64)$$

It should be noted that this derivation for the pressure dilatation correlation is strictly applicable for cases where the fluctuations cannot be considered to be isobaric.

#### 5.3.3.3 Effect of baroclinic torque

The modelling of the transport equation for  $\epsilon_s$  usually follows the incompressible form and ignores the effect of the baroclinic torque.  $\epsilon_s$  is usually defined as the correlation between the vorticity fluctuations, that is,  $\epsilon_s = \overline{v \omega_i'' \omega_i''}$  where  $\nu$  is the kinematic viscosity. The assumption made in the proposal for the algebraic modification for the dilatational dissipation is that the solenoidal dissipation rate is relatively unaffected in the case of compressible flows. DNS studies (Zeman, 1990 and Sarkar, 1991) of decaying isotropic turbulence and homogeneous free shear layers at low Reynolds numbers seem to warrant this assumption. But the validity of such an assumption in the case of high Reynolds number flows and flow fields of increased complexity is open to question. The solenoidal part of the rate of dissipation of TKE cannot be assumed to be independent of compressibility effects. A look at the exact form of the governing equation for  $\epsilon_s$  will reveal this.

The exact form of the governing equation for the solenoidal dissipation rate,  $\epsilon_s$ , is written as ( $\epsilon$ , in the equations that follow, is used to denote the solenoidal dissipation rate  $\epsilon_s$ ):

$$\frac{\partial}{\partial t}(\rho \epsilon) + \frac{\partial}{\partial x_k}(\rho U_k \epsilon) = P_\epsilon + D_\epsilon + \Phi_\epsilon - \nu \nabla^2 \epsilon + B_\epsilon \quad (5.65)$$

where

$$P_\epsilon = -2\nu \overline{\omega_p'' u_k''} \frac{\partial \Omega_p}{\partial x_k} + 2\nu \overline{\omega_p'' \omega_k''} \frac{\partial U_p}{\partial x_k} + 2\nu \Omega_k \left( \overline{\omega_p'' \frac{\partial u_p''}{\partial x_k}} \right) \quad (5.66)$$

$$D_\epsilon = -\overline{u_k'' \frac{\partial}{\partial x_k} (v \omega_p'' \omega_p'')} + 2\nu \overline{\omega_p'' \omega_k''} \frac{\partial u_p''}{\partial x_k} \quad (5.67)$$

$$\Phi_\epsilon = -2\nu^2 \left( \frac{\partial \omega_p''}{\partial x_k} \right) \left( \frac{\partial \omega_p''}{\partial x_k} \right) \quad (5.68)$$

$$B_\varepsilon = 2\nu \frac{\varepsilon_{pqj}}{Q^2} \left\{ \underbrace{\frac{\partial Q}{\partial x_q} \overline{\omega_p'' \frac{\partial p'}{\partial x_i}}}_{\text{Term 1}} + \underbrace{\frac{\partial P}{\partial x_i} \overline{\omega_p'' \frac{\partial Q'}{\partial x_q}}}_{\text{Term 2}} + \underbrace{\overline{\omega_p'' \frac{\partial Q'}{\partial x_q} \frac{\partial p'}{\partial x_i}}}_{\text{Term 3}} \right\} \quad (5.69)$$

In the equations above,  $P_\varepsilon$  represents the “production of dissipation”,  $D_\varepsilon$  represents the “turbulent diffusion of dissipation”,  $\Phi_\varepsilon$  represents the “destruction of dissipation”. The fourth term in equation 5.65 represents the viscous dissipation of  $\varepsilon$ .

$B_\varepsilon$  (equation 5.65), represents the baroclinic term and arises due to differences in direction between the gradients of pressure and density, i.e., the term arising due to  $\left[ \vec{\nabla} \left( \frac{1}{Q} \right) \times (\vec{\nabla} p) \right]$ . In the case of the mean flow, the baroclinic term represents a production of vorticity due to the interaction of the pressure and density gradients. We, therefore, assume that this term represents a production of fluctuations in vorticity. To evaluate and to suitably account for the effect of this term we conducted an order of magnitude analysis comparison of the three terms.

A characteristic length scale,  $L_d$  is chosen as representing the spatial extent of the distortion.  $\Delta Q$  and  $\Delta U$  are chosen to represent variations in  $Q$  and  $U_i$  respectively. The gradient in mean pressure is assumed to be of the order of  $(Q \Delta U / L_d)$  and the fluctuations in vorticity are assumed to be of the order of  $\varepsilon/k$ , where the reciprocal represents a characteristic time scale of the turbulent fluctuations (in second-order eddy-viscosity models). With these the order of magnitude of the terms in the expression for  $B_\varepsilon$  work out to be :

$$\text{Term 1} = \left\{ \frac{\partial Q}{\partial x_q} \overline{\omega_p'' \frac{\partial p'}{\partial x_i}} \right\} = \frac{\Delta Q}{L_d} \frac{\varepsilon}{k} \left( \frac{\Delta p'}{L_d} \right) \quad (5.70)$$

$$\text{Term 2} = \left\{ \frac{\partial P}{\partial x_i} \overline{\omega_p'' \frac{\partial Q'}{\partial x_q}} \right\} = \left( \frac{Q \Delta U}{L_d} \right) \frac{\varepsilon}{k} \left( \frac{\Delta Q'}{L_d} \right) \quad (5.71)$$

$$\text{Term 3} = \left\{ \overline{\omega_p'' \frac{\partial Q'}{\partial x_q} \frac{\partial p'}{\partial x_i}} \right\} = \frac{\varepsilon}{k} \left( \frac{\Delta Q'}{L_d} \right) \left( \frac{\Delta p'}{L_d} \right) \quad (5.72)$$

Comparing the orders of magnitude of terms 1 and 2 we get

$$\text{Term1/ Term2} = \frac{\left[ \frac{\Delta \rho}{L_d} \frac{\varepsilon}{k} \frac{\Delta p'}{L_d} \right]}{\left[ \frac{\rho U \Delta U}{L_d} \frac{\varepsilon}{k} \frac{\Delta \rho'}{L_d} \right]} = \frac{\Delta \rho}{\rho} \left( \frac{1}{U \Delta U} \right) \left( \frac{\Delta p'}{\Delta \rho'} \right) \ll 1 \quad (5.73)$$

where it has been assumed that  $(\Delta p')$  and  $(\Delta \rho')$  are of the same order.

Comparing the orders of magnitude of terms 2 and 3 we get

$$\text{Term2 / Term3} = \frac{\left[ \frac{\rho U \Delta U}{L_d} \frac{\varepsilon}{k} \frac{\Delta \rho'}{L_d} \right]}{\left[ \frac{\varepsilon}{k} \frac{\Delta \rho'}{L_d} \frac{\Delta p'}{L_d} \right]} = \frac{\rho U \Delta U}{\Delta p'} > 1 \quad (5.74)$$

where we have assumed that the fluctuations in pressure are of the order of magnitude (suggested by Lele, 1994)  $\frac{p'^2}{p^2} = \gamma^2 M^2 M_t^2$ , where  $M = \frac{Sl}{c}$  and  $M_t^2 = \frac{q}{c^2}$  where  $S$  is representative of the mean flow time scale,  $l$  is a characteristic length scale of the turbulent eddies,  $c$  is the speed of sound and  $q = u_i'' u_i''$ . It should be pointed out that the order of magnitude analysis is just a first order estimate and the orders of magnitude used can be debated. Additionally, it has also been assumed that the fluctuations in vorticity and the gradient of fluctuations in pressure and density are well correlated. However, due to a lack of information to provide us a better estimate of the orders of magnitude, we will use these estimates to obtain a modification for the term representing the effect of the baroclinic term.

Thus from the order of magnitude analysis it turns out that the second term in equation 5.69 is the more dominant term in comparison with the other two terms that make up  $B_\varepsilon$ .

Comparing this term with the transport equation for TKE it is modelled as  $- C_{\varepsilon 1} \frac{\varepsilon}{k} \overline{u_i''} \frac{\partial P}{\partial x_i}$ .

We chose to model the second term in equation 5.69 as a production term because we know that for the mean flow the baroclinic term acts as a production of vorticity. The constant is based on conventional modelling of the “production of dissipation” term in the  $\varepsilon$  equation. There is no experimental or DNS data to guide our choice of this constant. Future experimental observations or DNS studies may help us in making a better estimate of the constant.

Therefore the modelled form of the transport equations representing the evolution of  $k$  and  $\varepsilon$  are given as

$$\frac{\partial}{\partial t}(\bar{\rho} \tilde{k}) + \frac{\partial}{\partial x_j}(\bar{\rho} \tilde{u}_j \tilde{k}) = P_k - \bar{\rho} \tilde{\varepsilon} + \frac{\partial}{\partial x_j} \left[ \mu + \frac{\mu_t}{\sigma_k} \left( \frac{\partial \tilde{k}}{\partial x_j} \right) \right] - \overline{u_i''} \frac{\partial P}{\partial x_i} + \overline{p' \frac{\partial u_i''}{\partial x_i}} \quad (5.75)$$

and

$$\frac{\partial}{\partial t}(\bar{\rho} \tilde{\varepsilon}) + \frac{\partial}{\partial x_j}(\bar{\rho} \tilde{u}_j \tilde{\varepsilon}) = C_{\varepsilon 1} \frac{\varepsilon}{k} \left( P_k - \overline{u_i''} \frac{\partial P}{\partial x_i} \right) - C_{\varepsilon 2} \bar{\rho} \frac{\tilde{\varepsilon}^2}{k} + \frac{\partial}{\partial x_j} \left[ \mu + \frac{\mu_t}{\sigma_\varepsilon} \left( \frac{\partial \tilde{\varepsilon}}{\partial x_j} \right) \right] \quad (5.76)$$

#### 5.3.3.4 Comment on proposed modifications

The advantages of the current modifications are :

a) *A representation for the turbulent mass flux term, using experimentally validated assumptions.* The representation for the turbulent mass flux proposed by Rubesin [1990] has the inherent problem of an arbitrary parameter in terms of the polytropic coefficient. Also, Rubesins' modification (Rubesin, 1990) will predict no turbulent mass flux when there is no heat flux.

b) *A representation for the enthalpic production,* which tends to be an important term when considering flows involving strong expansions and compressions. This representation, again, avoids the use of an arbitrary polytropic coefficient. Also, the entire modification proposed by Rubesin [1991] is based on an ad hoc hypothesis.

c) *A representation for the effect of the baroclinic term on the dissipation rate of TKE.* The necessity for modelling this term in highly compressible or stratified flows is clear and in fact this will become abundantly clear when we look at the solutions to the flow past the axi-symmetric afterbody.

These representations help solve the exact form of the transport equations, albeit in a modelled form. Huang et al. [1992], have shown that in the case of wall boundary layers the  $k$ - $\varepsilon$  form of modelling show a strong dependence on the density gradients. It remains to be seen whether the modifications presented here for the  $\varepsilon$  equation may help in offsetting this

dependence. A more detailed analysis, particularly of the  $\epsilon$  equation, needs to be conducted to clarify this issue.

It should also be pointed out that the effectiveness of such modifications in the case of reacting flows and also hypersonic flowfields with strong wall cooling is in question. Further tests are needed to validate and/or to improve the modifications for such flowfields.

#### 5.3.4 Additional Issues

The modifications given by equations 5.27 through 5.47 were intended for mixing layers. Consequently, they have been shown to be successful in predicting the reduction in the growth rates of free shear layers (Zeman, 1990 and Zeman, 1991; Sarkar and Lakshmanan, 1991; Sarkar, 1992; El Baz and Launder, 1993 and Wilcox, 1992).

From their DNS study of homogeneous shear layers, Blaisdell et. al. [1993] conclude that the Sarkar et al. [1991] model gave a better estimate of  $\epsilon_d$  than the model proposed by Zeman [1990]. However the validity of these algebraic modifications in predictions made of time dependent flow fields is in question. For turbulent boundary layers (Wilcox, 1992) they predict reduced levels of TKE thereby aggravating the model deficiencies in predicting skin friction coefficient and wall heat transfer rates. All these modifications have not been adequately tested to infer their applicability for more complex flow fields which is one of the issues being addressed in this dissertation.

For incompressible flows, equilibrium in the logarithmic region yields the following relation between the coefficients in the dissipation rate equation.

$$\kappa^2 = (C_{\epsilon 2} - C_{\epsilon 1}) \sqrt{c_\mu} \sigma_\epsilon \quad (5.77)$$

where  $\kappa$  is the von Karman constant and is 0.41. It follows from Huang et al. [1992] that if the model satisfies the above equation then in the case of compressible flows there is a balance of terms expressing a dependence on the spatial gradients in density. None of the proposed compressibility modifications address this issue. This balance of terms is responsible for the deficiencies seen in the computations made of turbulent wall layers. Huang et al. [1992] also indicate that the  $k-\omega$  model is dependent on the spatial gradients of



density to a lesser extent than the  $k$ - $\epsilon$  model. The dependence of the modelling procedure on the spatial gradients of density can be shown as follows.

We will first address the dependence of the  $\epsilon$  equation on the spatial gradients in density and next address the same in the  $\omega$  equation. The  $k$ - $\omega$  model in its current form indicates that it is dependent on the density gradients to a lesser degree. But this is mainly because of the neglecting of cross-diffusion terms in the  $\omega$  equation. We intend to show this in the next few paragraphs.

Consider the region in the log layer of a flat plate boundary layer. The equations for  $k$  and  $\epsilon$  reduce to :

$k$  equation

$$-\frac{\partial}{\partial y} \left( \frac{\mu_t}{\sigma_k} \frac{\partial k}{\partial y} \right) = P_k - \rho \epsilon \quad (5.78)$$

$\epsilon$  equation

$$-\frac{\partial}{\partial y} \left( \frac{\mu_t}{\sigma_\epsilon} \frac{\partial \epsilon}{\partial y} \right) = C_{\epsilon 1} \rho \frac{\epsilon}{k} P_k - C_{\epsilon 2} \rho \frac{\epsilon^2}{k} \quad (5.79)$$

where

$$\mu_t = C_\mu \frac{\rho k^2}{\epsilon} ; \quad P_k = - \overline{\rho u'' v''} \frac{\partial U}{\partial y} \quad (5.80)$$

and the constants,  $C_\mu = 0.09$ ,  $C_{\epsilon 1} = 1.43$ ,  $C_{\epsilon 2} = 1.92$ ,  $\sigma_k = 1.0$  and  $\sigma_\epsilon = 1.3$ .

Since in the log layer we can assume an equilibrium between the rate of production of TKE and the rate of dissipation of TKE, that is,  $P_k = \epsilon$  (Huang et al., 1992). Following Huang et al. [1992] and using the compressible form of the wall function method the values of  $k$ ,  $\epsilon$  and  $P_k$  can be prescribed as :

$$k = \left( \frac{\tau_{wall}}{\rho} \right) \frac{1}{\sqrt{C_\mu}} ; \quad \epsilon = \left( \frac{\tau_{wall}}{\rho} \right)^{3/2} \frac{1}{\kappa y} = P_k \quad (5.81)$$

Substituting these assumptions into equation 5.79 and after mathematical manipulations we get

$$\frac{\sqrt{C_\mu}}{\kappa^2} \sigma_\epsilon (C_{\epsilon 2} - C_{\epsilon 1}) = 1 + 3 \left( \frac{y}{Q} \right)^2 \left( \frac{\partial Q}{\partial y} \right)^2 - \frac{3}{2} \frac{y^2}{Q} \left( \frac{\partial^2 Q}{\partial y^2} \right) + \frac{y}{Q} \frac{\partial Q}{\partial y} \quad (5.82)$$

For the  $k$ - $\omega$  model the equations reduce to

$k$  equation

$$-\frac{\partial}{\partial y} \left( \frac{\mu_t}{\sigma_k} \frac{\partial k}{\partial y} \right) = P_k - \rho C_\mu \omega k \quad (5.83)$$

$\omega$  equation

$$-\frac{\partial}{\partial y} \left( \frac{\mu_t}{\sigma_\omega} \frac{\partial \omega}{\partial y} \right) = C_{\omega 1} \rho \frac{\omega}{k} P_k - C_{\omega 2} \rho C_\mu \omega^2 \quad (5.84)$$

and the eddy viscosity is defined as

$$\mu_t = \frac{k}{\omega} \quad (5.85)$$

where  $C_\mu = 0.09$ ,  $C_{\omega 1}$ ,  $C_{\omega 2}$  and  $\sigma_\omega$  are modelling constants. The exact values of these constants are not important for our analysis, they can be found in Wilcox [1992].

The reciprocal time scale variable  $\omega$  is defined as  $\omega = \frac{\epsilon}{C_\mu k}$ . Conducting an analysis similar

to the one above for the  $k$ - $\epsilon$  model with  $\omega = \left( \frac{\tau_{\text{wall}}}{Q} \right)^{\frac{1}{2}} \frac{1}{\kappa y} \frac{1}{\sqrt{C_\mu}}$  in the log region and

substituting the values for  $k$  and  $P_k$  from equations 5.81 and the value of  $\omega$  given above, we get

$$\frac{\sqrt{C_\mu}}{\kappa^2} \sigma_\omega (C_{\omega 2} - C_{\omega 1}) = 1 + \frac{1}{2} \left( \frac{y}{Q} \right)^2 \left( \frac{\partial Q}{\partial y} \right)^2 - \frac{1}{2} \frac{y^2}{Q} \left( \frac{\partial^2 Q}{\partial y^2} \right) \quad (5.86)$$

Comparing equations 5.82 and 5.86, we see that the  $k$ - $\omega$  model depends to a lesser extent on the spatial gradients in density than the  $k$ - $\epsilon$  model. This is the analysis used by Huang et al. [1992]. However, they have not included the effect of the cross-diffusion term in their analysis. As Speziale et al. [1992] point out, the cross-diffusion term needs to be included in the  $\omega$  equation to get asymptotically consistent values for  $k$  (as we approach the wall). The

cross-diffusion term is written as  $\frac{\mu_L}{k} \left( \frac{\partial k}{\partial y} \right) \left( \frac{\partial \omega}{\partial y} \right)$ . If we conduct the same analysis on this cross-diffusion term we end up with

$$\frac{\mu_L}{k} \left( \frac{\partial k}{\partial y} \right) \left( \frac{\partial \omega}{\partial y} \right) = \frac{(\tau_{\text{wall}})^{1/2}}{\kappa} \frac{1}{\sqrt{C_\mu}} \left[ \left( \frac{1}{\rho^3 y} \right) \left( \frac{\partial \rho}{\partial y} \right)^2 + \left( \frac{1}{\rho^2 y^2} \right) \frac{\partial \rho}{\partial y} \right] \quad (5.87)$$

The cross-diffusion term in essence adds extra terms which when taken along with the terms for the equation for  $\omega$  considered by Huang et al. [1992] would lead to an equivalent dependence on the spatial gradients in density. Therefore, the  $k$ - $\omega$  model in the form given by Wilcox [1992] while dependent to a lesser extent on the spatial gradients in density will not produce asymptotically consistent values for  $k$ , in regions close to wall boundary. When the cross-diffusion term is added to the  $\omega$  equation to achieve this asymptotic consistency, we have to pay the price of increased dependence on the spatial gradients in density.

#### 5.4 Summary

In this Chapter, we have considered the exact form of the governing equations and identified terms that are unique to compressible turbulent flows. We have discussed the modifications that have been proposed to address the extra dissipation introduced by the non-divergent velocity field. Additional effects of this non-divergent field have also been addressed in the context of the pressure dilatation correlation. Modelling options for this correlation have also been addressed. The deficiencies associated with the models for the dilatational dissipation term and the pressure dilatation term have been highlighted.

The drawbacks in the current modelling procedure, in terms of solving the exact form of the governing equations, has been our main focus. Modifications have been proposed for the turbulent mass flux (and hence the enthalpic production term) and for the effect of the baroclinic term. Also, the issue regarding the increased dependence of the  $k$ - $\epsilon$  model on the spatial gradients in density in comparison with the  $k$ - $\omega$  model has been addressed.

## CHAPTER 6

### COMPUTATIONAL ANALYSIS OF COMPRESSIBILITY MODIFICATIONS

Compressibility modifications have been proposed in the literature to address the effect of compressibility on the growth of turbulent shear layers. In addition two new modifications have been proposed in Chapter 5 to help solve the governing equations in their exact form, albeit in a modelled manner. The effectiveness of these modifications in predicting flow fields of increased complexity is addressed in this chapter. Particularly, the capabilities of these modifications have been evaluated for the flow past an axi-symmetric afterbody and for the flow past a projectile forebody. Additionally, modifications that have been proposed to address the added time scale introduced due to non-equilibrium effects are analyzed.

#### 6.1 Introduction

The effects of compressibility on the growth of a turbulent shear layer has been addressed in Chapter 2. DNS studies of Zeman [1990] and Sarkar et al. [1991] seem to indicate that the effect of compressibility on both decaying compressible turbulence and homogeneous shear turbulence is a dissipative one. Models have been proposed to address this extra dissipation (due to the non-divergent nature of the velocity field). Models have also been proposed to account for the pressure dilatation correlation. The modifications for the extra dissipation due to dilatational effects and the pressure dilatation correlation have been successful in predicting the reduction in growth rate and reduction in magnitudes of turbulence correlation coefficients of free shear layers (Sarkar and Lakshmanan, 1991). But these modifications have been shown to aggravate the deficiencies of the eddy viscosity

models in predicting the growth of turbulent wall shear layers (Wilcox, 1992 ; Huang et al., 1994).

In Chapter 5, we have looked at the exact form of the governing equations and identified additional terms (unique to compressible turbulent flows) that have not been suitably accounted for. These are the turbulent mass flux term (and hence the enthalpic production) and the effect of the baroclinic term. Modifications have been proposed to account for these terms with the aim of solving the governing equations in their exact form.

In addition, modifications have been proposed (Chen and Kim, 1987 and Thakur et al. 1996) to suitably modify the constants in the transport equation for the rate of dissipation of TKE. These modifications have been proposed to address turbulent flow fields where the rate of production of TKE and the rate of dissipation of TKE are not in equilibrium (this is an implicit assumption in the eddy viscosity based models).

Table 6-1 Modifications to be evaluated.

Modifications.	Details	Author(s)
1. Non-equilibrium modification.	Modification for a) imbalance between production of TKE and its dissipation rate. b) added time scale	Chen and Kim [1987] Thakur et al. [1996]
2. Sarkar et al. Modifications	Modification for a) dilatational dissipation and b) pressure dilatation terms.	Sarkar et al. [1991] and Sarkar [1992]
3. El Baz Modification	Modifications for a) compressibility effects and b) pressure dilatation term.	El Baz and Launder [1993]
4. Current Modification	Modifications for a) Turbulent Mass Flux b) Enthalpic Production	Current work

All these modifications have been tested to analyze their effectiveness in predicting simple turbulent flows. The issue of their applicability in predicting more complicated flows is being addressed in this chapter. The modifications that are being tested, in this dissertation are listed in Table 6-1.

Three flow fields with complex flow features are computed here with an aim to understand the applicability of such modifications. These are the flow past an axi-symmetric afterbody and the flow field in the forebody region of a projectile.

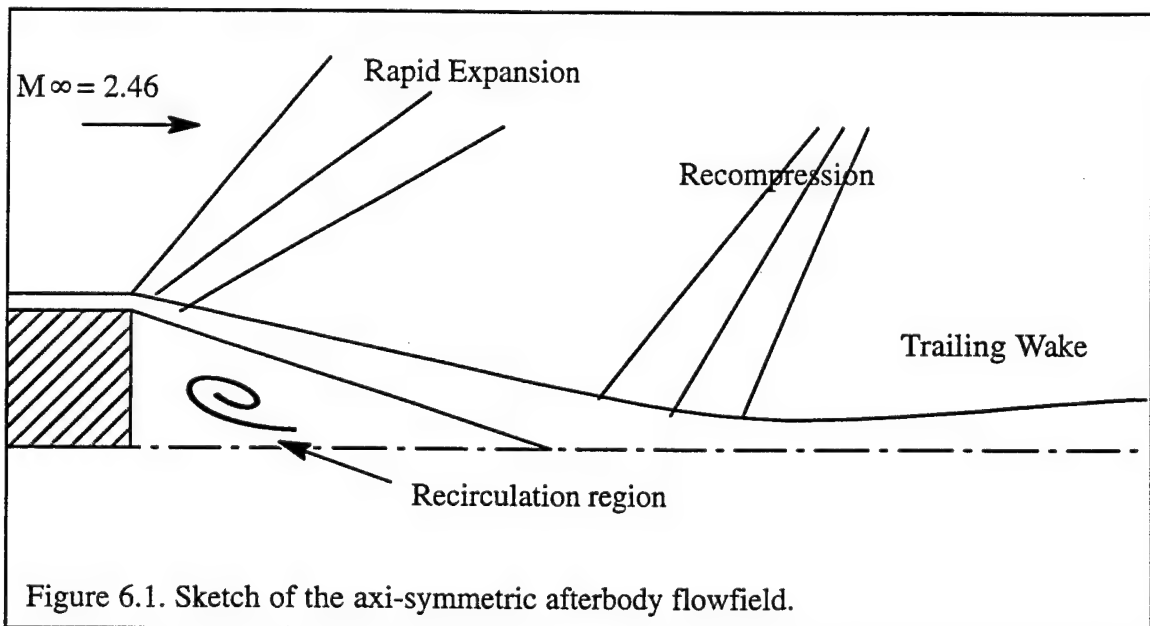
## 6.2 Base Flowfield

The accuracy of the various modifications in predicting the flow past an axi-symmetric afterbody is being tested here. In particular, the compressibility modifications of Sarkar et al. [1991], Sarkar [1992] and the modifications of El Baz and Launder [1993] and the two additional modifications for the turbulent mass flux term (thereby a representation for the enthalpic production) and the baroclinic term are tested in this paper and a comparative study is presented.

### 6.2.1 Description of the Base Flowfield

Figure 6.1, shows a sketch of the flow past an axi-symmetric afterbody. The flow field is characterized by,

1. An incoming turbulent boundary layer which undergoes separation at the base edge,
2. a rapid expansion region,
3. a mixing layer region where the shear layer interacts with the recirculating region



behind the base,

4. a recompression region and
5. a trailing wake region.

In what follows, a brief description is given of the individual regions of the flow field (highlighting some of the drawbacks with reference to eddy-viscosity based two-equation models, in particular the  $k$ - $\epsilon$  model).

#### 6.2.1.1 Turbulent wall boundary layer

Some of the main problems in  $k$ - $\epsilon$  models are :

- i) asymptotic consistency in approaching the wall: This refers to the problem of prescribing the correct variation in  $k$  and  $\epsilon$  in the region close to the wall. As  $y^+ \rightarrow 0$ ,  $k \sim \mathcal{O}(y^2)$  and  $\epsilon \sim \mathcal{O}(1)$ . Currently this variation in  $k$  and  $\epsilon$  is obtained by either wall functions or by using a low Reynolds number form of the modelling equations. In this study, the wall function treatment is being used. Viegas et al. [1985] and Huang and Coakley [1993] have, from their computational studies, concluded that the wall function treatment can be used to obtain a reasonably accurate prediction of the wall quantities as long as the first grid point (adjacent to a wall), is located in the log layer. That is, as long as the computed value of  $y^+ = \frac{yU_\tau}{\nu_L}$  is  $\geq 20$ , where  $y$  is the perpendicular distance of the first grid point from the wall,  $U_\tau$  is the friction velocity (defined in attached wall layers as  $U_\tau = \sqrt{\frac{\tau_{\text{wall}}}{\rho}}$ ),  $\nu_L$  is the laminar viscosity at the wall and  $\tau_{\text{wall}}$  is the shear stress at the wall. The formulation of the wall function is modified to account for the variation of density within the boundary layer. Here use is made of the van Driest transformation for compressible turbulent boundary layers.
- ii) the correct prescription of  $\epsilon$  at the wall: Currently, curve fits based on empirical observations are used to prescribe the value of  $\epsilon$  at the wall. Unfortunately, these values provide accurate values for  $\epsilon$  at the wall only in the case of attached boundary layers. In the case of separated flows, the accuracy of these prescriptions is open to question.

iii) Additional deficiencies: In addition to these deficiencies in the two-equation based modelling approach there is the issue regarding the dependence of the k- $\epsilon$  modelling approach on the density gradients which results in incorrect prediction of the skin friction coefficient and the heat transfer rates at the wall. However, for the freestream Mach numbers that are encountered in this study, the wall function based treatment outlined in Viegas et al. [1985] is quite reliable and makes satisfactory predictions regarding the wall shear and the value of  $\epsilon$  at the wall as long as the first grid location is well inside the log layer. In the computations presented in this article care has been taken to ensure that the first grid location is at a  $y^+$  of about 40.

#### 6.2.1.2 Rapid expansion region

This region is characteristic of a shear layer undergoing a rapid distortion. The streamlines in this region are flattened. As pointed out by Gaviglio et al. [1977], this region is also characterized by reduced levels of production.

The rate of production of TKE is expressed as :

$$P_k = - \overline{\rho u_i'' u_j''} \frac{\partial \tilde{U}_i}{\partial x_j} - \overline{u_i''} \frac{\partial P}{\partial x_i} \quad (6.1)$$

where the first term on the right hand side of equation 6.1 is called the kinetic production rate and the second term is referred to as the enthalpic production rate. The kinetic production rate is therefore written as

$$P_{\text{kinetic}} = - \overline{\rho u_i'' u_j''} \frac{\partial \tilde{U}_i}{\partial x_j} \quad (6.2)$$

The kinetic part of the rate of production of TKE can be split into a dilatational part ( $P_{kd}$ ) and an iso-volumetric part ( $P_{kiv}$ ). These are given as

$$P_{kd} = \left( \frac{1}{3} \overline{\rho u_k'' u_k''} \right) \frac{1}{\bar{\rho}} \frac{D\bar{\rho}}{Dt} \quad (6.3)$$

$$P_{kiv} = \left[ \left( \overline{\rho u_i'' u_j''} - \frac{1}{3} \overline{\rho u_k'' u_k''} \delta_{ij} \right) \left( S_{ij} - \frac{1}{3} \tilde{U}_{k,k} \delta_{ij} \right) \right] \quad (6.4)$$

The enthalpic part of the rate of production of TKE is given as



$$P_{\text{enthalpic}} = - \overline{u_i''} \frac{\partial P}{\partial x_i} \quad (6.5)$$

The split up is useful in understanding the effect of a rapid distortion, such as an expansion or compression, on the evolution of the turbulent flow field. As the turbulent shear layer moves through the rapid expansion region at the base corner it undergoes a streamwise acceleration (resulting in flattened streamlines). The three parts of the production term, given by equations 6.3, 6.4 and 6.5, are of the same order of magnitude. Since the dilatational part,  $P_{kd}$ , varies in direct proportion to the density changes it introduces a negative contribution as does the enthalpic production. In fact, for a strong expansion the production can be negative (Gaviglio et al. 1977). The dissipation rate and diffusion terms do not affect the intensity of the fluctuations because of the relatively small time period over which the flow passes through the expansion. In fact, the distortion time scale is roughly 1/3rd of the integral time scale (Gaviglio et al. 1977). Dawson and Samimy [1994] show that the rapid expansions quench the small scale turbulence in supersonic turbulent boundary layers while enhancing the turbulence energy in the large scale structures. To a lesser degree, the stabilizing streamline curvature also contributes to a decrease in the Reynolds stresses.

#### 6.2.1.3 Mixing region

This is the region where the inner region from the incoming turbulent boundary layer interacts with the recirculating region. The production of TKE in this region is mainly due to the entrainment of the recirculating fluid. The compressibility effects are minimal here. Experimental observations (Gaviglio et al. 1977) indicate that the peak shear stress value increases by about 4–6 times the value in the incoming boundary layer. The increase in shear stress is attributed to an increase in the Reynolds shear stress  $-\overline{u''v''}$ . Since it is also observed that there is a reduction in  $\frac{\partial \tilde{U}}{\partial y}$ , a gradient transport hypothesis representation for the Reynolds stresses could be erroneous. The standard k- $\epsilon$  model is based on the assumption of equilibrium between the production and dissipation of TKE. Studies, (Chen and Kim, 1987) have shown that this kind of flowfield is characterized by strong non-equilibrium

effects. This is the motivation behind the need to test the predictive capabilities of the non-equilibrium modifications of Chen and Kim [1987].

#### 6.2.1.4 Recompression region

The recompression takes place over a distance several times larger than the thickness of the shear layer. Consequently,  $\frac{\partial \tilde{U}}{\partial x} \ll \frac{\partial \tilde{U}}{\partial y}$ . Gaviglio et al. [1977], suggest that a practical model for the production term in this region would be  $P_k = \left[ -\overline{u''v''} \frac{\partial \tilde{U}}{\partial y} \right]$ . This model predicts a rate of increase of TKE that is much greater than what is actually observed.

Currently, there is no single model that can successfully account for all the observed variations in this flowfield.

#### 6.2.2 Overview of Prior Computational Efforts

There have been several computational studies of the base flow field. These are well documented in the report of Herrin and Dutton [1993]. Of particular relevance to this study are the results obtained by Childs and Caruso [1987], Peace [1990] and Tucker and Shyy [1993]. Extensive work has also been done by Sahu and co-workers (Sahu et al. 1985 and Sahu, 1994). In the following paragraph a brief description of the computational efforts to predict this axi-symmetric flowfield are presented.

Childs and Caruso [1988], performed a computational study to evaluate the adequacy of grid resolution and the errors associated with the turbulence model in modelling this complex flowfield. Though not a comprehensive study, they concluded from their computations that the inadequacy of grid resolution could act to cancel out the errors in the modeling of the turbulence structure. In fact their results seemed to indicate that the standard k- $\epsilon$  model, with its inability to accurately model Mach number effects on the turbulence structure, was more accurate in capturing the mean flow variations than a model which was modified to account for the Mach number effects. Peace [1990] conducted a comparative study to evaluate the predictions made by zero-equation models against two-equation models. The computations were made using the thin-layer form of the Navier-Stokes

equations. The thin-layer form is valid over the attached boundary layer upstream of the base corner but in the recirculating downstream of the base and in fact over the expansion region, the use of a thin-layer form of the Navier-Stokes equations is highly questionable. The results obtained indicate that the zero equation and the two equation models of turbulence are very accurate as long as the flow is attached, i.e., upstream of the base corner. But there is a severe loss of accuracy in the recirculating region. However, inaccuracies in the predictions made of the "turbulence" quantities do not or have a negligible impact on the predictions made of the pressure distribution over the base of the afterbody. More recently, Sahu [1994] conducted a computational comparison of the predictions made by zero-equation models with those made by a low-Reynolds number form of the  $k$ - $\epsilon$  model. The results do show the expected trend in the predictive capabilities of these models. The  $k$ - $\epsilon$  model did seem to display a superior predictive capability in comparison with the zero-equation models. While both Peace [1990] and Sahu [1994] used the low-Reynolds number model of Chien [1982] the only difference between their calculations was the form of the Navier-Stokes equations. The calculations of Peace [1991] were made using the thin-layer form of the equations, while those presented by Sahu [1994] were made using the full form of the equations.

Tucker and Shyy [1993] conducted a study on the predictions made of this axi-symmetric flowfield. Their studies parallel the current study in the sense that they compared the effectiveness of the non-equilibrium modification of Chen and Kim [1988] and other modifications that have been proposed to address the effect of Mach number variations on the turbulent flowfield. They also used the low-Reynolds number model of Chien [1982]. One of the outcomes of their study was that the standard form of the  $k$ - $\epsilon$  model modified using the non-equilibrium modification for the  $\epsilon$  equation and the compressibility correction for  $\epsilon_c$  proposed by Sarkar et al. [1991], yielded a better prediction of the flowfield including the "turbulence" quantities. Results of their study will be frequently alluded to in a later section of this chapter. In a more recent report, Chuang and Chieng [1996] present a comparison between the predictions made using a Reynolds Stress Closure model, a hybrid

model (using both Algebraic Reynolds Closure and k- $\epsilon$  model) and the k- $\epsilon$  model. Their studies indicate that the Reynolds Stress Closure model yields the better prediction, however suffering from inaccuracies of its own. Their computations do not address the Mach number dependency of the turbulent fluctuations. Furthermore, they do not present enough information within the recirculating zone, making it difficult to assess the overall performance of the turbulence models investigated.

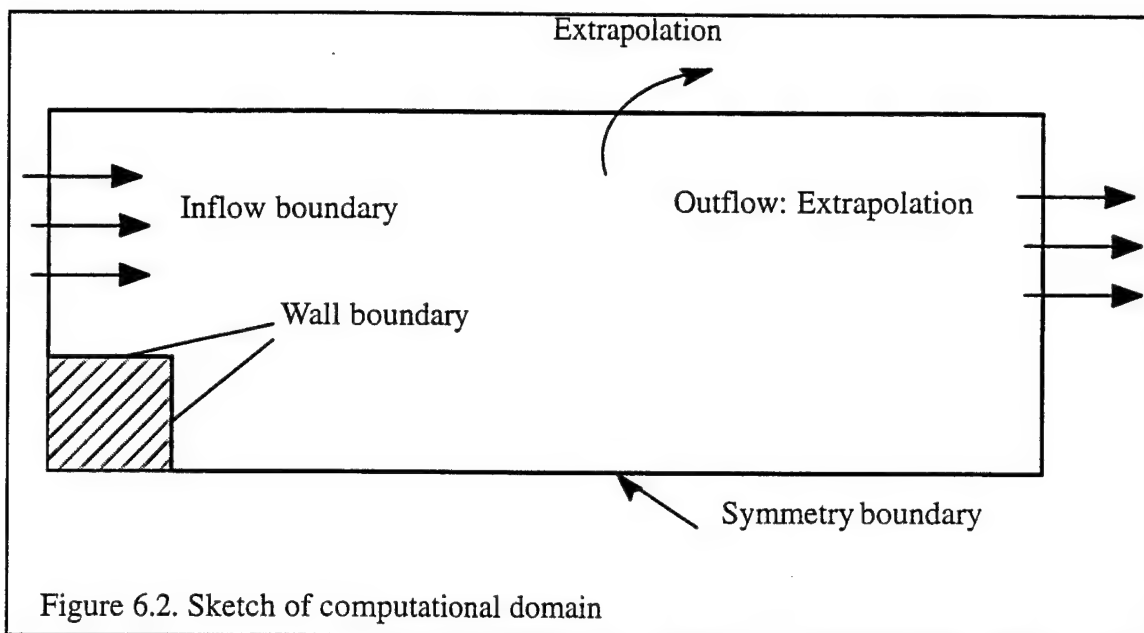
All of the computational efforts that have been expended in computing this particular flowfield have provided evidence for the need to adequately model the physics of the flowfield (particularly turbulence modelling) and also the need for adequate grid resolution. But as will be shown in this article there is a definite dependence of the solution on the discretization of the convection terms. In fact, it has been observed in this study that grid independence of the solution does not necessarily imply adequate resolution of the flowfield. The order and nature of the differencing used in the discretization of the convection terms does have a definite impact on the solution accuracy.

### 6.2.3 Present Computational Study

The computational domain with the boundary conditions used is shown in Figure 6.2. The domain extends from slightly upstream of the base corner to 6 diameters downstream of the base. The far field extends 2 diameters from the top of the base. The freestream conditions are an inlet Mach number,  $M_\infty = 2.46$  and an inlet Reynolds number  $Re_\infty = 52.1 \times 10^6/m$ . The inflow boundary conditions are obtained from the experimental measurements of Herrin and Dutton [1993]. The inlet boundary layer profile is obtained using the curve fit of Sun and Childs [1973] and the inlet TKE distribution is obtained using an interpolation of the measured data. Extrapolation is used to obtain the boundary conditions at the far field and at the outflow. At the symmetry boundary, the boundary condition used is

$$\frac{\partial}{\partial y} \{p, u, T, k \text{ and } \epsilon\} = 0 \text{ and } v = 0 \quad (6.6)$$

The pressure is assumed to be constant over the inlet wall boundary layer and the temperature is computed using constant stagnation temperature conditions at the inlet. The



recovery factor,  $r=0.89$  is used to compute the wall temperature. The density in the incoming boundary layer is computed from the equation of state. Wall functions (Viegas et al., 1985) are used to prescribe the boundary conditions at the wall for  $k$  and  $\epsilon$ . Computations were made using the multi-stage, Runge-Kutta time stepping, finite volume scheme based on the one developed by Jameson et al. [1981] with a TVD type dissipation scheme (Yee, 1985). But, as will be pointed out later in this chapter, this artificial dissipation scheme introduced excessive amounts of numerical dissipation that we had to switch to a second-order upwind scheme for the convective fluxes. The chief issues addressed in this article are listed in Table 6-1.

Figures 6.3(a) through (c) and Figure 6.4(a) show representative contours of density, pressure, temperature and Mach number. The main regions of the base flowfield are clearly discernible. The incoming turbulent boundary layer undergoes a rapid expansion at the base corner. The separated boundary layer interacts with the recirculating fluid downstream of the base resulting in an increase in the production of TKE. As the flow continues downstream it tends to realign itself with the symmetry boundary (or centreline) which results in the recompression region. A portion of the trailing wake region is also evident.

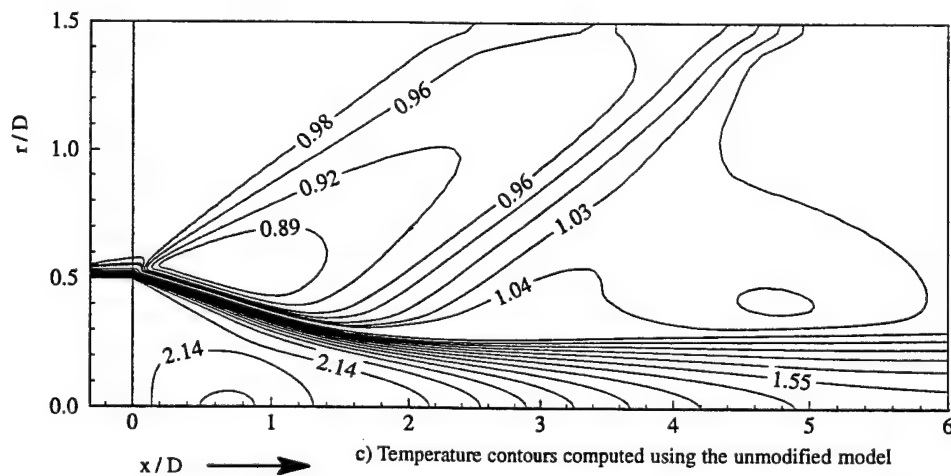
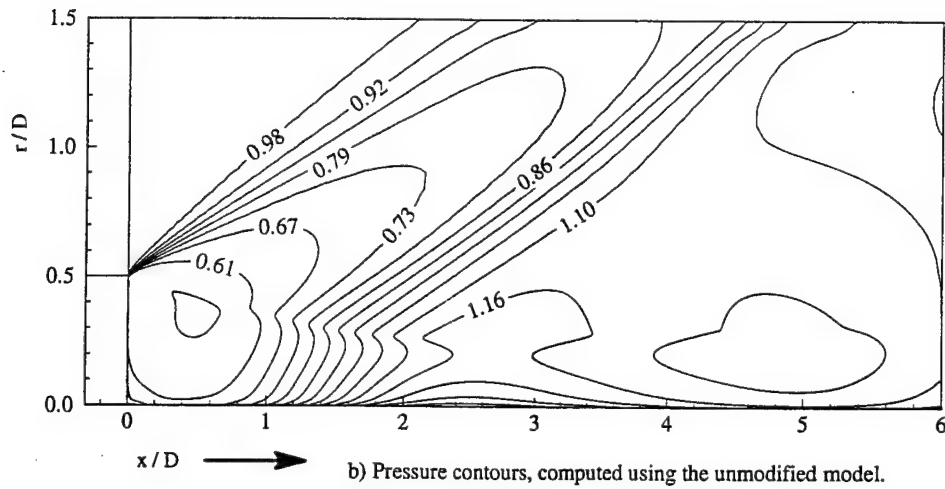
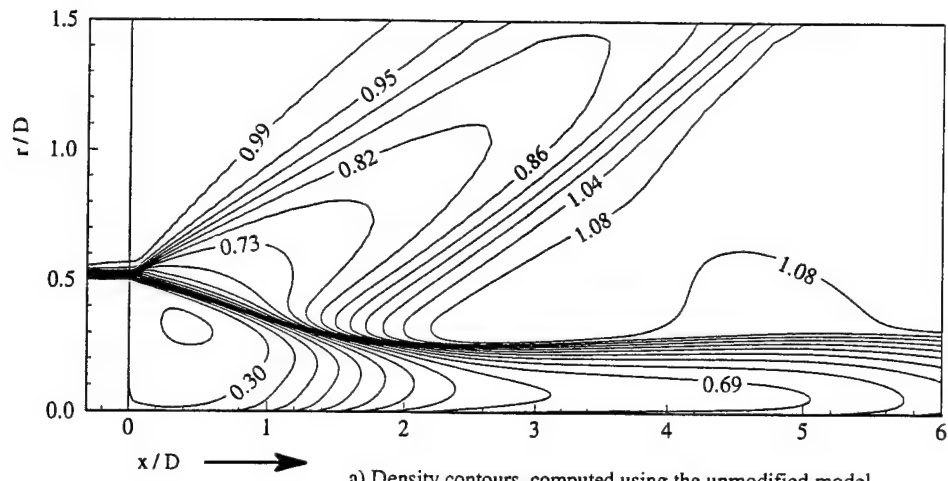


Figure 6.3. Representative contour plots of density, pressure and temperature.

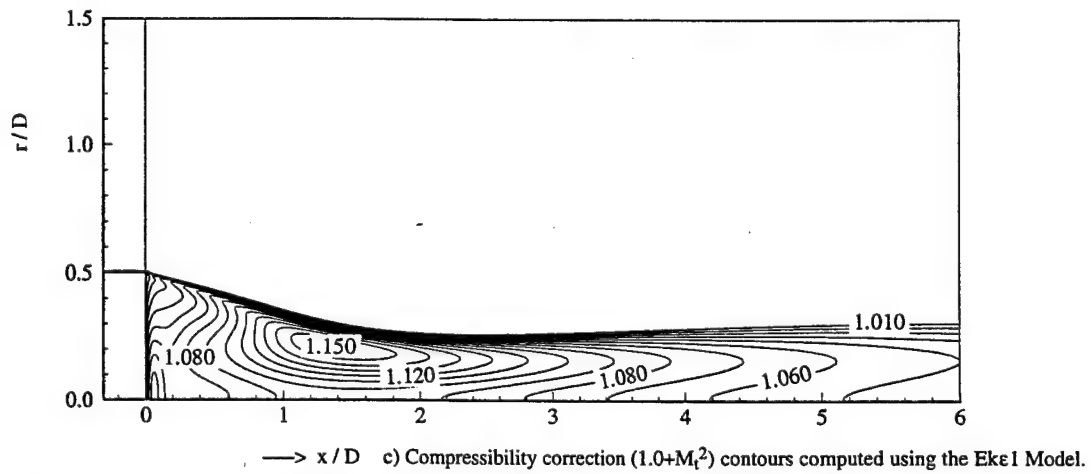
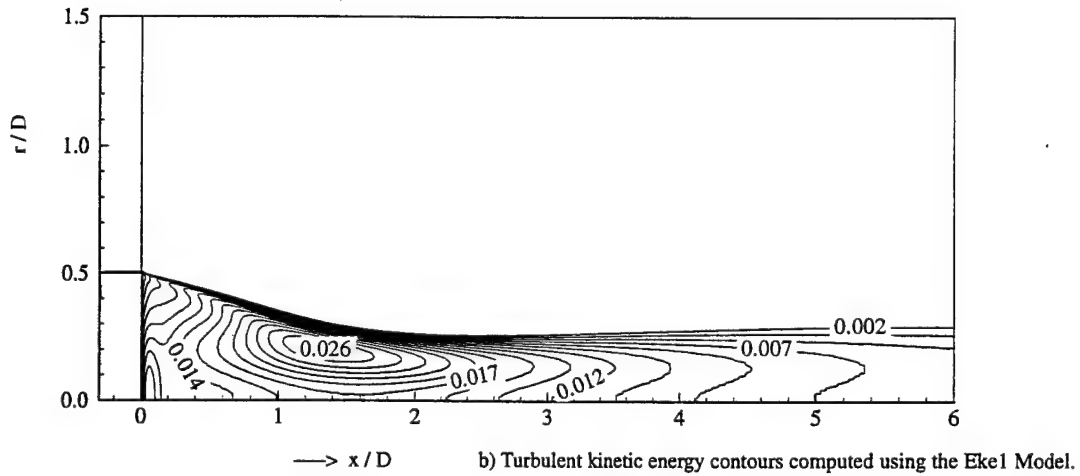
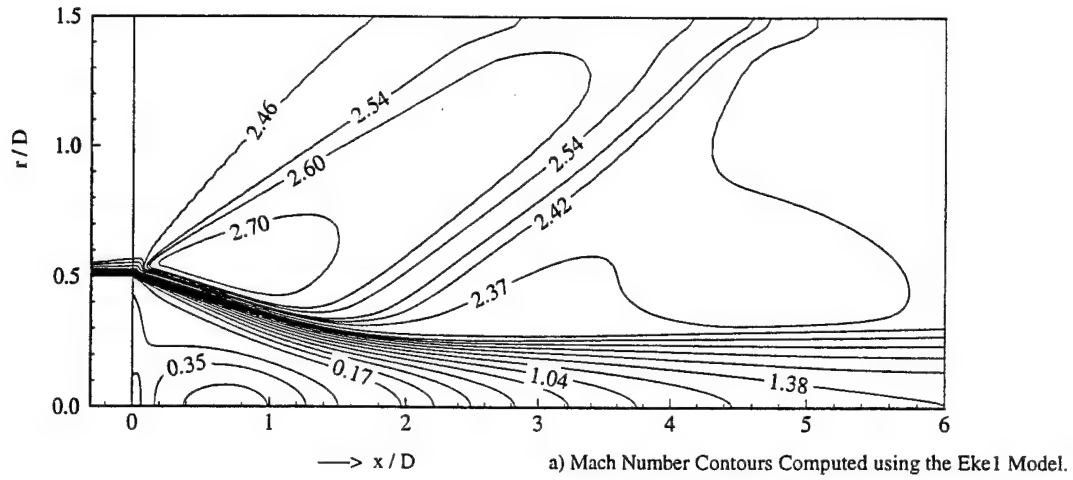


Figure 6.4. Representative contours of Mach number, TKE and Turbulent Mach number, computed using the Eke1 model.

The freestream is essentially inviscid. The free shear layer separating the inviscid region from the recirculating region is marked by sharp velocity gradients. One of the interesting things to note in these contour plots is the direction of the gradients in density and pressure. While the density gradients are along a direction perpendicular to the shear layer, the pressure gradients are along a direction parallel to the flow in the shear layer. Since the gradients are almost perpendicular to each other, the baroclinic torque could be an important factor in defining the development of the turbulent flow field thereby justifying our concerns regarding the need to model the effect of this torque on the fluctuations.

Figures 6.4(b) and (c) show representative contour plots of TKE levels and the compressibility modification  $(1.0 + M_t^2)$ . The maximum value of turbulent Mach number predicted is seen to be about 0.4. This value will be relevant when we consider the effect of the compressibility modifications that have been proposed (as functions of this Mach number). Table 6-2 presents a summary of the comparison between experimental data and the computational cases in terms of a few select quantities such as the maximum level of TKE, the peak reverse velocity along the centreline, reattachment length and the average coefficient of base pressure.

The average flow turning angle presented in Table 6-2 is computed as an average of the angles computed over a distance from  $x/R = 0.5$  to  $x/R = 2.5$ , at the midpoint location of the shear layer. In the table, the following definitions apply :

Skε = Standard k-ε model;  $\epsilon_d$  modification = modification due to Sarkar et al. [1991], i.e.,  $\epsilon_d = \epsilon_s M_t^2$ ;  $C_{\epsilon 1}$  modification = non-equilibrium modification due to Chen and Kim [1987], where the constant  $C_{\epsilon 1}$  in the standard k-ε model is changed to  $\left(1.15 + 0.25 \frac{P_k}{\epsilon}\right)$ ;

Ekε1 = Standard k-ε model extended using the above mentioned modifications for  $\epsilon_d$  and  $C_{\epsilon 1}$ ; Ekε2 = Standard k-ε model extended using the modifications for  $\epsilon_d$ ,  $C_{\epsilon 1}$  and  $C_{\epsilon 2}$ ;  $C_{\epsilon 2}$  modification (Thakur et al., 1996) refers to the modification where  $C_{\epsilon 2}$  in the unmodified



k- $\epsilon$  model is changed to  $\left(1.45 + 0.45 \frac{P_k}{\epsilon}\right) \cdot \epsilon_d + \overline{p'd''}$  = Compressibility modifications for the dilatational dissipation and pressure dilatation due Sarkar et al. [1991] and Sarkar [1992], respectively. El Baz = refers to the modifications to account for compressibility that have been proposed by El Baz and Launder [1993], for the effects of increased dissipation due to dilatational effects and pressure dilatation.  $\epsilon_d$  and  $-\overline{u_i'''} dP/dx_i$  refers to the modification for compressibility due to Sarkar et al. [1991] and enthalpic production term.

Table 6-2 Comparison of some representative mean quantities.

No.	Model	Ave. Turning Angle	$\overline{Cp}_{base}$	Reattachment length $x/R_0$	Maximum TKE Level	Peak Reverse Velocity
1.	Experiment	-15.1	-0.102	2.67	0.044 (At $x/R_0 = 2.2$ )	0.27 (At $x/R_0 = 1.5$ )
2.	Sk $\epsilon$	-15.19	-0.116	2.61	0.049 (At $x/R_0 = 2.24$ )	0.34 (At $x/R_0 = 1.02$ )
3.	$\epsilon_d$ Modification only	-13.68	-0.105	3.06	0.034 (At $x/R_0 = 2.41$ )	0.37 (At $x/R_0 = 1.14$ )
4.	$C_{\epsilon 1}$ modification only	-13.04	-0.102	3.06	0.037 (At $x/R_0 = 2.47$ )	0.31 (At $x/R_0 = 1.28$ )
5.	Ek $\epsilon 1$	-12.17	-0.096	3.43	0.028 (At $x/R_0 = 2.6$ )	0.34 (At $x/R_0 = 1.4$ )
6.	Ek $\epsilon 2$	-14.42	-0.110	2.93	0.038 (At $x/R_0 = 2.24$ )	0.39 (At $x/R_0 = 1.02$ )
7.	$\epsilon_d + \overline{p'd''}$	-12.9	-0.1	3.3	0.028 (At $x/R_0 = 2.54$ )	0.37 (At $x/R_0 = 1.24$ )
8.	El Baz.	-10.24	-0.078	4.49	0.013 (At $x/R_0 = 3.18$ )	0.41 (At $x/R_0 = 1.48$ )
9.	$\frac{\epsilon_d}{-\overline{u_i'''} dP/dx_i}$	-13.56	-0.105	3.3	0.033 (At $x/R_0 = 2.36$ )	0.36 (At $x/R_0 = 1.2$ )

### 6.2.3.1 Grid independence

In order to ascertain the grid independence of the computations, calculations were made of the flow field using three different grid sizes. These computations made use of the

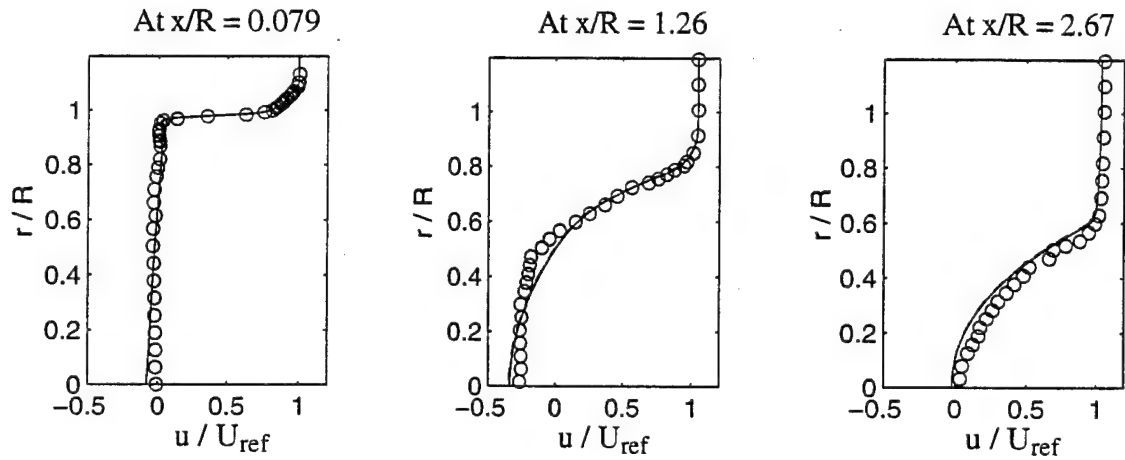
standard form of the k- $\epsilon$  model. The results obtained using two grids with 361 x 201 mesh points and 251 x 111 mesh points are compared in Figure 6.5. The mean flow field as represented by the axial and radial velocity components prove that grid independence is indeed achieved using the 251 x 111 grid. The TKE profiles show minimal differences between the two solutions. Solutions presented throughout the rest of this article have been obtained using the 251 x 111 grid.

#### 6.2.3.2 Treatment of convective fluxes

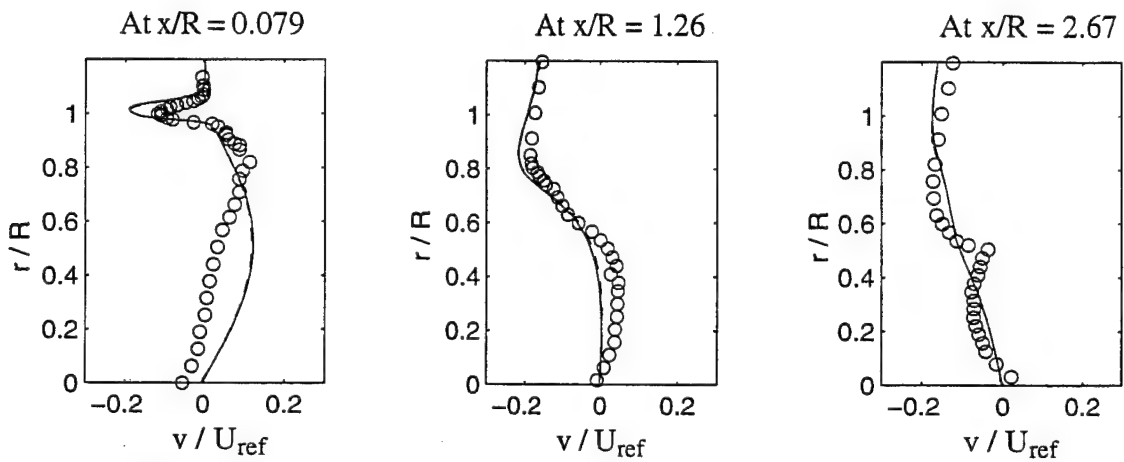
In the study of Tucker and Shyy [1993] the extensions to the unmodified k- $\epsilon$  model, based on the modifications suggested by Chen and Kim [1987] and the modification for compressible dissipation ( $\epsilon_d$ ) due to Sarkar et al. [1991] gave a better accounting of the flow field development than the unmodified model which was in sharp contrast to the results that were seen in some of our earlier calculations using the finite volume algorithm developed by Jameson et al. [1981] (with the TVD type artificial dissipation scheme) described in Chapter 4. One of the differences between these calculations and the study of Tucker and Shyy [1993] is the treatment of the convection terms. In that study the computations were made using a second-order central difference scheme while those of Tucker and Shyy [1993] used a weighted higher and first order upwind schemes for the convection terms in the mean flow equations and a first order upwind scheme for the k and  $\epsilon$  equations.

To clarify this issue, regarding the convection schemes, a set of computations were made using the second order upwind scheme based on the Steger-Warming flux-splitting approach (described in Chapter 4). The variables at the interfaces were extrapolated based on a MUSCL extrapolation technique (Shuen, 1992). Definite differences between the results of the two computations i.e., the second-order upwinding and the second-order central differencing of the convection terms were seen and some of these representative quantities are presented in Table 6-3.

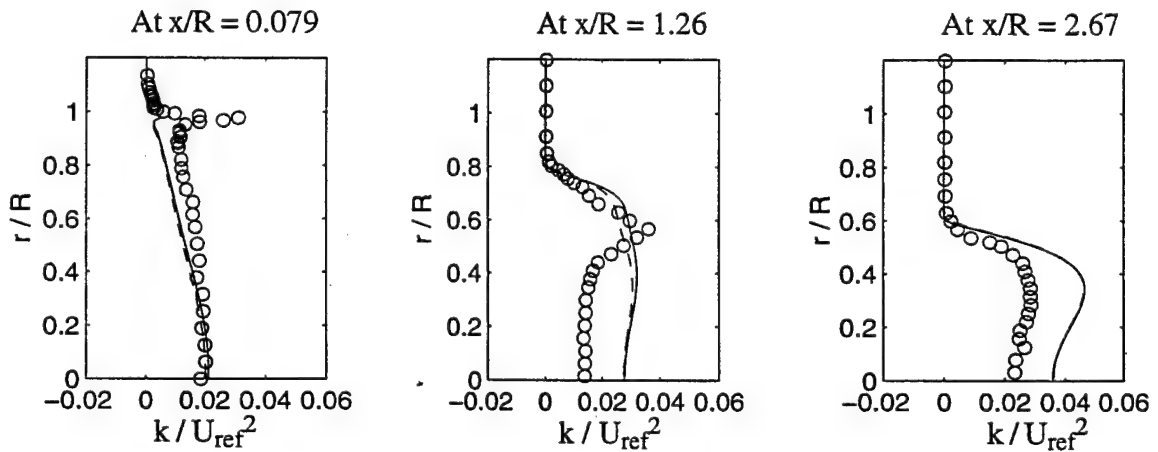
Results obtained using the upwind method are presented in figures 6.6 (a), (b) and (c). These figures show profiles of the axial and radial velocity components and the Reynolds



a) Computed axial velocity component.



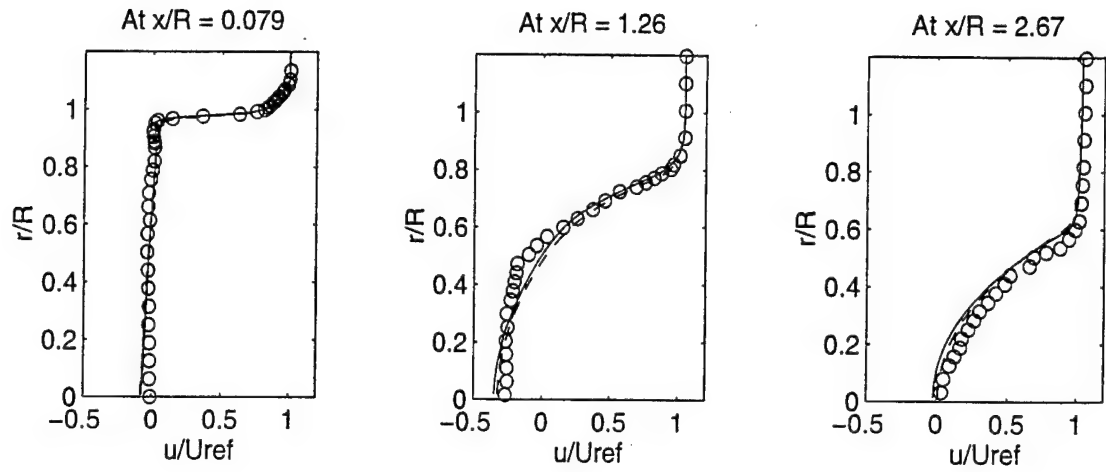
b) Computed radial velocity component.



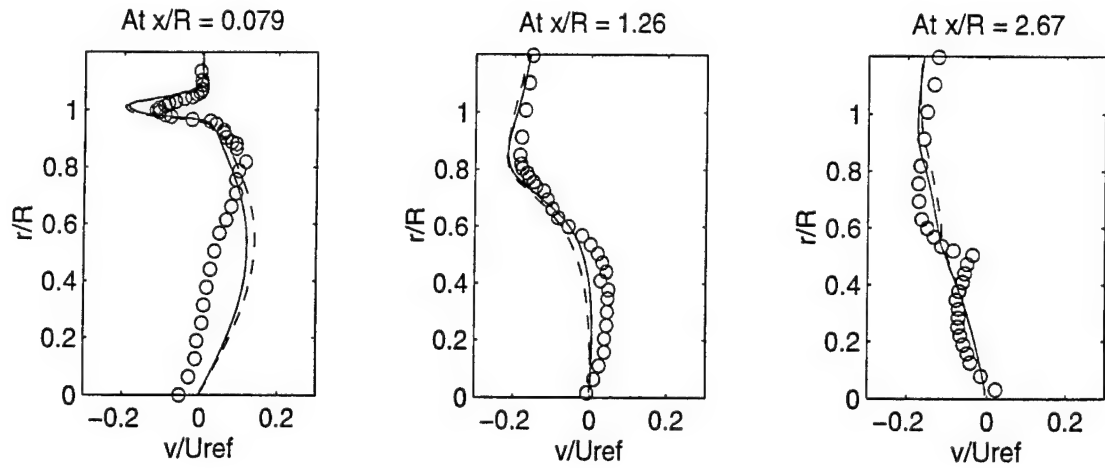
c) Computed values of TKE.

Figure 6.5. Grid Independence test : Comparison of  $u$ ,  $v$  and TKE computed using the Standard  $k-\epsilon$  Model.

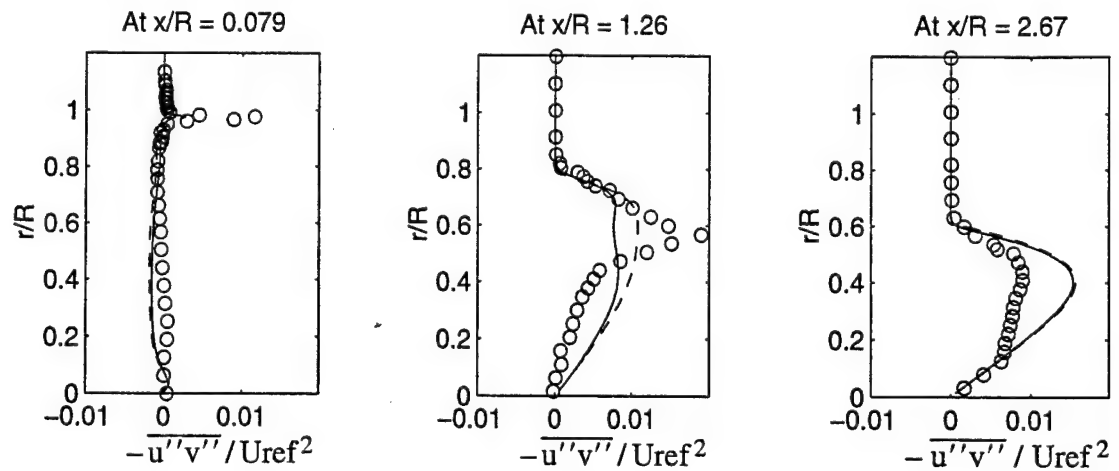
— = 361x201 grid ; --- = 251x111 grid "o" = Experiment.



a) Computed axial velocity component.



b) Computed radial velocity component.



c) Computed primary Reynolds shear stress component.

Figure 6.6. Comparison of convection schemes, using the unmodified  $k-\epsilon$  model.

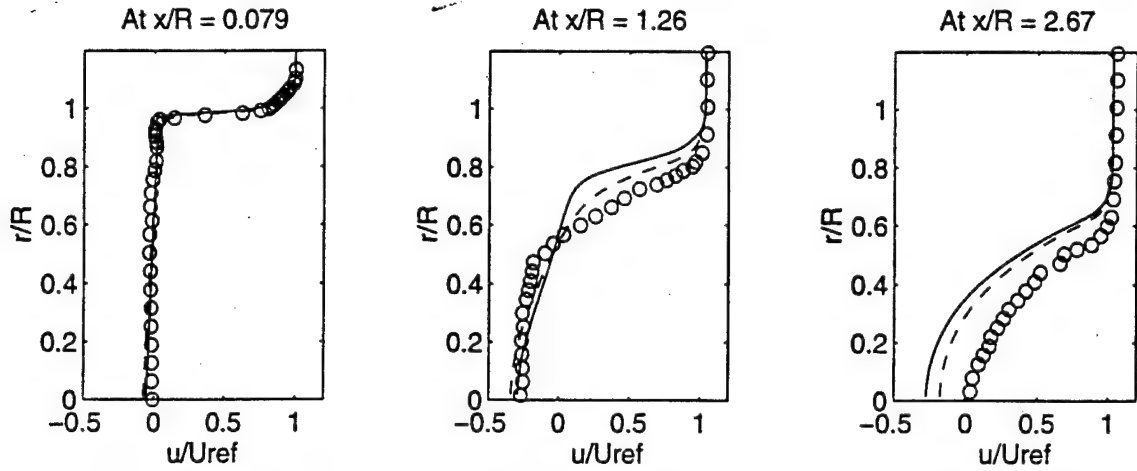
— = central difference ; - - - = 2nd order upwind and "o" = Experiment.

shear stress. A comparison is presented between the predictions made, using the second order central difference scheme and the second order upwind scheme, with the unmodified k- $\epsilon$  model. The differencing scheme used seems to have very little impact on the standard k- $\epsilon$  model based computations. Computations made using the Ek $\epsilon$ 1 model showed considerable differences between the two convection treatments. These are shown in Figures 6.7 (a), (b) and (c) where a comparison is presented between the predictions made of the axial and radial velocity components and the Reynolds shear stress.

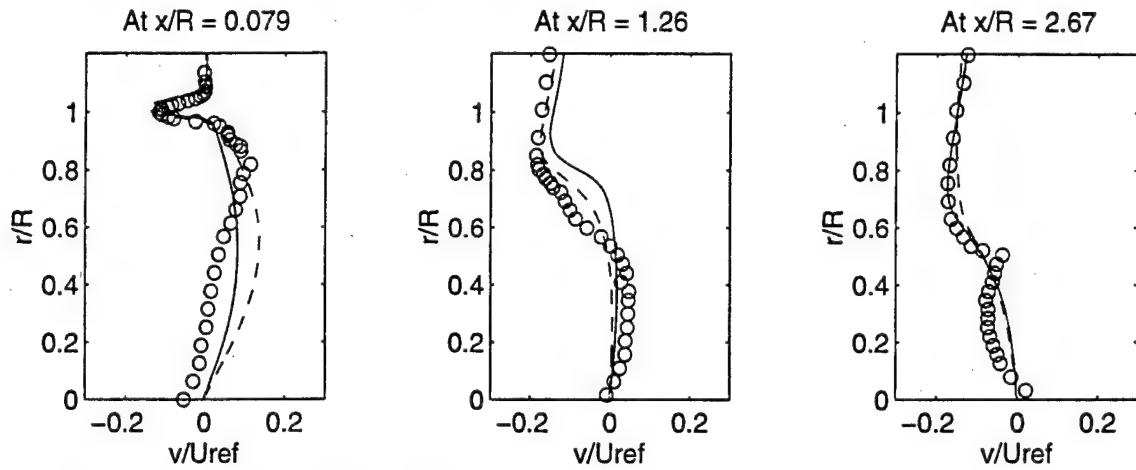
Table 6-3. Comparison between convection schemes.

No.	Model	Ave. Turning Angle	$\overline{C_{p,base}}$	Reattachment length $x/R_o$	Maximum TKE Level	Peak Reverse Velocity	Scheme
1.	Experiment	-15.1	-0.102	2.67	0.044 (At $x/R_o = 2.2$ )	0.27 (At $x/R_o = 1.5$ )	-
2.	Sk $\epsilon$	-14.73	-0.112	2.715	0.047 (At $x/R_o = 2.3$ )	0.35 (At $x/R_o = 1.21$ )	2nd order Central
3.	Sk $\epsilon$	-15.19	-0.116	2.61	0.049 (At $x/R_o = 2.24$ )	0.34 (At $x/R_o = 1.02$ )	2nd order Upwind
4.	Ek $\epsilon$ 1	-10.65	-0.085	3.786	0.025 (At $x/R_o = 3.06$ )	0.35 (At $x/R_o = 1.98$ )	2nd order Central
5.	Ek $\epsilon$ 1	-12.17	-0.096	3.43	0.028 (At $x/R_o = 2.6$ )	0.34 (At $x/R_o = 1.4$ )	2nd order Upwind

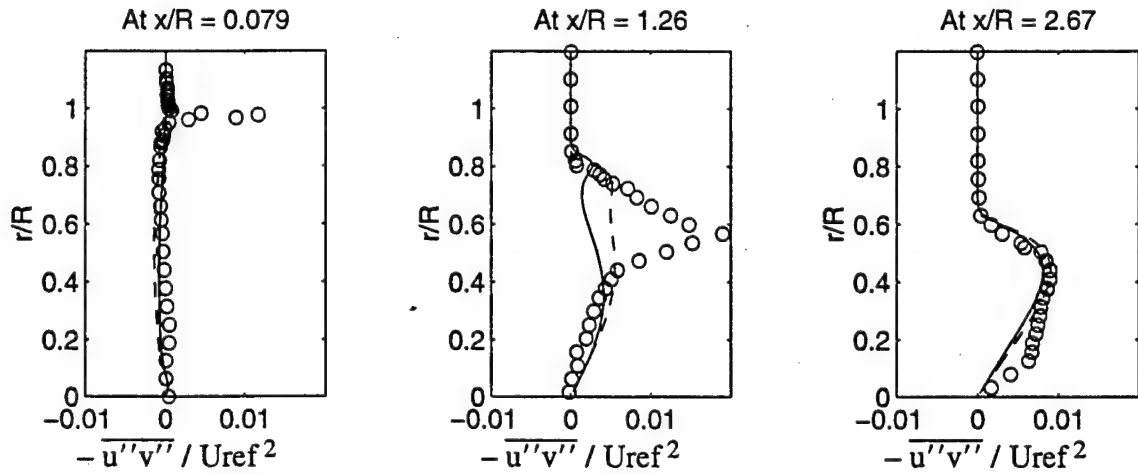
The comparison between the predictions made using the extended model (Ek $\epsilon$ 1) and the standard model (Sk $\epsilon$ ) with the 2nd order upwind differencing are shown in figures 6.8 (a), (b) and (c). The results shown here are very similar to the ones presented in Tucker and Shyy [1993]. However, there is still the question of the apparent difference between the second-order central difference and the second-order upwind difference solutions. In order to probe this a little, we zoomed into the region close to base corner. Profiles are presented at locations just upstream and immediately downstream of the base corner. These figures,



a) Computed values of axial velocity component



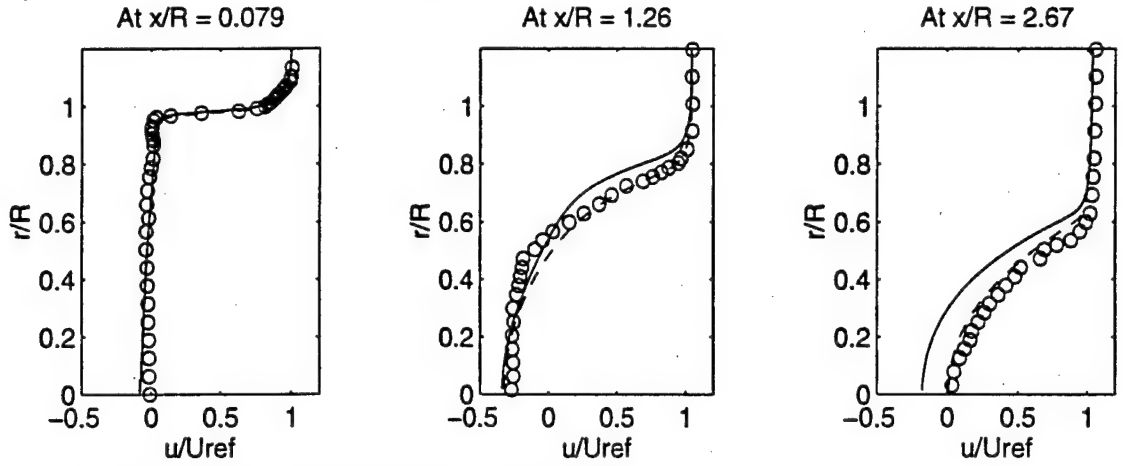
b) Computed values of radial velocity component



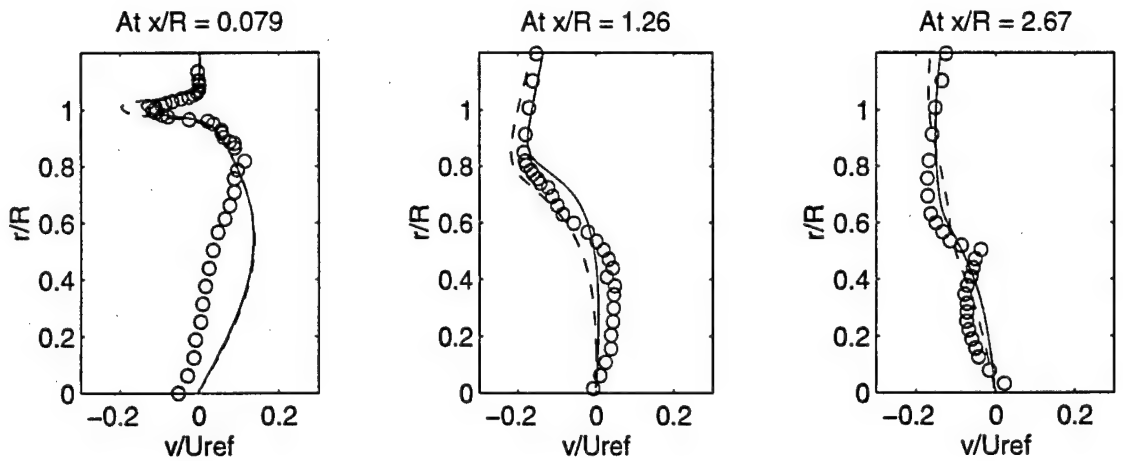
c) Computed primary Reynolds shear stress component

Figure 6.7. Comparison of convection schemes, using the Eke1 model.

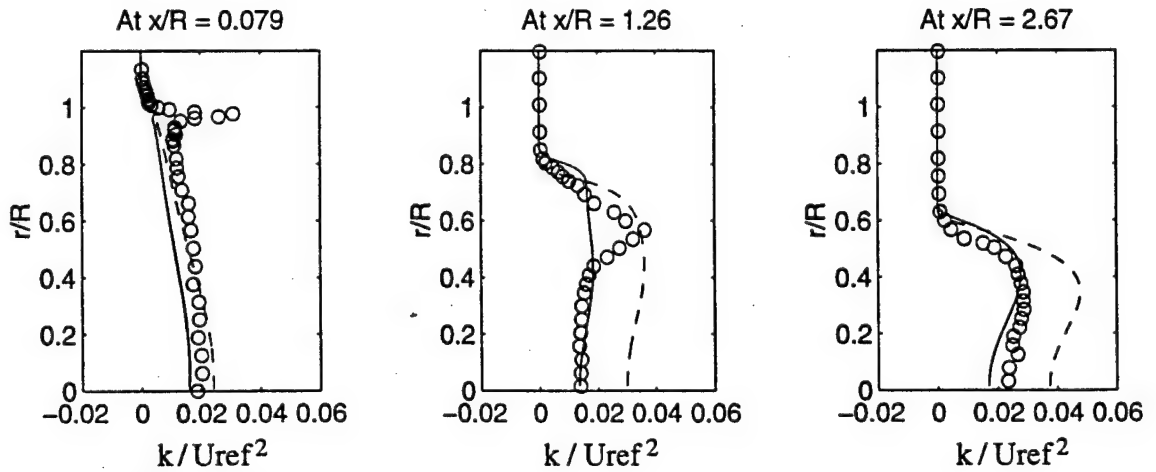
———— = central difference ; - - - - = 2nd order upwind and "o" = Experiment.



a) Computed values of axial velocity component



b) Computed values of radial velocity component



c) Computed levels of TKE

Figure 6.8. Comparison of  $Sk\epsilon$  and  $Ek\epsilon$  model predictions.

———— =  $Ek\epsilon$     - - - - =  $Sk\epsilon$     "o" = Experiment

also help to clarify to a certain extent the problems associated with the eddy-viscosity based  $k$ - $\epsilon$  model.

Figure 6.9 shows the computed values of TKE and Figure 6.10 shows the computed values of the rate of dissipation of TKE. At the first cell upstream of the base corner, the central differencing scheme does show some influence of the expansion at the base, possibly contributing to the differences seen in the results obtained with the central difference scheme and the results presented by Tucker and Shyy [1993]. At the first cell downstream of the base corner, it can be seen quite clearly that there is marked reduction in the magnitude of TKE due to the decreased production rates as the flow goes through the expansion region. All the computations show a reduction in the rate of dissipation of TKE as well, in direct contrast to experimental observations.

In order to explain the observed discrepancies between the different convection schemes, it is worthwhile to look at the flow angles at locations downstream and upstream of the base. This is shown in figure 6.11. The upstream influence of the rapid expansion is seen in the profiles upstream of the base corner, in the case of the central differencing based treatment of the convection terms. This influence is not seen in the second-order upwinding based treatment of the inviscid fluxes. Also, at locations upstream of the base corner the flow angle should be expected to be close to zero. This is not the case in the finite volume algorithm with the artificial dissipation added to it. This is the effect of the addition of artificial dissipation and has been reported recently by McNeil [1996]. The second-order upwinding based calculations, on the other hand, display pretty much the correct behaviour at locations upstream of the base corner. With this in mind we decided to use the 2nd order upwind differencing of the inviscid fluxes for all our comparisons. All the comparisons that are given throughout the rest of this article are based on computations which used the 2nd order upwind differencing technique to discretize the convection terms. Also the same treatment was used for the mean flow equations as well as equations governing the transport of TKE and its dissipation rate.



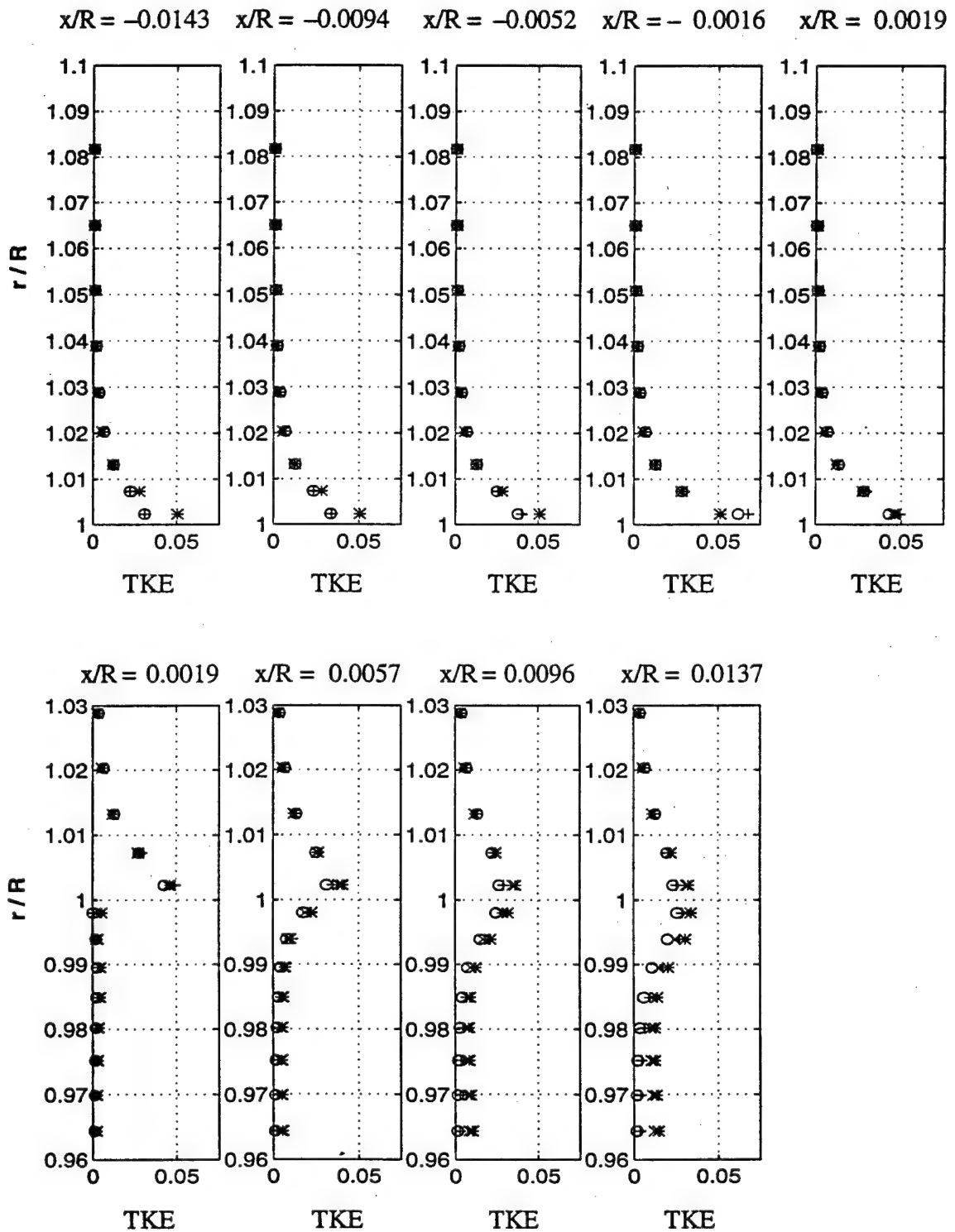


Figure 6.9. Computed values of TKE at locations slightly upstream of the base corner and immediately downstream of it.

+ =  $Sk\epsilon$  (central)   o =  $Ek\epsilon_1$  (central)   \* =  $Sk\epsilon$  (upwind)   x =  $Ek\epsilon_1$  (upwind)

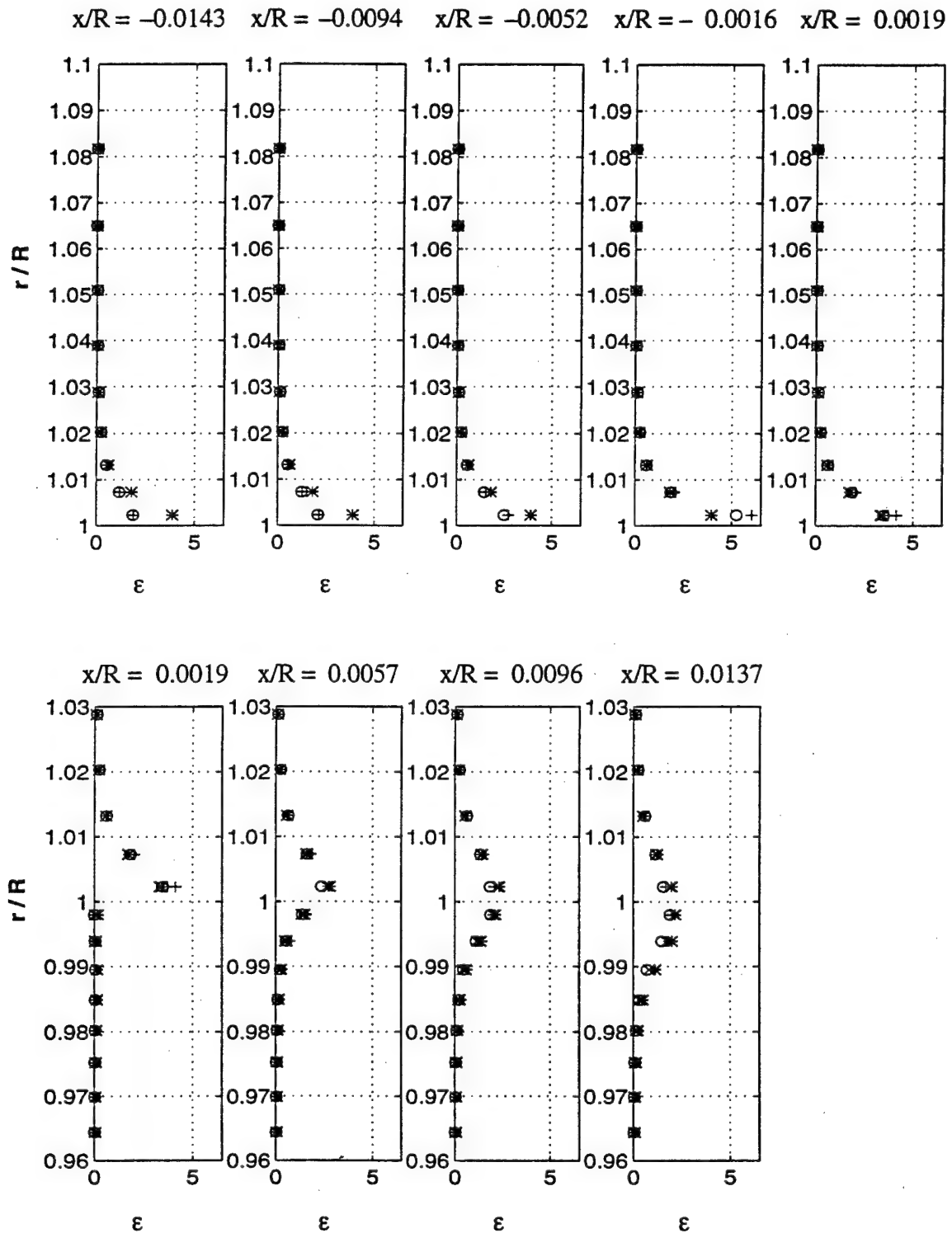


Figure 6.10. Computed values of TKE dissipation rate at locations slightly upstream of the base corner and immediately downstream of it.

+ =  $Sk\epsilon$  (central)   o =  $Ek\epsilon_1$  (central)   \* =  $Sk\epsilon$  (upwind)   x =  $Ek\epsilon_1$  (upwind)

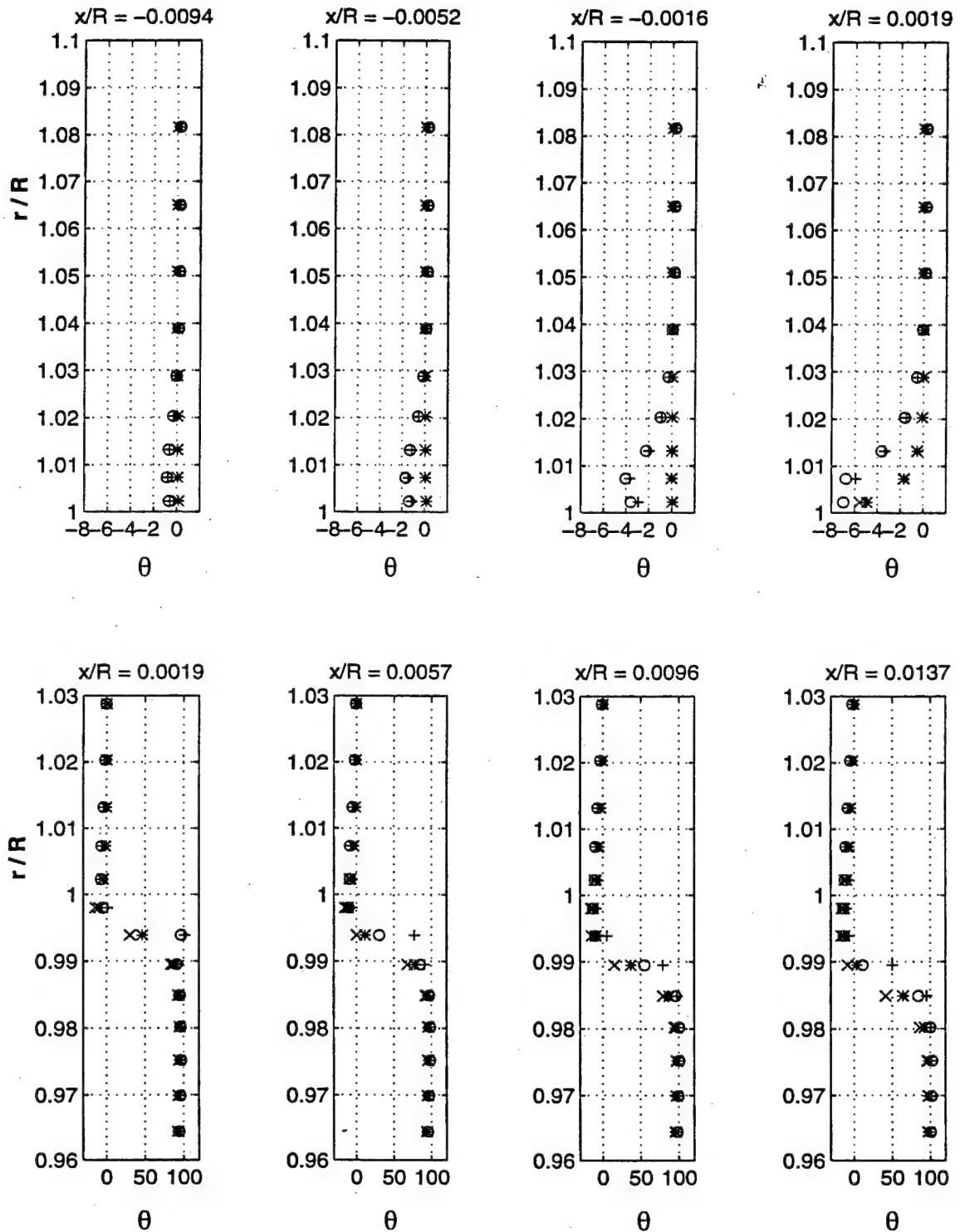


Figure 6.11. Comparison of the computed value of flow angle  $\theta$  (deg).

### 6.2.3.3 Non-equilibrium modifications

The mixing region, where the separated shear layer interacts with the recirculating fluid downstream of the base, has been documented to be strongly influenced by non-equilibrium effects. Several modifications have been proposed in order to extend the applicability of the  $k$ - $\epsilon$  model. These are algebraic modifications with an intent to modify one or more of the constants used in the  $\epsilon$  equation and the definition of the eddy-viscosity. In this section we address two such modifications, one proposed for  $C_{\epsilon 1}$  (Chen and Kim, 1987) and the other proposed to modify  $C_{\epsilon 2}$  (Thakur et al., 1996).

The non-equilibrium modification due to Chen and Kim [1987], alters the coefficient  $C_{\epsilon 1}$  in the incompressible form of the  $\epsilon$  equation to  $\left(1.15 + 0.25 \frac{P_k}{\epsilon}\right)$ . Chen and Kim [1987] observe that this alteration of the coefficient, allows  $\epsilon$  to respond faster to the variations in the mean strain rate. It works to enhance the development of  $\epsilon$  when the mean strain is strong (or large production rate) and to reduce it when the mean strain is weak (or small production rate).

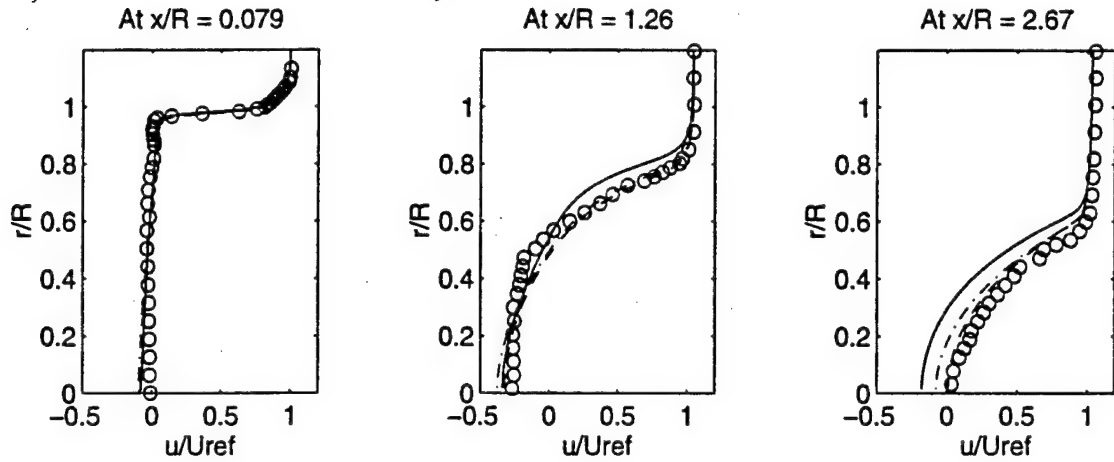
The non-equilibrium modification due to Thakur et al. [1996] alters the constant  $C_{\epsilon 2}$  in the  $\epsilon$  equation to  $\left(1.45 + 0.45 \frac{P_k}{\epsilon}\right)$ . The modification has been proposed to be used in conjunction with  $C_{\epsilon 1}$ , because of observations (Thakur et al., 1996) made from the computational studies of flow past a backward facing step and the hill flow inside a channel. The  $C_{\epsilon 1}$  modification reportedly overpredicts the length of the recirculating flow due to increased levels of the “production of dissipation” term. Further tests (Thakur et al. 1996) conducted using this modification seem to indicate an improvement over the non-equilibrium modification due to Chen and Kim [1987]. The standard model in its unmodified form indicates that there is an equilibrium between the production and dissipation of TKE. The  $C_{\epsilon 2}$  modification has the effect of an added time scale. The time scale may be thought of as representing the relaxation time required for any imbalance

between production and dissipation rates of TKE to return back to an equilibrium situation. However, the modification in this form will tend to overpredict the rate of decay of TKE in the case of decaying isotropic turbulence. To avoid this, some form of a limiter needs to be applied to enable the modification to predict experimentally observed decay rates. One modification, albeit not an elegant one, could be  $\left\{ \max \left[ 1.92, \left( 1.45 + 0.45 \frac{P_k}{\epsilon} \right) \right] \right\}$ . This is just suggested as a temporary fix to the problem. It should be noted here, that previous studies on homogeneous shear flows (Bernard and Speziale, 1992) have shown that there is definitely a need for a "relaxation time-scale" based modification.

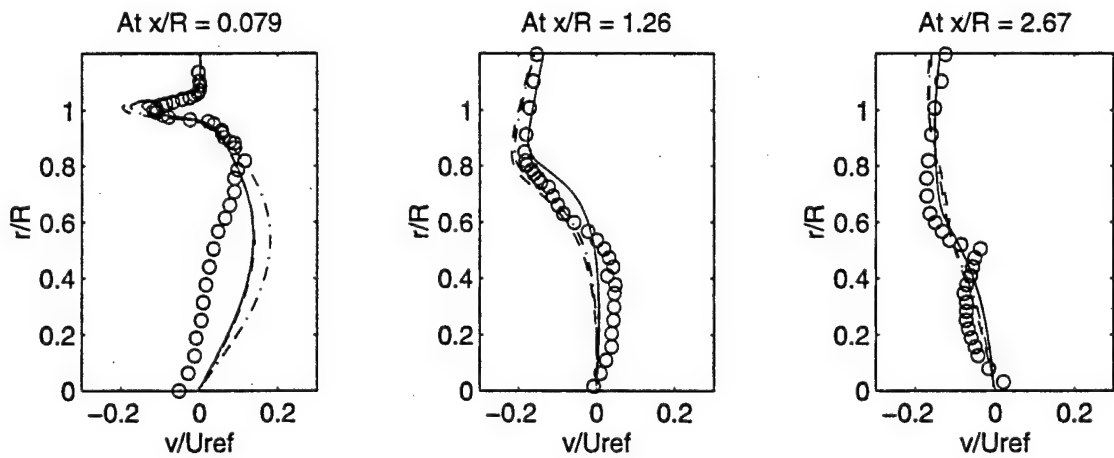
Before we analyze the effect of such modifications it might be informative to consider the development of the shear layer from its point of inception, i.e., as a separated boundary layer at the base corner. Using an order of magnitude analysis, Gaviglio et al. [1977] showed that through the expansion there is a reduction in the rate of production of TKE while the rate of dissipation of TKE is relatively unaffected which is due to the short time duration that a volume of fluid spends in the expansion region. Referring to the experimental analysis of Herrin and Dutton [1993], the strength of the expansion at the base corner decreases with increasing distance from the wall. Consequently, fluid particles in the viscous region experience a more sudden expansion than the particles farther away from the wall resulting in a larger discontinuity in the velocity profile immediately downstream of the expansion, displaying a larger peak mean velocity gradient downstream of the expansion. Hence, for only moderate changes in the mean shear stress there is an increase in the primary turbulent kinetic energy production rate. This is experimentally observed in the higher turbulence levels downstream, as the shear layer develops. Thus, there are regions in the flowfield where higher production rates do not necessarily imply an increase in the rate of dissipation of TKE. Whether such non-equilibrium modifications are indeed consistent with the flow physics is debatable. These modifications are curve fits to the empirically observed details of the flow field. From an engineering perspective it does, however, offer a "quick fix" solution to the

problem. In the remainder of this section comparisons will be presented between the predictions made using the unmodified  $k-\epsilon$  model (referred to as the standard model and designated as  $Sk\epsilon$ ) and the non-equilibrium based extensions to the standard model. Throughout the rest of this chapter, the standard model modified using the  $C_{\epsilon 1}$  modification (Chen and Kim, 1987) and the compressibility modification for  $\epsilon_d$  due to Sarkar et al. [1991] will be designated as  $E_k\epsilon 1$  and the standard model modified using both the  $C_{\epsilon 1}$  and the  $C_{\epsilon 2}$  modifications and the compressibility modification for  $\epsilon_d$  due to Sarkar et al. [1992] will be designated as  $E_k\epsilon 2$ .

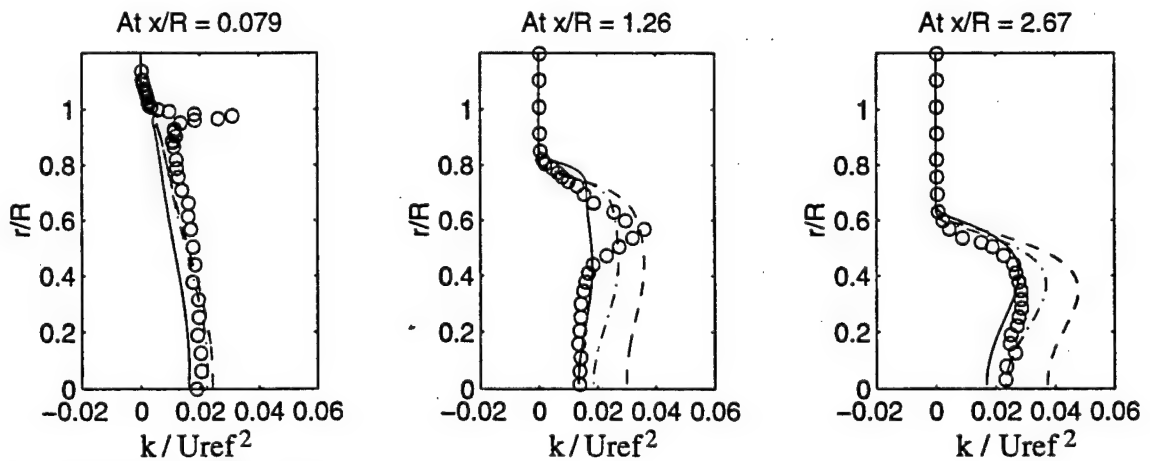
To evaluate the effectiveness of these non-equilibrium modifications, comparisons are presented of the predictions made using the modified models with the standard model. Profiles are presented at three representative locations. These represent a location close to the base of the afterbody ( $x/R = 0.079$ ); a location that is midway to the experimentally observed reattachment point ( $x/R = 1.26$ ) and a location that is at the experimentally observed reattachment point ( $x/R = 2.67$ ). Profiles of the mean velocity components and the TKE at these three locations are presented in Figures 6.12 (a), (b) and (c), respectively. At the  $x/R = 0.079$  location, close to the base region, very minor differences are seen in the predictions made using the two models. While the mean flow profiles show next to negligible differences, the predictions of TKE show some observable differences. In the predictions made of the TKE the location of the peak value is picked up but all three models grossly underpredict the magnitude of this peak, possibly due to the inherent assumption of isotropy in eddy-viscosity based models. Marked differences in the predictions made using the two models can be seen in the profiles at the downstream locations. At both the downstream locations presented in this figure, the standard model (unmodified  $k-\epsilon$  model) seems to make the better prediction in terms of the mean velocity components. At the  $x/R = 1.26$  location it is clearly seen that there is some kind of a lateral shift in the predictions made of the axial and radial velocity components, using the  $E_k\epsilon 1$  model. However, the TKE seems to be better represented by the  $E_k\epsilon 1$  model. The standard model predicts increased levels of TKE as



a) Computed axial velocity component.



b) Computed radial velocity component.



c) Computed TKE levels.

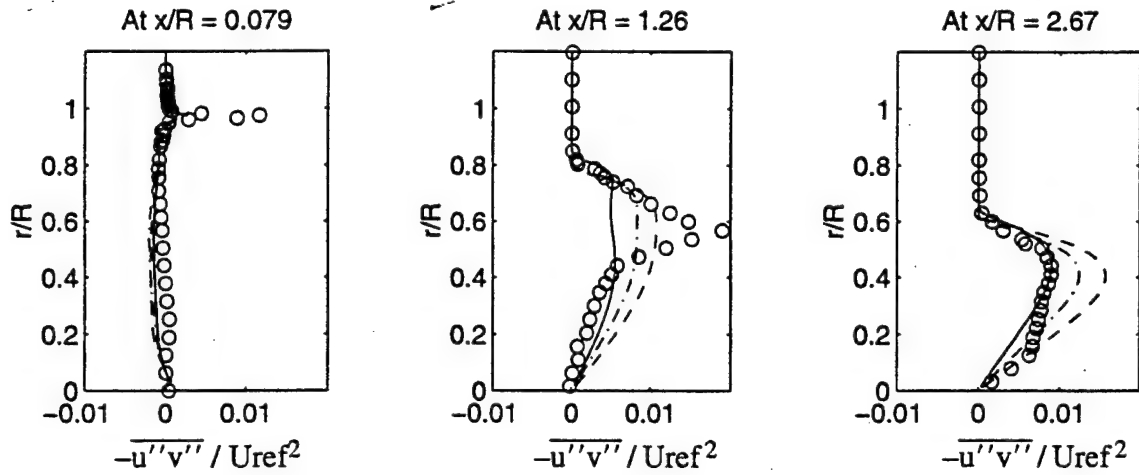
Figure 6.12. Comparison of the computations made using the non-equilibrium modifications with the unmodified model.

----- =  $Sk\epsilon$  ——— =  $Ek\epsilon_1$  -.-.- =  $Ek\epsilon_2$  and "o" = Experiment.

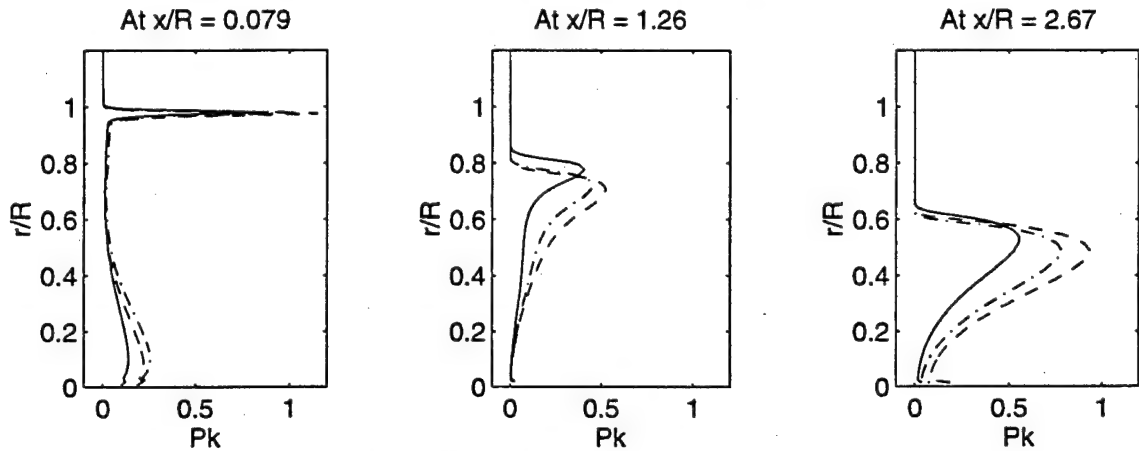
compared to the experimentally observed levels, obviously a result of an increased rate of production of TKE which is clearly seen in the computed values of rate of production of TKE, presented in Figure 6.13 (b). The  $E\kappa 2$  model predictions of the mean velocity components seems much closer to the the predictions of the standard model while its predictions of the turbulent kinetic energy is about midway between the predictions made using the  $S\kappa$  and the  $E\kappa 1$  model. This trend is continued in the comparisons presented in Figures 6.13 (a), (b) and (c).

Figures 6.13 (a), (b) and (c) show profiles of the primary Reynolds shear stress, the primary rate of production of TKE and the total rate of dissipation of TKE. The rate of dissipation profiles show the magnitude of the dissipation rate used in the transport equation for TKE. Therefore, if  $\epsilon$  is the solenoidal component of the rate of dissipation of TKE used in the unmodified model, then for the  $E\kappa 1$  and  $E\kappa 2$  models the profile shows the sum total of the solenoidal dissipation rate and the compressible dissipation rate, i.e.,  $\epsilon(1.0 + 0.5M_t^2)$ . The profiles of the Reynolds shear stress follow the same trends observed in the predicted values of TKE with the  $E\kappa 1$  model offering a better representation of the variation compared to the standard model and the  $E\kappa 2$  predicting a variation which can be thought of as an average of these two predictions. Profiles of production and dissipation rates show that the standard or unmodified model predicts increased levels of production and dissipation. At what can be thought of as the interface between the shear layer and the recirculating fluid, the production and dissipation rates are not in equilibrium (clearly indicative of the non-equilibrium effects). A key feature to note in the profiles of production and dissipation rates are the location of the peak values. The peak location refers to the point where the inner edge of the shear layer interacts with the recirculating fluid and results in increased production rates. This location is relevant in interpreting the results when comparing the predictions made using the standard model and the extended models. From the figures the radial shift in the peak locations is very evident. As will be shown later, this is due to the reduced turning angle of the shear layer computed using the  $E\kappa 1$  model.

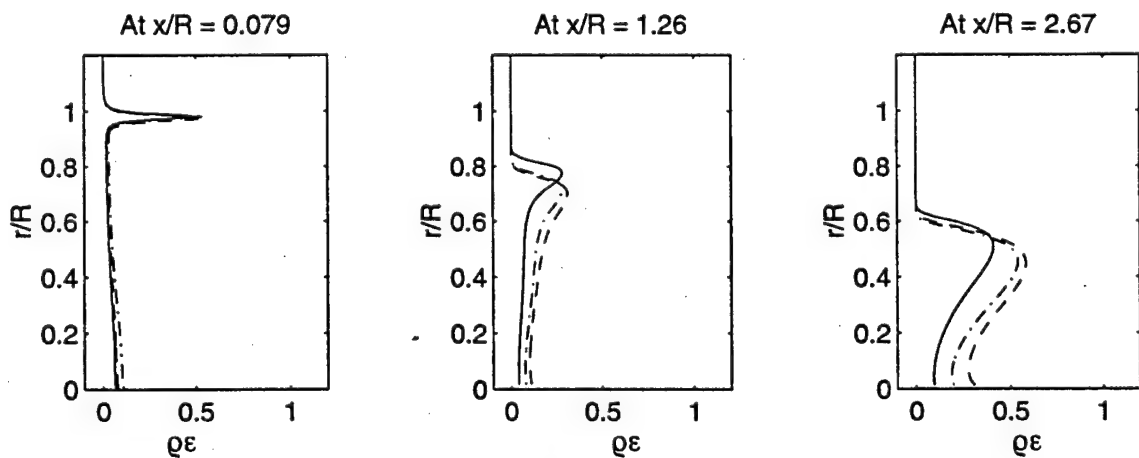




a) Computed values of the primary Reynolds shear stress component.



b) Computed values of the rate of production of TKE.



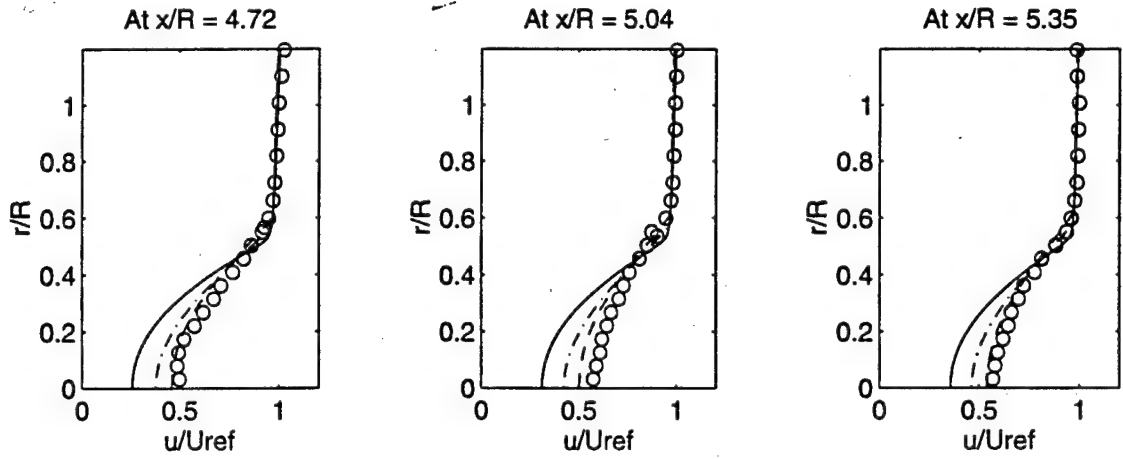
c) Computed values of the total rate of dissipation of TKE.

Figure 6.13. Comparison of the computations made using the non-equilibrium modifications with the unmodified model.

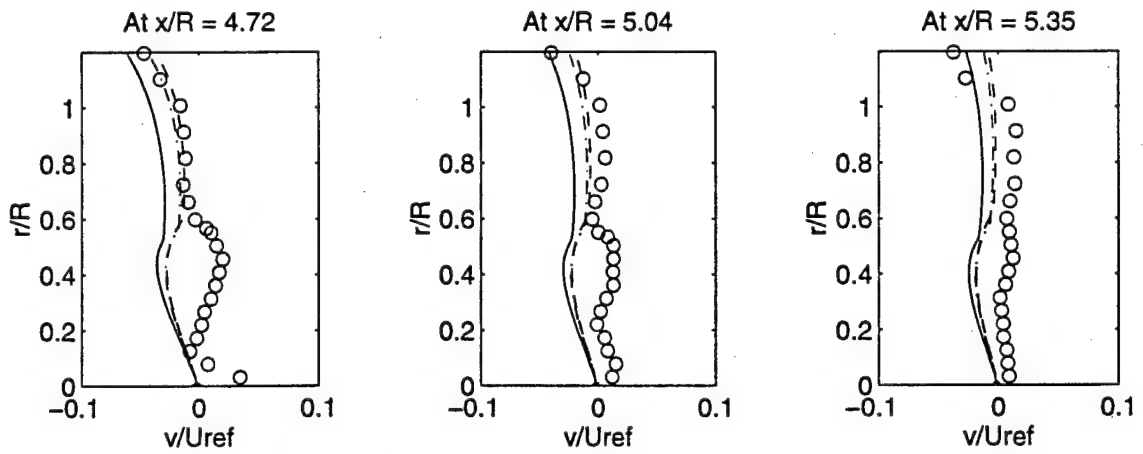
----- =  $Sk\epsilon$  ——— =  $Ek\epsilon_1$  and -.-.- =  $Ek\epsilon_2$  and "o" = Experiment.

To better understand the predictive capabilities of the models, profiles of the velocity components and the TKE are shown in Figures 6.14 (a), (b) and (c) at locations far downstream of reattachment. Again it is interesting to observe that while the non-equilibrium based modifications predict more accurately the turbulence structure parameters, the standard model does a better job in terms of the mean velocity profiles. Clearly, two different flow structures most directly influence the predictive capabilities namely the free shear layer and the recirculating zone. The mean angle through which the shear layer turns following its separation at the base corner, dictates the development of the mean velocity components. The non-equilibrium between the rate of production of TKE and its dissipation rate in the recirculating region, is better represented by the non-equilibrium modification to  $C_{\varepsilon 1}$ . This is observed in the better agreement of the predicted values of the mean turbulence quantities, such as the TKE and Reynolds shear stress, with the experimental values.

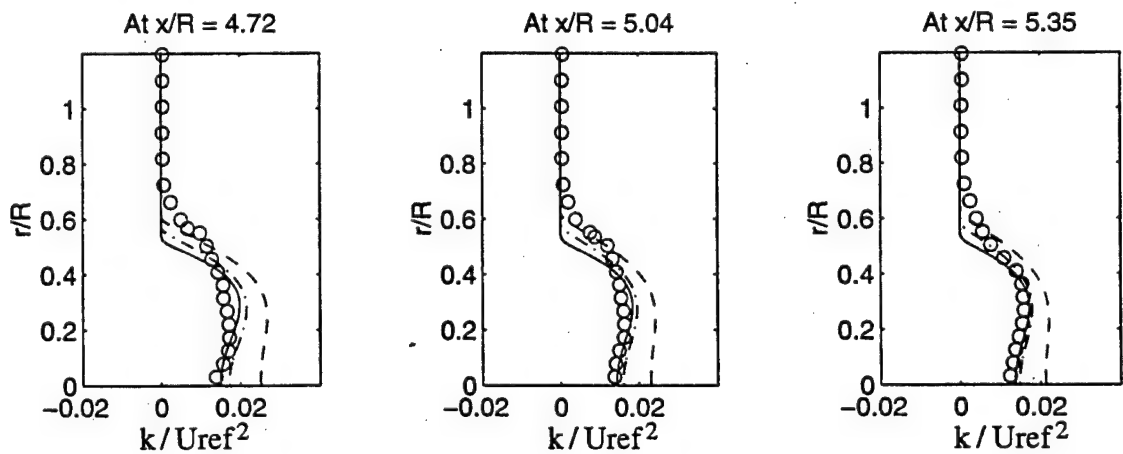
Details regarding the development of the shear layer were calculated. These details help in getting a better insight into the relative capabilities of the various modifications tested here. There is a difference between the way the extent of the shear layer is currently computed to the way Herrin and Dutton [1993] define the extent of the shear layer. The mean turning angle in the shear layer is computed in exactly the same way as described in Herrin and Dutton [1993]. The flowfield is then rotated by this mean angle and the velocity vector parallel to the streamwise direction, in the shear layer, is computed. The experimental measurements indicate that the streamwise velocity component reaches a constant value at a certain location. These constant velocity values are used to define the faster and slower streams of the two-dimensional mixing layer. Let us designate the fast and slow streams of the mixing layers as  $U_1'$  and  $U_2'$  respectively. A reference velocity is defined as  $\Delta U' = U_1' - U_2'$  and the variation of the streamwise velocity component is computed. The 10% velocity line is defined as the location where  $U' = U_2' + 0.1\Delta U'$ , where  $U'$  is the streamwise velocity component. The 90% velocity line and the 50% velocity lines are



a) Computed axial velocity component.



c) Computed radial velocity component.



c) Computed TKE levels.

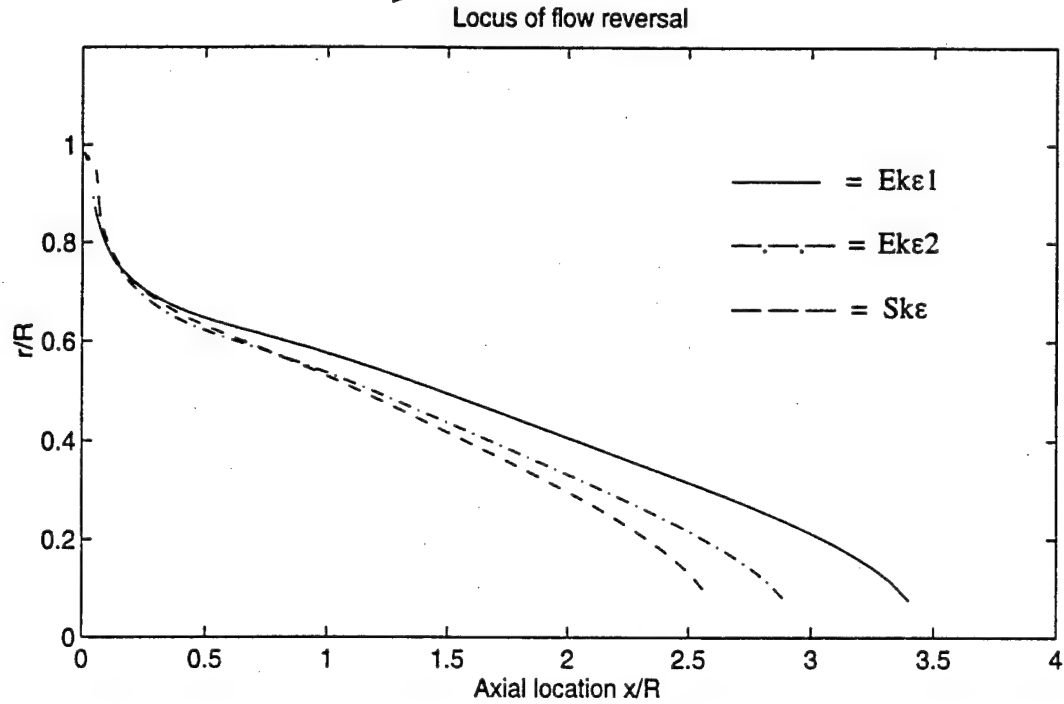
Figure 6.14. Comparison of the computations made using the non-equilibrium modifications with the unmodified model.

----- =  $Sk\epsilon$     ————— =  $Ek\epsilon_1$     -.-.-.- =  $Ek\epsilon_2$  and "o" = Experiment.

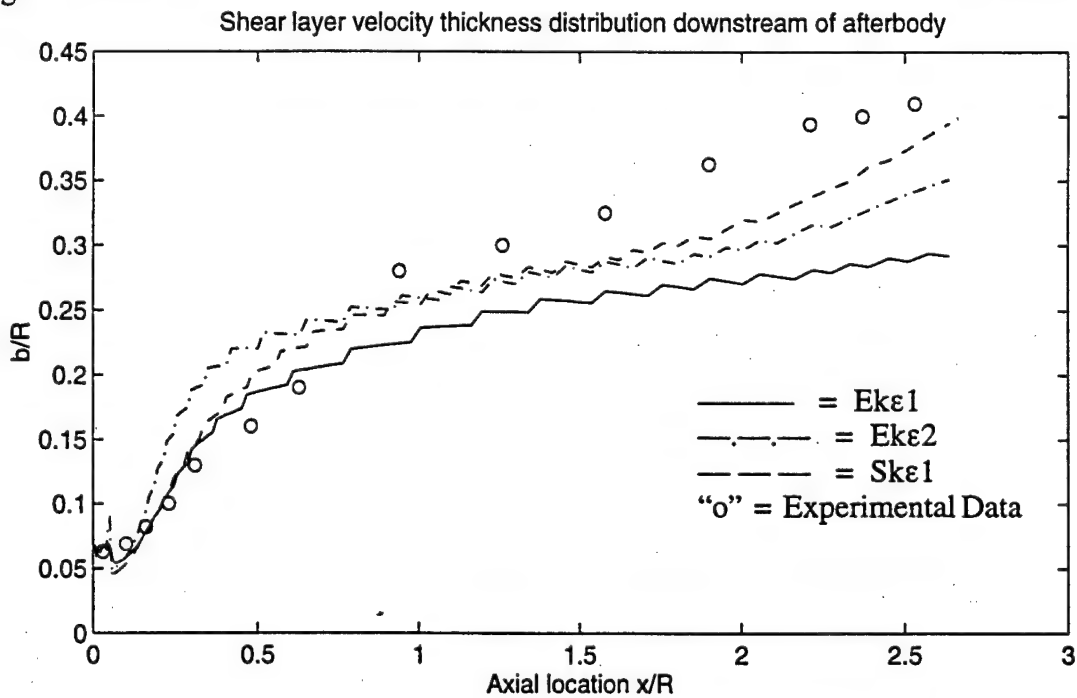
defined in a similar way. The thickness of the shear layer, "b", is defined as the distance between the radial location of the 90% velocity line and the 10% velocity line.

In the computations made using the eddy-viscosity models after computing the streamwise velocity component it was observed that the velocity does not reach a constant value. Therefore, the location of  $U_2'$  had to be defined in an alternate way. The location of  $U_2'$  is defined in the computational case as follows: The location where the streamwise velocity component changes sign from positive to negative is computed on the numerical grid. The streamwise velocity component just below this location on the numerical grid was chosen to define the magnitude of  $U_2'$ . The location of  $U_1'$  was relatively easy to define because it is dictated chiefly by the inviscid flow development. Therefore, there are significant differences in the definition of the slow stream side of the shear layer. The plots presented are not meant as a measure of the relative accuracy of the prediction methods (though the apparent difference between the definitions does indicate to a certain extent the inaccuracies of eddy viscosity models in predicting flow fields with an increased degree of complexity). These plots are presented here because they help in understanding the differences between the various modifications.

Figures 6.15 through 6.16 (a), (b) and (c) show computed details of the shear layer downstream of the base. In all these figures it may be noticed that the shear layer locations do not start at  $x/R = 0$  (denoting the corner of the base), because of difficulties in computing the exact locations and sharp gradients in the mean velocity field. Figure 6.15 (a) shows the locus of flow reversal for the computed flow field. The locus of flow reversal is defined as the location where the axial component of the velocity vector changes sign. The figure shows that the  $S_{k\epsilon}$  model does seem to present a better estimate of the recirculation length (experimentally observed to be extending out to  $x/R = 2.67$ ). Figure 6.15 (b) shows the growth of the shear layer in the axial direction. The standard model predicts a thicker shear layer in comparison to the  $E_{k\epsilon 1}$  model and  $E_{k\epsilon 2}$  model which is to be expected because of the modification for compressibility effects that goes into the definition of the  $E_{k\epsilon 1}$  and

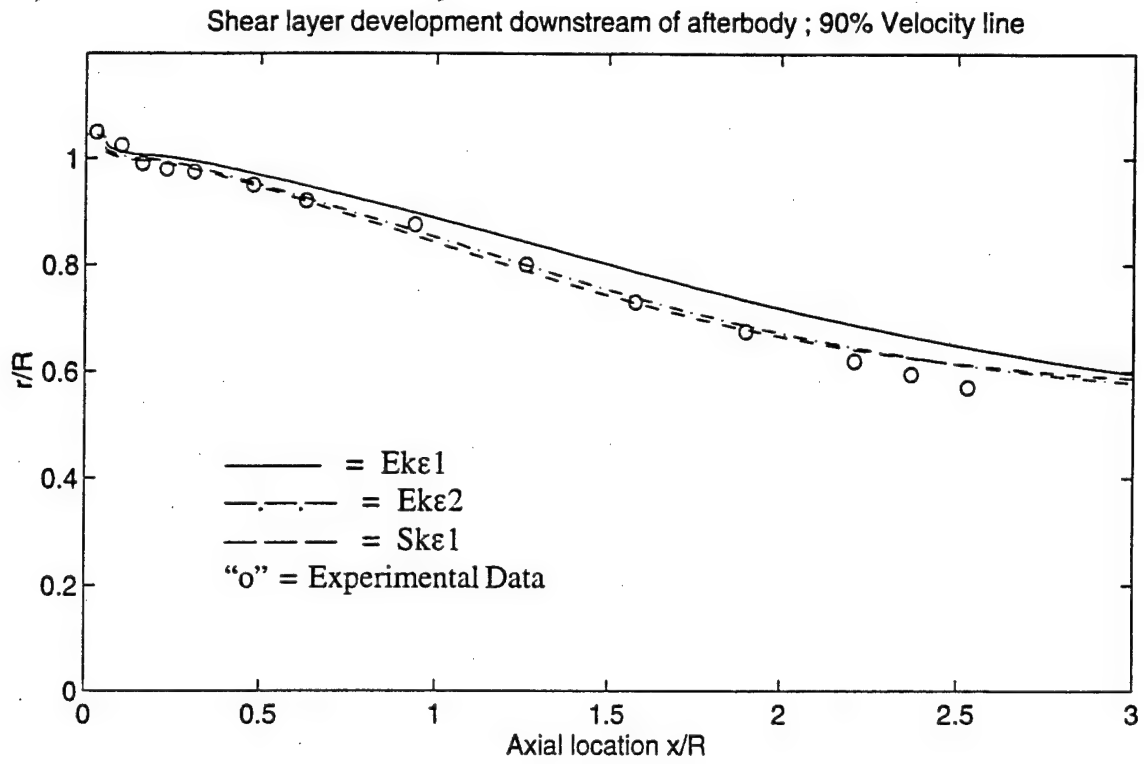


(a). Computed Locus of Flow Reversal, i.e., where the axial velocity component changes sign.

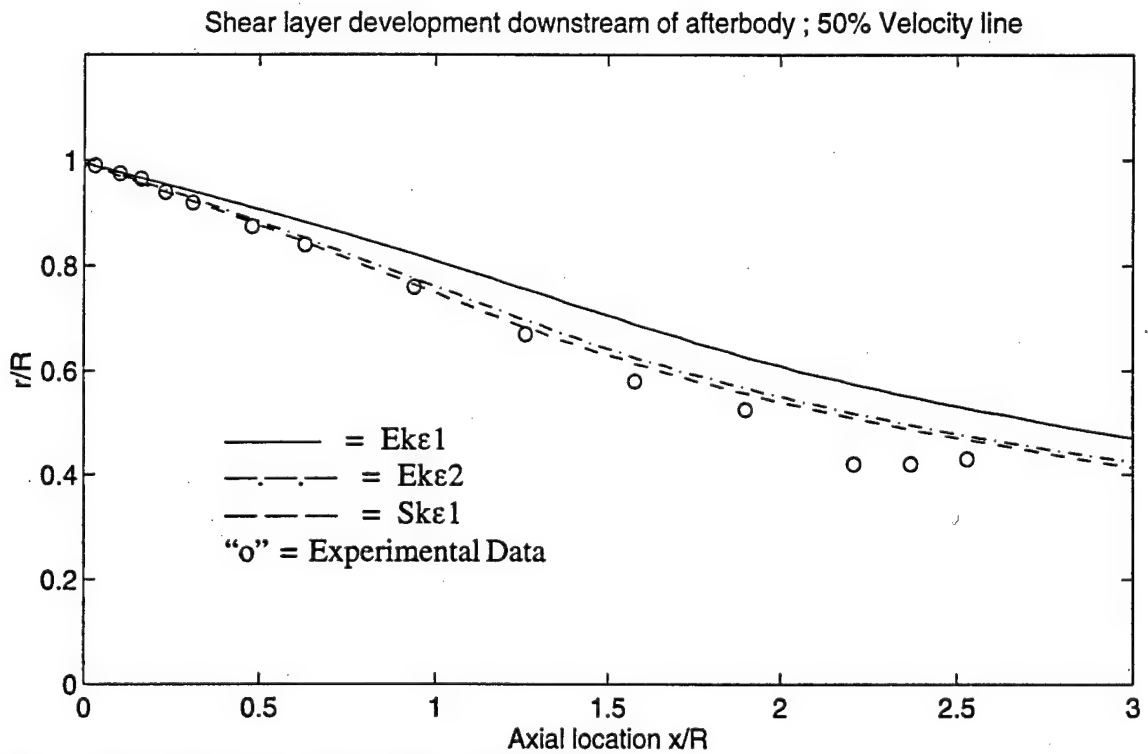


(b). Computed Thickness of the Shear Layer. The edges of the shear layer are defined as between  $U_2' + 0.1 \Delta U'$  and  $U_2' + 0.9 \Delta U'$ .

Figure 6.15. Development of the shear layer downstream of the afterbody.

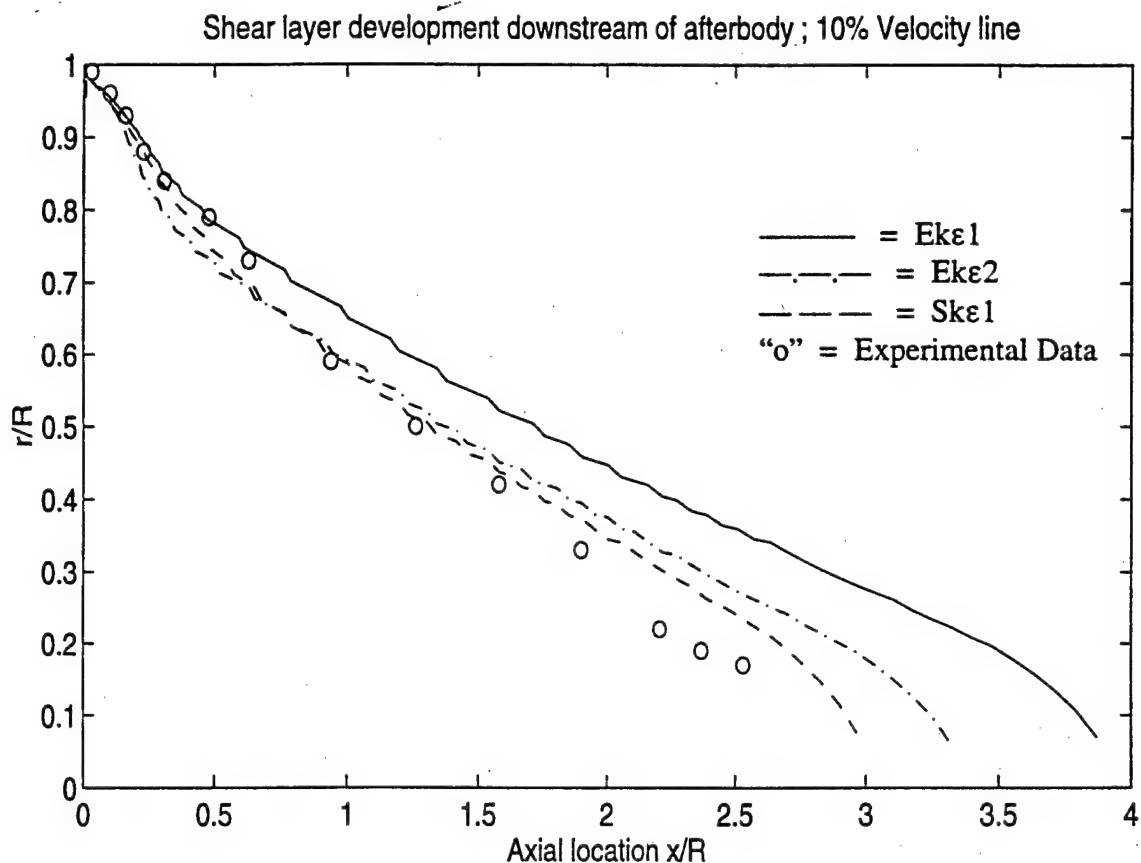


(a). Computed locus of the 90% velocity line.



(b). Computed locus of the 50% velocity line.

Figure 6.16. Computed development of the shear layer downstream of the afterbody.



(c). Computed locus of the 10% velocity line.

Figure 6.16 (Contd). Development of the shear layer downstream of the afterbody.

$\text{Ek}\epsilon 2$  models. Figures 6.16 (a), (b) and (c) show the computed locations of the 90%, 50% and the 10% velocity lines. As mentioned before, these plots are presented to compare the various modifications tested in this article and not necessarily as a comparison with the experimental data. However, these plots show that the unmodified model offers a better representation of the development of the shear layer.

The reason for the apparent inability of the  $\text{Ek}\epsilon 1$  model in accurately predicting this flow field can be explained as follows. The angle through which the incoming boundary layer turns while passing through the expansion seems to dictate to a fairly great extent the development of the flow downstream of the base. The shear layer predicted using the  $\text{Ek}\epsilon 1$  model seems to show a shift in the radial direction as compared to the standard  $k-\epsilon$  model. This is also reflected in the plots of production of TKE and the rate of dissipation of TKE,

which indicate a radial shift in the locations of the peak values (for the extended model in comparison with the standard model). A comparison was made between the predictions made by the standard model, the standard model with only the compressibility modification, the standard model with the non-equilibrium modification only and the Ekε1 model. The average flow turning angles are documented in Table 6-2. There is a distinct gradation in the predictions made leading to the increased inaccuracy of the extended model.

The flow turning angle at locations slightly upstream and downstream of the base are compared in Figure 6.17. The  $u$  and  $v$  components denoted in Figure 6.17 are the axial and radial velocity components respectively. The figure shows clearly that upstream of the base corner there is very little change in the turning angles computed. But almost immediately downstream of the base corner there is a significant difference between each one of the models. The difference in the turning angle of the shear layer leads to the inaccuracies seen in the predictions made of the flow field. Figure 6.18 shows plots of the 90% velocity line and the 10% velocity line, for the same four cases compared above in Figure 6.17. From this plot it can be seen that the impact of the various modifications are seen on the lower edge of the shear layer rather than on the upper edge. This is understandable because the development of the shear layer is chiefly governed by the interaction of the separated shear layer with the recirculating fluid. Thus any artificial modification to the rate of dissipation of TKE in this region seems to inhibit the true development of the shear layer.

#### 6.2.3.4 Compressibility modifications

In Chapter 5, a comparison has been made between the compressibility modifications of Sarkar et al. [1991] and those of El Baz and Launder [1993] for the simple case of decaying isotropic turbulence. It can be seen that the impact of both these modifications are essentially the same, with those of El Baz and Launder [1993] predicting a slightly increased level of rate of dissipation. Comparison of the predictions made using the modification proposed by Sarkar et al. [1991] for the dilatation dissipation term and modification proposed by Sarkar [1992] for the pressure dilatation term, El Baz and Launder [1993] modifications and the



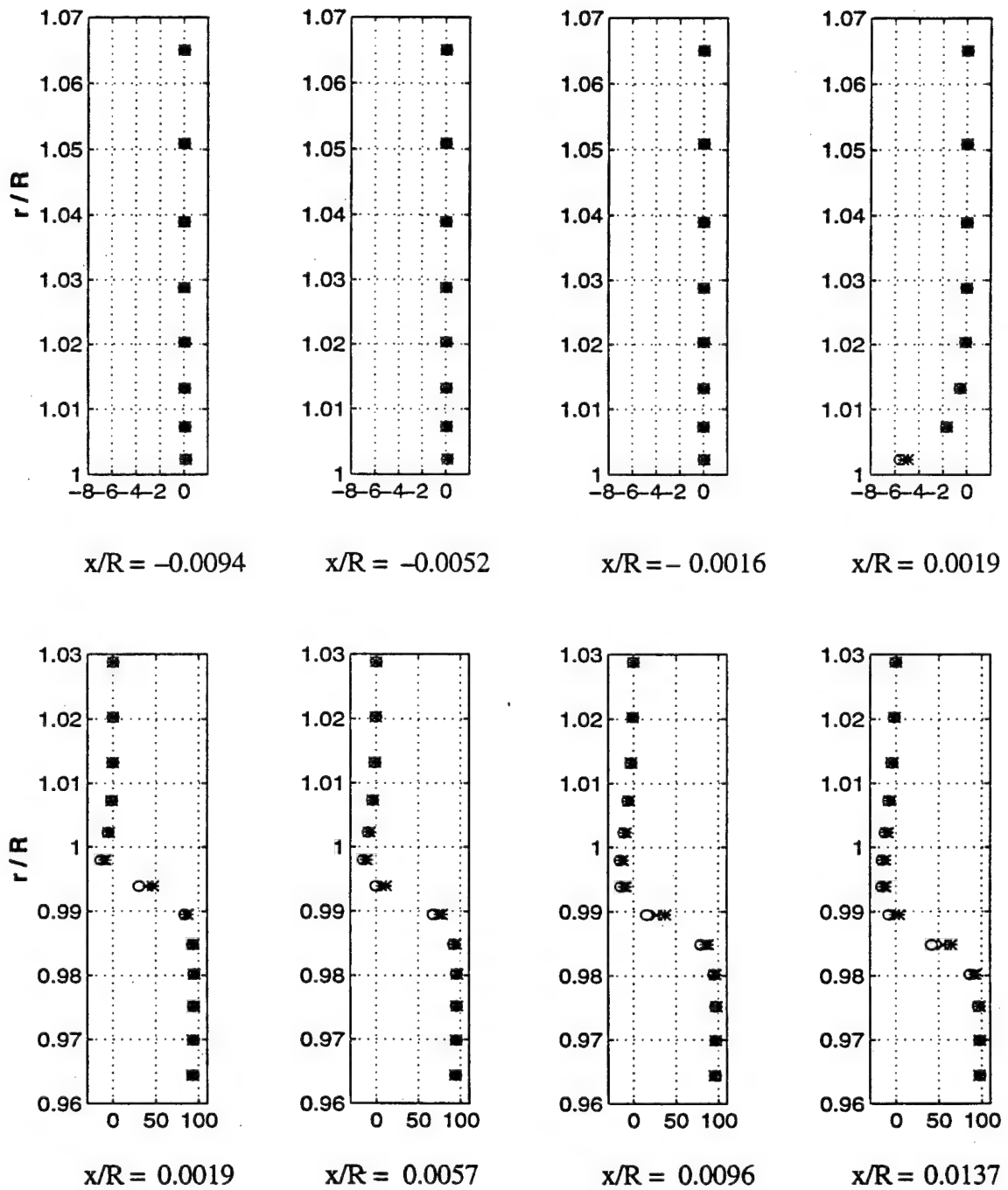
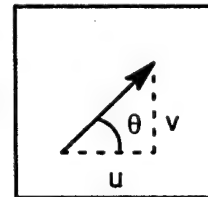


Figure 6.17. Computed values of flow turning angle  $\theta$ , (in degrees), at locations slightly upstream and immediately downstream of the base corner.

$o = Sk\epsilon$  ;  $*$  =  $Ek\epsilon_1$  ;  $+$  =  $C_{\epsilon_1}$  modification only and  $x = \epsilon_d$  modification only.



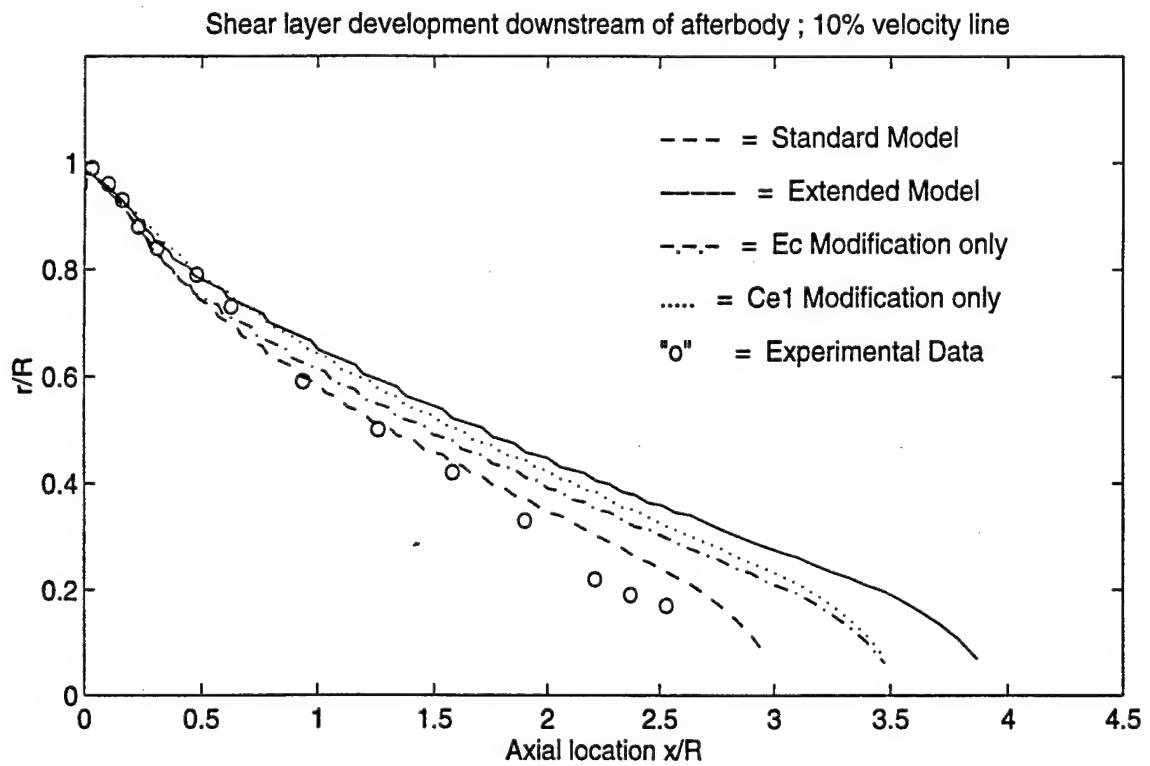
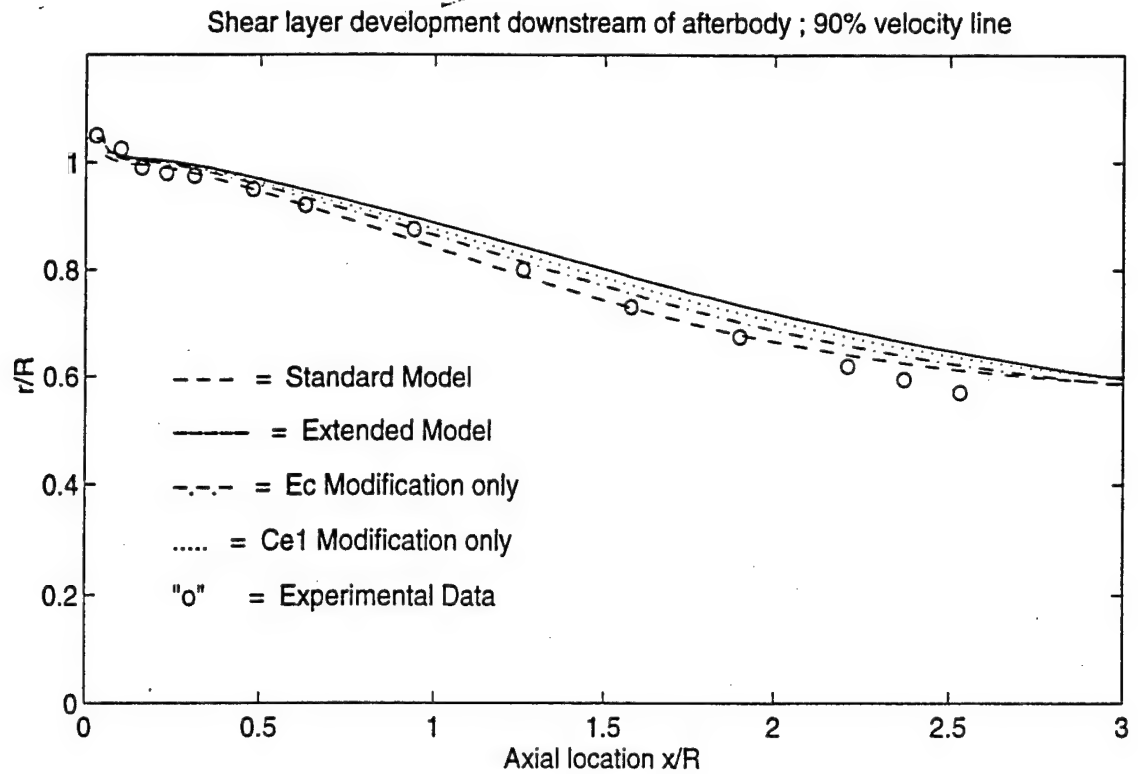
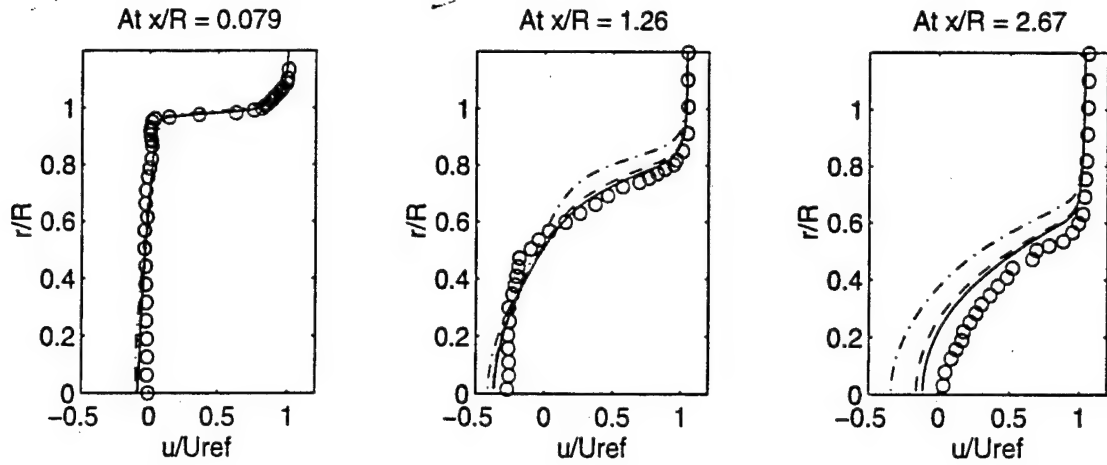


Figure 6.18. Computed development of the shear layer downstream of the afterbody.

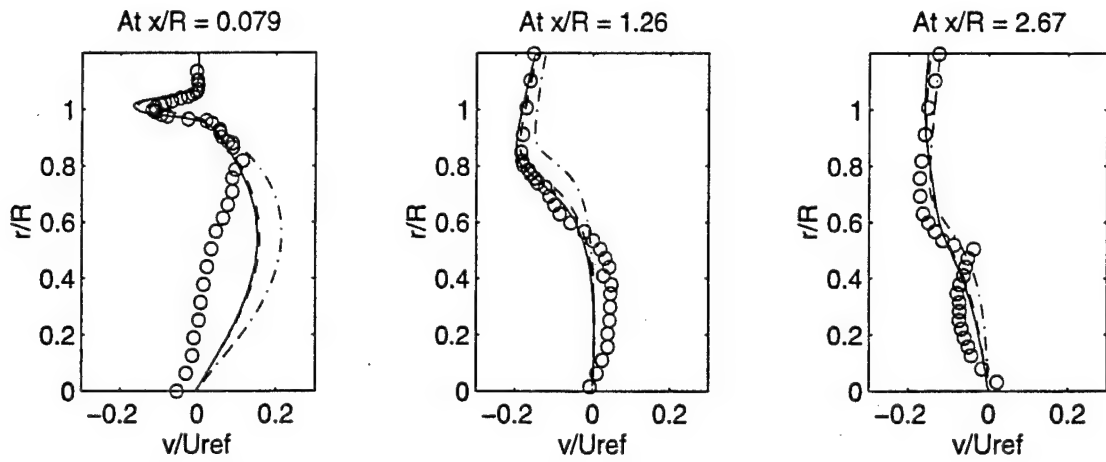
current modifications are presented here. It should be noted that the current modifications are not meant as a substitute for the afore-mentioned modifications but to be used in conjunction with these modifications. In the predictions made with the current modifications for the turbulent mass flux and the enthalpic production terms, the Sarkar et al. [1991] modification for  $\varepsilon_d$  has been used. In all the figures presented here, the "current" modification refers to the results obtained using the modifications proposed here and the modification for  $\varepsilon_d$ , "Sarkar" refers to the results obtained using the modifications due to Sarkar et al. [1991] and Sarkar [1992] and "El Baz" refers to the results obtained using the modifications proposed by El Baz and Launder [1993].

Figures 6.19 (a), (b) and (c) present profiles of the axial and radial velocity components and the TKE at the three locations downstream of the base. At the location close to the base there is very little difference between the three cases. At this location there is considerable difference in the computed values of the radial velocity component and the TKE with the modification due to El Baz and Launder [1993] predicting the lowest levels of TKE. This is possibly due to the increased dissipation rate, implied by this modification (also borne out in the comparisons made of the total dissipation rate). At locations downstream, all models suffer from inaccuracies with the errors associated with the El Baz and Launder [1993] modification being the largest. The modifications proposed here for the turbulent mass flux and the modification to the enthalpic production rate show a positive impact on the computations, albeit a small one.

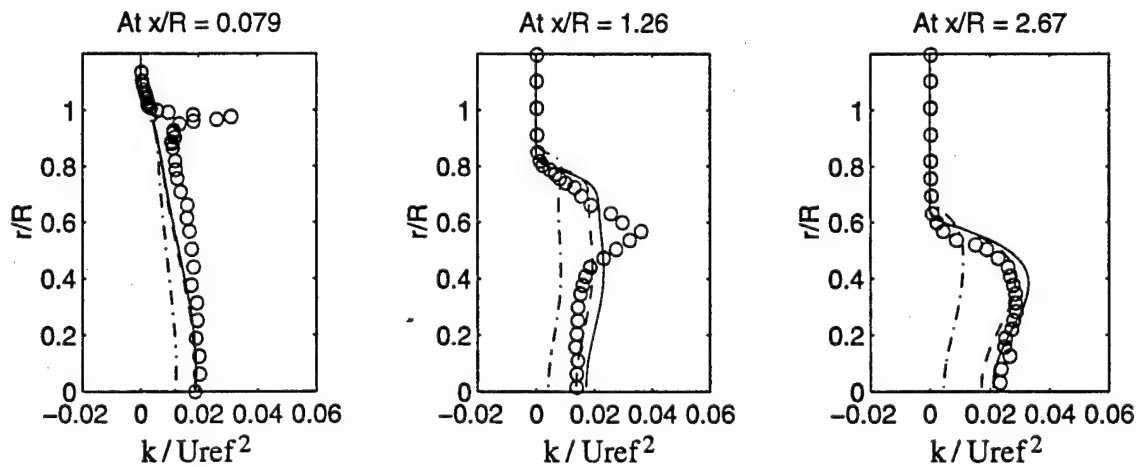
Figures 6.20 (a), (b) and (c) show plots of the primary Reynolds shear stress component, the TKE production rates used in these modifications and the total dissipation rate of TKE. In terms of the predictions made of the Reynolds shear stress component, the trend that is observed in Figures 6.19 (a), (b) and (c) seem to continue. The El Baz and Launder [1993] modification does seem to predict the largest dissipation rate. The level of dissipation rate predicted in the computations made using the current modifications are essentially identical to those predicted by the modifications of Sarkar et al. [1991] and Sarkar



a) Computed values of axial velocity component



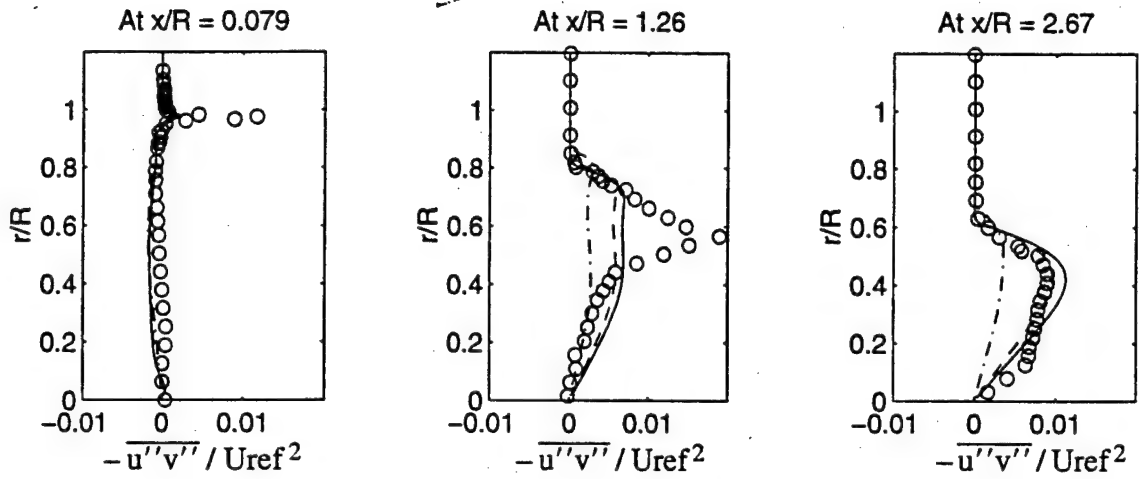
b) Computed values of radial velocity component



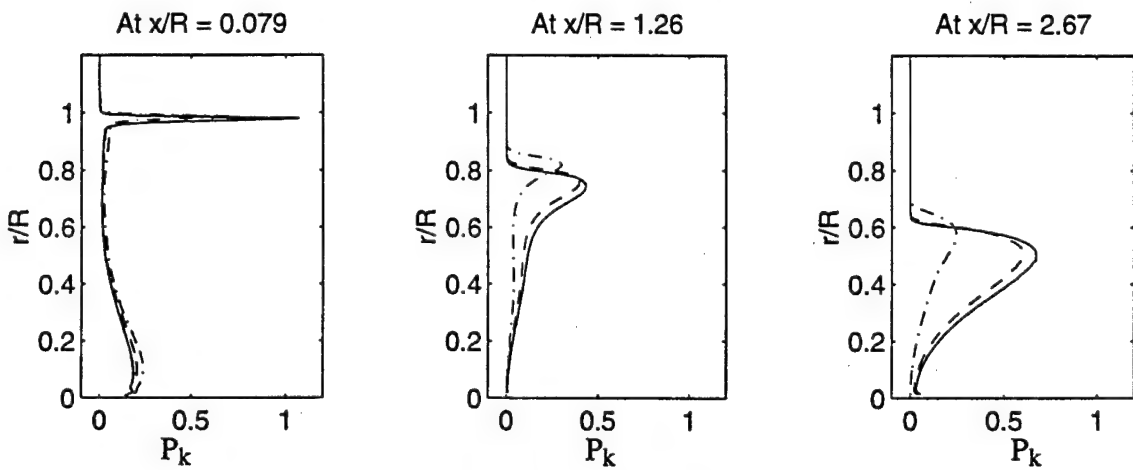
c) Computed levels of TKE

Figure 6.19. Comparison of predictions made using the compressibility modifications.

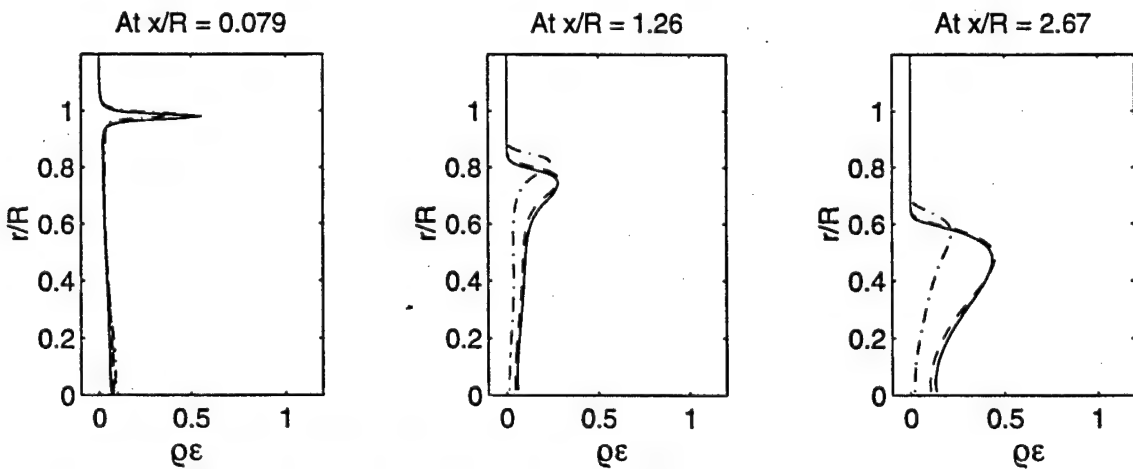
— = current    - - - = Sarkar    - . - = El Baz    and "o" = Experiment.



a) Computed magnitudes of the primary Reynolds shear stress.



b) Computed levels of the rate of Production of TKE.



c) Computed levels of total rate of dissipation of TKE

Figure 6.20. Comparison of the predictions made using the compressibility modifications.  
 — = current, --- = Sarkar and —.— = El Baz and "o" = Experiment.

[1992]. This is to be expected, because the modification for  $\varepsilon_d$  proposed by Sarkar et al. [1991] has been used in conjunction with the modifications for the enthalpic production rate. Again note the location of the peaks in the rate of production of TKE. A common theme seems to be evident in all the computations presented in this article. The amount of turbulence dissipation added to the flow field results in a reduction in the angle through which the separated shear layer turns and consequently in an overprediction of the variation of the velocity components and overprediction of the reattachment length.

In order to analyze the effect of the modifications for compressibility, profiles were made of the skin friction (upstream of the base corner) the eddy-viscosity, the TKE level and its dissipation rate  $\varepsilon$ . These profiles were computed at locations slightly upstream of the base and immediately downstream of the base. Comparisons were made of the predictions made using the three compressibility modifications tested in this article and the predictions made using the standard k- $\varepsilon$  model. The quantities compared did not show any glaring differences, both upstream and immediately downstream of the base corner. One of the comparisons made is shown in Figure 6.21. The figure shows the predicted level of TKE. The various modifications yield virtually identical results. What this implies is that the compressibility modification has very little impact on the incoming boundary layer. But at the freestream Mach number of 2.46 the effects of compressibility are almost negligible. An important outcome of this comparison, shown in Figure 6.21, is that it reduces the number of factors that could be held accountable for the observed changes on the flow turning angle. Where the compressibility modifications seem to breakdown is when they start artificially reducing the level of TKE. That situation is very evident in this study. The increase in TKE level and its production rate, observed in experiments, is due to the interaction of the separated boundary layer with the recirculating fluid downstream of the base. Part of the apparent inability of the compressibility modifications (that model the extra dissipation due to dilatational effects) could be due to enforcement of extra dissipation. This is very clearly

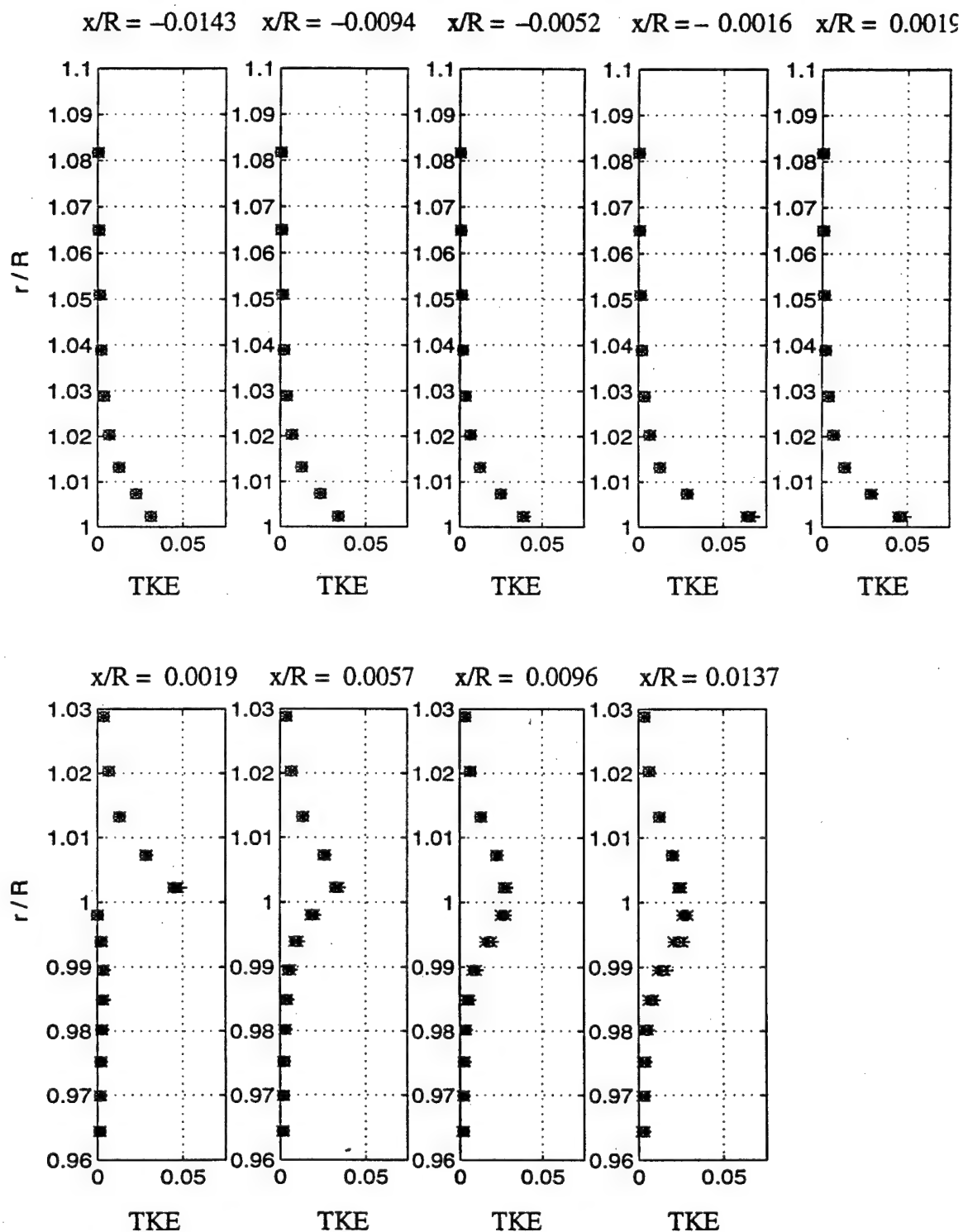


Figure 6.21. Computed values of TKE at locations slightly upstream of the base corner and immediately downstream of it.

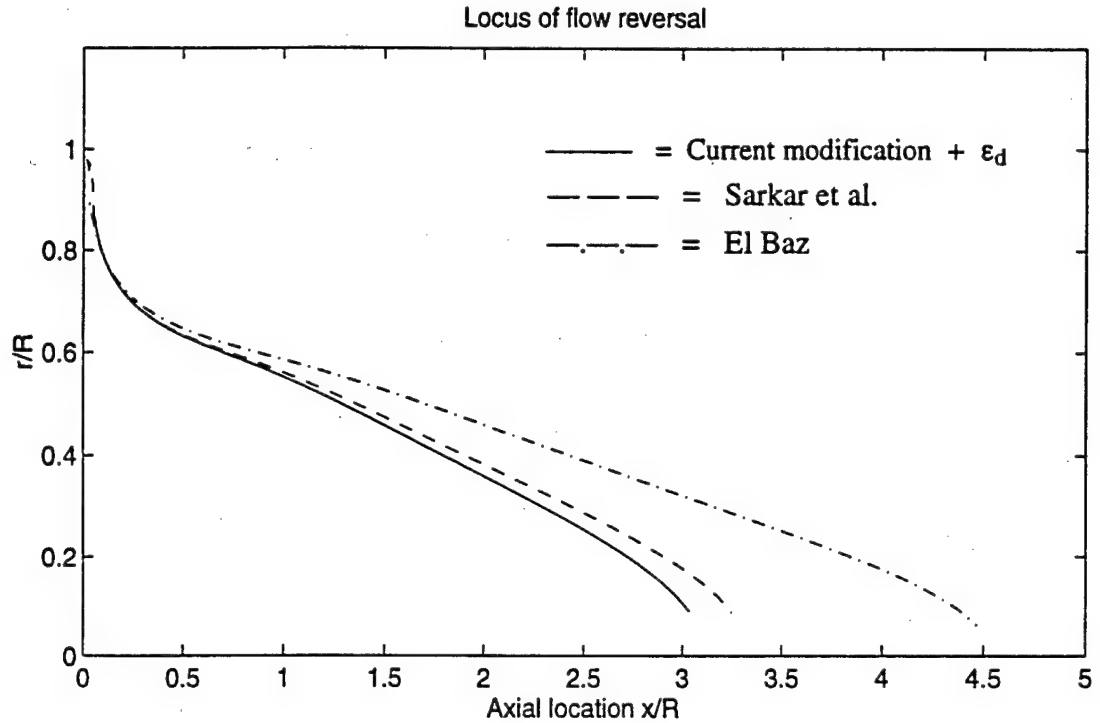
+ = Skε ; o = Sarkar et al. ; \* = El Baz ; x = Current + ε<sub>d</sub>

seen in the predictions made of the TKE levels and the Reynolds shear stress at the  $x/R = 1.26$  location which is at about the centre of the recirculation region.

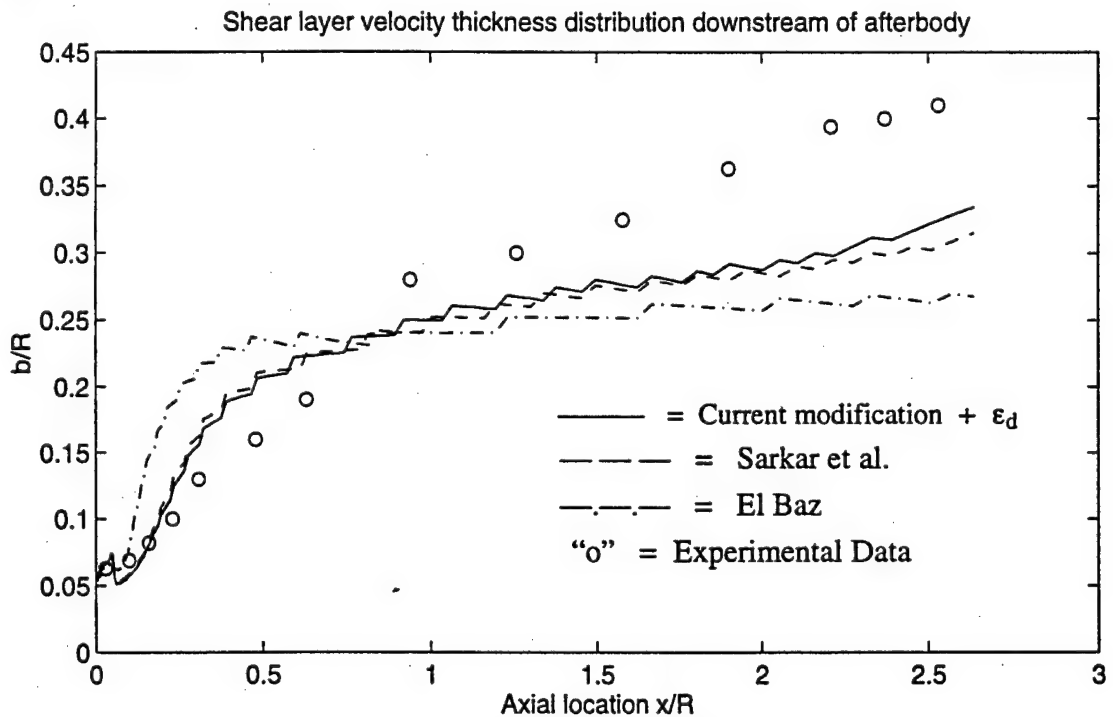
Figure 6.22 (a) shows a comparison of the locus of flow reversal computed using the three modifications. The current modifications seem to make the better prediction in terms of the extent of the recirculation region. Figures 6.22 (b) through 6.23 present computed details of the shear layer for the three modifications. Again as observed in the previous set of comparisons, the modifications seem to reduce the turning angle of the flow through the expansion region, thereby resulting in a lateral shift in the locations of the shear layer. All the modifications have the maximum impact on the lower extent of the shear layer rather than on the upper edge. This is to be expected because (as mentioned before) the lower edge of the shear layer is responsible for the growth of the shear layer.

Figure 6.24(a), shows a comparison between the Sarkar [1992] modifications for the pressure dilatation term and those due to El Baz and Launder [1993]. It is very evident from this figure that the modifications proposed by El Baz and Launder [1993] do result in much larger dissipation rates. The magnitudes of pressure dilatation predicted by the computations are about 1/10th of the magnitude of the solenoidal dissipation rates, similar to the observations in DNS studies. Figure 6.24(b) shows a comparison between the current modification for the enthalpic production term and the primary rate of production of TKE. The enthalpic production rate is almost negligible in comparison to the primary production rate. A explanation for the reduced magnitude of enthalpic production rate could be that the fluctuations are isobaric (or at least, not far from it). Of course, we could have tweaked the constants in the modification for the enthalpic production term. But, due to lack of experimental evidence or DNS results this was not feasible. Also, the intent is to bring out the need for modelling this term and to show that the compressibility effects should not be modelled by just increasing the rate of dissipation of TKE. Compressibility does affect the rate of production of TKE as is evidenced by some of the recent studies of compressible turbulent flows (Sarkar, 1994 and Huang et al., 1995). Figure 6.24(c) shows the predicted



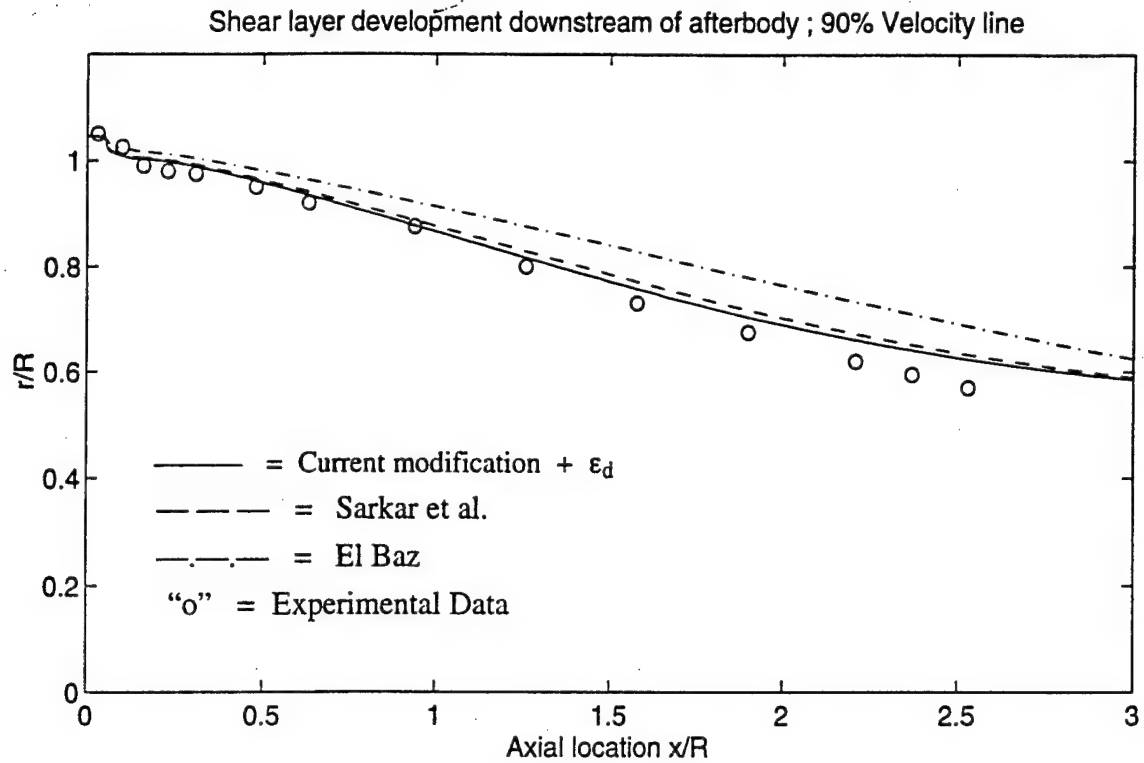


a) Computed Locus of Flow Reversal, i.e., where the axial velocity component changes sign.

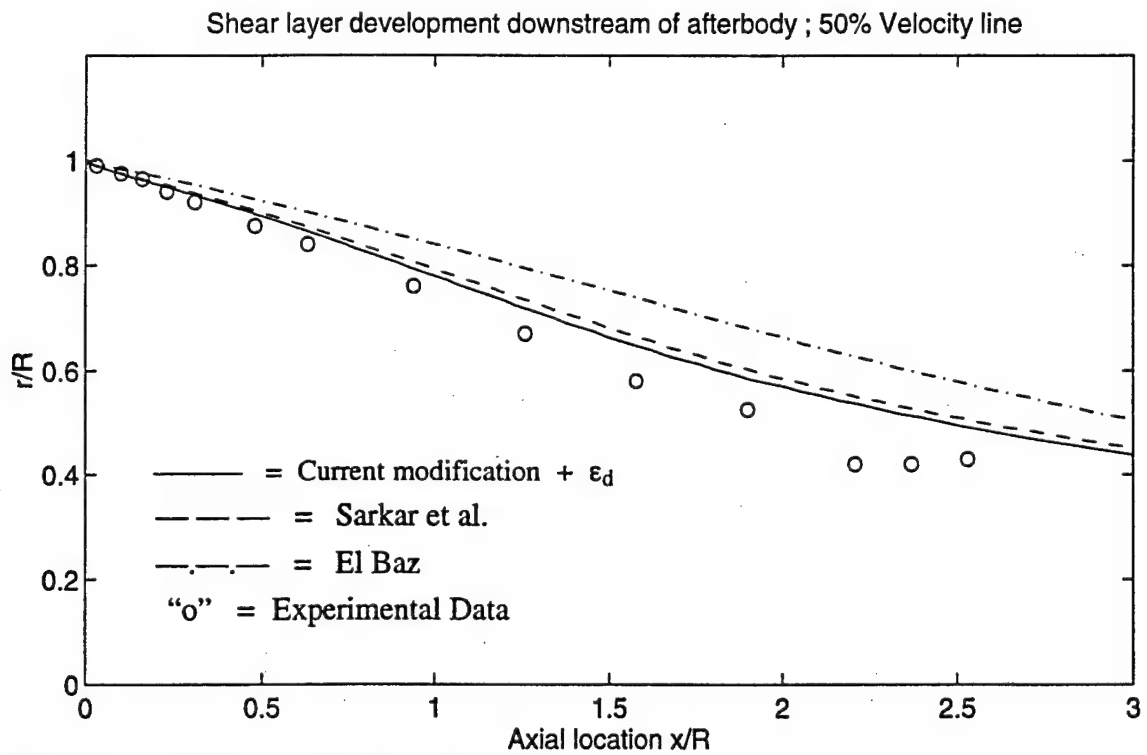


b) Computed Thickness of the Shear Layer. The edges of the shear layer are defined as between  $U_2' + 0.1 \Delta U'$  and  $U_2' + 0.9 \Delta U'$ .

Figure 6.22. Development of the shear layer downstream of the afterbody.

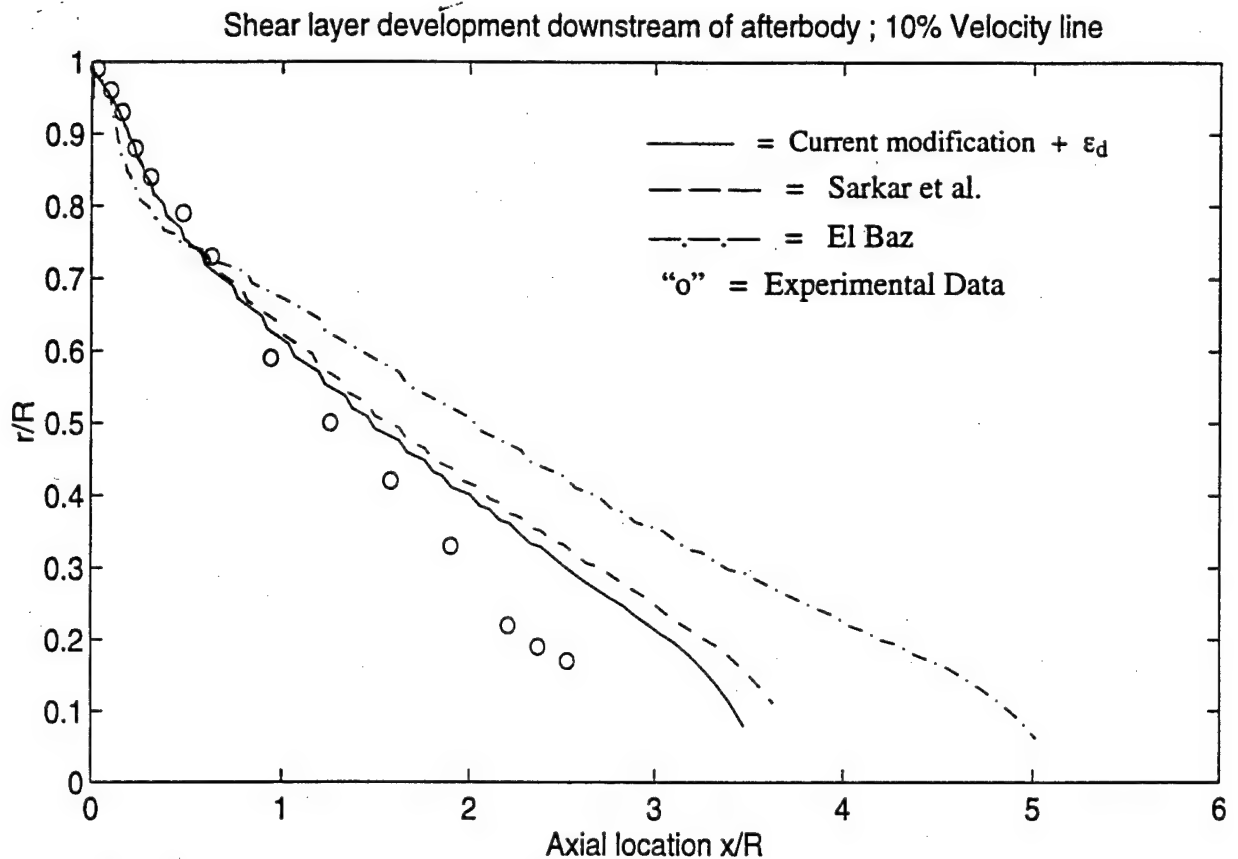


(a). Computed locus of the 90% velocity line.



(b). Computed locus of the 50% velocity line.

Figure 6.23. Development of the shear layer downstream of the afterbody.

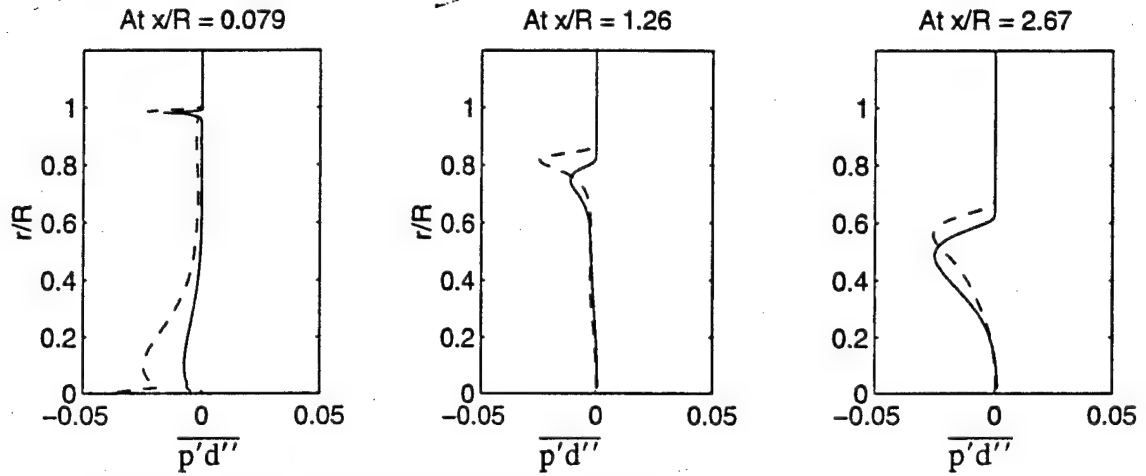


(c). Computed locus of the 10% velocity line.

Figure 6.23 (Contd.) Development of the shear layer downstream of the afterbody.

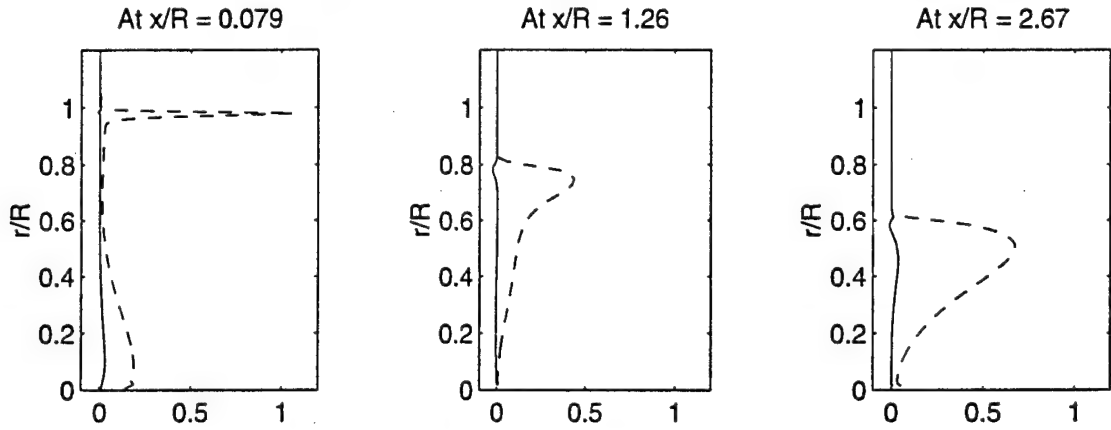
values of the averaged values of the Favre fluctuation velocity components. The predicted values showed the correct trends based on qualitative comparisons with the experimental observations of Gaviglio et al. [1977].

Figures 6.25 (a), (b) and (c) show the computed values of the axial velocity and radial velocity components and the level of TKE in the trailing wake region. The modifications due to El Baz and Launder [1993] and those due to Sarkar et al. [1991] and Sarkar [1992], predict essentially the same thickness of the shear layer. The thickness predicted using these modifications is considerably less than that predicted by the standard model which is to be expected, because of the effect of compressibility on free shear layers. The standard model predictions, in terms of the velocity components seem to match the experimentally observed values. However, the compressibility modifications seem to predict the turbulent kinetic



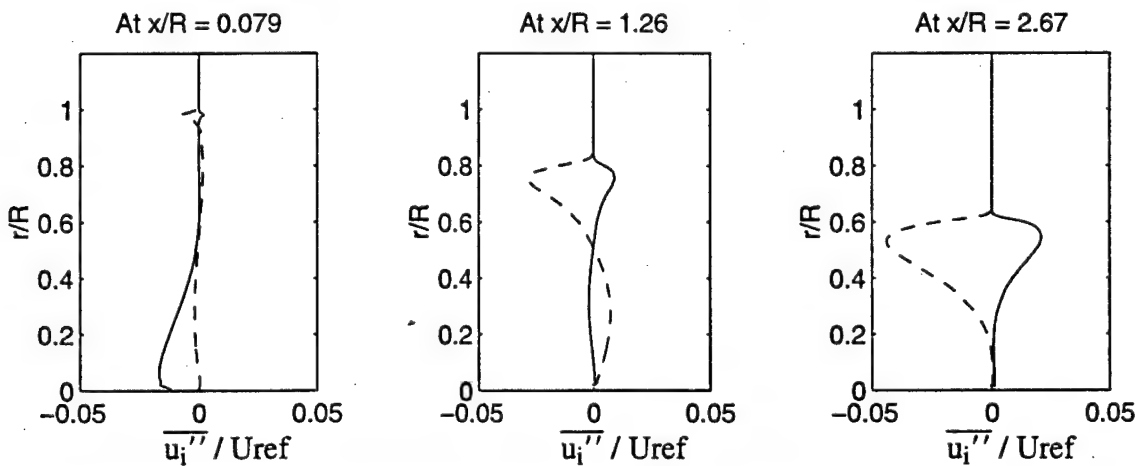
a) Computed values of the pressure dilatation term.

———— = Sarkar    - - - - = El Baz



b) Computed values of the rate of production of TKE :

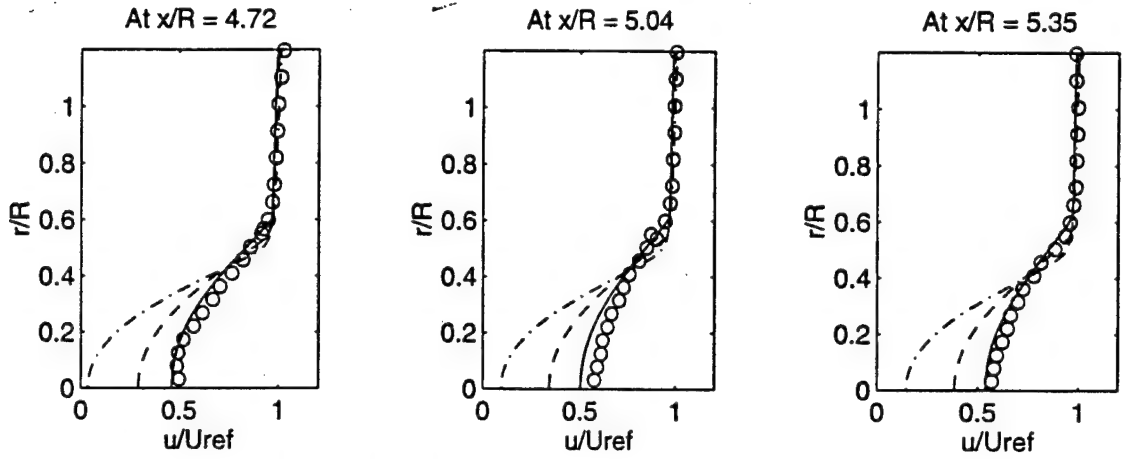
———— =  $-\overline{u_i'''} dp/dx_i$     - - - - =  $-\overline{\rho u_i'' u_j''} dU_i/dx_j$



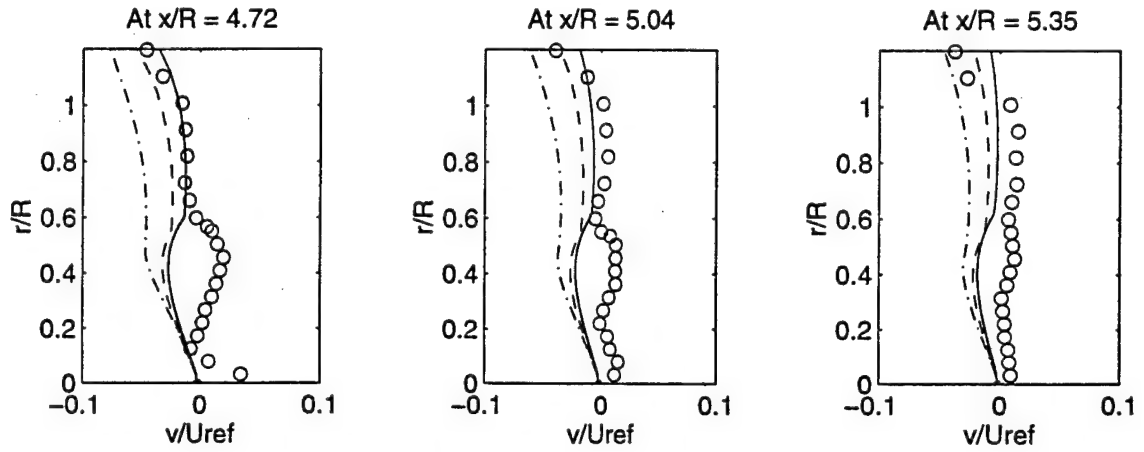
c) Computed values of the averaged Favre fluctuation velocity :

———— =  $\overline{u''}$     - - - - =  $\overline{v''}$

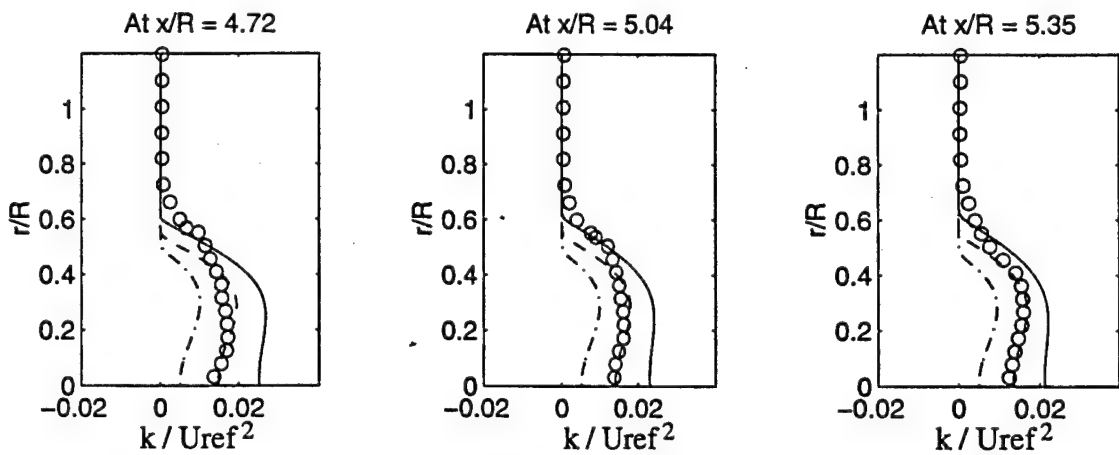
Figure 6.24. Comparison of the compressibility modifications.



a) Computed values of the axial velocity component.



b) Computed values of the axial velocity component.



c) Computed values of the level of TKE.

Figure 6.25. Comparison of compressibility modifications with the unmodified model.  
 — =  $Sk\epsilon$     - - - = Sarkar    - · - · - = El Baz    "o" = Experiment.

energy values much better than the unmodified model. In a recent article, Clemens and Mungal [1995] note that jets and wakes develop similar to their incompressible counterparts, in sharp contrast to the development of the two stream mixing layer. This is certainly observed in the current modifications.

### 6.3 Summary

Based on the computational cases presented here, the following observations can be made:

- 1) The treatment of the convection term has a strong impact on the results obtained. This seems to be important especially when dealing with flows with strong pressure gradients or streamline curvature. Of course, with proper tuning of the artificial dissipation terms, the upstream impact of the rapid expansion at the base corner could have been reduced but that may not be robust.
- 2) The non-equilibrium based modifications to  $C_{\epsilon 1}$  are not sufficient to make reasonable predictions of the flow field and from the current set of computations, of the three models, i.e.,  $Sk\epsilon$ ,  $Ek\epsilon 1$  and  $Ek\epsilon 2$ , the  $Ek\epsilon 2$  model seems to offer the optimum set of predictions in terms of the mean flow quantities as well as the turbulence structure.
- 3) The compressibility modifications due to Sarkar et al. [1991] for  $\epsilon_d$  and those due to El Baz and Launder [1993] for  $C_{\epsilon 2}$ , appear to be different in functional form, but in essence produce the same effect. Of the two compressibility modifications tested here, the modifications due to Sarkar et al. [1991] and Sarkar [1992] offer the better prediction. The modifications of El Baz and Launder [1993] are overly dissipative and result in unsatisfactory predictions, at least for the flow field tested here.
- 4) Conceptually, addressing the compressibility effects as a dissipative one or modelling compressibility based on the turbulent Mach number does not offer a complete description of the physics. Recent research (Sarkar, 1994) has indicated that another parameter the gradient Mach number may be an important parameter.

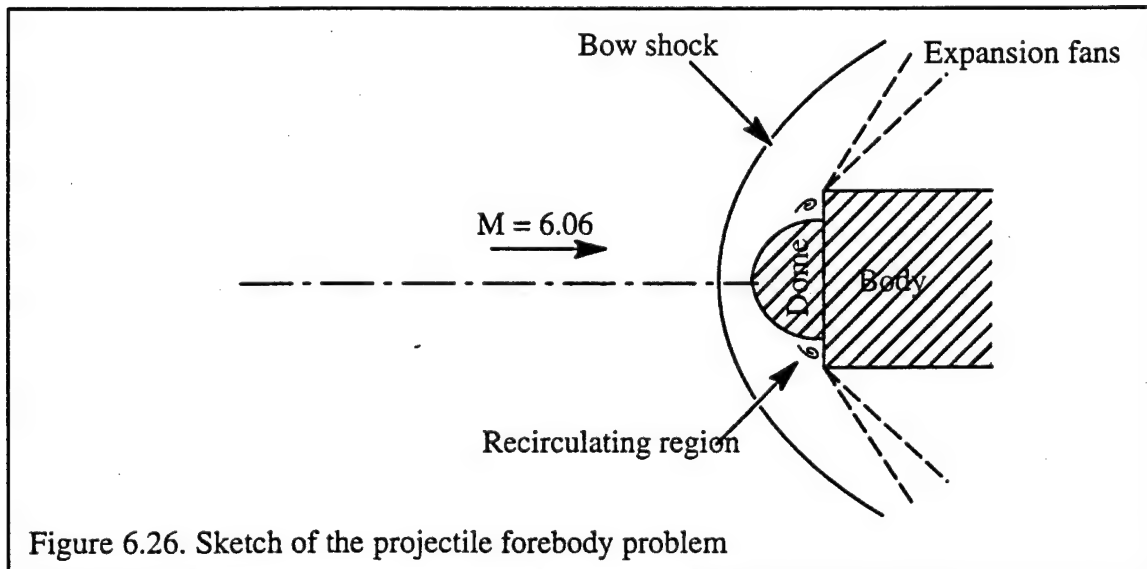
5) The current modifications show a positive impact on the predictions made. These predictions indicate that there is a need to account for the enthalpic production term and the term representing the baroclinic torque. These terms were hitherto considered negligible and have not been accounted for in the modelling of compressible turbulent flows. But the impact of the current models on the mean flow field is not strong in this test case. However in terms of the extent of the recirculation region, the current modifications are definitely a step in the right direction. Further study into the modelling of these terms is necessary to improve the predictive capabilities for quantities such as TKE and to ascertain their role in determining the mean flow field.

#### 6.4 Projectile Forebody Flowfield

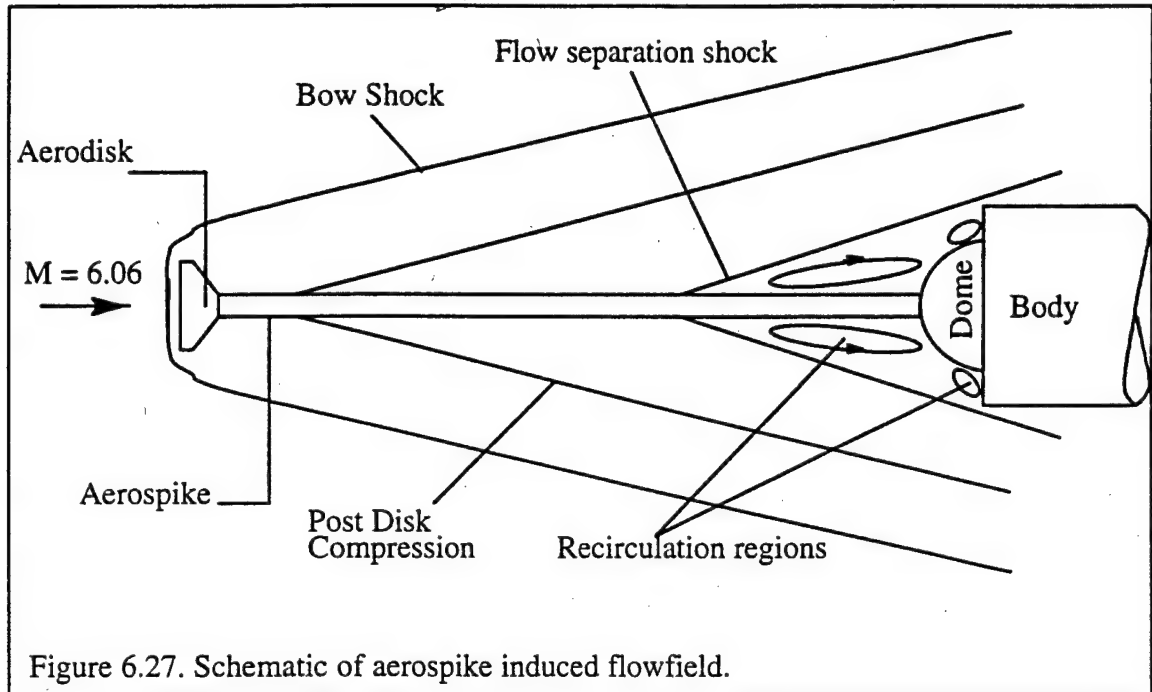
The computational study of the flow past an axi-symmetric afterbody indicated that the impact of the current modifications were minor. Possible reasons for this observation could be that these terms (for which modifications have been proposed in this dissertation) are of an order of magnitude smaller than the other terms (in the respective transport equation) or the compressibility effects are not really a major factor in the development of these shear layers. The latter reason could have played a more important role in the results obtained for the axi-symmetric afterbody flowfield. The flow field (the baseflow) is at an inlet Mach number of 2.46, relatively low for compressibility effects to play a major role in the development of the shear layer. In addition, as was pointed in the earlier section, two different flow structures seem to determine the evolution of the shear layer downstream of the afterbody. These are the recirculating region and the free shear layer. The interaction of the developing free shear layer with the recirculating, low speed fluid, makes a major contribution to the production of energy for the turbulent fluctuations. This is not really a compressibility effect, which would explain the reason for the inadequacy of the models addressing the dissipative effect of compressibility. The modifications proposed in this dissertation are intended to address the terms that are unaccounted for in the exact form of

the governing equations (for compressible turbulent flows). Also, we chose to address the issue of reduced production in compressible turbulent shear layers.

In order to clarify the issues raised by our observations of the predictions made of the axi-symmetric afterbody flow field we decided to compute a flow field at hypersonic speeds. One such flow field is that past a projectile travelling at hypersonic speeds. Recently, Huebner et al. [1995], conducted experimental studies of the flow past a hemisphere-cylinder at a Mach number  $M_\infty = 6.06$ . They made measurements of the pressure and temperature distribution on the surface of the projectile. A sketch of this flow field is given in Figure 6.26. The strong shock ahead of the dome of the projectile causes a huge jump in the pressure and also the temperature on the surface of the hemispherical dome. These cause, in addition to the increased drag on the projectile, adverse conditions for the optical and other sensing equipment typically mounted in the dome of the projectile (due to the excessive heating of the dome surface). The experiments conducted by Huebner et al. [1996] were intended to investigate the effect of a long slender spike and an aerodisk combination. A sketch of this flow structure is given in Figure 6.27. The recirculating regions upstream of the dome drastically reduce the pressures and to a certain extent the temperature on the dome surface.







Through the rest of this section details are presented of the computational study conducted to: a) address the effectiveness of the various modifications that were tested for the afterbody flowfield, in predicting this flow field with the involved complex flow physics and b) address the effectiveness of the spike-aerodisk assembly in reducing the heating of the dome surface.

The relevant flow structure of the turbulent flow field we are considering in this case is the interaction of the isotropic turbulence with the bow shock ahead of the dome of the projectile. Additionally, effects of the turbulent wall layer that separates upstream of the shoulder (the shoulder formed at the junction of the dome and the cylinder) and the expansion fan (Figure 6.26) need to be considered in the analysis of the flowfield. We have addressed the impact of a rapid expansion on a turbulent shear layer earlier when we considered the afterbody flowfield. We will concentrate (in the next few paragraphs) on the physics of shock-turbulence interaction.

### 6.4.1 Shock-Turbulence Interaction

Using a linear analysis of the equations of motion, Kovasznay [1953] showed that compressible turbulence can be split up into modes which act independently (to first order) of one another. Consider the inviscid form of the equations of motion with the mean velocity set to zero. Assuming that the fluctuations of density, pressure and temperature are small with respect to their mean values and also that the magnitude of the fluctuating velocities are small (that is, low turbulent Mach number) and keeping only the linear terms we can obtain the linearized inviscid equations. From these the equations for vorticity, pressure and entropy can be derived. These equations are written as (following Kovasznay, 1953)

$$\frac{\partial \omega_i''}{\partial t} = 0 \quad (6.7)$$

$$\frac{\partial^2 p'}{\partial t^2} - c^2 \frac{\partial^2 p'}{\partial x_j \partial x_j} = 0 \quad (6.8)$$

$$\frac{\partial s'}{\partial t} = 0 \quad (6.9)$$

where  $\omega_i''$ ,  $p'$ ,  $s'$  are the fluctuations in vorticity, pressure and entropy respectively.  $c$  is the speed of sound. These represent the three modes (Kovasznay, 1953) and are referred to as the vorticity mode, acoustic mode and entropy mode. To a first order, (with no mean velocity gradients) the equations 6.7, 6.8 and 6.9 show that the three modes are independent of one another. Also, the vorticity and entropy modes are frozen. If one accounts for viscosity, a diffusion equation is obtained for the vorticity mode. That is,

$$\frac{\partial \omega_i''}{\partial t} = \nu \frac{\partial^2 \omega_i''}{\partial x_j \partial x_j} \quad (6.10)$$

The vorticity mode is still decoupled from the entropy and pressure modes. While the concept of splitting modes is a useful concept for understanding the physics of compressible turbulence, a general turbulent flow field cannot be decomposed into independent modes. But this split up is useful in understanding the physics of the interaction of an isotropic turbulent flow field with the bow shock (ahead of the projectile dome).

To a first order, the three modes of vorticity, pressure and entropy are independent of one another. But when any one of them interacts with a strong shock wave, it can result in the generation of three modes (Ribner, 1954). Ribner [1954] considered the interaction of a homogeneous turbulent flow with a shock wave. The turbulent flow field is expressed as the sum of Fourier components and linearized Rankine-Hugoniot jump conditions are imposed across the shock (Ribner, 1954). The amplification of the turbulence intensities, downstream of the shock, are then computed as a function of the upstream statistics. Predictions based on such linearized analysis have been confirmed by numerical simulations (Lee et al. 1993, Rotman 1991). Linearized analysis method to estimate the turbulence corrections, to the shock jump relations and the shock speed, have been reported in Lele [1992].

When the intensities of the turbulent pressure fluctuations are small compared to the pressure rise across the shock, the shock front is weakly distorted and the linearization of the Rankine-Hugoniot jump conditions is justified (Lele, 1994). However when the intensities of the incident (on the shock) pressure fluctuations are stronger, the shock front is considerably modified and from Lee et al. [1993] the pressure rise is no longer monotonic. Lele [1994] proposes a condition based on the turbulent Mach number, to restrict the use of linearized analysis. This is given as  $M_t^2 < 0.1(M_t^2 - 1)$  which implies that as long as the turbulent Mach number,  $M_t = \frac{q}{c}$  (where  $q = u_i''u_i''$  and  $c$  is the speed of sound) is less than 0.33 ( $M_t \leq 0.33$ ) the linearized analysis can be used with reasonable justification. Recent numerical simulations of Lee et al. [1993] and Jacquin et al. [1991] also confirm that the linearized analysis predicts the jump in vorticity fluctuations across the shock accurately. Due to the amplification of the vorticity fluctuations across the shock the rate of dissipation of TKE,  $\epsilon$ , is also increased.

Linear analysis of Jacquin et al. [1993] indicate a rise in TKE across the shock. DNS simulations also indicate a rise in TKE across the shock (Lee et al., 1992). They also indicate that in addition to the increase in TKE at the shock there is an increase in TKE downstream

of the shock (Lee et al., 1992). This increase in TKE, downstream of the shock, has been attributed to an exchange of energy between the potential energy and kinetic energy (Lele, 1994). The increase in potential energy (amplification of acoustic mode) decays downstream of the shock, if the flow downstream of the shock is subsonic. Since the total energy in the fluctuations is conserved, the decay of potential energy results in an increase in the TKE of the fluctuations. The increase in TKE downstream of the shock has been attributed to pressure dilatation effects (Lele, 1994). Jacquin et al. [1992] also note that the rise in TKE across the shock is a function of the isotropy of the incident turbulent field. For an upstream Mach number of  $M=1.4$ , Jacquin et al. [1992] report no significant rise in the level of TKE across the shock which is in direct contrast to the experimental observations of Honkan and Andreopoulos [1992]. Jacquin et al. [1992] also note a significant increase in the level of TKE if the upstream turbulence is anisotropic. Recent calculations based on rapid distortion theory (RDT) by Mahesh et al. [1993] confirm the linear theory estimates of Jacquin et al. [1992].

The linearized theory estimates of Ribner [1954] and the DNS results of Lee et al. [1993] indicate a reduction in the characteristic length scales of the turbulent eddies. These include longitudinal and lateral correlation length scales. Honkan and Andreopoulos [1992], from their measurements of velocity correlations, observe an increase in the Taylor

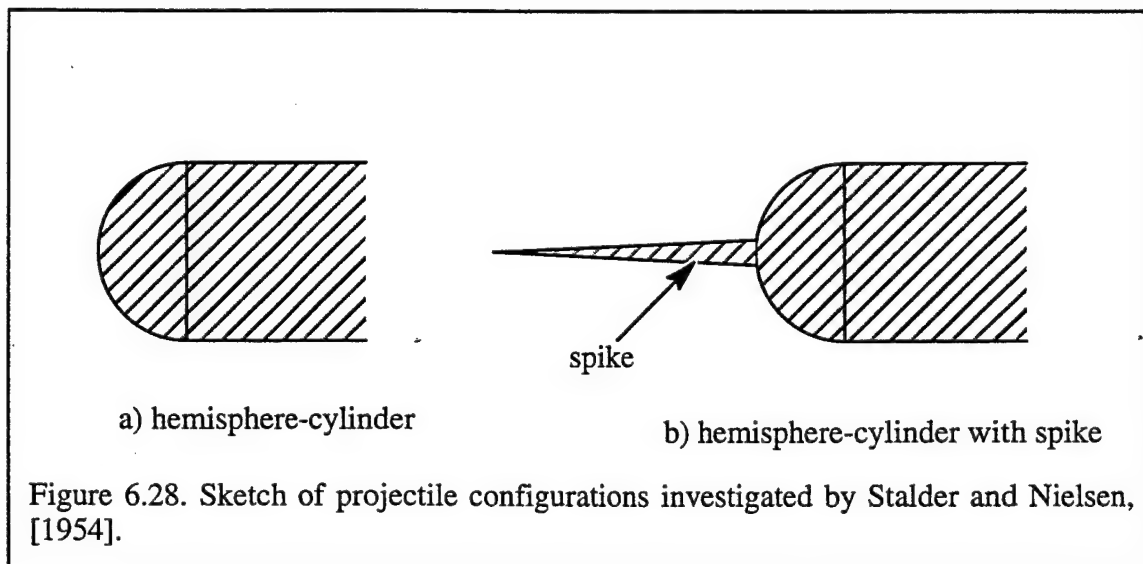
micro-scale  $\left[ L_\epsilon = \frac{(\overline{u'^2})^{3/2}}{\epsilon} \right]$  across the shock where  $u''$  are the fluctuations in the

streamwise velocity components and  $\epsilon$  is the rate of dissipation of TKE. Similar measurements of density fluctuations by Keller and Merzkirch [1990] and velocity fluctuations by Barre et al. [1996] suggest an amplification of length scales across the shock. It should be noted that DNS simulations are limited to low Mach numbers and the interaction of turbulence with weak shocks. This apparent conflict between experimental measurements and DNS studies has not been resolved (Lele, 1994).

#### 6.4.2 Experimental Studies of Projectile Flowfield

Several experimental studies have been conducted to investigate the projectile forebody flowfield. Most of these studies, in the 1950's, concentrated on the issues of strong pressures and heating rates at the dome of the projectile and means to reduce it. Stalder and Nielsen [1954] conducted experiments on a simple hemisphere-cylinder configuration similar to the one shown in Figure 6.28 at Mach numbers of 1.75, 2.67 and 5.0. Their experiments indicated a reduction in the pressure (consequently the drag) on the surface of the dome, with the addition of the spike. It did not, however, show a reduction in the temperature on the nose of the projectile. In fact, it showed an increase in heat transfer rates with the addition of the spike (in comparison with the "un-spiked" case). They explain the increase in heat transfer rates as a result of the separated turbulent boundary layer (upstream of the nose) periodically impinging on the outer region of the boundary layer on the nose of the hemisphere.

Bogdonoff and Vas [1959] conducted experimental investigations on the variations in pressure at the nose of the projectile forebody as a function of the spike length. These investigations showed an initial drop in the pressure at the nose of the forebody with increase in spike length (upto about an  $L/D = 3$ ) but asymptotes with any further increase in the spike



length. The experimental investigation of Crawford [1959] was chiefly concerned with the phenomena of flow transition (from laminar to turbulent).

More recently, Huebner et al. [1995] investigated the projectile flow field. They conducted experimental measurements of the pressure and temperature at the nose of the projectile and the effect of the aerospike and aerodisk assembly (sketches of the flow field investigated are given in Figures 6.26 and 6.27) at various angles of attack. They observe that at moderate angles of attack ( $\alpha \leq 15^\circ$ ) the spike and aerodisk assembly was very useful in reducing the pressure and temperature distributions on the surface of the dome. But at higher angles of attack the combination aggravates the situation at the dome surface with the shock impinging directly on the boundary layer on the dome surface.

### 6.5 Projectile Flowfield Computations

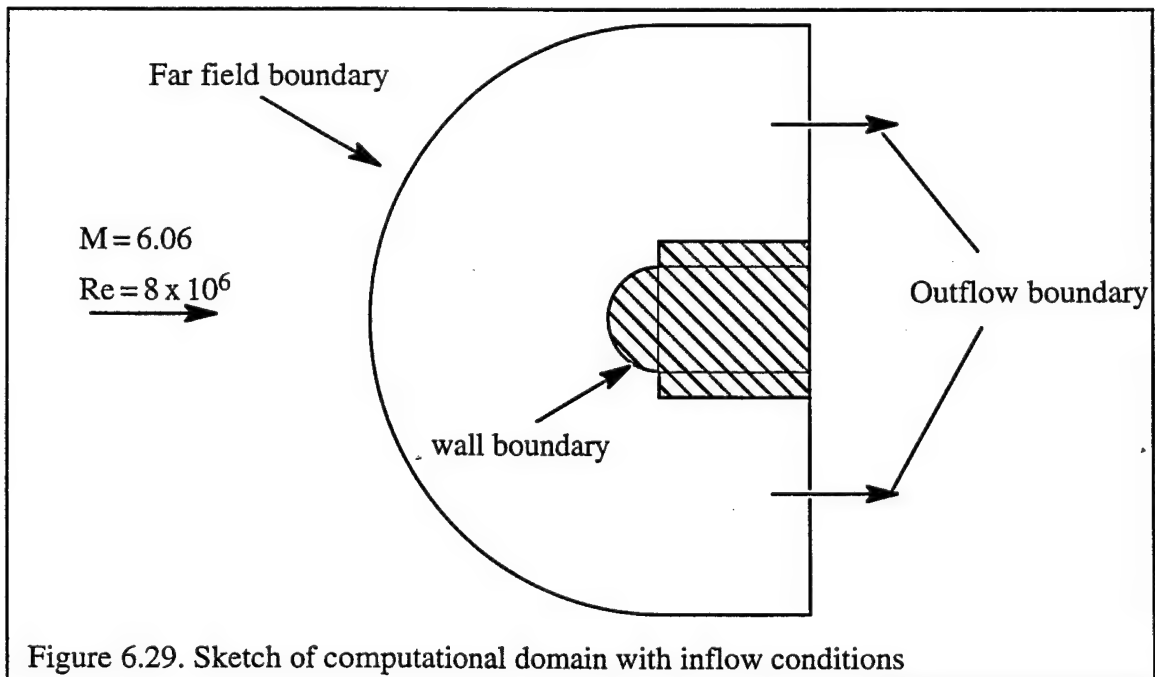
Computations have been performed to investigate the capabilities of the non-equilibrium modifications (Chen and Kim, 1987 and Thakur et al., 1996) and the compressibility modifications (discussed in Chapter 5). The compressibility modifications proposed by Sarkar et al. [1991] and Sarkar [1992] (for the compressible dissipation rate and the pressure dilatation correlation) the modifications proposed by El Baz and Launder [1993] (for  $C_{\epsilon 2}$  and the pressure dilatation correlation) and our modifications for the turbulent mass flux (hence the enthalpic production) and the baroclinic term are being investigated.

In the remainder of this dissertation we will refer to the projectile forebody problem as the spike-off case and the problem with the spike and aerodisk assembly as the spike-on case. Unless specified otherwise all spatial locations presented in this section are in inches. From the results of Crawford [1959] we know that the inflow conditions are such that the flowfield can be expected to be turbulent. The measurements of Huebner et al. [1996] (used in comparing computational predictions) were not concerned with the nature of the flow field.

### 6.5.1 Spike-off Case

A sketch of the computational domain (for the spike-off case) is shown in Figure 6.29. The geometry of the projectile is obtained from the experimental study of Huebner et al. [1996]. The diameter of the hemisphere is 3.0 inches and the diameter of the cylinder is 4.0 inches. The length of the cylinder is 4.0 inches. The dome is offset from the cylindrical body with a 0.25 inches long, 3.0 inches diameter cylindrical extension. The outer boundary of the computational domain extends out to 6.0 inches from the cylinder surface.

The boundary conditions at the far field were fixed at the experimental inflow conditions. A freestream turbulence intensity of 0.3% was used to prescribe the turbulent kinetic energy and the dissipation rate,  $\epsilon$ , in the freestream. This value is consistent with intensities of turbulence observed in most supersonic wind tunnels. At the outflow boundary a simple extrapolation procedure was used because the flow is supersonic at this boundary. At the wall boundary, the compressible form of the wall function technique (described in Chapter 3) has been used.



Computations were initially conducted using the artificial dissipation schemes discussed in Chapter 4. As mentioned in Chapter 4 the artificial dissipation schemes tend to dampen the amplitude of the dispersive errors introduced by the “central difference” scheme. They do not suppress the oscillations about the shock discontinuity. In the case of the projectile flow field calculations we found the artificial dissipation schemes inadequate, to obtain a solution. We had to resort to the second order upwind scheme based on the Steger-Warming flux-vector splitting technique (Shuen, 1991). All the results presented here have been computed using this second order upwind scheme. The fluxes at the cell faces are computed using a MUSCL extrapolation method (Shuen, 1991).

#### 6.5.1.1 Non-equilibrium modifications

Computations made with the unmodified form of the  $k$ - $\epsilon$  model will be denoted as  $Sk\epsilon$ . The computations made using the non-equilibrium modification of Chen and Kim [1987], wherein the constant  $C_{\epsilon 1}$  is modified to  $\left(1.15 + 0.25 \frac{P_k}{\epsilon}\right)$  in conjunction with the compressibility modification due to Sarkar et al. [1991] for the extra dissipation due to compressibility (that is  $\epsilon = \epsilon_s + \epsilon_d = \epsilon_s(1 + M_t^2)$ ) will be referred to as  $Ek\epsilon 1$ . The computations made using the  $C_{\epsilon 1}$  modification of Chen and Kim [1987] and the  $C_{\epsilon 2}$  modification of Thakur et al. [1996] where the constant  $C_{\epsilon 2}$  is modified to  $\left(1.45 + 0.45 \frac{P_k}{\epsilon}\right)$  and the compressibility modification due to Sarkar et al. [1991] is referred to as the  $Ek\epsilon 2$ .

Figure 6.30, shows plots of the static pressure variation and the Reynolds shear stress variation along the stagnation line. The shock is at a distance of about 0.22 inches ahead of the nose of the projectile. There is a slight increase in the pressure downstream of the shock but the magnitude of the jump (across the shock) is comparable to that predicted by one-dimensional gas dynamics. The plot of the Reynolds shear stress variation is to indicate



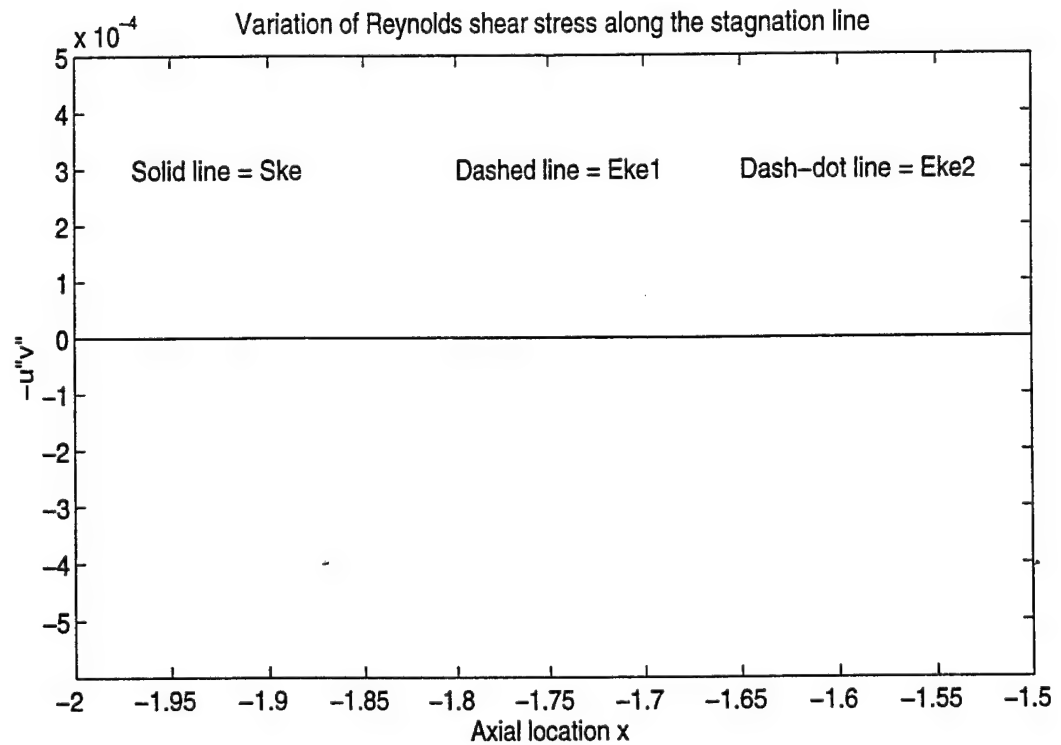
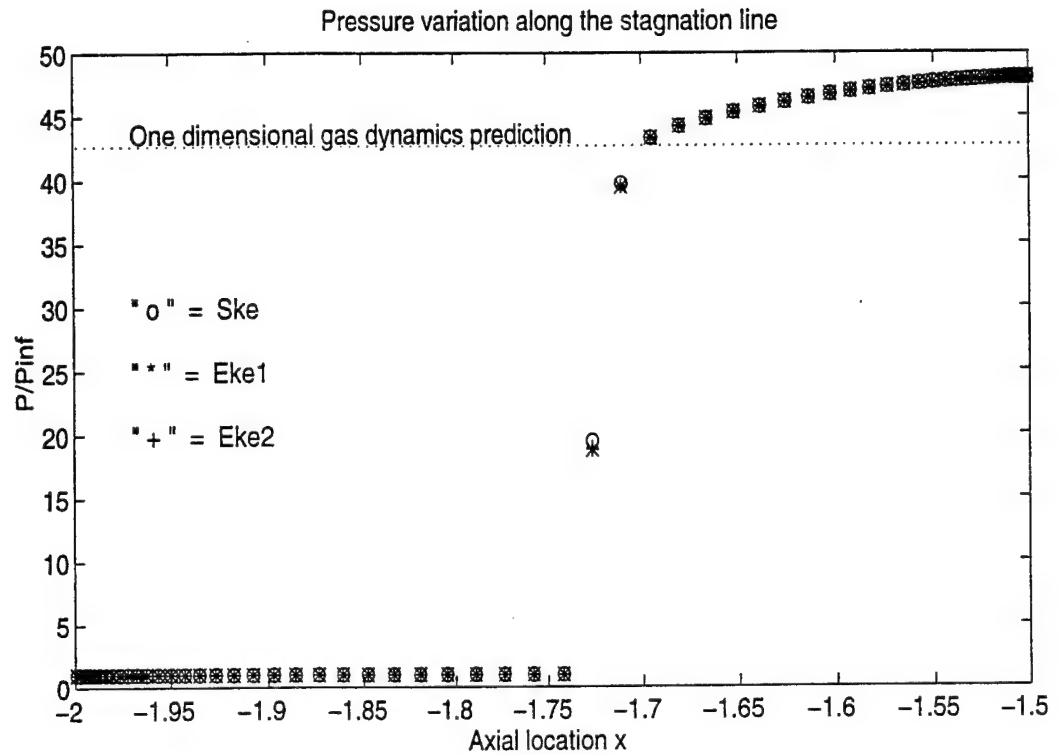


Figure 6.30. Computed variations of static pressure and Reynolds shear stress along the stagnation streamline for the spike-off case.

the symmetry in the predicted solutions. No differences between the various modifications need be expected here.

Figure 6.31 shows a comparison between the computed values of TKE along the stagnation line. The unmodified model predicts a much higher value of TKE compared to the modified models,  $E_k\epsilon_1$  and  $E_k\epsilon_2$ . Figure 6.32 shows a comparison between the predictions made by the unmodified model and the models modified to take into account the non-equilibrium effects. The rate of production and rate of dissipation show a similar trend as far as the peak levels in  $P_k$  and  $\epsilon$  are concerned. However, the level of production and dissipation predicted by the unmodified model is much larger than that predicted by the modified models and the predictions made by the modified models ( $E_k\epsilon_1$  and  $E_k\epsilon_2$ ) are virtually identical. Let us consider the predictions made by the unmodified model at a given

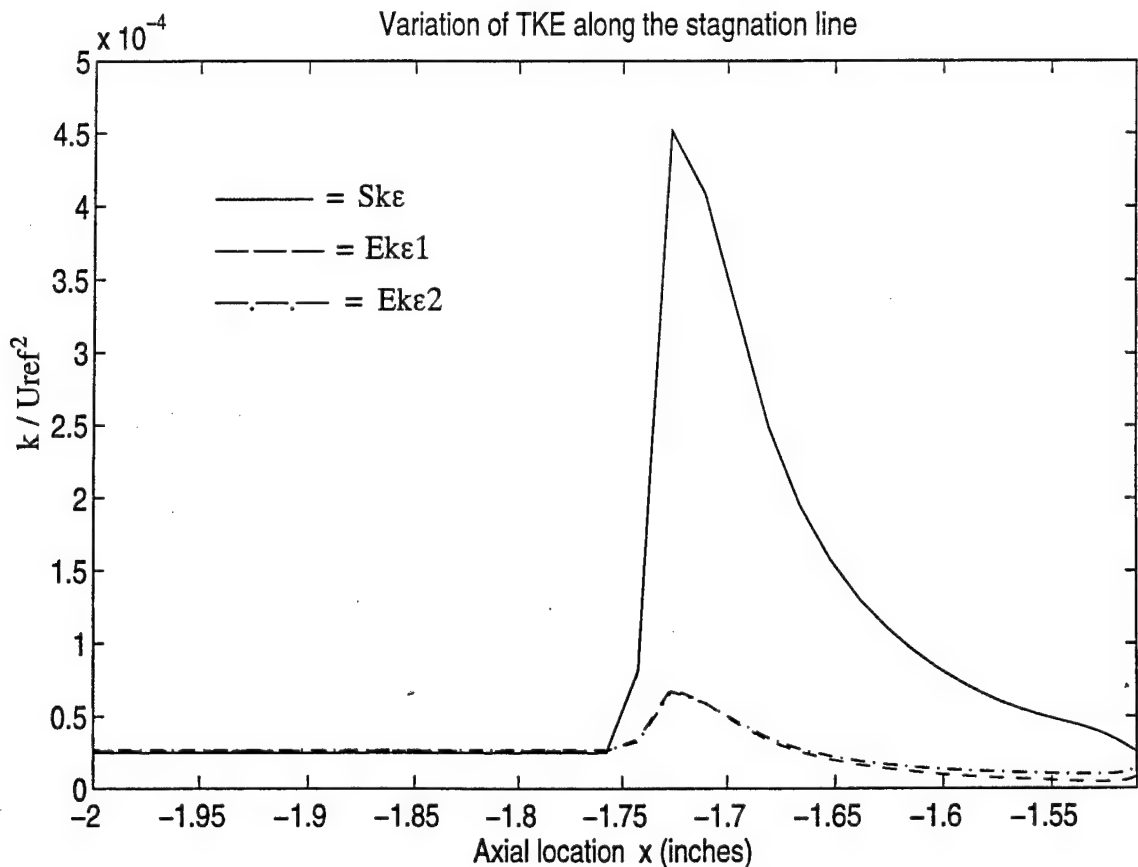


Figure 6.31. Computed variation of TKE for the spike-off case.

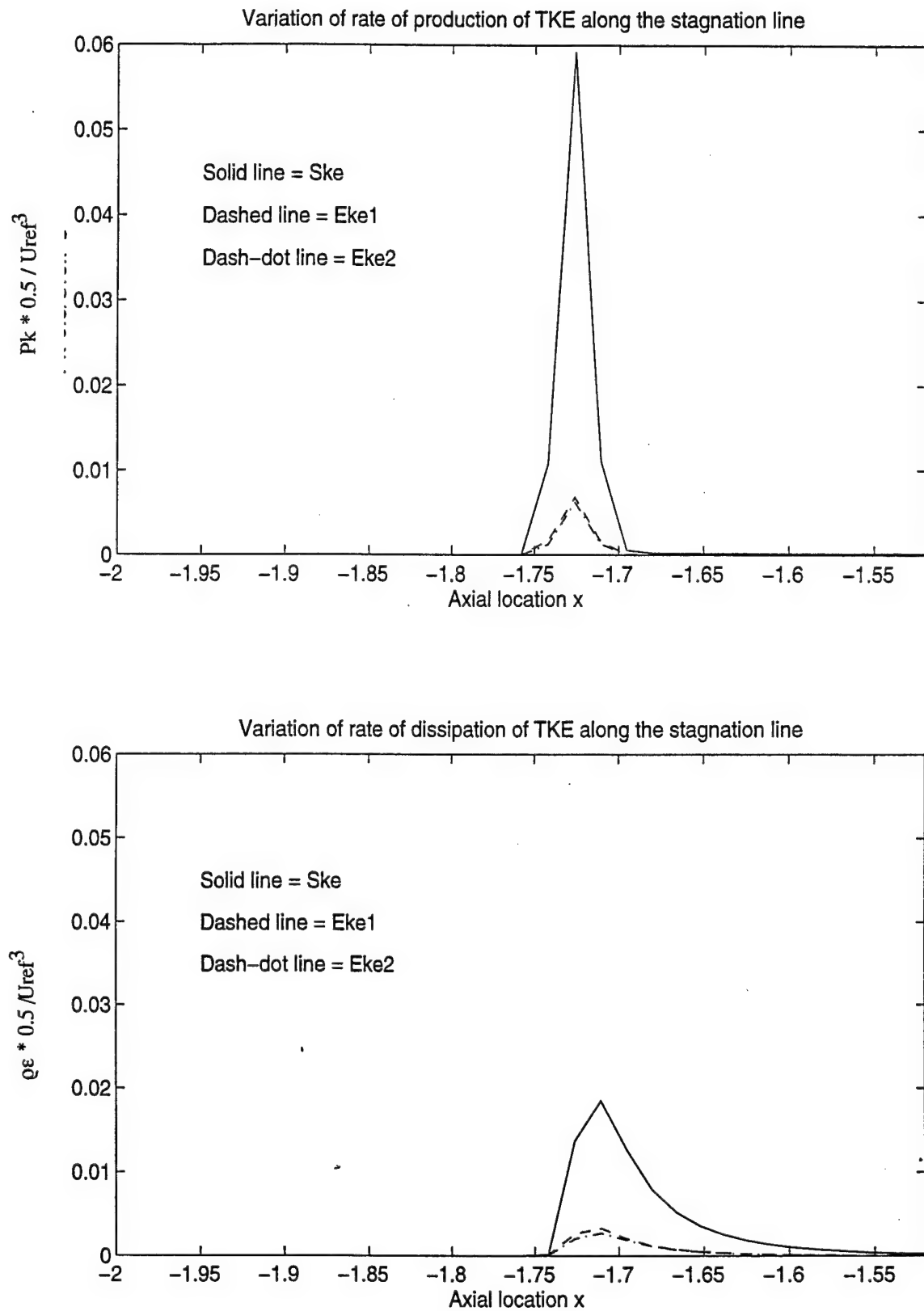


Figure 6.32. Variation of the rate of production and rate of dissipation along the stagnation line for the spike-off case.

instant in time. The rate of production is about three times the rate of dissipation and so results in a substantial increase in the rate of “production of dissipation” term in the  $\epsilon$  equation (using the  $C_{\epsilon 1}$  modification). The result is an increase in the predicted value of dissipation rate and when this magnitude of dissipation rate is added to the  $k$  equation it results in a decrease in the predicted value of  $k$  and the eddy viscosity. The reduction in eddy viscosity leads, in turn, to a reduction in viscous stresses and thereby a reduction in the production rate. As the flow evolves it results in substantially reduced values of TKE,  $\epsilon$  and  $P_k$ . In Figure 6.32, the location of the peak levels indicate that the peak in the dissipation rate is displaced one cell downstream from the peak in the production rate. It is difficult to explain the reason for this behaviour.

Figure 6.33 shows a plot of the pressure distribution on the surface of the projectile and a comparison of the predicted values with experimental data. The predictions made by the various models are very much identical to one another, which could be expected, because there is an equilibrium between the production and dissipation in the log-layer of the boundary layer on the surface of the projectile. The compressibility modification does not play a major role because the flow is almost subsonic downstream of the shock. A possible difference between the predictions made by the models could be expected in the region where the boundary layer separates. But the differences seen in the predictions made are very minimal.

In the figure, a region of discrepancy between the experimental measurements and the computational predictions has been highlighted. The jump in pressure is because of the separation of the boundary layer on the dome surface. To accommodate this separation the flow goes through a weak compression wave. The shadowgraphs and Schlieren pictures of the flow field clearly indicate this weak compression wave. But the pressure taps on the dome of the hemispherical surface fail to pick up this jump. The experimentalists, Huebner et al. [1995], confirmed that there is a weak compression wave but could not account for the

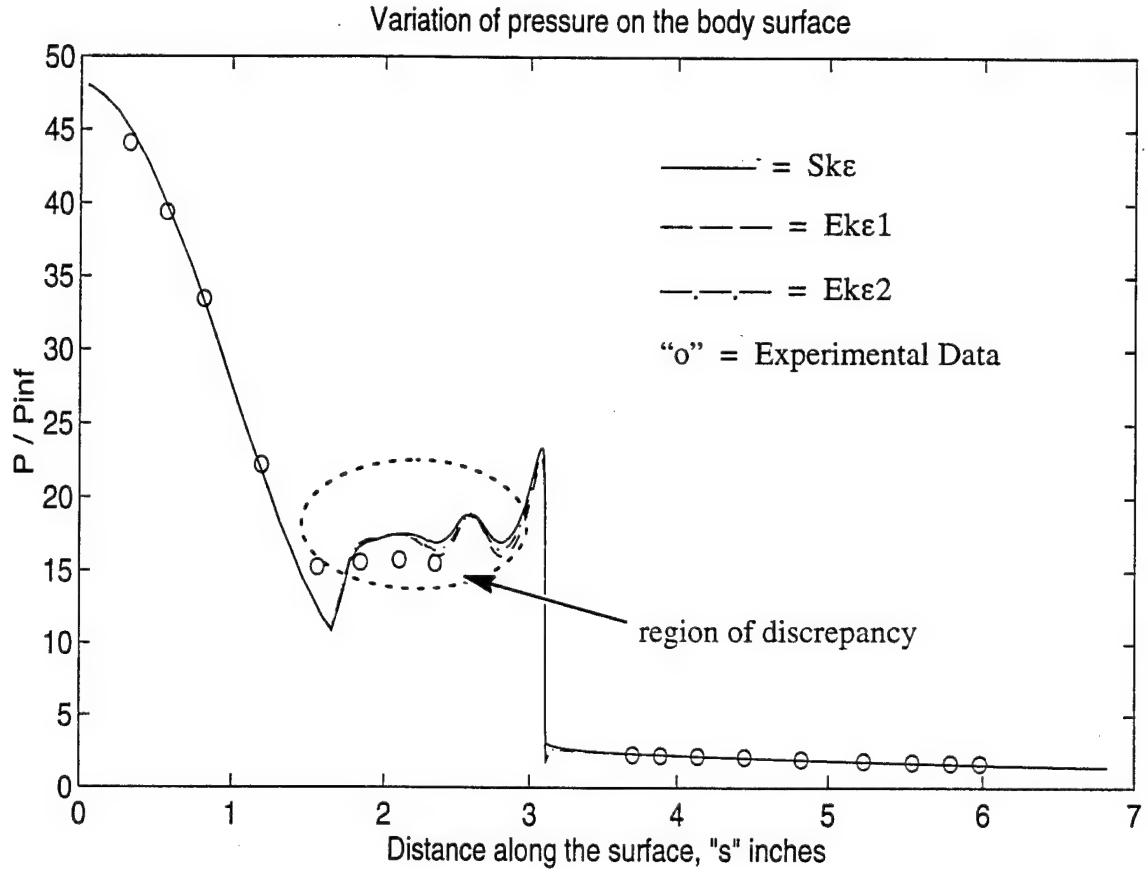


Figure 6.33. Comparison of computed values of pressure with experimental data

experimentally observed pressure distribution. Other computational studies have also confirmed the jump in pressure (private communication from L. Huebner).

#### 6.5.1.2 Compressibility modifications

Computations using the compressibility modifications, of Sarkar et al. [1991] and Sarkar [1992] and El Baz and Launder [1993] for the extra dissipation due to compressibility effects and the pressure dilatation correlation and the compressibility modifications for the turbulent mass flux and the baroclinic term (proposed in this dissertation), were performed to compare and contrast their effectiveness and applicability. It was observed in the computational study of the base flow field that the compressibility modifications of El Baz and Launder [1993] were overly dissipative resulting in unsatisfactory predictions of the afterbody flow field.

Figure 6.34 presents a comparison of the predicted variation of static pressure and Reynolds shear stress, along the stagnation line. There is no difference between the values predicted by the various models that address the effect of compressibility. The plot of the Reynolds shear stress confirms the symmetry in the solutions obtained. The lack of differences seen in the predicted values of static pressure along the stagnation line could be because the jump across the shock is dominated by “inviscid” effects. Also, as was pointed out earlier, as long as the intensity of the turbulent field upstream of the shock is not large the Rankine-Hugoniot jump conditions can be expected to hold true.

Figure 6.35, presents a plot of the predicted values of turbulent kinetic energy along the stagnation line. The comparison, between the various compressibility modifications, does not show any distinct difference between the various modifications but the El Baz and Launder [1993] modification does seem to predict consistently lower levels of TKE (see section on afterbody flow field computations).

Figure 6.36 presents a comparative plot of the predicted values of rate of production and dissipation of TKE along the stagnation line. The values predicted by the current modifications and that predicted by the Sarkar et al. [1991] and Sarkar [1992] models are virtually identical. The reason for this can be seen from a plot of the enthalpic production rate compared with the dilatational component of the production rate and the iso-volumetric part of the production rate (equations 6.3, 6.4 and 6.5), as shown in figure 6.37. The figure shows that the enthalpic production rate as predicted by the current modification is not of the same order of magnitude as the other two parts of the production which explains the minor impact of the current modifications on the mean flow solution.

Figure 6.38 presents a comparison (between the various compressibility modifications) of the predicted value of pressure on the surface of the projectile with experimental data. There is no appreciable difference seen in the predictions made by the various models that address the effect of compressibility on the turbulent flowfield.

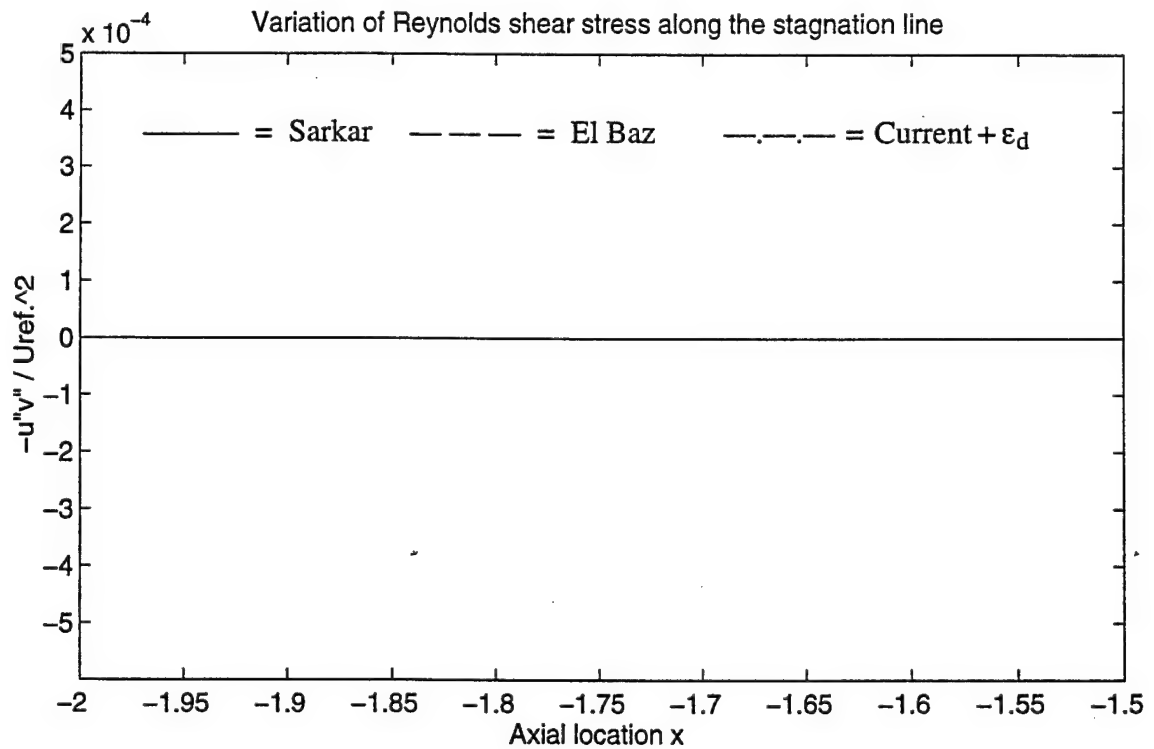
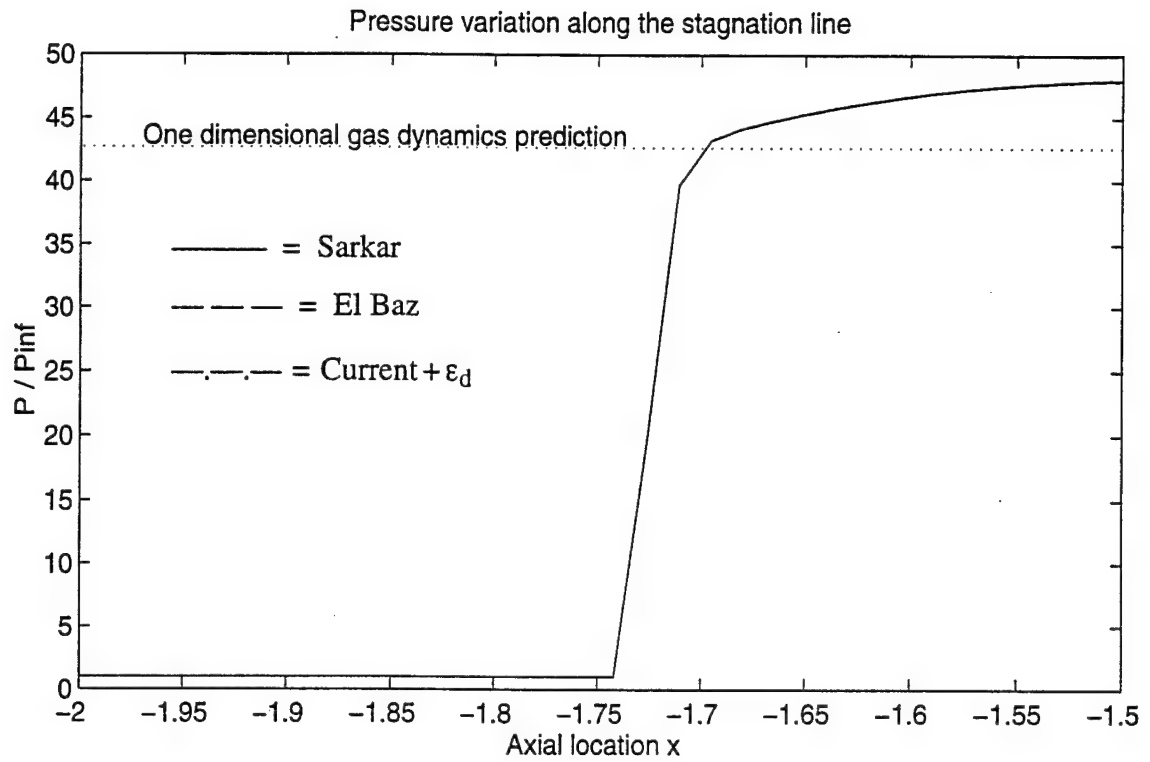


Figure 6.34. Computed variations of static pressure and Reynolds shear stress along the stagnation line for the spike-off case.

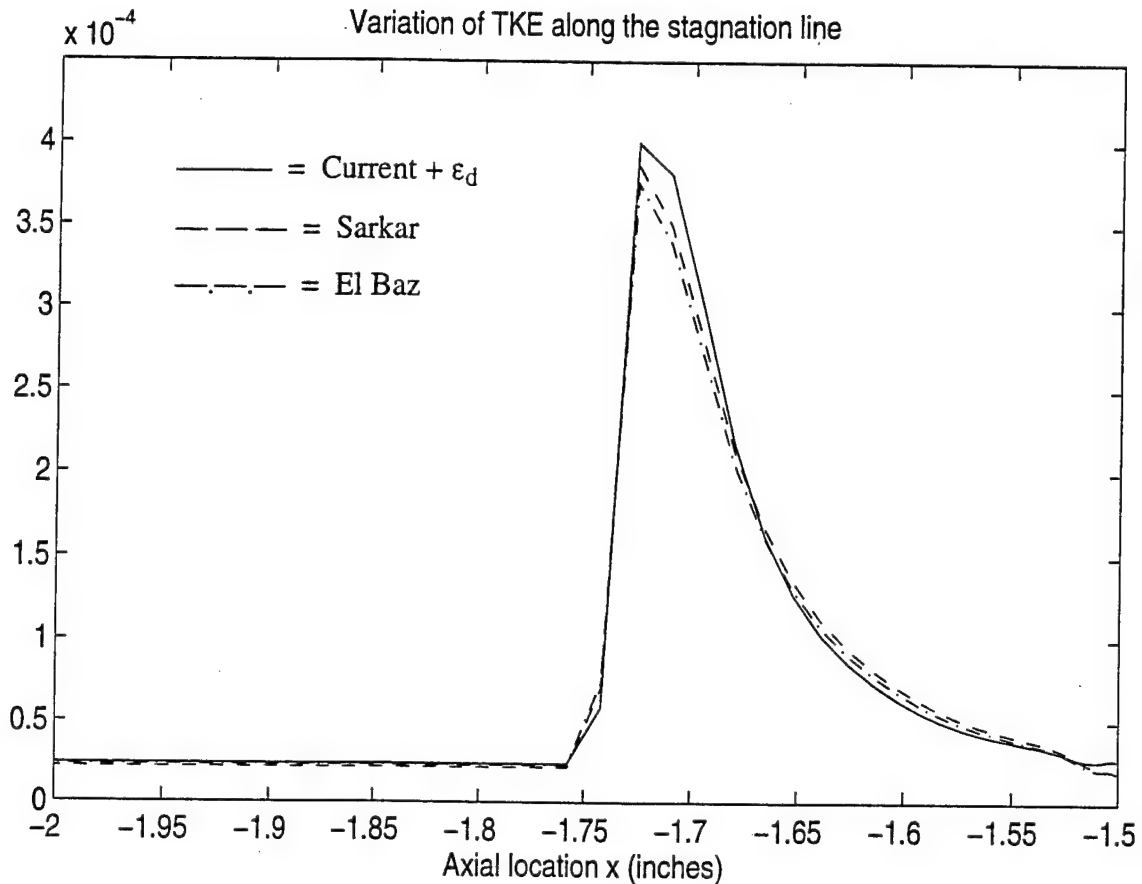


Figure 6.35. Computed variation of TKE for the spike-off case.

### 6.5.2 Spike-on Case

Figure 6.39 shows a sketch of the computational domain used in the calculations. The geometry of the spike and the projectile are obtained from the experimental study of Huebner et al. [1995]. The domain extends out about 6 inches from the top of the cylinder surface. The geometry of the projectile is the same as the one described in the previous sub-section. The length of the spike-aerodisk assembly is 12.00 inches and the inflow boundary is at a distance 3.00 inches from the aerodisk surface. The diameter of the aerodisk is 1.156 inches and the diameter of the spike is 0.375 inches. The computational domain had to be split into four blocks to achieve a reasonable distribution of grid points. The blocks have continuous grid lines and so there was no need for any special interface treatment excepting the conservation of fluxes at interfaces.



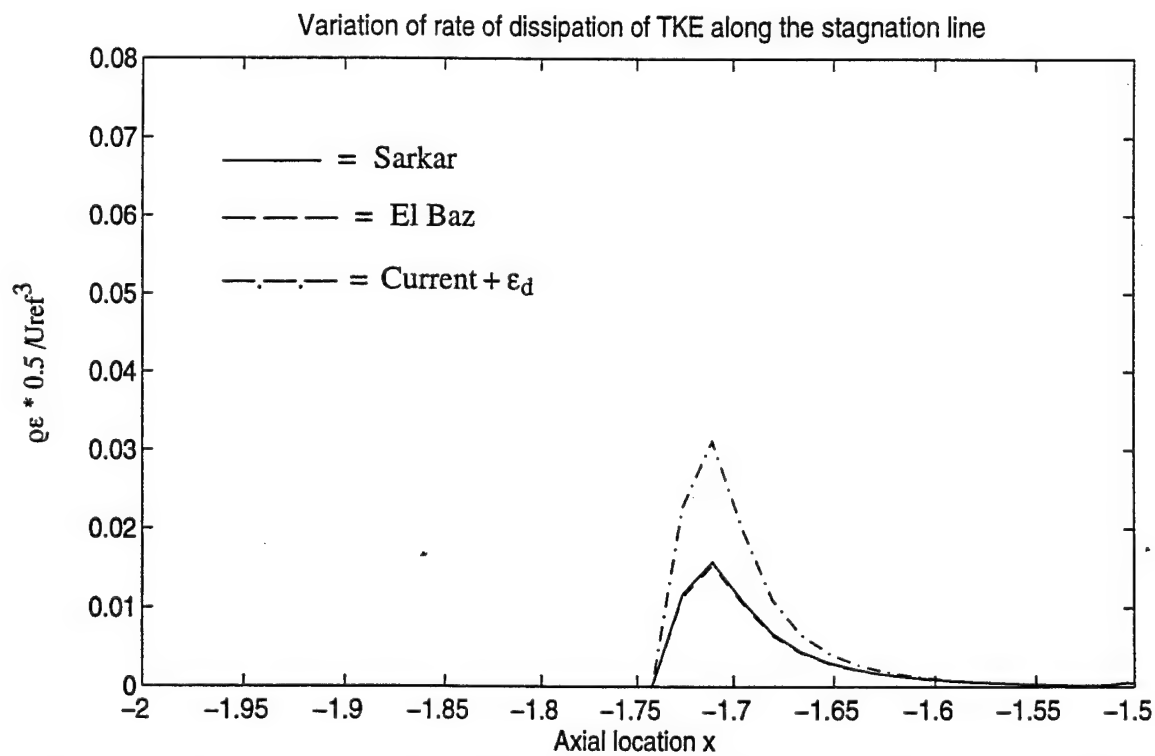
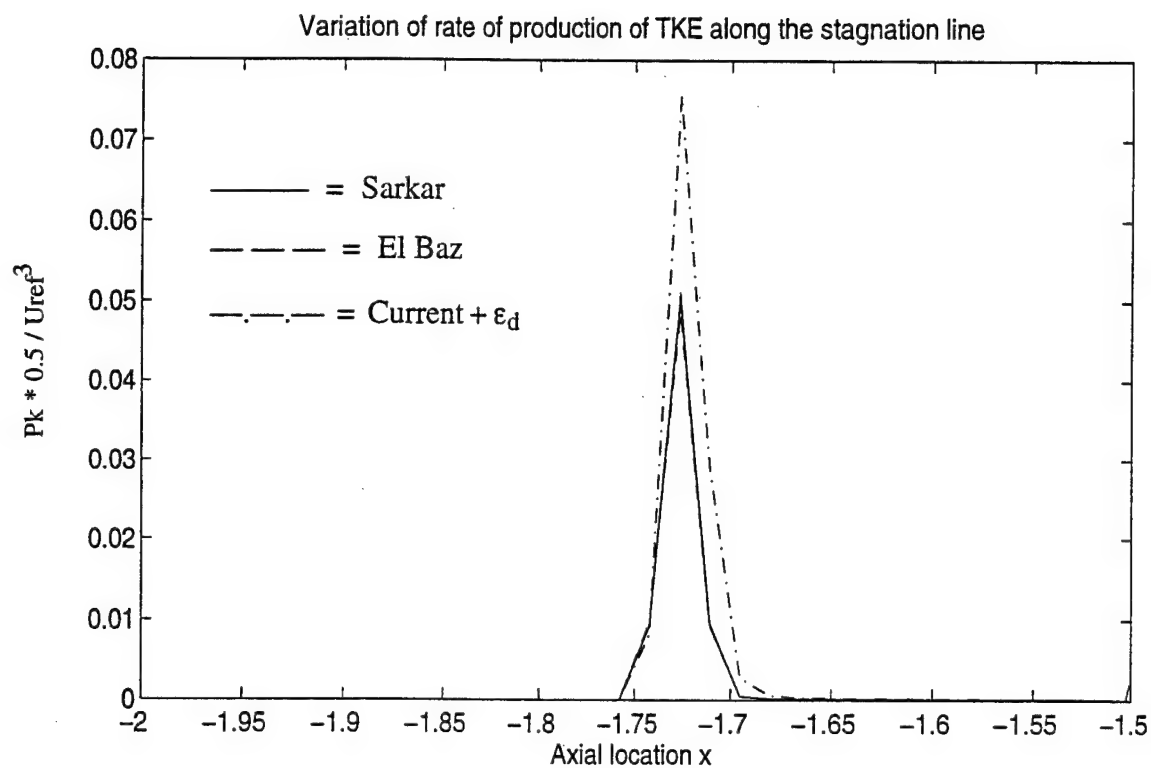


Figure 6.36. Variation of rate of production and dissipation along the stagnation line for the spike-off case.

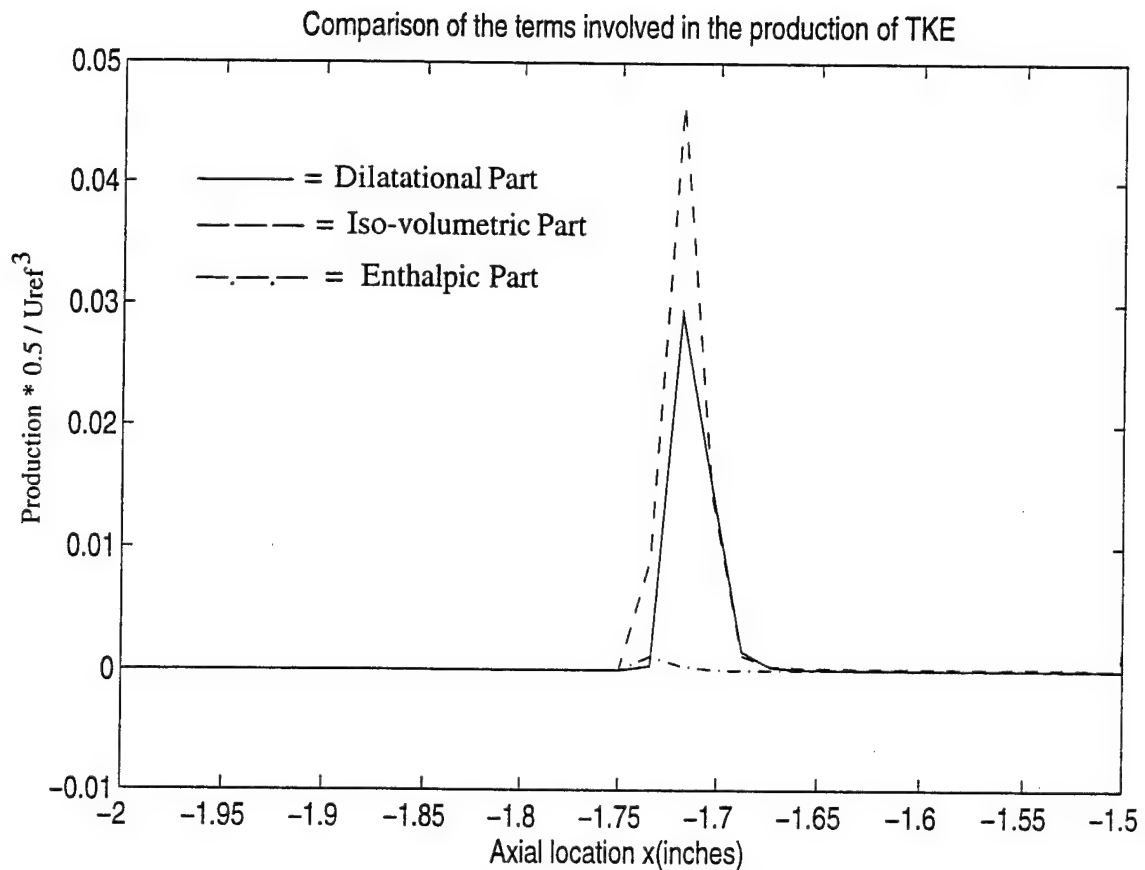


Figure 6.37. Variation of the three parts of production of TKE, along the stagnation line.

At the inflow boundary the inflow Mach number and Reynolds number were specified and the pressure and temperature were held constant. The inflow Mach number and Reynolds numbers are respectively, 6.06 and  $8.0 \times 10^6$ . The Reynolds number is based on the projectile diameter. At the far field boundary and at the outflow boundary a simple variable extrapolation was used. At the wall boundary the compressible form of the wall function technique has been used. At the symmetry boundary the gradients, of axial component of velocity, temperature, density, TKE and  $\epsilon$ , in the radial direction and the radial component of the velocity were set to zero.

Figure 6.40, shows representative contour plots of density, pressure and temperature. As the flow behind the bow shock expands around the aerodisk a weak compression is formed at its base. The wake flow caused by the aerodisk and the nearly stagnant flow near the dome creates the conically shaped recirculation region. The region is separated from the

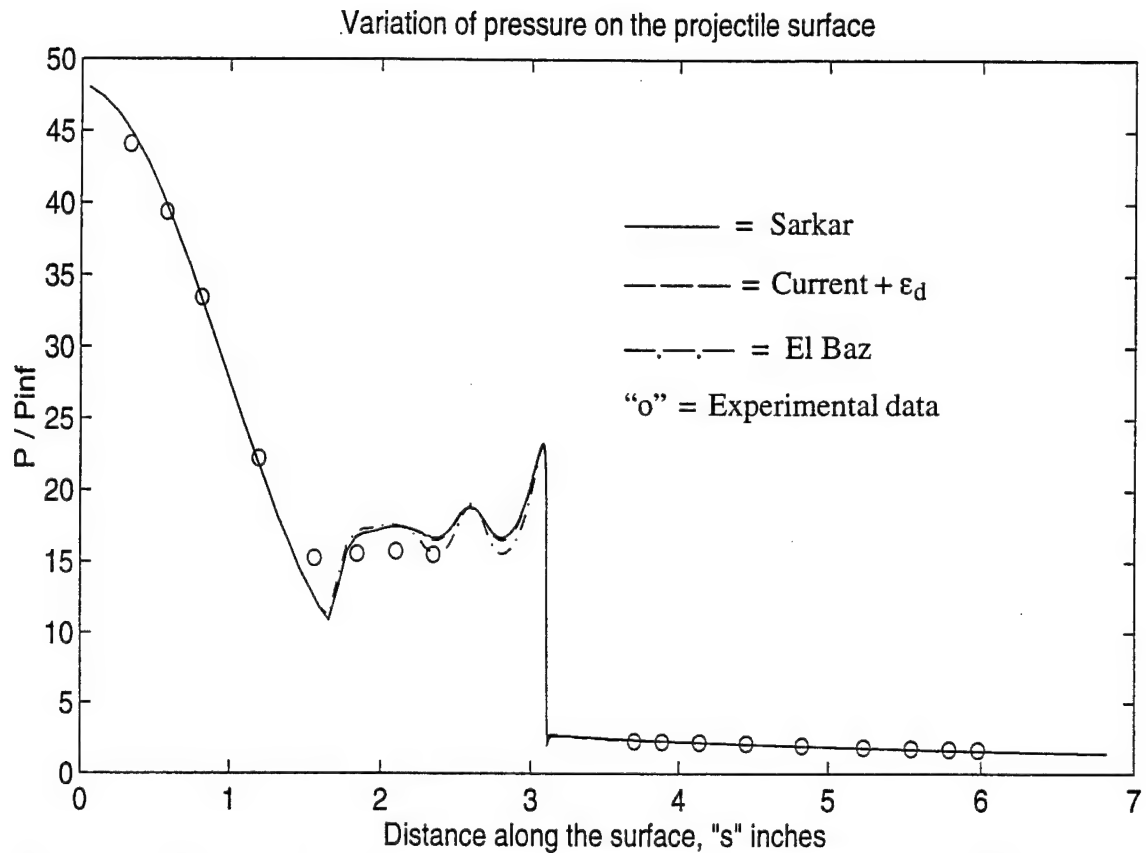
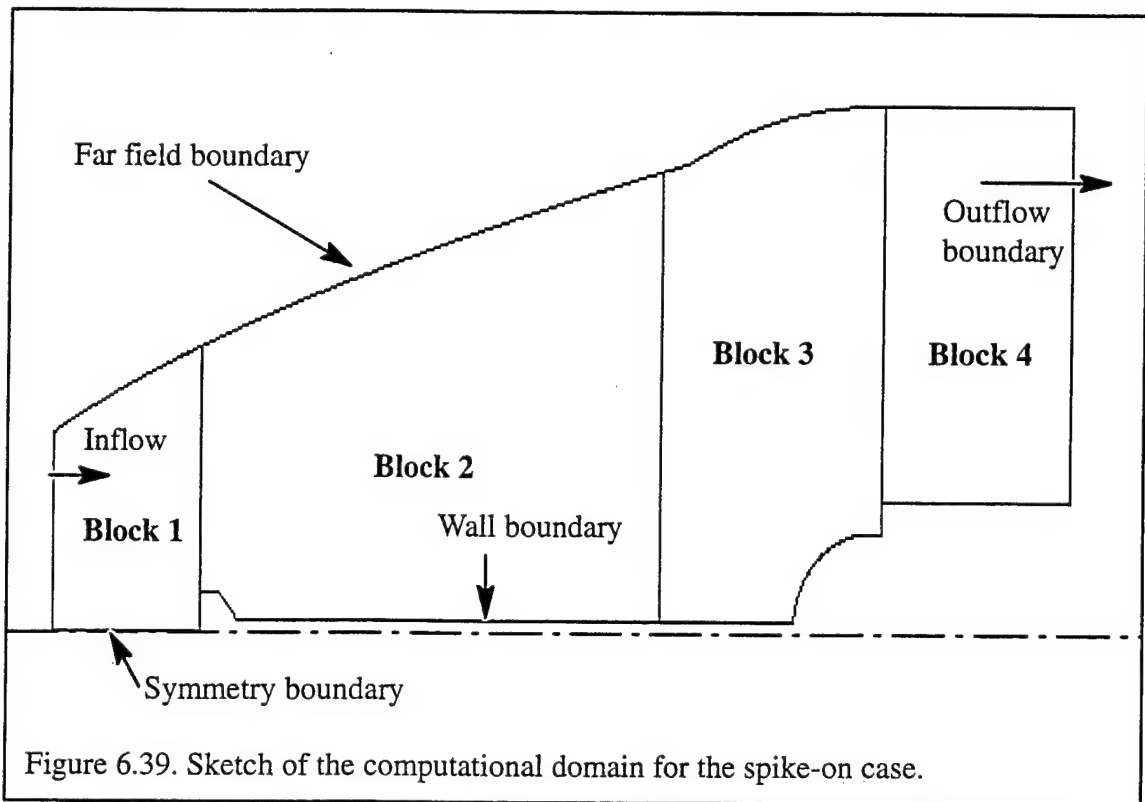


Figure 6.38. Comparison of computed values of pressure with experimental data.

inviscid flow by a flow separation shock. It is expected that this shock will isolate the recirculation region thereby enabling the reduction of pressure and heating rates on the dome surface. Additional pockets of recirculation region are created at the shoulder region between the hemispherical dome and the cylindrical body of a larger diameter.

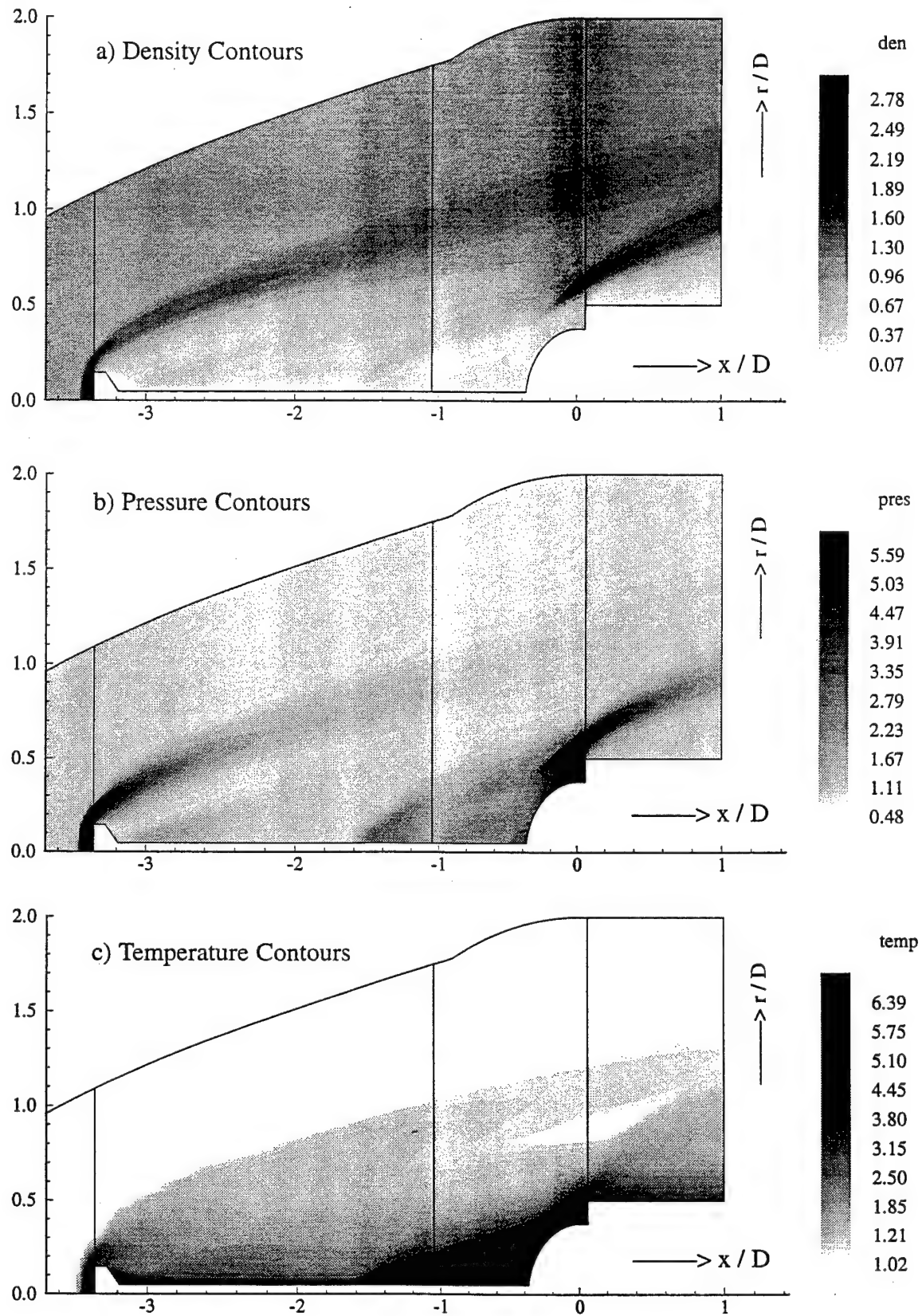
Figure 6.41 presents a comparison between the pressure distributions on the dome surface, with and without the spike and aerodisk combination. The results presented here are those obtained with the modifications (proposed in this dissertation) for enthalpic production and baroclinic torque and dilatational dissipation rate. It is quite clear from this plot that the spike-disk combination certainly helps in reducing the pressure on the projectile surface. The decrease in pressure is almost ten times the value obtained in the spike-off case. The distribution of temperature on the surface of the projectile, with and without the spike, is shown in Figure 6.42. Even though the drop in temperature at the dome surface is not as



dramatic as the pressure drop there is definitely an appreciable drop in temperature, which justifies the use of the spike-aerodisk combination. Also, the temperature on the dome of the projectile remains fairly constant in comparison for the spike-on case. However, it should be noted that the current computations were restricted to an angle of attack of zero degrees. Huebner et al. [1996] have reported that there is a limited range (in terms of angle of attack), of application of the spike-aerodisk combination.

#### 6.5.2.1 Non-equilibrium modifications

Computational studies of the afterbody flowfield indicated that the non-equilibrium modification of Thakur et al. [1996] when used in conjunction with the non-equilibrium modification of Chen and Kim [1987] and the compressibility modification of Sarkar et al. [1991] resulted in an “optimum” prediction. The predictions in the afterbody case gave reasonable predictions of the both the mean flow quantities as well as the turbulence quantities, such as the turbulent kinetic energy and the Reynolds shear stress. With this in mind, we decided to compare only this combination of non-equilibrium modifications (with



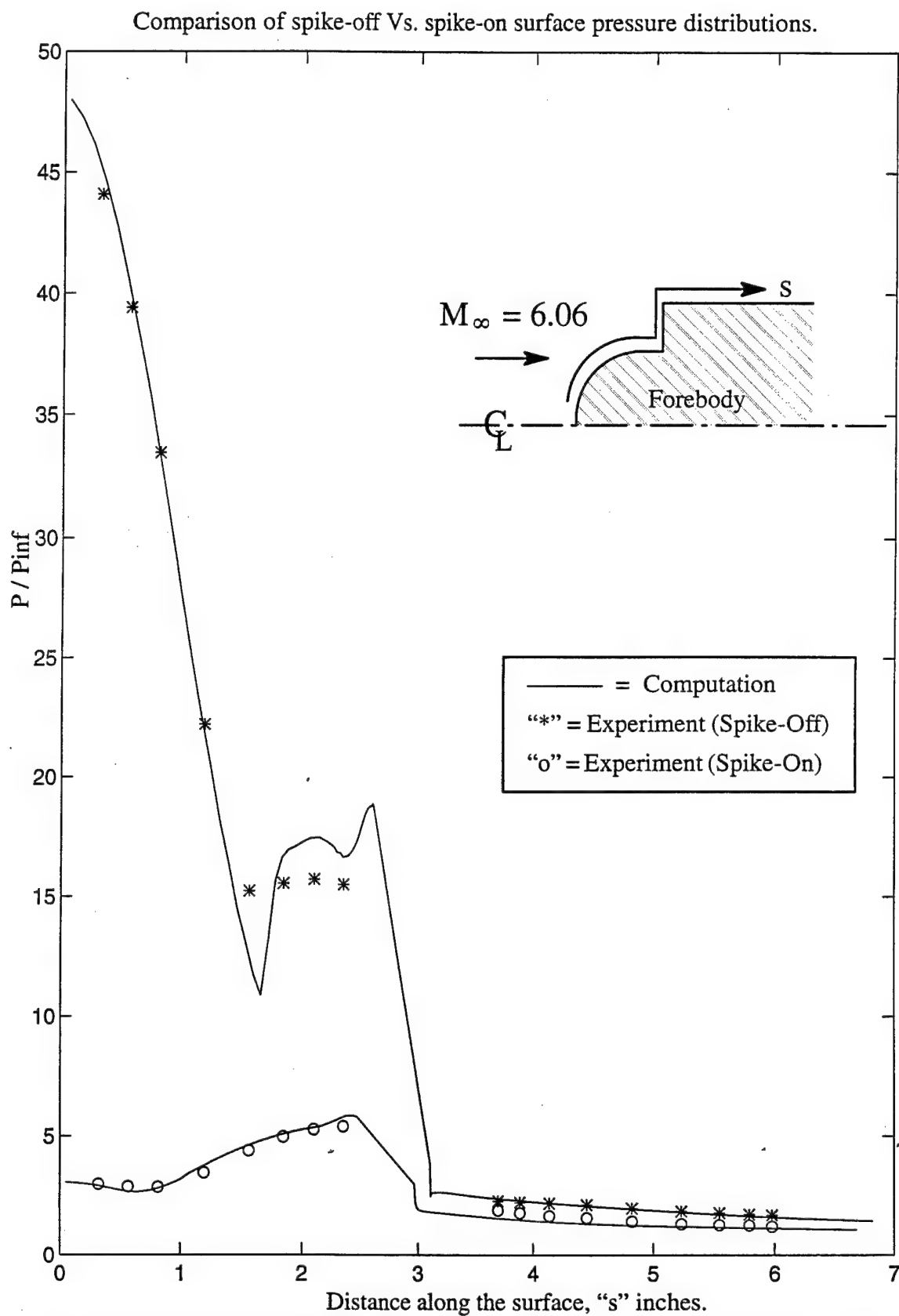


Figure 6.41. Comparison of the pressure distributions on the projectile surface, with and without the spike. Computed with the "current" model.

Comparison of spike-off Vs. spike-on surface temperature distributions.

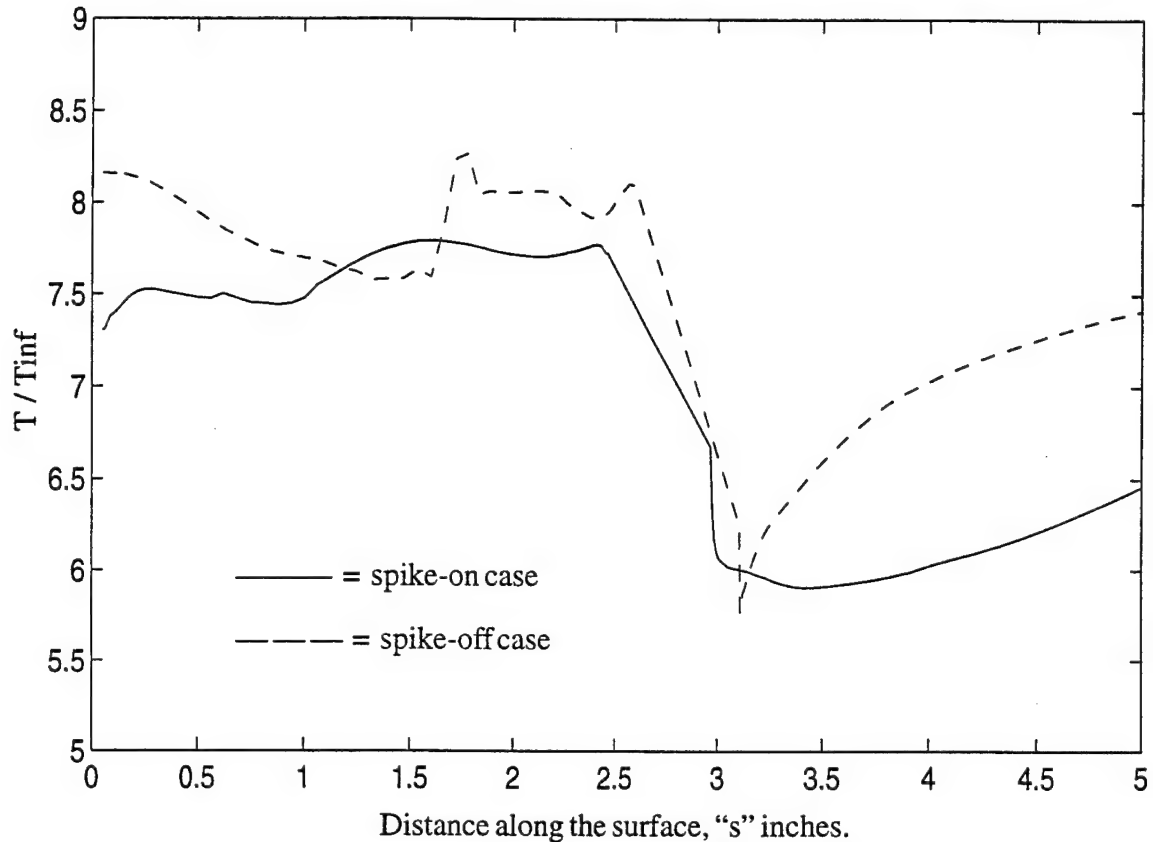


Figure 6.42. Comparison of the temperature distributions on the projectile surface, with and without the spike. Computed with the "current" model.

the compressibility modification of Sarkar et al., 1991) against the predictions made by the unmodified model.

Figure 6.43 presents a comparison of the predictions made of the pressure and temperature distributions along the surface of the spike. The axial location starts from the tip of the aerodisk and extends to the nose of the dome surface. The axial location is given in inches. The distinct regions of the flowfield that is the postdisk compression at the base of the aerodisk and the compression through the separation shock are clearly seen in these plots. Since there are no experimental data along the spike these comparisons can only be qualitative. The location of the jump in temperature, across the separation shock, indicates the location of the separation shock and hence a rough estimate of the extent of the recirculation region. The extent of the recirculation region predicted by the extended model

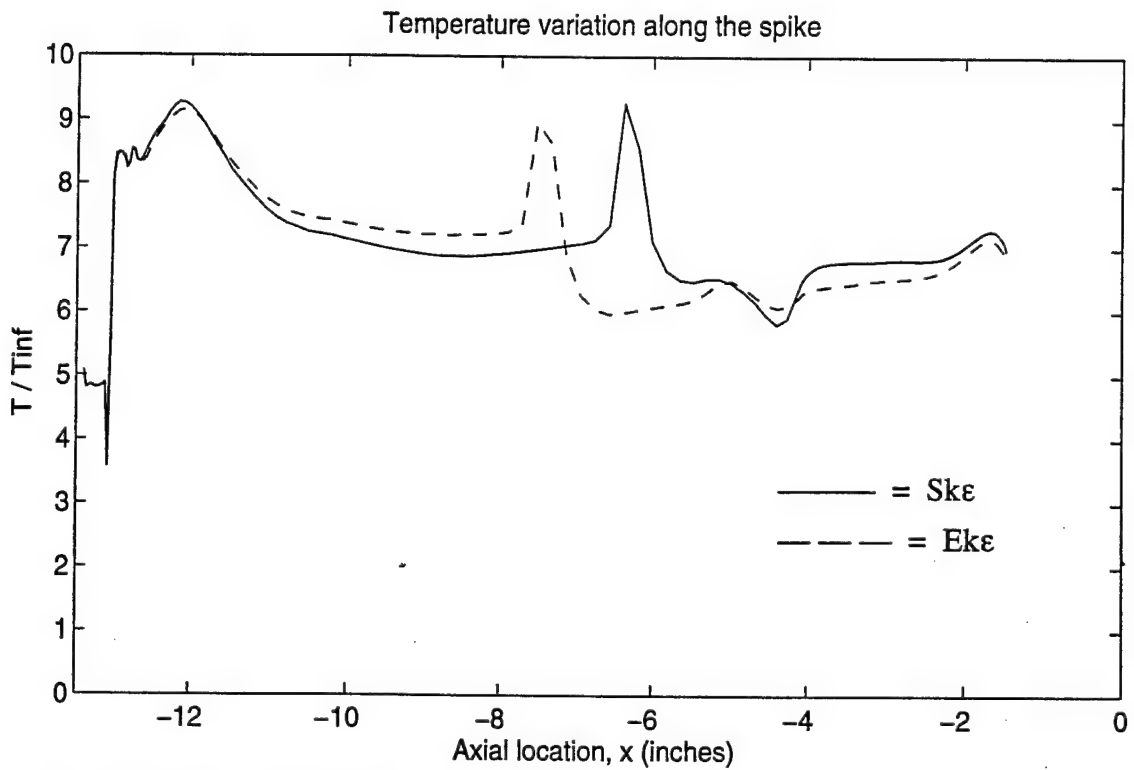
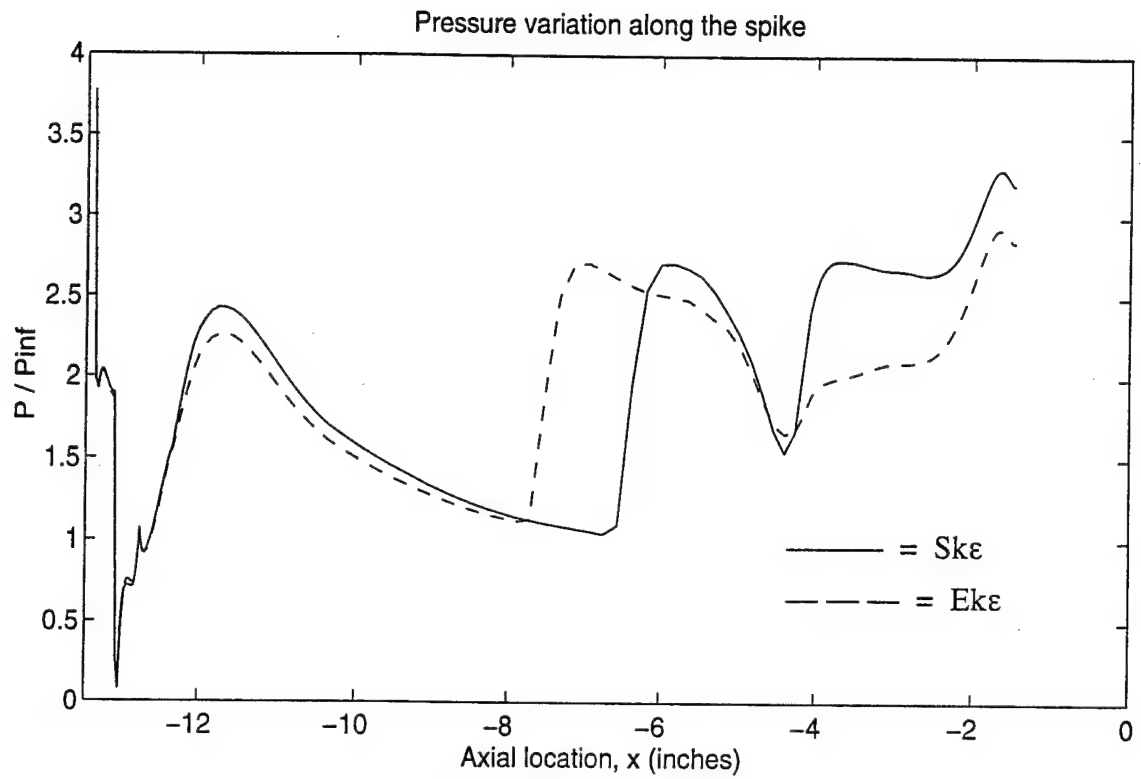


Figure 6.43. Pressure and temperature distributions along the spike.  
Comparison of non-equilibrium modification with unmodified model.



is much larger than that predicted by the unmodified model which is possibly a reflection of the extra dissipation of turbulent kinetic energy introduced by the non-equilibrium modifications. Due to the extra dissipation rate, the eddy-viscosity is reduced with the consequent reduction in the magnitudes of the viscous stresses. The velocity profiles tend to be smoothed out resulting in larger recirculation lengths and a shift in the location of peak values, very similar to the observations made for the axi-symmetric afterbody flowfield.

Figure 6.44 presents a comparison between the predictions made, of the pressure distribution on the surface of the projectile. There is a distinct difference between the predictions made by the eddy-viscosity models and the experimental data, which could be expected, because the variations in pressure on the surface are dictated largely by the

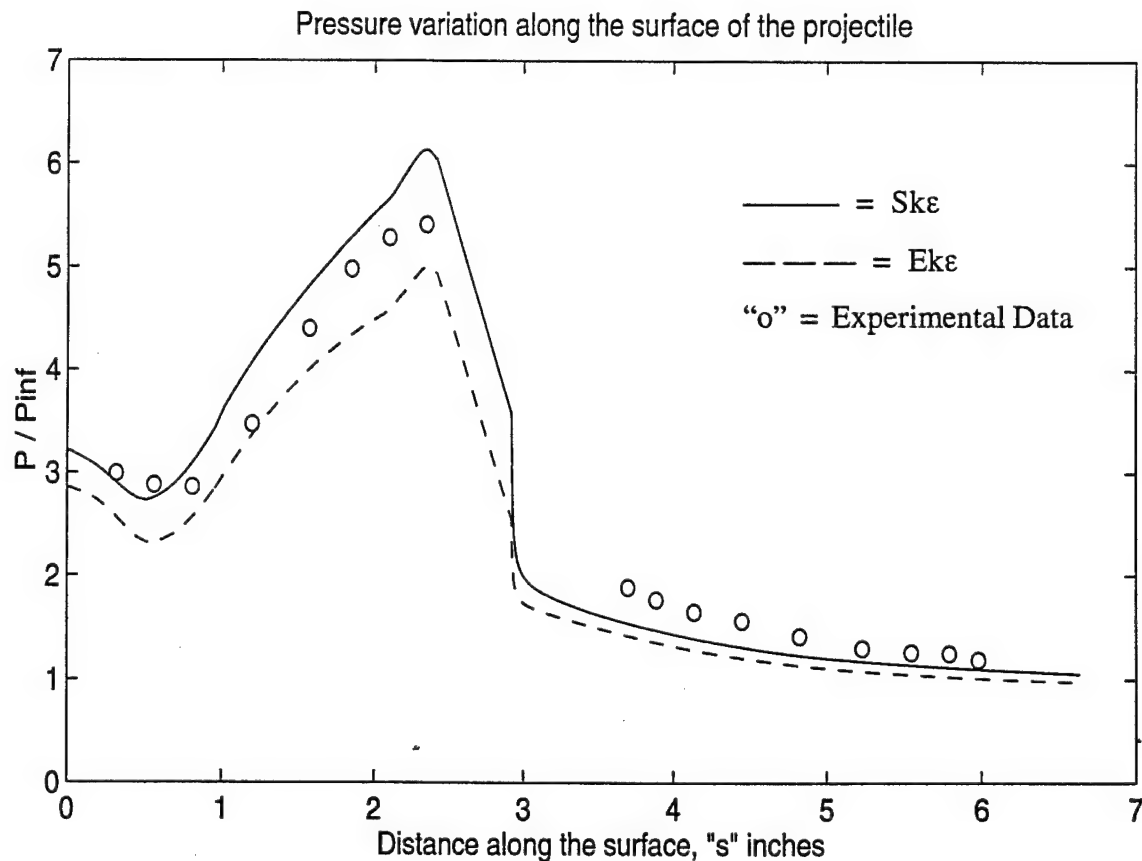


Figure 6.44. Pressure distribution along the surface of the projectile.  
Comparison of non-equilibrium modification with unmodified model.

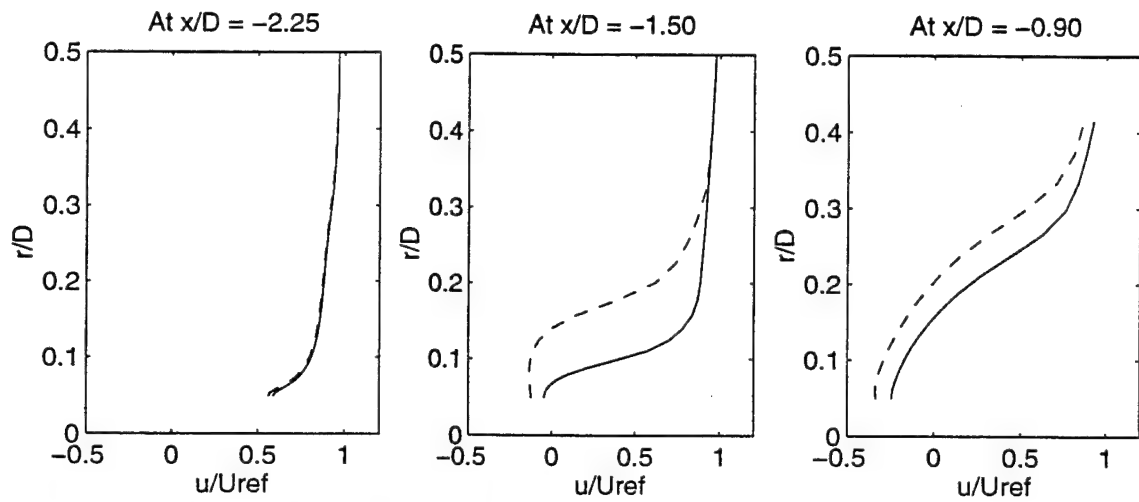
mechanism at play in the recirculating region. The pressure distributions on the dome surface show distinct differences between the two models with the unmodified model predicting a much higher values of pressure on the surface of the projectile and the extended model predicting a lower value of pressure.

To compare the effectiveness of the modifications in predicting the mean flow field comparisons were made at three select locations along the spike. These locations are at an  $x/D = -2.25$ , and  $x/D = -1.50$  and  $x/D = -0.90$ . The  $x/D = -2.25$  location corresponds to a location just outside the conical recirculation region. The  $x/D = -0.90$  location corresponds to about the midway point of the recirculation region. Profile plots of the components of velocity and the turbulent kinetic energy are presented in Figure 6.45. The plots show a lateral shift in the peak locations very similar to the shift seen in the predictions made of the afterbody flow field. However, in the afterbody flow field case the combination of non-equilibrium modifications yielded a prediction comparable to the prediction made using the unmodified model. The non-equilibrium based modification of Chen and Kim [1987] revealed marked shifts in the location peak values (in comparison with the unmodified model). The reason for the lateral shift seen in these computations is presumably due to the dominating influence of the  $C_{\epsilon 1}$  modification.

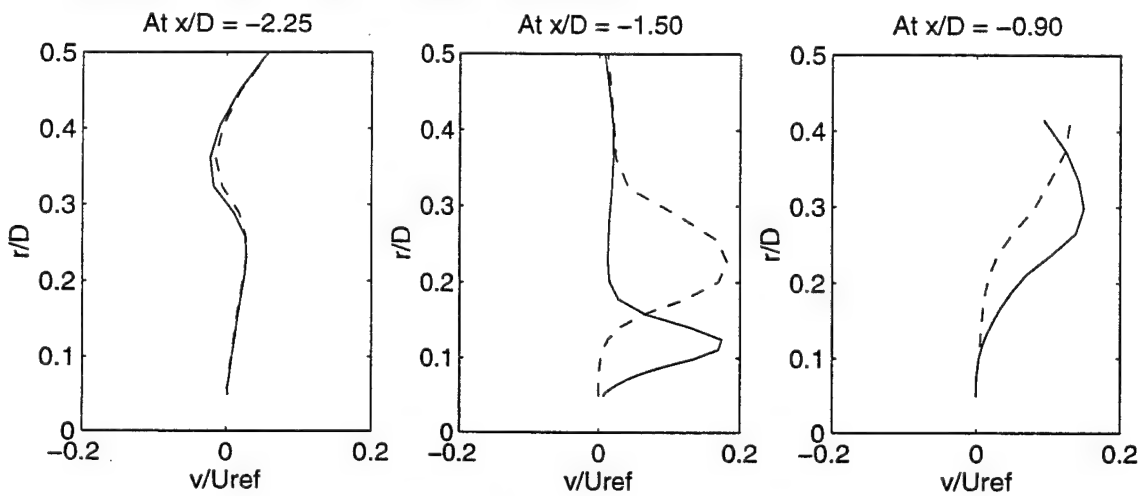
Figure 6.45 shows profile plots of the axial and radial velocity components and the level of TKE, at the three locations mentioned above. There is no difference in the predictions made using the two models at the  $x/D = -2.25$  location. There are substantial differences seen at the other two locations with the standard model predicting a much higher level of TKE due to the larger rate of production of TKE predicted by the standard model. Again, due to the lack of experimental information, these comparisons are purely qualitative.

#### 6.5.2.2 Compressibility modifications

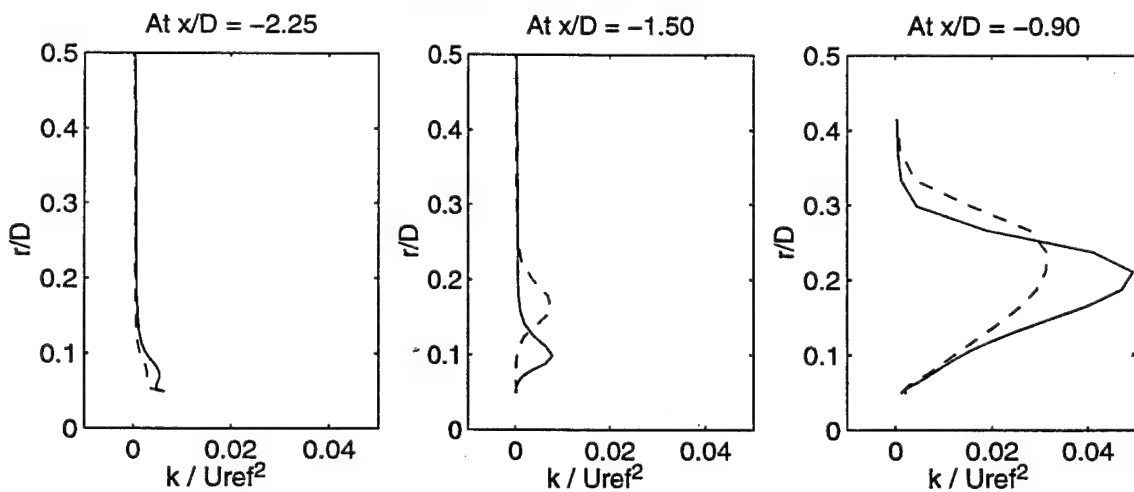
The modifications of Sarkar et al. [1991] and El Baz and Launder [1993] (for the extra dissipation due to dilatational effects) and the modifications of Sarkar [1992] and El Baz and Launder [1993] (for the pressure dilatation correlation) and the modifications proposed in



a) Computed values of axial velocity component



b) Computed values of radial velocity component



c) Computed levels of TKE

Figure 6.45. Comparison of predictions made by the unmodified model and the extended model. — =  $Sk\epsilon$  ; --- =  $E_k\epsilon$ .

this dissertation (that is, the modifications for the enthalpic production term and the baroclinic term) are being compared in this sub-section. In the plots shown below, the modifications due to Sarkar et al. [1991] and Sarkar [1992] is denoted as “Sarkar”. The modifications due to El Baz and Launder [1993] is being denoted as “El Baz”. The term “current” has been used to denote the computations made using the modifications proposed in this dissertation. It should be noted that the current modifications are used in conjunction with the modification for compressible dissipation rate proposed by Sarkar et al. [1991].

Figure 6.46 shows a comparative plot of the pressure and temperature distributions along the surface of the spike. The rise in pressure at about  $x/D = -11.5$  is due to the “post-disk compression” (see Figure 6.27). All three models predict identical variations in pressure and temperature upto this location (from the tip of the aerodisk), but the level of pressure jump across this compression predicted by the El Baz and Launder (El Baz and Launder, 1993) modification is considerably lesser than that predicted by the “Sarkar” modifications and the “current” model. Downstream of this location the pressure and temperature variations predicted by the three models are about the same. The “El Baz” modification predicts a smaller recirculation zone in comparison with the other the two models. Inside the recirculation zone all three models predict considerable variations in the pressure and temperature distribution. It is difficult to provide a reasonable explanation for this variation due to a lack of experimental data in this region.

Figure 6.47 shows a comparison between the predictions made, using the compressibility modifications, of the pressure distribution along the surface of the projectile. The current modifications offer a slight improvement over the other two modifications with the possible implication that the current modifications are a step in the right direction (albeit a small step).

Figure 6.48 presents profile comparisons, of the compressibility modifications, at the three locations along the spike, mentioned earlier. The El Baz modification (El Baz and Launder, 1993) predicts the lowest level of TKE in the flow field. The current modifications

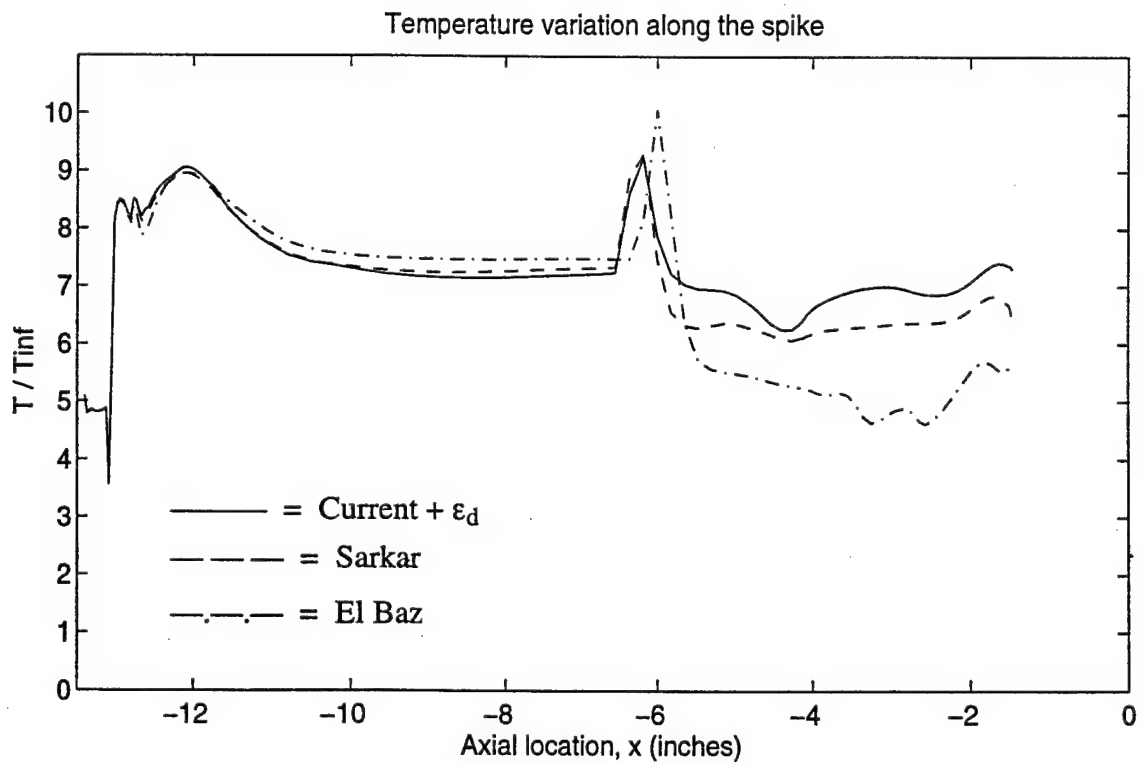
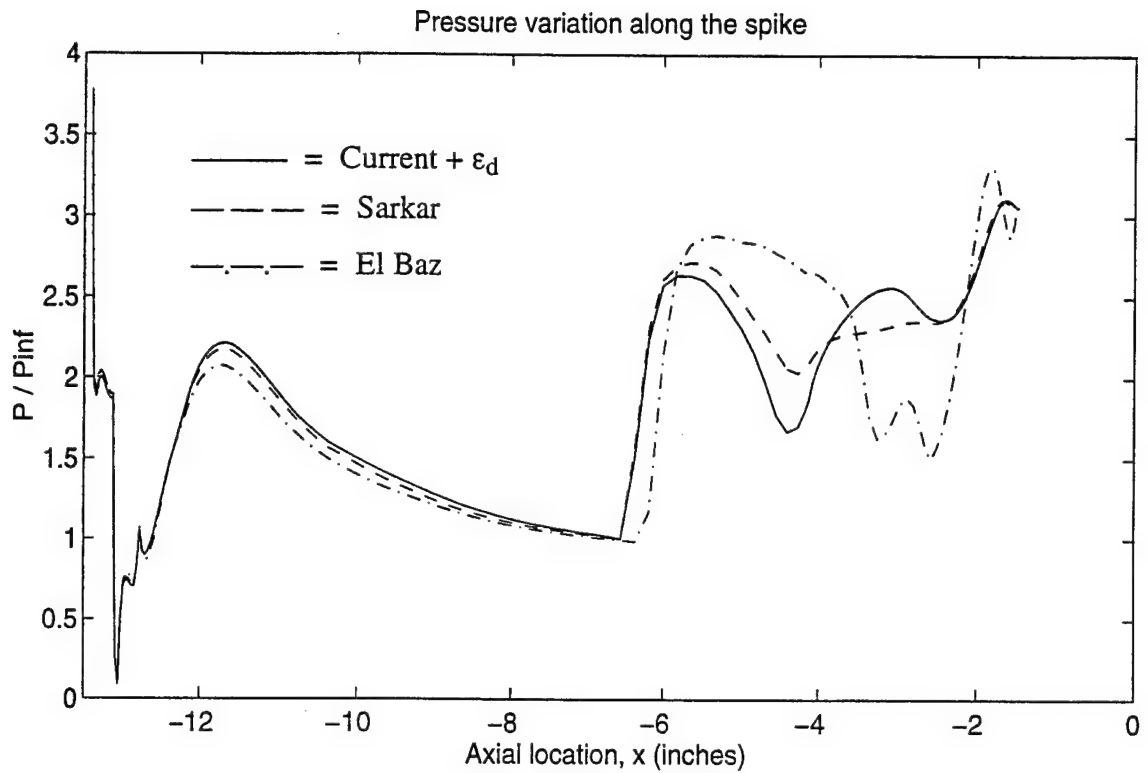


Figure 6.46. Comparison of the compressibility modifications : Pressure and temperature distributions along the spike surface.

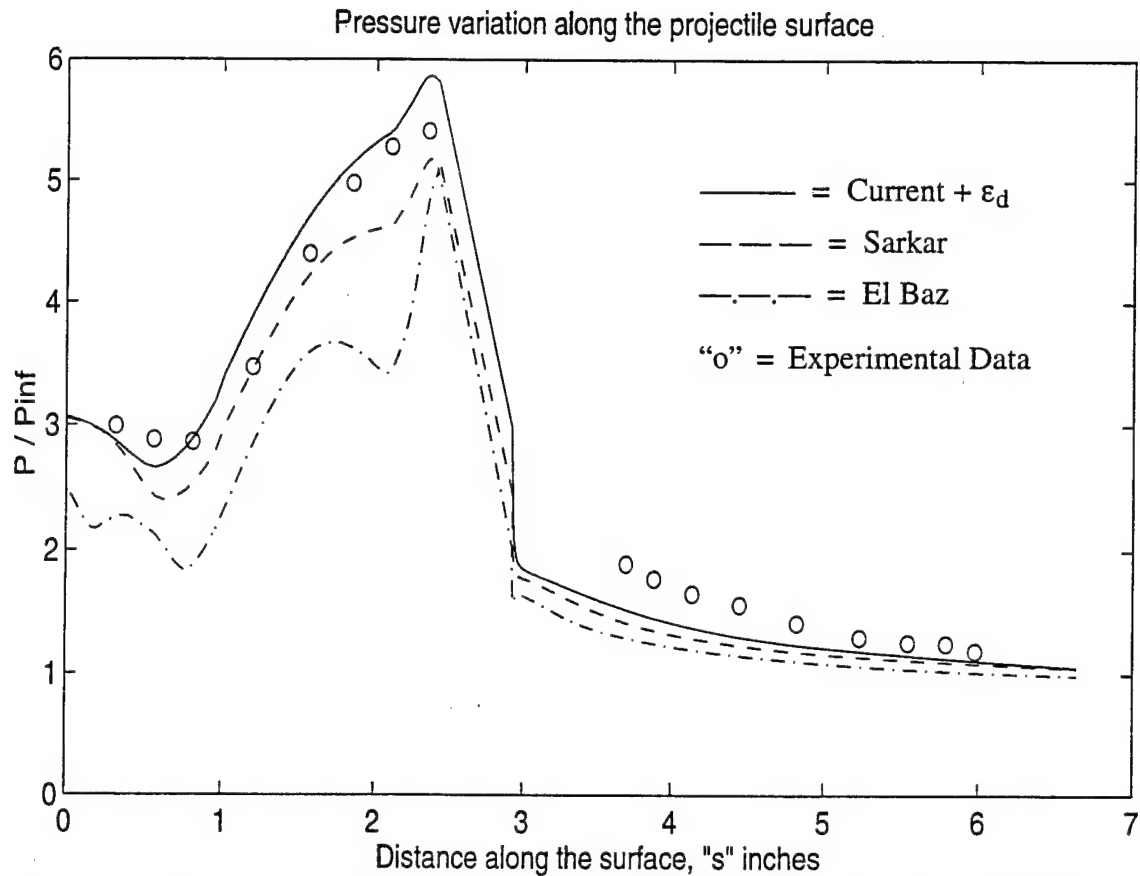
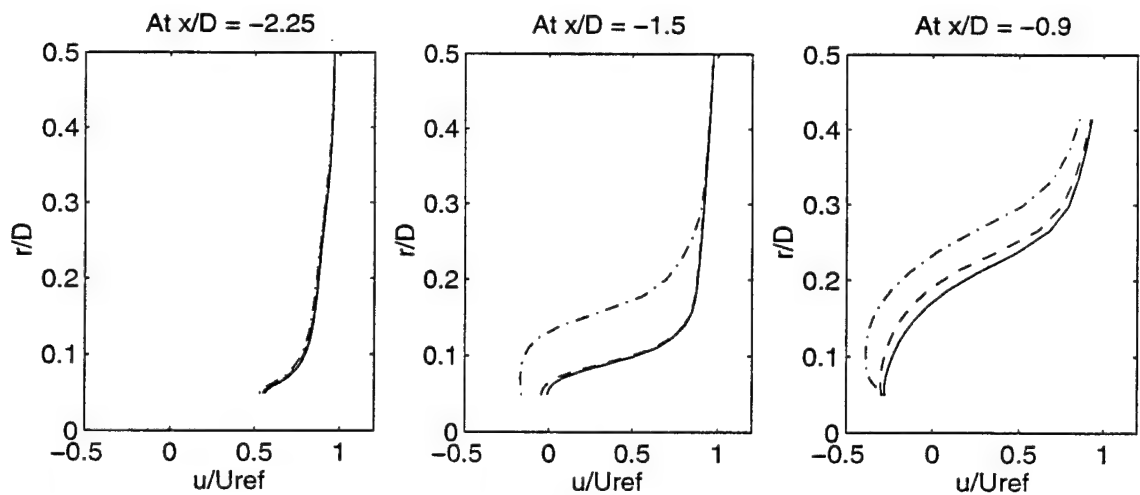


Figure 6.47. Comparison of the compressibility modifications : Pressure distribution along the projectile surface.

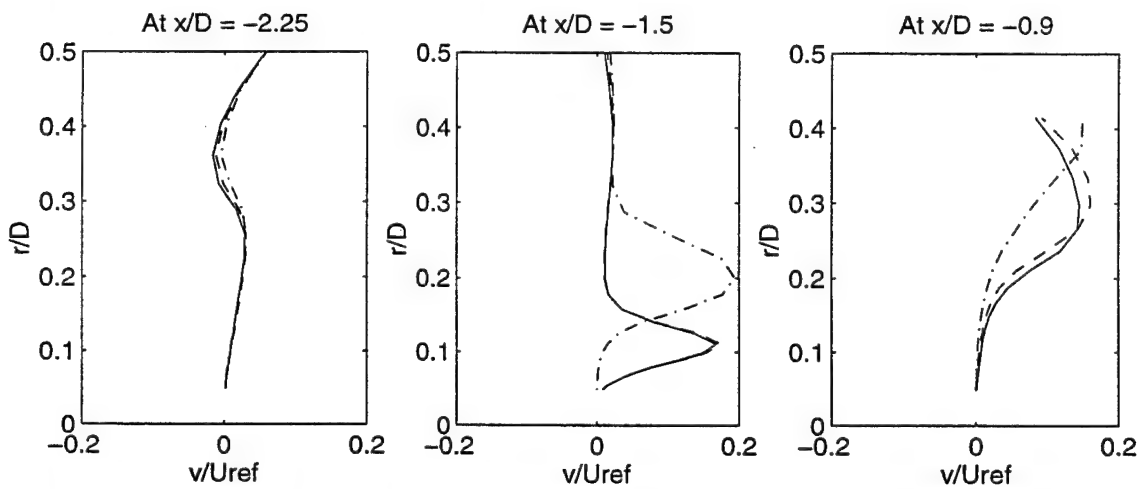
predict an increased level of TKE which is again very similar to our observations for the afterbody flowfield. The reduced level of TKE predicted by the modifications due to El Baz and Launder [1993] is largely due to the increased dissipation rates predicted by that model. The lateral shift in the location peak values is observed in the computations made using the El Baz model.

### 6.6 Summary

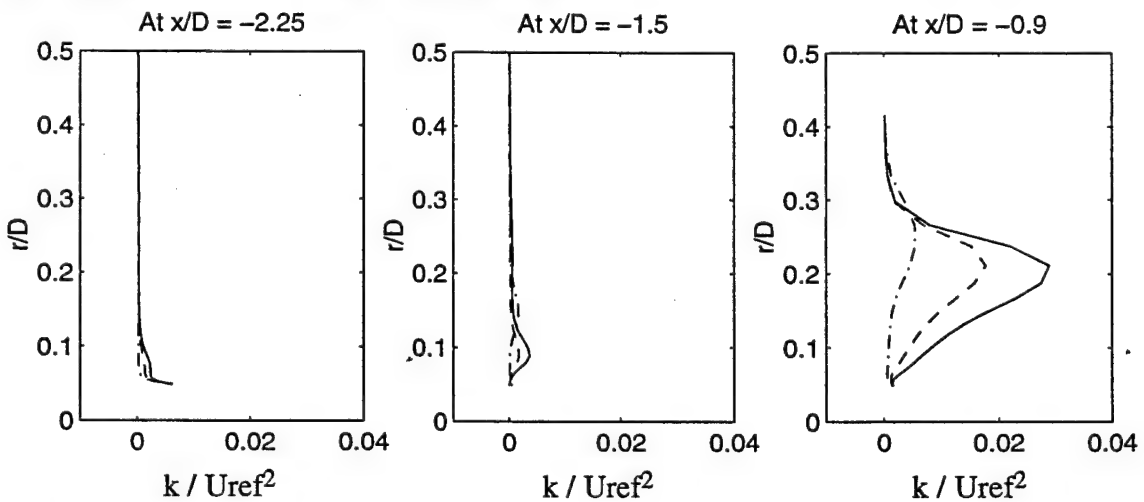
Modifications that have been proposed to address the issue of non-equilibrium between the rate of production and dissipation have been tested for the projectile forebody flow field. Due to the lack of sufficient experimental measurements of this flow field the comparisons had to be qualitative. The standard model predicts higher rates of production of TKE, across the shock wave, in comparison with the non-equilibrium models. There are still



a) Computed values of axial velocity component



b) Computed values of radial velocity component



c) Computed level of TKE

Figure 6.48. Comparison of predictions made using the compressibility modifications.  
 — = Current, --- = Sarkar and -.- = El Baz.

some unresolved issues and conflicting observations (between experiment and DNS). With more insight into the phenomena of shock-turbulence interaction, the validity of the predictions made by the various models can be ascertained.

The modifications that have been proposed to address the effect of compressibility on the turbulent flow field have been tested to evaluate their effectiveness and capability. In terms of the pressure distributions, on the projectile forebody surface, there are no marked differences between the various models. However the El Baz modification (El Baz and Launder, 1993) does consistently overpredict the rate of dissipation.

The use of the spike-aerodisk assembly, in front of the projectile, does reduce the pressure at the projectile surface (by almost a factor of 10). The temperature distributions on the projectile surface do not display such a dramatic reduction, However, the drop in temperature at the nose of the projectile is considerable with a significant rise in temperature at the separation-shock location.

For the spike-on case, the extended model (combination of the modifications for  $C_{\varepsilon 1}$ ,  $C_{\varepsilon 2}$  and compressible dissipation  $\varepsilon_d$ ) predicts a longer recirculating region. The current modifications do not make a significant impact on the mean flow field predictions. However it does predict a pressure distribution that is marginally closer to the experimental data. The modifications also predict higher values of TKE in comparison with the modifications of Sarkar et al. [1991] and Sarkar [1992]. The modifications proposed by El Baz and Launder [1993] predict the lowest levels of TKE, indicative of the overly dissipative nature of these modifications.



## CHAPTER 7

### CONCLUDING REMARKS

Conceptually, addressing the compressibility effects as a dissipative one or modelling compressibility effects based on the turbulent Mach number does not seem to offer a complete description of the physics. Compressibility modifications that have been proposed to address the extra dissipation due to the dilatational velocity field have been analyzed to contrast their predictive capabilities (of decaying compressible turbulence). The study indicated that these modifications were similar in nature, save a constant.

From an analysis of the exact form of the governing equations, additional terms have been identified which are unique to compressible turbulent flows and have been hitherto ignored. These are the terms representing the enthalpic production rate and the term representing the effect of the baroclinic effect. Modifications have been derived to model these terms via a model for the turbulent mass flux.

Additional modifications that have been proposed to address the added time scale effects arising due to the non-equilibrium between the rates of production and dissipation of turbulent kinetic energy have been considered. Suggestions have been made, for possible improvements that could be made to the modification for  $C_{\epsilon 2}$

The various modifications have been evaluated in terms of their predictive capabilities, through computational analysis of flow fields of increased complexity. These are the flow past an axi-symmetric afterbody at supersonic Mach number, the flow past a projectile forebody at hypersonic speeds and the flow past the projectile forebody with a drag reduction spike. A computational procedure using a finite volume, cell-centered scheme with second-order multi-stage Runge-Kutta time stepping has been used in this study. The

artificial dissipation scheme has been found to be unsatisfactory in terms of maintaining the integrity of the flow physics (at least, for the afterbody flow field). The artificial dissipation scheme is also unsatisfactory in predicting flowfields with strong gradients, such as shocks. The added dissipation is not sufficient enough to suppress the spurious oscillations at a discontinuity, such as a shock.

The results of the afterbody flow field indicated that the non-equilibrium based modification to  $C_{\epsilon 1}$  is not sufficient to make reasonable predictions of the flow field and the modification to  $C_{\epsilon 2}$ , when used in conjunction with the  $C_{\epsilon 1}$  modification, offers a more satisfactory set of predictions in terms of the mean flow quantities as well as the turbulence structure.

Of the two compressibility modifications to the compressible dissipation rate and the pressure dilatation correlation, the modifications of El Baz and Launder [1993] are overly dissipative, at least for the flow fields tested in this dissertation. The current modifications show a positive impact on the predictions made. These predictions indicate that there is a need to account for the enthalpic production term and the term representing the baroclinic effect. But the impact of the current model on the mean flow field is not strong for the test cases considered here. However, in terms of the extent of the recirculation region (in the case of the afterbody flow field) or the distribution of pressure on the surface of the projectile, the current modifications are definitely a step in the right direction. Further study into the precise nature of the enthalpic production term and the baroclinic effects may be needed to improve the predictive capabilities of quantities such as the turbulent kinetic energy and to ascertain their role in determining the mean flow field.

The issue regarding the reduced sensitivity of  $k-\omega$  models to spatial gradients in density has been studied. It has been shown that this is an artifact of the neglect of cross-diffusion terms in the transport equation for  $\omega$ .

To further the understanding of the effects of compressibility on the turbulence structure the following suggestions can be made. The afterbody flow field that has been

investigated in this dissertation has been extensively studied, experimentally. However, the measurements are at a relatively low Mach number with the effects of compressibility playing a relatively minor role in the development of the flow field. Investigations of the flow structure at higher Mach numbers are needed to improve our understanding and to study the impact of the various modifications.

From the point of view of evaluating the model that has been proposed for the turbulent mass flux, measurements of the fluctuating velocity components based on Reynolds and Favre averages would be very useful to evaluate the need to account for the turbulent mass flux. Detailed measurements of high Mach number flow fields would be helpful in evaluating the orders of magnitude of the various terms that appear in the exact form of the governing equations and to fine tune the coefficients used in the models. A detailed study, either experimental or DNS, would be very helpful in addressing the baroclinic effect.

There is still no consistency in the definition of the non-dimensional distance,  $y^+$ , from the wall. A computational study of the impact of the various definitions of  $y^+$  would prove to be an useful exercise to improve the near wall modelling of turbulent flows. The dependence of the two-equation based models on the spatial gradients in density has been briefly considered in this dissertation. A more thorough study of the effect of the cross-diffusion term (in the  $k-\omega$  model) should be conducted and the differences between the predictive capabilities of the  $k-\epsilon$  and  $k-\omega$  models should be studied.

Very little information is available of the high velocity projectile flow field. For the particular case that we have considered in this dissertation there are discrepancies between the flow visualization results and the measurements made of the pressure distribution which renders a detailed analysis of the models of compressibility incomplete. The discrepancies need to be resolved and measurements of the mean velocity and temperature field need to be made to help evaluate the models of turbulence and understand the effect of compressibility in flow fields characterized by an interaction between complicated flow structures. Additionally, a resolution of the discrepancies between DNS studies and

experimental measurements regarding the interaction of turbulent field with a shock will help further our understanding of compressibility effects.

## REFERENCES

- Aupoix, B. and Viala, S., 1995, "Compressible turbulent boundary layer modelling", *The 2nd Joint ASME/JSME Fluids Engineering Conference & ASME/EALA 6th International Conference on Laser Anemometry*.
- Barre, S., Alem, D. and Bonnet, J. P., 1996, "Experimental study of a normal shock/homogeneous turbulence interaction", *AIAA Journal*, Vol. 34, pp. 968-974.
- Bernard, P. S. and Speziale, C. G., 1992, "Bounded energy states in homogeneous turbulent shear flow — An alternative view", *Journal of Fluids Engineering*, Vol. 114, pp. 29-39.
- Birch, S. L. and Eggers, J. M., 1972, "A critical review of the experimental data on turbulent shear layers", *NASA SP 321*, pp. 943-949.
- Blaisdell, G. A., Mansour, N. N. and Reynolds, W. C., 1993, "Compressibility effects on the growth and structure of homogeneous turbulent shear flow", *Journal of Fluid Mechanics*, Vol. 256, pp. 443-485.
- Blumen, W., Drazin, P. G. and Billings, D. F., 1975, "Shear layer instability of an inviscid compressible fluid — Part 2", *Journal of Fluid Mechanics*, Vol. 71, pp. 306-316.
- Bogdanoff, D. W., 1983, "Compressibility effects in turbulent shear layers", *AIAA Journal*, Vol. 21, pp. 926-927.
- Bogdanoff, S. M. and Vas, I. E., 1959, "Preliminary investigations of spiked bodies at hypersonic speeds", *Journal of the Aero/Space Sciences*, Vol. 26, pp. 65-74.
- Bradshaw, P., 1977, "Compressible turbulent shear layers", *Annual Review of Fluid Mechanics*, Vol. 9, pp. 33-54.
- Breidenthal, R., 1992, "Sonic eddy — A model for compressible turbulence", *AIAA Journal*, Vol. 30, pp. 101-104.
- Brown, G. L. and Roshko, A., 1974, "On density effects and large structure in turbulent mixing layers", *Journal of Fluid Mechanics*, Vol. 64, pp. 775-816.
- Chen, Y. S. and Kim, S. W., 1987, "Computation of turbulent flows using an extended k- $\epsilon$  turbulence closure model", *NASA CR 179204*.

- Chien, K. Y., 1982, "Predictions of channel and boundary layer flows with a low-Reynolds number turbulence model", *AIAA Journal*, Vol. 20, pp. 33-38.
- Childs, R. E. and Caruso, S. C., 1987, "On the accuracy of turbulent base flow predictions", *AIAA Paper* 87-1439.
- Chuang, C.-C and Chieng, C.-C., 1996, "Supersonic base flow computation using higher order closure turbulence models", *AIAA Paper* 96-0566.
- Clemens, N. T. and Mungal, M. G., 1995, "Large-scale structure and entrainment in the supersonic mixing layer", *Journal of Fluid Mechanics*, Vol. 284, pp. 171-216.
- Coakley, T. J. and Huang, P. G., 1992, "Turbulence modelling for high speed flows", *AIAA Paper* 92-0436.
- Coles, D., 1981, "Prospects for useful research on coherent structure in the turbulent shear flow", *Proceedings of the Indian Academy of Sciences*, Vol. 4, pp. 111-127.
- Cook, P. H., McDonald, M. A. and Firmin, M. C. P., 1979, "Aerofoil RAE 2822—Pressure distributions and boundary layer and wake measurements", *AGARD-AR-138*.
- Crawford, D. H., 1959, "Investigation of the flow over a spiked-nose hemisphere cylinder at a Mach number of 6.8", *NASA TN D-118*.
- Dawson, J. A. and Samimy, M. A., 1994, "The effects of expansion on a supersonic boundary layer : Surface pressure measurements", *AIAA Paper* 94-0648.
- El Baz, A. M., and Launder, B. E., 1993, "Second-moment modelling of compressible mixing layers", *Engineering Turbulence Modelling and Experiments*, edited by Rodi, W. and Martelli, F., Elsevier Science Publishers B. V., pp. 63-72.
- Elliott, G. S. and Samimy, M., 1990, "Compressibility effects in free shear layers", *Physics of Fluids A*, Vol. 2, pp. 1231-1240.
- Fernholz, H. H. and Finley, P. J., 1980, "A critical commentary on mean flow data for two-dimensional compressible turbulent boundary layers", *AGARD-AG-253*.
- Gaviglio, J., Dussauge, J. P., Debieve, J. F. and Favre, A., 1977, "Behaviour of a turbulent flow, strongly out of equilibrium, at supersonic speeds", *Physics of Fluids*, Vol. 20, pp. S179-S192.
- Gropengesser, H., 1970, "Study of the stability of boundary layers in compressible fluids", *NASA TT-F-12-786*.
- Hanjalic, K. and Launder, B. E., 1976, "Contribution towards a Reynolds stress closure for low-Reynolds number turbulence", *Journal of Fluid Mechanics*, Vol. 74, Part 4, pp. 593-610.
- Herrin, J. L. and Dutton, J. C., 1993, "An experimental investigation of supersonic axi-symmetric base flows including the effects of afterbody boattailing", Technical Report, *UILU-ENG 93-4018*, University of Illinois, Urbana-Champaign, Illinois.

- Hirsch, C., 1990, *Numerical Computation of Internal and External Flows*, Vol. 2, Wiley, Inc.
- Honkan, A. and Andreopoulos, J., 1992, "Rapid compression of grid generated turbulence by a moving shock wave", *Physics of Fluids A*, Vol. 4, pp. 2562-2572.
- Huang, P. G., Bradshaw, P. and Coakley, T. J., 1992, "Assessment of closure coefficients for compressible flow turbulence models", *NASA TM 103882*.
- Huang, P. G., Bradshaw, P. and Coakley, T. J., 1994, "Turbulence models for compressible boundary layers", *AIAA Journal*, Vol. 32, pp. 735-740.
- Huang, P. G. and Coakley, T. J., 1993, "Calculations of supersonic and hypersonic flows using compressible wall functions", *Engineering Turbulence Modelling and Experiments*, edited by Rodi, W. and Martelli, F., Elsevier Science Publishers B. V., pp. 731-739.
- Huang, P. G., Coleman, G. N. and Bradshaw, P., 1995, "Compressible turbulent channel flows: DNS results and modelling", *Journal of Fluid Mechanics*, Vol. 305, pp. 185-218.
- Huebner, L. D., Mitchell, A. M. and Boudreaux, E. J., 1995, "Experimental results on the feasibility of an aerospike for hypersonic missiles", *AIAA Paper 95-0737*.
- Ikawa, H. and Kubota, T., 1975, "Investigation of supersonic turbulent mixing layer with zero pressure gradient", *AIAA Journal*, Vol. 13, pp. 566-572.
- Jackson, T. L. and Grosch, C. E., 1989, "Inviscid spatial stability of a compressible mixing layer", *Journal of Fluid Mechanics*, Vol. 208, pp. 609-637.
- Jacquin, L., Blin, E. and Geffroy, P., 1991, "Experiments of free turbulence/shock wave interaction", *Turbulent Shear Flows 8*, Edited by Durst, F., Friedrich, R., Launder, B. E., Schmidt, F. W., Schumann, U. and Whitelaw, J. H., pp. 229-248.
- Jacquin, L., Cambon, C., and Blin, E., 1992, "Turbulence amplification by a shock wave and rapid distortion theory", *Physics of Fluids A*, Vol. 5, pp. 2539-2550.
- Jameson, A., Schmidt, W. and Turkel, E., 1981, "Numerical solutions of the Euler equations by finite volume methods with Runge-Kutta time stepping schemes", *AIAA Paper 81-1259*.
- Kays, W. M. and Crawford, M. E., 1980, *Convective Heat and Mass Transfer*, McGraw-Hill, Inc.
- Keller, J. and Merzkirch, W., 1990, "Interaction of a normal shock wave with a compressible turbulent flow", *Experiments in Fluids*, Vol. 8, pp. 241-248.
- Kim, S. C., 1990, "A new mixing length model for supersonic shear layers", *AIAA Journal*, Vol. 28, p. 1999.

- Kovaszny, L. S. G., 1953, "Turbulence in supersonic flow", *Journal of the Aeronautical Sciences*, Vol. 20, pp. 657-682.
- Launder, B. E., Reece, G. J. and Rodi, W., 1975, "Progress in the development of a Reynolds stress turbulence closure", *Journal of Fluid Mechanics*, Vol. 68, pp. 537-566.
- Launder, B. E. and Spalding, D. B., 1972, *Lectures in Mathematical Models of Turbulence*, Academic Press.
- Lee, S., Lele, S. K. and Moin, P., 1993, "Direct numerical simulation of isotropic turbulence interacting with a weak shock wave", *Journal of Fluid Mechanics*, Vol. 251, pp. 533-562.
- Lele, S. K., 1993, "Notes on the effects of compressibility on turbulence", *Center for Turbulence Research Manuscript* Number 145, Stanford University.
- Lele, S. K., 1994, "Compressibility effects on turbulence", *Annual Review of Fluid Mechanics*, Vol. 26, pp. 211-254.
- Li, H. and Kroll, N., 1988, "Solutions of one- and two-dimensional Euler equations using TVD schemes", *DFVLR IB* 129-88 / 24, Braunschweig, Germany.
- Mahesh, K., Lele, S. K. and Moin, P., 1993, "Shock turbulence interaction in the presence of mean shear: an application of rapid distortion theory", *AIAA Paper* 93-0663.
- McNeil, C. Y., 1996, "The effect of numerical dissipation on high Reynolds number turbulent flow solutions", *AIAA Paper* 96-0891.
- Menter, F. R., 1994, "Two-equation eddy viscosity turbulence models for engineering applications", *AIAA Journal*, Vol. 32, pp. 1598-1605.
- Monin, A. S. and Yaglom, A. M., 1971, *Statistical Fluid Mechanics*, Vol. 1, Cambridge: MIT Press.
- Morkovin, M. V., 1987, "Transition at hypersonic speeds", *NACA CR* 178315, *ICASE Interim Report* No. 1, 1987.
- Morris, P. J., Giridharan, M. G. and Lilley, G. M., 1990, "On the turbulent mixing of compressible free shear layers", *Proceedings of the Royal Society of London, Series A : Mathematical and Physical Sciences*, Vol. 431, pp. 219-243.
- Papamoschou, D., 1991, "Structure of the compressible turbulent shear layer", *AIAA Journal*, Vol. 29, pp. 680-681.
- Papamoschou, D. and Lele, S. K., 1993, "Vortex induced disturbance field in a compressible shear layer", *Physics of Fluids A*, Vol. 5, pp. 1412-1419.
- Papamoschou, D. and Roshko, A., 1988, "The compressible turbulent shear layer : An experimental study", *Journal of Fluid Mechanics*, Vol. 197, pp. 453-477.



- Passot, T. and Pouquet, A., 1987, "Numerical simulation of compressible homogeneous flows in the turbulent regime", *Journal of Fluid Mechanics*, Vol. 181, pp. 441–466.
- Patel, V. C., Rodi, W. and Scheuerer, G., 1985, "Turbulence models for near-wall and low-Reynolds number flows : A review", *AIAA Journal*, Vol. 23, pp. 1308–1319.
- Peace, A. J., 1990, "Turbulent flow predictions for afterbody/nozzle geometries including base effects", *Journal of Propulsion*, Vol. 7, pp. 396–403.
- Poggie, J. and Smits, A. J., 1996, "Large-scale coherent turbulence structures in a compressible mixing layer flow", *AIAA Paper* 96-0440.
- Ragab, S. A. and Wu, J. L., 1989, "Linear instabilities in two-dimensional compressible mixing layers", *Physics of Fluids A*, Vol. 1, pp. 957–966.
- Reynolds, O., 1895, "On the dynamical theory of incompressible viscous fluids and the determination of the criterion", *Philosophical Transactions of the Royal Society of London*, A, Vol. 186, pp. 123–164.
- Ribner, H. S., 1954, "Shock-turbulence interaction and the generation of noise", *NACA TN* 3255.
- Ristorcelli, J. R., 1993, "A representation for the turbulent mass flux contribution to Reynolds stress and two-equation closures for compressible turbulence", *NASA CR* 191569.
- Rizzi, A., 1978, "Numerical implementation of solid-body boundary conditions for the Euler equations", *ZAMM*, Vol. 58, pp. T301–T304.
- Rizzi, A., 1981, "Computational mesh for Transonic Airfoils: The standard mesh", *Numerical Methods for the Computation of Inviscid Transonic Flows with Shock Waves*, Edited by Rizzi, A. and Viviand, H., Friedr. Vieweg & Sohn, pp. 222–253.
- Roe, P. L., 1981, "Approximate Riemann solvers, parameter vectors and difference schemes", *Journal of Computational Physics*, Vol. 43, pp. 357–372.
- Rotman, D., 1991, "Shock wave effects on a turbulent flow", *Physics of Fluids A*, Vol. 3, pp. 1792–1806.
- Rotta, J. 9151, "Statistical theory of inhomogeneous turbulence – Part I", *Zeitschrift für Physik*, Vol. 129, pp. 257–572.
- Rubesin, M. W., 1990, "Extra compressibility terms for Favre-average two-equation models for inhomogeneous turbulent flows", *NASA CR* 177556.
- Sahu, J., 1994, "Numerical computations of supersonic base flow with special emphasis on turbulence modelling", U. S. Army Research Laboratory, *ARL-TR-438*.
- Sahu, J., Nietubicz, C. J. and Steger, J. L., 1985, "Navier–Stokes computations of projectile base flow with and without base injection", *AIAA Journal*, Vol. 23, pp. 1348–1355.

- Samimy, M., Erwin, D. E. and Elliott, G. S., 1989, "Compressibility and shock wave interaction effects on free shear layers", *AIAA Paper* 89-2460.
- Samimy, M., Reeder, M. F. and Elliott, G. S., 1992, "Compressibility effects on large structures in free shear flows", *Physics of Fluids A*, Vol. 4, pp. 1251-1258.
- Sandham, N. D. and Reynolds, W. C., 1990, "Compressible mixing layer : Linear theory and direct simulation", *AIAA Journal*, Vol. 28, pp. 618-624.
- Sarkar, S., 1992, "The pressure dilatation correlation in compressible flows", *Physics of Fluids A*, Vol. 4, pp. 2674-2682.
- Sarkar, S., 1994, "The stabilizing effect of compressibility in turbulent shear flow", *NASA CR* 194932.
- Sarkar, S., Erlebacher, G., Hussaini, M. Y. and Kreiss, H. O., 1991, "The analysis and modelling of dilatational terms in compressible turbulence", *Journal of Fluid Mechanics*, Vol. 227, pp. 473-493.
- Sarkar, S. and Lakshmanan, B., 1991, "Application of a Reynolds-stress turbulence model to the compressible shear layer", *AIAA Journal*, Vol. 29, pp. 743-749.
- Schlichting, H., 1968, *Boundary Layer Theory*, McGraw-Hill, Inc.
- Shih, T.-H. and Lumley, J. L., 1993, "Remarks on turbulent constitutive relations", *NASA TM* 106116.
- Shuen, J.-S., 1992, "Upwind differencing and LU factorization for chemical non-equilibrium Navier-Stokes equations", *Journal of Computational Physics*, Vol. 99, pp. 233-250.
- So, R. M. C., 1991, "Near-wall modelling of compressible turbulent flow", *NASA CR* 189608.
- Sondak, D. L. and Pletcher, R. H., 1995, "Application of wall functions to generalized non-orthogonal curvilinear co-ordinate systems", *AIAA Journal*, Vol. 33, pp. 33-41.
- Speziale, C. G., 1992, "Analytical methods for the development of Reynolds stress closures in turbulence", *Annual Review of Fluid Mechanics*, Vol. 23, pp. 107-157.
- Speziale, C. G., Abid, R. and Anderson, E. C., 1992, "Critical evaluation of two-equation models for near-wall turbulence", *AIAA Journal*, Vol. 30, pp. 324-331.
- Stalder, J. R. and Nielsen, H. V., 1954, "Heat transfer from a hemisphere-cylinder equipped with flow-separation spikes", *NACA TN* 3287.
- Sun, C. C. and Childs, M. E., 1973, "A modified wall wake velocity profile for turbulent compressible boundary layers", *Journal of Aircraft*, pp. 381-383.

- Swanson, R. C. and Turkel, E., 1987, "Artificial dissipation and central difference schemes for the the Euler and Navier-Stokes equations", *Proceedings of the AIAA 8th Computational Fluid Dynamics Conference*, pp. 55-69.
- Tennekes, H. and Lumley, J. L., 1972, *A First Course in Turbulence*, Cambridge: MIT Press.
- Thakur, S. S., Wright, J. F., Shyy, W., Liu, J., Ouyang, H. and Vu, T., 1996, "Development of pressure-based composite multigrid methods for complex fluid flows", *Progress in Aerospace Sciences*, Vol. 32, pp. 313-375.
- Thibert, J. J., Grandjacques, M. and Ohman, L. H., "NACA 0012 airfoil — Pressure distributions and boundary layer and wake measurements", *AGARD-AR-138*.
- Thomas, J. L. and Salas, M. D., 1986, "Far-field boundary conditions for transonic lifting solutions to the Euler equations", *AIAA Journal*, Vol. 24, p. 1074.
- Thompson, P. A., 1972, *Compressible Fluid Dynamics*, McGraw-Hill, Inc.
- Tucker, P. K. and Shyy, W., 1993, "A numerical analysis of supersonic flow over an axi-symmetric afterbody", *AIAA Paper 93-2347*.
- Turkel, E., 1984, "Acceleration to a steady state for the Euler equations", *NASA CR 172398*.
- Viegas, J. R. and Rubesin, M. W., 1991, "A comparative study of several compressibility corrections to turbulence models applied to high-speed shear layers", *AIAA Paper 91-1783*.
- Viegas, J. R., Rubesin, M. W. and Horstman, C. C., 1985, "On the use of wall-functions as boundary conditions for two-dimensional separated compressible flows", *AIAA Paper 85-0180*.
- Wilcox, D. C., 1988, "Reassessment of the scale-determining equation for advanced turbulence models", *AIAA Journal*, Vol. 26, pp. 1299-1310.
- Wilcox, D. C., 1992, *Turbulence Modelling for CFD*, DCW Industries, Inc.
- Wilcox, D. C. and Traci, R. M., 1976, "A complete model of turbulence", *AIAA Paper 76-351*.
- Yee, H. C., 1985, "On symmetric and upwind TVD schemes", *Proceedings of the 6th GAMM Conference on Numerical Methods in Fluid Mechanics*, pp. 399-407.
- Yoshihara, H. and Sacher, P., 1985, "Test cases for inviscid flow field method", *AGARD-AR-211*.
- Zeman, O., 1990, "Dilatation dissipation : The concept and application in modelling compressible mixing layers", *Physics of Fluids A*, Vol. 2, pp. 178-188.

Zeman, O., 1993, "New model for super/hypersonic turbulent boundary layers", *AIAA Paper* 93-0897.

**DISTRIBUTION**  
**WL-TR-1997-7060**

Defense Tech Info Center  
ATTN: DTIC-OCP  
8725 John J Kingman Road, Suite 0944  
Ft. Belvoir VA 22060-6218

1

Eglin AFB Offices:

WL/CA-N	1
WL/MNP-1 (Tech Library)	1
WL/MNSI (Dr Belk)	1
WL/MNSI (R. Johnson)	2